Crustal Deformation and Geodetic Site Stability Determination using GPS

By

Willem Ludwig Combrinck

Thesis Presented for the Degree of
DOCTOR OF PHILOSOPHY
in the Department of Geomatics
UNIVERSITY OF CAPE TOWN
June, 2000.

DEDICATION This work is firstly dedicated to my parents, who gave me my first chemistry set, telescope and shortwave radio. They gave me freedom to explore and investigate using a multi-disciplinary approach.
Secondly, this work is dedicated to my wife Sandra, who manages to live with me regardless of an overflowing outbuilding, garage and house which is a result of the multi-disciplinary approach. She has lived with a mountain of books, folders and papers on my side of the bed, and probably feels she married a laptop. She has stood by me since my first university exam and has never left my side since.

ACKNOWLEDGEMENTS

I would like to express my sincere gratitude to several individuals and organisations whose support made this work possible;

The director of HartRAO, Dr George Nicolson, whose generous vision has allowed the development and expansion of the Geodesy Programme and whose unfaltering support in more ways than one has ensured completion of this work.

My supervisor, Prof. Charles Merry (UCT), who always stayed within reach and provided a solid foundation for this work.

Mr Richard Uytenbogaardt (Dick), who took me under his wing when I only had ideas and helped me to turn those ideas into reality, his dedication, generosity and friendship are greatly appreciated.

Mr Peter Stocker, for improving my grammar and preventing me from mixing American with English.

Mr William Moralo, who aided this work with his own enthusiasm and did not mind sleeping in a tent on a cold night.

Dave Stowers, James Zumberge and Martin Marcin of JPL, for supporting the densification of the IGS in southern Africa, not with words but with action.

Oivind Ruud of UNAVCO for packing jelly beans with GPS equipment, both are appreciated.

Matthijs van Domselaar, Pfeng Fang and Yehuda Bock for showing me the ropes with GAMIT.

Geoffrey Blewitt for allowing me to roam free in the libary of the University of Newcastle.

Angelyn Moore and Ruth Neilan for supporting my IGS activities.

Marisa Nickola for painstakingly drawing error ellipses.

Jan Kouba, who in his special way, with few words greatly encouraged me at a late hour of this work.

I, **Willem Ludwig Combrinck**, hereby declare that the work on which this thesis is based is original (except where acknowledgements indicate otherwise) and that neither the whole work nor any part of it has been, is being, or is to be submitted for another degree at this or any other University.

I empower the University to reproduce for the purpose of research either the whole or any portion of the contents in any manner whatsoever.

.....

.....

(Date)

Abstract

This work describes crustal deformation and local site stability as determined by Global Positioning System (GPS) measurements at HartRAO. A novel approach is used to conduct geodetic site *footprint* surveys by utilising relevant disciplines such as geology and geomorphology in a systems approach. The monument and the technique used to measure its position is seen as part of an open dynamic system, which is closely related to the Earth's surface system. It is shown that footprints can no longer be seen as only a collection of vector components between reference points, but is in fact a complex system which is continuously affected by various exogenic and endogenic factors and processes. These factors and processes cannot be ignored in the quest for millimetre and submillimetre geodetic positioning, whether it be on a global or local scale.

Monumentation is described and discussed with the emphasis on long term stability. Using a holistic approach, the minimising of monument instability due to local effects such as slope movement and poor interface to bedrock is investigated.

The effect of solar radiation on monument stability is investigated using GPS measurements. A simple Distinct Element Method numerical model is developed to support these measurements. The GPS measurements indicate thermal expansion of a hill which results in a diurnal positional variation at the several millimetre level in the position of the geodetic monument. The Distinct Element Method model indicates that thermal expansion can be responsible for a diurnal and longer term positional instability of a geodetic monument. The GPS and thermal model results agree very well and indicate independently that thermal expansion could lead to geodetic monument positional variation. It is shown that although many other factors have a near diurnal period, such as influences of the ionosphere, troposphere and satellite geometry, these factors are not responsible for the diurnal signal present in the monument position.

A regional network and its preliminary results are discussed. Several permanent GPS stations were installed during the course of this work, leading to densification of the International Terrestrial Reference Frame and making an important contribution to the International GPS Service (IGS). This contribution was enhanced by establishing an IGS regional data centre at HartRAO. The results from the regional network are promising in that close agreement with Very Long Baseline Interferometry results as well as independently processed data are achieved on a weekly basis.

This work shows that the HartRAO site is stable. It provides the background material and data for site integrity, ties between various space geodetic techniques and the ability to detect and quantify any anomalous geodetic movement on site. It also lays the foundation for further research concerning local effects on monument stability and crustal motion interpretation using a systems approach.

Contents

List of Figures

List of Tables

Acronyms

BKG Bundesampt für Kartographie und Geodäsie.

COSPAR Committee on Space Research

DEM Distinct Element Method

DOP Dilution of Precision

ERS-1 Earth Resources Satellite of the European Space Agency

GDOP Geometrical Dilution of Precision

GGAO Goddard Geophysical and Astronomical Observatory

GPS Global Positioning System

HartRAO Hartebeesthoek Radio Astronomy Observatory

HDOP Horizontal Dilution of Precision

HEMTS High Electron Mobility Transistors

IEEE Institute of Electrical and Electronics Engineers, Inc.

IERS International Earth Rotation Service

IfAG Institut für Angewandte Geodäsie

IGS International GPS Service

ILRS International Laser Ranging Service

IRI International Reference Ionosphere

ITRF International Terrestrial Reference Frame

IVS International VLBI Service

MIT Massachusetts Institute of Technology

NTM Numerical Thermal Model

NSSDC National Space Science Data Center

SLR Satellite Laser Ranging

SINK Name given to sinking monument located on expansive clay

SOPAC Scripps Orbit and Permanent Array Center

SPD Surge Protection Device

Topex-Poseidon USA/French system to measure sea surface topography for determination of global ocean circulation and to improve the earth's gravity model

TEC Total Electron Content

UHF Ultra High Frequency (300-3000 Mhz)

UNAVCO University NAVSTAR Consortium

URSI International Union of Radio Science

VHF Very High Frequency (30-300 MHz)

VLBI Very Long Baseline Interferometry

Chapter 1

Space Geodesy at HartRAO

"The revolution in Geodesy has only just begun and we are privileged to be taking part in it" - **A. R. Robbins, Oxford University, 1978**

1.1 Introduction

The Hartebeesthoek Radio Astronomy Observatory (HartRAO), which is located north of Johannesburg, South Africa, regularly participates in space geodetic experiments using different space geodetic techniques. HartRAO uses a 26 metre equatorially mounted Cassegrain radio telescope built by Blaw Knox in 1961. The telescope was part of the NASA deep space tracking network until 1975 when the facility was converted to an astronomical observatory. Currently approximately 15 % of the radio telescope time is allocated to geodetic Very Long Baseline Interferometry (VLBI) in various International VLBI Service (IVS) networks. HartRAO participates as IGS Regional Data Centre for Africa in the International GPS Service (IGS) network. In addition a permanent Satellite Laser Ranging (SLR) station (MOBLAS6) is being installed at HartRAO as part of the International Laser Ranging Service (ILRS) network. Each of these different space geodetic techniques makes a unique contribution to geodesy, although some overlapping is inevitable. GPS networks allow relatively economical and efficient densification of permanent geodetic stations on a local scale, VLBI uniquely determines accurate Earth orientation in an inertial frame and SLR allows accurate definition of Earth scale. The main focus and content of this work by the author has been to initiate and develop GPS capabilities at the HartRAO site, for short baseline crustal stability studies ('footprint' surveys) as well as densification of the IGS network in southern Africa and the continous processing of a regional GPS network. The GPS work supports and enhances VLBI and SLR results and is an important player in the field of geodesy on a local and global scale. This chapter briefly introduces the different space geodetic techniques, with emphasis on HartRAO's unique contribution and sketches the background against which the rest of this work should be read.

The basic structure of this work is set out as follows:

- Chapter 1 describes the geodesy programme at HartRAO, briefly introduces

the space geodetic techniques in use as well as their operational status in order to present a background for the rest of the work.

- Chapter 2 contains an overview of and describes the motivation behind footprint studies. The systems approach for footprint studies is introduced.
- Chapter 3 sketches the HartRAO site geological background and mentions geomorphological factors which could influence footprint results.
- Chapter 4 defines the Earth's crust from a monumentation perspective, outlines methods and procedures for selecting a monument site and critically overviews different monument locations.
- Chapter 5 investigates possible GPS error sources which might have a diurnal component. It is shown that the magnitude of these GPS errors are too small to account for the measured thermal expansion.
- Chapter 6 describes the footprint network, processing strategy and results.
- Chapter 7 singles out the effect of diurnal thermal variation on geodetic monument stability. The effect of this variation on a hill is investigated to ascertain the amplitude of the positional changes of a monument caused by thermal expansion.
- Chapter 8 discusses the development of a numerical thermal model based on the distinct element method to model monument instability due to diurnal temperature changes.
- Chapter 9 introduces the HartRAO regional network and participation in the IGS.
- Chapter 10 contains a short summary of the results, conclusions and some recommendations for future work.
- Appendix A contains some additional background material on some of the mathematical concepts used in this work.
- Appendix B describes thermal data reduction procedures
- Appendix C contains an example of the regional network baseline repeatability.
- Appendix D contains tables and plots of footprint results.
- Appendix E contains data tables and plots of the thermal expansion (Hill 411) results.
- Appendix F lists a table containing the results of a monument located on expansive clay.
- Appendices G and H contain error ellipses and footprint baseline plots respectively.

1.2 VLBI

1.2.1 Introduction

VLBI is a technique developed by radio astronomers to accurately measure the positions and spatial structure of astronomical radio sources utilising radio telescopes. Radio astronomers use radio interferometers for aperture synthesis imaging, which allows radio telescopes with resolutions equivalent to very large effective apertures, to be built by using an array of radio telescopes. These telescopes can be separated by hundreds of metres or one can have intercontinental networks by having telescopes on different continents.

Geodesy has benefitted from radio astronomy by using the radio interferometry technique in an inverse sense. VLBI has been used since the early seventies in high precision geodynamical studies for determining the position of and baseline between stations. HartRAO currently supports several long term international geodetic VLBI projects, using its 26 m diameter radio telescope (figure 1.1). The geodetic VLBI technique utilises very distant extragalactic radio sources (known as quasars), as apparently motionless objects of reference and for this purpose are taken to be point sources. This characteristic of quasars allows the implementation and maintenance of a very stable reference frame which is required for the measurement of slow geodynamical processes which normally exhibit motions in the range of millimetres to tens of millimetres per year.

The use of VLBI, GPS and SLR furthers the scientific understanding of Earth dynamics, earthquake mechanisms and tectonophysics by applying these techniques to the following:

- Studies of the Earth's variable rotation, this includes the motion of the Earth's rotation axis with respect to the Earth as shown by polar motion and the angular position around the Earth's rotation axis describing universal time (UT1).
- Studies of angular momentum transfer from the atmosphere and its effect on the rotation of the Earth.
- Crustal dynamics - e.g. tectonic motion and monitoring of active regions.
- Global studies of true variation of ocean levels by linking tide gauges to fundamental GPS, VLBI and SLR sites.
- Geophysical studies - e.g. VLBI has significantly improved our knowledge of the shape of the core-mantle boundary.
- Geomorphological studies - e.g. global and tectonic geomorphology.

Figure 1.1: The HartRAO 26 m antenna.

- Geopotential field measurements - SLR data from LAGEOS is very important in the measuring of long wavelength temporal components of the gravity field.
- SLR allows special tests of the theory of General Relativity.
- Using SLR, sub-nanosecond global time transfer is possible.
- Precision orbit determination for spaceborne radar altimeter missions.

1.2.2 Technical parameters of the HartRAO telescope

The feed-horns used for the 13 cm and 3.5 cm wavelengths are single polarised conical feeds. Both S and X bands have right hand circular polarisation. The rf amplifiers are cryogenically cooled HEMTS (High Electron Mobility Transistor). The radio telescope is being upgraded and we have recently (November 1998) replaced the hydraulic drive with an electric drive. A project has been launched to upgrade the perforated surface panels of the telescope to higher tolerance solid panels to increase the antenna efficiency, especially at the higher frequencies.

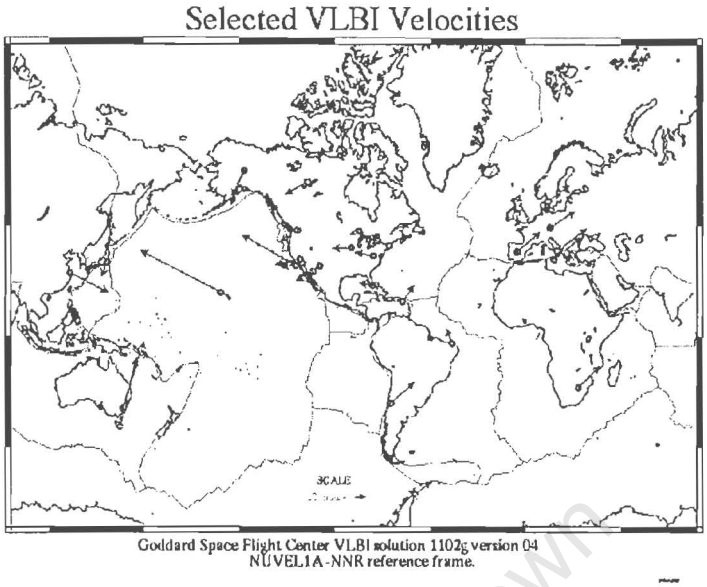

Figure 1.2: Depiction of global VLBI station velocities. (Ma and Ryan 1998)

1.2.3 Basic Principles of Geodetic VLBI

In general, the travel time of a wavefront between antennas at two or more sites is measured by maximising the cross-correlation function of the different signals received at the antennas. The difference in travel time (known as the group delay) is a function of (Kolaczek 1989):

- geometry of the participating stations
- spatial distribution of the radio sources
- effects of the propagation medium
- instrumentation effects

The latter includes clock drifts and the offset of the antenna axis, which is by definition, the distance between the Hour Angle (HA) rotational axis and the Declination (DEC) rotational axis. Group delay is one of the parameters which is necessary for the calculation of the baseline coordinates. If the antennas in an array are separated by relatively short distances, phase-synchronised local oscillators can be used and the antennas can feed directly into a correlator. Currently, if antennas are situated on different continents they cannot be connected in real time. Therefore Hydrogen MASER atomic clocks are used to synchronise the signals from the antennas and the signals from the radio sources are then stored on very high density magnetic tape. This technique requires specialised recording equipment and a correlator system, but

then the antennas can be located far apart, allowing the measurement of intercontinental baselines.

1.2.4 Geodetic VLBI Applications

Geodetic VLBI allows one to accurately determine the relative positions of the radio antennas in an array. These relative positions can then be used to study the motion of the continents on which the antennas are located as well as the motion of the Earth itself. The basic concept of plate tectonics is that the lithosphere, the crust and uppermost mantle which is of the order of 100 km thick, is divided into a small number of nearly rigid plates, which are moving over the astenosphere. Apart from plate tectonics, the Earth undergoes dynamic processes such as rapid and complex rotation about it's axis. The lithosphere behaves elastically on a geological time scale, so there is also a gradual rebound of the land after the retreat of continental glaciers. It is only by careful investigation of all the complex dynamical processes that a deep enough understanding can be had of the physics of the earth which will enable us to predict earthquakes and monitor global changes. (Figure 1.2) (Ma & Ryan 1998) depicts VLBI station velocities on a world map. These VLBI plots are results from NASA Goddard Space Flight Center's VLBI terrestrial reference frame solution number 1102g, 1998 August. (Figure 1.3) (Ma & Ryan 1998) is a time series plot of HartRAO, the time baseline is more than ten years. It is interesting to compare this with our GPS solution(Figure 1.7), which has a time baseline of about one year. Note that when comparing, the VLBI solution has the up component on the top part of the figure, followed by the east and north component, whereas the GPS solution has the sequence reversed.

1.2.5 HartRAO Geodetic VLBI Participation

The number of geodetic VLBI experiments conducted at HartRAO have increased from 38 in 1995 to 44 in 1998. A substantial increase in number were allocated for 1999 (57). The experiments are each of 24 hour duration. The Space Geodesy Programme currently participates in the following projects:

- IRIS-S
- CORE-A (Earth Orientation Parameters)
- SYOWA
- CRF
- CORE-OHIG
- RDV/VLBA

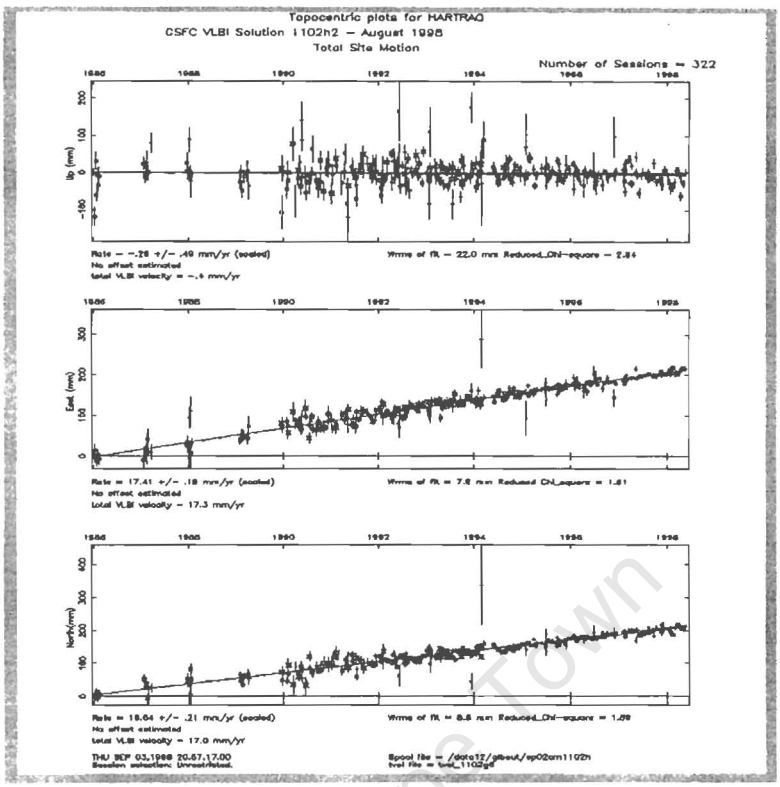

Figure 1.3: Time series of the HartRAO Geodetic VLBI station. (Ma and Ryan 1998)

The bulk of these experiments are IRIS-S and Core-A. The IRIS-S sessions continue the series of measurements for the determination of earth rotation parameters. These experiments are set up to provide baseline components, all earth orientation parameters (UT1, polar motion, and nutation), as well as the positions of extragalactic radio sources. The standard configuration of the monthly observed IRIS-S (South) experiments consists of four stations; United States of America (Westford), South Africa (HartRAO), Europe (Wettzell,Germany) and one radio telescope in South America (Fortaleza, Brazil). Since January 1997 the network has been augmented by station Fairbanks (Alaska). During the O'Higgins occupations two more stations located in the southern hemisphere are added to this network; with O'Higgins (Antarctica) and Hobart (Tasmania) there are seven stations in this network. The purpose of CORE-A (Continuous Observations of the Rotation of the Earth) is to validate the CORE concept of measuring EOP continuously using different networks. The network for CORE-A includes Fairbanks (Alaska), HartRAO (South Africa), Algonquin (Canada), Westford (USA), Matera (Italy), Medicina (Italy), Tsukuba (Japan) and Hobart (Tasmania). This set of 8 stations includes two geographically paired stations: Algonquin/Westford and Matera/Medicina. More detailed information can be had from the CORE white paper;

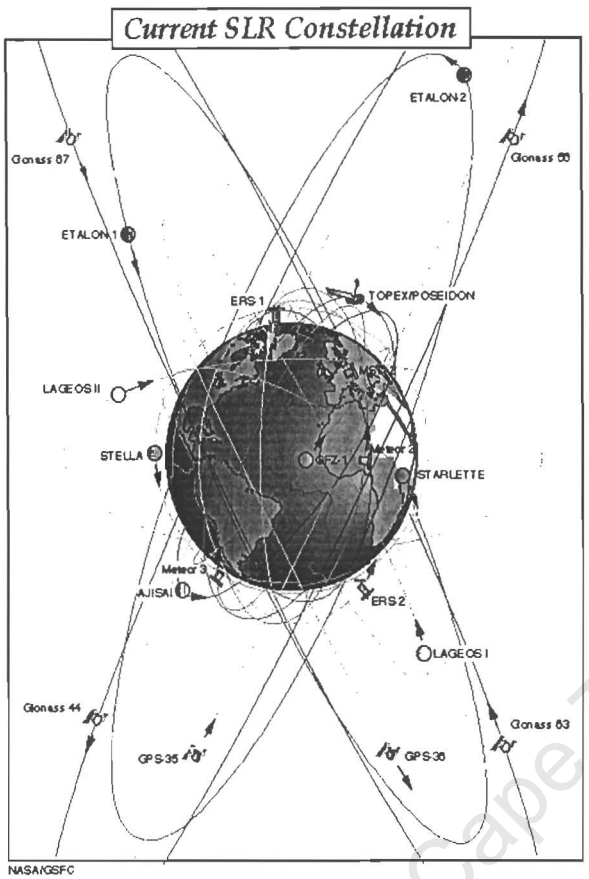

Figure 1.4: Constellation of satellites tracked by SLR. (source NASA, CDDIS, http://cddis.gsfc.nasa.gov)

(http://lupus.gsfc.nasa.gov/core/final1.html).

1.3 SLR

1.3.1 Introduction

A Satellite Laser Ranging (SLR) station can be regarded as an optical radar. This technique makes very precise measurements of the range and rate of motion between an SLR station and an orbiting satellite. (Figure 1.4) depicts the current SLR constellation. The satellite needs to be equipped with special mirrors called retroreflectors which reflect the laser light back to the SLR station. There are about 45 SLR stations in operation worldwide, but even more so than with GPS and VLBI, the African continent is not covered as is clearly shown in Figure 1.5. This lack of an SLR station in Africa has resulted in a large gap in the coverage of many geodetic and remote sensing satellites and this gap is affecting scientific results in an adverse way; establishing an

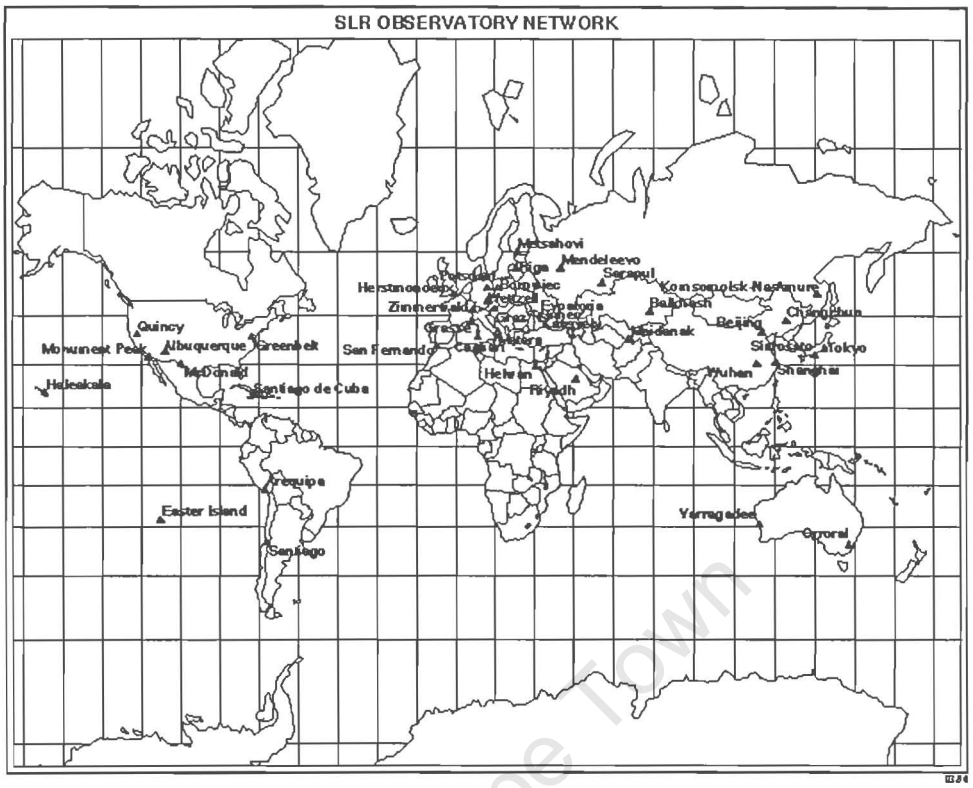

Figure 1.5: World map showing current distribution of SLR sites. (source NASA, CDDIS, http://cddis.gsfc.nasa.gov)

SLR station at HartRAO would overcome this to a large extent.

1.3.2 SLR Monument

Early in 1993, NASA and IfAG (Institut für Angewandte Geodäsie), now BKG (Bundesampt für Kartographie und Geodäsie), expressed an interest in establishing a satellite laser ranging system in South Africa. HartRAO proceeded to construct an SLR pad and geodetic monument for the German Modular Transportable Laser Ranging System (MTLRS) which subsequently occupied the pad in June 1993. Unfortunately the MTLRS never re-occupied the pad, but very satisfactory results were obtained for the SLR pad reference point. Afterwards the MTLRS was moved to occupy an SLR pad at Sutherland, at the site of the South African Astronomical Observatory (SAAO).

1.3.3 Initial Objectives of the SLR Campaign

Initial objectives of the SLR campaign were not fully attained, as the SLR pad was not re-occupied after the initial measurements were made but in the event of a permanent SLR unit being stationed at HartRAO these goals should be

achieved. In any event the SLR measurements proved valuable in that they provided an independent reference point, using another technique than VLBI. The main objectives were:

- Provide an inter-comparison at the cm level of the position of the 26-m radio telescope as determined by VLBI and that determined by the SLR technique.
- Models of the earth's gravity field over southern Africa and the adjoining oceans would be improved.
- Orbits of satellites such Topex-Poseidon and ERS-1 would be improved with consequent improvements in ocean level altimetry.
- A precise baseline would be established between Sutherland and HartRAO, which would be useful for national surveying and geodetic applications.

At the time of writing, we are making preparations to bring a MOBLAS6 SLR unit to HartRAO in collaboration with Goddard Space Flight Centre (GSFC) and we hope to have this station operational by mid 2000. The addition of this station to the global network will improve scientific results over a wide range of applications.

1.4 GPS

1.4.1 Introduction

The Global Positioning System (GPS) was developed by the USA Department of Defence to provide instantaneous positioning and velocity determination data for its armed forces. To ensure that four satellites are always visible to a receiver, a system was developed whereby 21+3 evenly spaced satellites placed in 12-hour orbits inclined at 55° to the equatorial plane would provide the required coverage most economically. Currently there are 27 operational satellites in orbit. GPS is now used for many more applications than it was originally intended for and is successfully used in high precision geodetic research. We routinely achieve 10-15 ppb (parts per billion) repeatability per 24 hour data set in our weekly GPS analyses. This equates to a precision of about 10 mm in 1000 km.

1.4.2 HartRAO GPS Activities

During the 1995-1998 period HartRAO assisted IfAG in the Geodetic Antarctic Project (GAP95) which fall within the SCAR (Scientific Committee for Antarctic Research) program to establish a precise geodetic network in the Atlantic sector of Antarctica (Dietrich 1996). The 1998 GPS observations

at HartRAO were conducted in cooperation with the Alfred Wegener Institute for Polar and Oceanic Research which had taken over the responsibility from IfAG after their transformation to the BKG. Several other GPS related projects were undertaken during this period. We developed a method to determine the VLBI antenna axis offset and reference point using GPS (Combrinck and Merry 1997) which allows simultaneous eccentricity determinations between geodetic reference points occupied by different measuring systems. A footprint survey of the HartRAO site was initiated during 1997 to determine local crustal and monumentation stability (the core of this work) as well as ties between the reference points of the different space geodetic techniques.

1.4.3 HartRAO IGS Participation

The International GPS Service (IGS) in cooperation with a multinational membership of organisations and agencies, provides precise GPS orbits, tracking data, and other high-quality GPS data and data products to meet the objectives of a wide range of scientific and engineering applications and studies. GPS stations which meet certain criteria can be included in the IGS network. During September 1996 HartRAO installed an IGS station (HRAO) which is currently equipped with a ROGUE SNR12 RM receiver and Dorne Margolin choke ring antenna (IGS 1996 Annual Report). The monumentation is tied to bedrock. The use of a Hydrogen MASER as a clock reference has allowed HRAO to be included in a small network of globally distributed GPS receivers equipped with precise time references. This special network is used to estimate GPS clock parameters every 30 seconds. The accuracy obtained allows post-processing of high-rate single receiver kinematic GPS data with few-cm-level precision when used with precise GPS orbits (Zumberge et al. 1998).

Towards the end of 1997 HartRAO installed an IGS station (SUTH) at the Sutherland site of the SAAO. This station is equipped with a ROGUE SNR8000 and Dorne Margolin antenna. Monumentation for a future IGS site (NAMI) at Windhoek, Namibia was installed during November 1998 at the location of the Surveyor General's office of Namibia. It is envisaged that this site will become an IGS station during mid 2000 after an equipment upgrade. The equipment for the IGS sites is provided by the Jet Propulsion Laboratory (JPL) of NASA. From April 1999 HartRAO has officially commenced to function as an IGS Regional Data Centre for Africa. In this function we gather data from various operational data centres and maintain an archive for users interested in stations in the Africa region. This reduces electronic network traffic and allows local users to obtain IGS products and data more timeously. Currently we archive data for 15 IGS stations and one regional station (NAMI). These data can be downloaded from our webpage: *(http://www.hartrao.ac.za/geodesy/geodesy_index.html).*

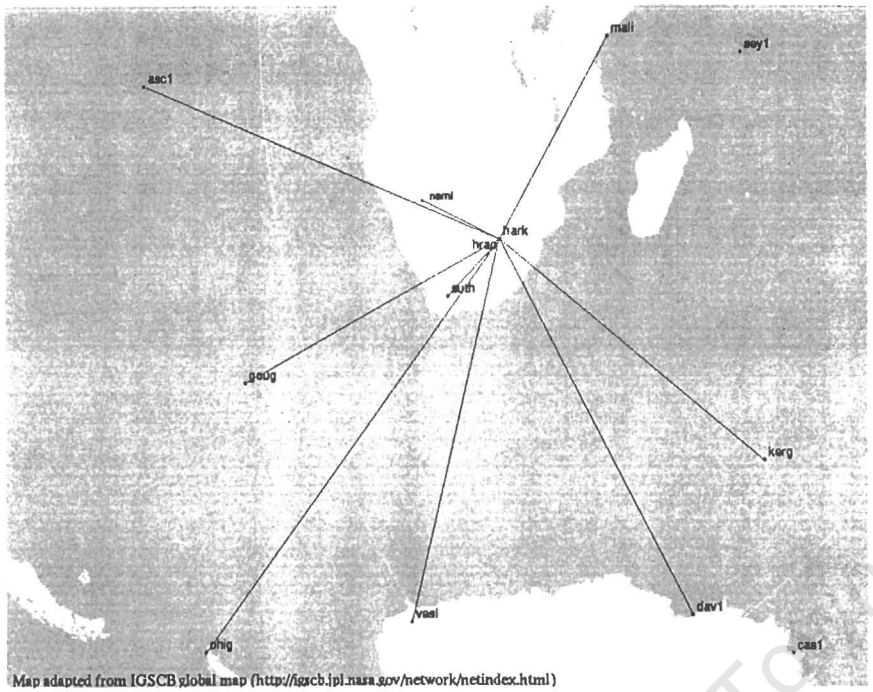

Figure 1.6: HartRAO regional GPS network. It is obvious that the network requires strengthening towards the north. Densification of the IGS network in Africa will benefit global geodesy.

1.4.4 Regional GPS Network

With the co-operation of Scripps Orbit and Permanent Array Centre (SOPAC) located at the Scripps Institute of Oceanography, La Jolla, we have started to process a regional network (figure 1.6) in the southern hemisphere using the GAMIT software package. The reference frame is maintained through the IGS orbit and IERS Earth orientation values using HRAO as origin. These stations are located on the African and Antartica tectonic plates. Preliminary results are shown in the form of a time series plot (figure 1.7) for HRAO. The north and east components show close agreement with the VLBI results, even though the time baseline is much shorter. The vertical component is weaker, but is showing closer agreement every time more data is added. There is a noted improvement in the GPS timeseries at about 1998.3 due to the addition of the the Sutherland IGS station which strengthened the network and subsequently reduced the rms noise level. We plan to expand this network by establishing IGS stations north of South Africa as there is an obvious gap in the distribution of stations in Africa. Adding stations will not only improve our regional network but will densify the global network to the benefit of all IGS product users. GPS users in southern Africa can easily download this data for postprocessing with their own measurements for the purpose of improved accuracy from our website. The data has been used by local and other users

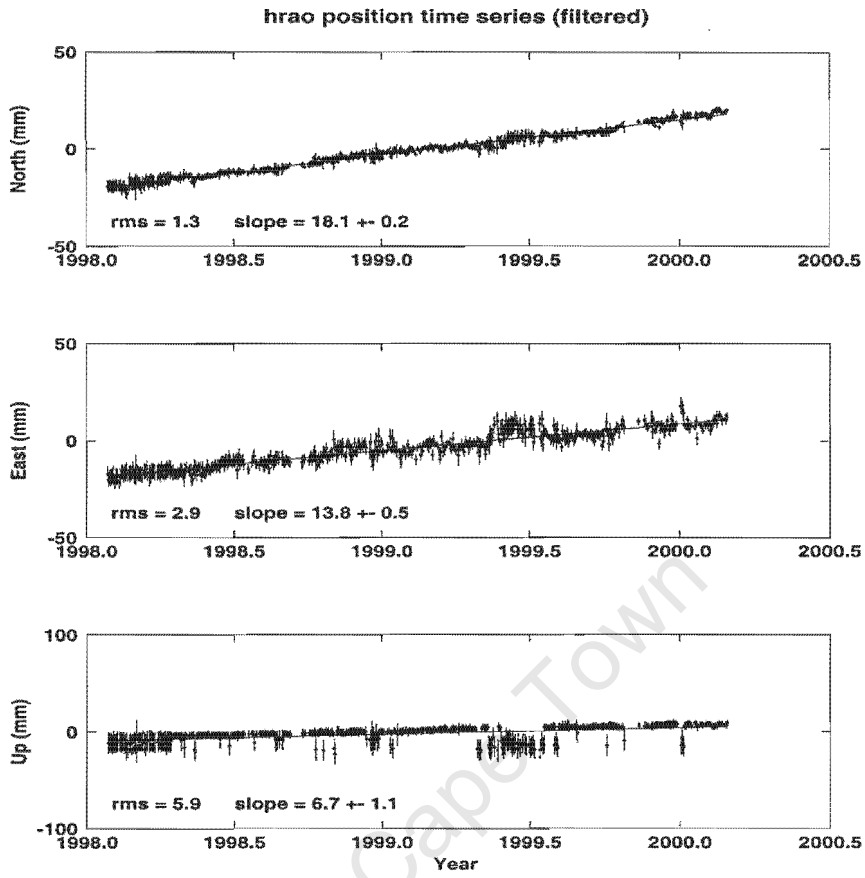

Figure 1.7: Time series of the HartRAO IGS station, HRAO. The north and east components are showing good agreement with VLBI results.

for various purposes, from local cadastral mapping to clearing minefields in Mozambique.

1.5 Contribution to the ITRF

HartRAO's participation in space geodesy adds a positive contribution towards all parameters which enter into the establishment and maintenance of the International Terrestrial Reference Frame (ITRF). Table 1.1 lists the eccentricities between the reference points of the three geodetic techniques (Combrinck and Merry 1997) and Table 1.2 lists the ITRF 96 Epoch 1997 coordinates for the respective reference points.

The ITRF is realised by a set of positions and velocities derived from combining results from VLBI, GPS and SLR. These techniques complement each other and the combination of results leads to an improved ITRF.

Table 1.1: Table of eccentricities, VLBI telescope to SLR and GPS (HRAO) reference points.

Reference	Coordinate	Δ	σ (mm)
SLR	X	41.680	15.8
SLR	Y	-66.564	7.5
SLR	Z	-8.131	3.9
HRAO	X	90.236	15.8
HRAO	Y	-132.190	7.5
HRAO	Z	-34.704	3.9

Table 1.2: Table of Geodetic reference points, ITRF96 Epoch 1997, VLBI, SLR and GPS (HRAO).

Reference	Coordinate	Cartesian (m)	σ (m)	Velocity (m)	σ (m)
VLBI	X	5085442.780	0.006	0.0007	0.0009
VLBI	Y	2668263.483	0.005	0.0192	0.00101
VLBI	Z	-2768697.034	0.005	0.0164	0.0007
GPS	X	5085352.500	0.009	0.0007	0.0009
GPS	Y	2668395.681	0.007	0.0192	0.00101
GPS	Z	-2768731.692	0.006	0.0164	0.0007
SLR	X	5085401.135	0.101	0.0007	0.0009
SLR	Y	2668330.108	0.063	0.0192	0.00101
SLR	Z	-2768688.865	0.071	0.0164	0.0007

The unique contributions to the ITRF (Ma et al. 1994) of each technique are:

SLR:

- centre of mass
- longest pole and length of day series
- scale

VLBI:

- tie to inertial frame
- stable pole, UT1, nutation series
- precision/accuracy
- site velocities

GPS:

- daily measurements of position

- pole densification

1.6 Summary

The Geodesy Programme at HartRAO is actively involved in and contributes to space geodesy using the techniques of VLBI, SLR and GPS. We are expanding our activities to enable us to make a more worthwhile contribution to geodesy not only in a local context, but to the international geodetic community. Participation in international experiments and active involvement in data analysis and interpretation will provide us with the necessary expertise and technological exposure to contribute to science in a field where there is still much to be done. Acting as the IGS Regional Data Centre for Africa is of benefit to the local and international community. Conducting local ties (footprint surveys) at HartRAO maintain local site integrity through the monitoring of the relative positions of reference points on site and provides necessary high accuracy ties between the different space geodetic techniques.

Chapter 2

Footprint Concepts

"The divisions of the sciences are not like different lines that meet in one jungle, but rather like the branches of trees that join in one trunk" - **Bacon**

2.1 Introduction

The last three decades have made the study of crustal movements increasingly effective, particularly through the development of space geodesy. Popular literature during the past century has laid a foundation for more theoretical and practical urgency, leading to the development of advanced models of crustal motion and the design and construction of high accuracy measurement techniques. Even before the general acceptance of plate tectonics, works such as *Our Mobile Earth* (Daly 1926), *The Deformation of the Earth's Crust* (Bucher 1933), *Our Wandering Continents* by Alexander du Toit, (du Toit 1937), *The Pulse of the Earth* (Umbgrove 1942) and *The Unstable Earth* (Steers 1945) served to stir the scientific world into action. Although there is more or less general acceptance of plate tectonics, crustal stability may have different meanings to the various Earth sciences. A seismologist may regard an area to be stable if it is free from earthquakes, a geomorphologist may find the same area unstable due to large slope movements, a geologist may suppose it to be stable if it is located on the supposedly stable central portion of a continent such as the HartRAO area, located on the Kaapvaal craton. Each scientist will also be able to define the Earth crust from the viewpoint of his particular science. Each scientist will have a particular time frame in mind. Quaternary geologists and geomorphologists will regard a stable coast as one that has not shifted much in the last 2 million years, whereas the neotectonics scientist, will be interested in the last 10 000 years, which he will call recent movements.

The word "geodesy" is derived from the ancient Greek prefix "geo" which means "the Earth" and the verb "daiein", to divide. Geodesy is therefore the branch of applied mathematics which is concerned with determining the

shape of the Earth, or a part of its surface, using precise measurements. It is concerned with locating precise points on the Earth's surface and with measurement of the Earth's gravity field. The major goals of geodesy may be summarised as: (NASA Technical Paper 2147, 1983)

(1) Establish and maintain national and global three-dimensional geodetic control networks on land, recognising the time-variant aspects of these networks;

(2) Measure and mathematically represent geodynamic phenomena, such as polar motion, Earth rotation, Earth tides, and crustal motion;

(3) Determine the gravity field of the Earth, including temporal variations.

In order to achieve the aims of geodesy as defined, different techniques are used in modern geodesy and currently there are several space geodetic techniques which are utilised at facilities all over the world. Very Long Baseline Interferometry (VLBI), Global Positioning System (GPS) and Satellite Laser Ranging (SLR) are the three main space geodetic techniques supported at HartRAO. In order to determine the stability of each geodetic fiducial site on a local scale, tie reference points and determine the eccentricities between these points, small networks are measured which surround the geodetic sites. These footprint networks cover a radius of some tens of metres to tens of kilometres.

For instance Goddard Space Flight Centre's (GSFC) Crustal Dynamics Project and now its successor, the NASA Space Geodesy Program has been involved in the acquisition of GPS data at footprint networks located around primary VLBI and SLR sites since 1990.

2.2 Overview of Footprint Studies

In order to give a general background on previous and current footprint studies conducted by NASA, a short overview is given based on and using extracts from an unpublished report by Bell et al. (1994) and personal communication received from C Noll (CDDISA) and R Allenby.

At the time of writing, two epochs of GPS data had been taken by NASA at footprint networks at six different observing sites. Three of these are in California (Quincy, Pinyon Flat and Monument Peak), two in the continental U.S. (Fort Davis, Texas and the Goddard Geophysical and Astronomical Observatory (GGAO) in Greenbelt, MD) and one in Alaska (Sourdough). Conventional geodetic surveys are usually performed to ascertain reference points of fixed observing instruments such as SLR and VLBI and the relative positions of reference monuments or other collocated geodetic instruments within the immediate site area. The classical and GPS surveys are used at the local reference and regional footprint scale to determine each site's stability.

The measurements are done in order to differentiate between local instability effects (local groundwater fluctuations, soil movement or monument instability) and geodetically measured motion from larger scale effects. The larger scale effects include coseismic displacement during an earthquake, subsidence or uplift due to glacial or fluvial loading or unloading, steady state slip resulting from plate motion, or displacement due to volcanic eruptions. A footprint measurement can provide crucial information when a site suddenly exhibits anomalous displacement. This is supported by the case of the Pinyon Flat Observatory in California, which had footprint measurements taken in 1992 and 1994, before and after the Landers earthquake. This earthquake sequence ruptured an area which is located about 40 to 50 kilometres away from the Pinyon Flat Observatory, during June 1992. The average slip was about 3 to 4 meters with maximum slip being 6 meters (see for instance Bock et al. 1997).

2.2.1 NASA/GSFC Site Stability Program

The site stability program of NASA/GSFC was initiated in the late 1980s with the aim to insure geodetic site integrity as outlined by a special committee of principal scientific investigators of the CDP. Through collaboration with local specialists basic guidelines were established for selecting, monumenting and surveying 'footprint' or site stability networks around primary geodetic sites. The footprint measurements then provided a basis for the analysis of both the tectonic and physical stability of these sites. As mentioned by Bell et al. (1994) the objectives of the Site Stability Program are:

(1) Assuring the integrity of geodetic measurements taken at principal space geodetic observing sites (VLBI, SLR, and GPS)

(2) Implementing and measuring local GPS networks around the main observing monument that are representative of the local tectonic environment they encompass (5-30 km scale)

(3) Repeating conventional surveys of the reference markers relative to the main observing monument (less than 1 km) to assure monument stability

(4) Providing first and second epoch GPS footprint measurements at many of the essential fiducial geodetic sites used in the worldwide global networks, beginning with the U.S.

(5) Providing raw survey data and final geodetic results to NASA's CDDIS.

2.2.2 Conventional Site Surveys

Physical stability of the main observing monuments are assessed by conventional geodetic surveys of the reference markers. If a permanent tracking instrument (VLBI, SLR, GPS) is installed at the site, these conventional surveys determine the reference point of the fixed observing instrument, and the

relative positions of reference monuments, an azimuth mark, as well as other collocated geodetic instruments within the site area. When a site contains a marker that is frequently used by mobile geodetic systems, a mark to mark survey is simply conducted. The relative station position estimates from these classical surveys generally agree at the several mm level.

2.2.3 GPS Footprint Surveys

From 1990 onwards, NASA's Site Stablity Program has implemented and measured local GPS networks (1-30 km scale) centred around main observing monuments with the aim to determine local stability of the area occupied by the main reference point. In comparison to the footprint survey, local GPS networks have been and are being measured by scientific teams in areas of tectonic interest to identify geological structures that are accommodating strain seen between and around geodetic fiducial sites. There is a basic difference between these two efforts. The footprint encompasses a single tectonic feature which is occupied by the main site, whereas the regional strain network encompasses an entire deformation field including all of its regional characteristics. The results of the NASA footprints are not reported here as they are discussed by Bell et al. (1994). The results are mainly in the form of cartesian coordinate differences between points, which indicate the relative stability of the footprint networks.

2.2.4 Footprints at Other Geodetic Sites

A survey conducted during December 1999 using the IGS logfiles as source, indicated that approximately 50% of geodetic sites have had or are in the process of doing a footprint. The word footprint is used very loosely, but in general indicates some local survey, using some high precision surveying technique and it may include the determination of ties between reference points of different geodetic techniques. The information is more often than not inadequate, so a follow up survey was conducted via the IGS mail exploder, which brought forth about a 2% response. This survey did have the advantage of creating some discussions of the footprint topic. A short summary of some of the major points and concerns raised are given; (with special thanks in particular to J Manning (AUSLIG), M Chin (NOAA), A Neill (MIT), J Long (NASA/GSFC/ATSC)).

- Considering the stability of results across a particular network, one is uncertain if extensive regional area footprint surveys are worth their considerable expense.
- Are there any examples where the footprint surveys have been significant?
- One is not sure if the footprint concept is still valid for every site.

- Footprints are rather outdated, things have changed in the last ten years, and the concept should be reviewed.
- Densified networks across plate provides a quality check on the results from each site.
- A driving issue is, as we move towards combination solutions, the quality of integrating surveys between different geodetic techniques for combined global solutions for IERS/IRTF. So the precise connection between the telescope reference point of an SLR system, and the centre of the electrical system for VLBI, the antenna phase centre of GPS, and the reference point for different DORIS antennae, and the connection to absolute gravity is a major concern.
- Local precise surveys (say 30-100 metres) at sites to reference marks and to collocated different observation types, are not footprints, footprints cover many kilometres.
- Footprints are important and this should be brought to the attention of all involved.
- Different interpretations of the term **Footprint** exist.

These concerns and opinions are not without merit and it is hoped that this work will address most of these points. There is no formal definition of the term footprint except as discussed already and one should think of the term in a broader sense, as a concept and not limit it by formal definition. Formal definitions of concepts often lead to suppressed and confined research with non-optimal return, which tells one that an axiom was disregarded: the course of science as a whole determines the progress of its parts, in their greater or lesser degrees. Therefore, if in the researcher's opinion his footprint should be small, cost effective, and this meets his objectives, he has succeeded. If on the other hand the researcher decides more is required, which perhaps includes different measuring techniques, in-depth study of local effects, a large area, mathematical modelling, and this meets his objectives, he has succeeded. Geodetic sites are all unique and there is no grand unification of a single concept which will suit all geological structures, manpower, equipment and available expertise. Perhaps the approach of operationalism could be used to specify the meaning of footprint. Using this approach the difference between implicit and explicit definition disappears, establishing a rigid procedure for determining the meaning of the term. Quoting Ackoff et al. 1962 as quoted by Harvey 1969,

The formal requirements for (operationally) defining properties are that we specify what is to be observed, under what (changing and unchanging) conditions the observations are to be made, what operations are to be performed, what instruments and measures are to be used, and how the observations are to be made and treated.

Therefore, the meaning of the footprint concept is determined by specifying

the operations which determines its application, which will rarely be the same for any two sites.

2.3 Footprint System for HartRAO

The first question which was asked by myself during the design phase of this study was whether a footprint can be adequately described by cartesian differences between reference points. Surely an area of the Earth's crust has many different unique features and different processes which will affect the stability of each reference point ? Would it be possible to investigate the various sources of error which would influence the differential cartesian coordinates ? What factors and processes should be considered when interpreting sets of differential cartesian coordinates ? How can one weight a particular monument for site stability determination ?

Basically the stability of the footprint area is inferred from the measured stability of the footprint reference points, referred to (in HartRAO's case) the SLR pad, radio telescope and the IGS station HRAO. Several of the reference points are located on rocky outcrops, which are essentially free of soil and can be regarded as continuous or nearly continuous bodies of exposed rock. These outcrops owe their form to the intact strength of the rock, the continuity, dip, strike and spacing of their partings. Any movement of the rock on which the monument is located might not be due to crustal instability in the footprint area, but might be the result of other natural factors which influence and even control the nature and extent of the dominant processes in rock slope evolution. The current form of such an outcrop is a result of long term evolution of the ridge or 'koppie' on which the outcrop is located. Each outcrop will have its own inherent stability, dependent on the current state of balance with the dominant processes in its evolution.

Sometimes the rock slopes have forms which are in equilibrium with the total strength of the rock mass (Moon and Selby 1983), but it is probable that rock slope development controlled by orientation of joints critical for stability is the norm (Selby 1982). In this study 'form' means the physical dimensions of a landform or area of relief - its shape and size. The branch of geomorphology that deals with form is called morphometry. Measurement of form is of course relevant to all geomorphology, therefore morphometric studies can be carried out in all branches of the subject. The reason why form is an important parameter in this study is clear when one realises that the processes which created the form are the same processes which will cause movement of the monument. So the study does not concentrate on the evolution of the form, but on the effect the processes have on the stability of the monument. The footprint study is therefore not a study concerned with only the baseline and

relative position GPS measurements. In order to understand and correctly interpret small movements of the reference points one has to approach the footprint in a holistic way. Therefore, consideration needs to be given to the individual reference point as a system, and a combination of all these systems into the footprint system. These systems can be simply defined as structured sets of objects and/or attributes with specific relationships between them.

Many attempts at defining the scope and functions of geodesy have been made, and will be made in the future and a short account of this can be found in Vaníček and Krakiwsky (1986). For instance the mentioned authors quote the definition of geodesy which was adopted by the National Research Council of Canada in 1973:

Geodesy is the discipline that deals with the measurement and representation of the Earth, including its gravity field, in a three-dimensional time varying space.

During the formulation and slow process of setting up boundaries for this footprint study, it became very clear that in order to solve this particular geodetic problem, use should be made of all relevant disciplines, in a multi-disciplinary approach. Free use is therefore made of techniques and approaches used to solve problems in geodesy, geology, geophysics, electronics and other useful and sometimes seemingly unrelated sciences.

2.3.1 The Open Dynamic System

The type of system which will be used to describe the footprint and its components is the **open dynamic system**, as its main matter component is the surface of the Earth, which is open to the flow of matter and energy. The system's main measurement component is GPS, which is open to influence from other systems, such as the ionosphere, troposphere and time. We have thus an external input, some processes internal to the system, such as rock movement or soil heave and an output consisting of radiated energy or matter which leaves the system. Each component in the footprint system can be described as a subsystem and this approach allows a methodical, structured approach which aids in describing the footprint system holistically.

The footprint as an open system, in the case of HartRAO can be described as having:

(1) **Boundaries**, an inner boundary set by the five inner monuments, an intermediate boundary, set by the four intermediate monuments and an outer boundary set by the three reference points of the outer network.

(2) A **focal point**, chosen as the main reference point, which is the area surrounding the radio telescope and which contains the radio telescope, the SLR pad and IGS reference point HRAO.

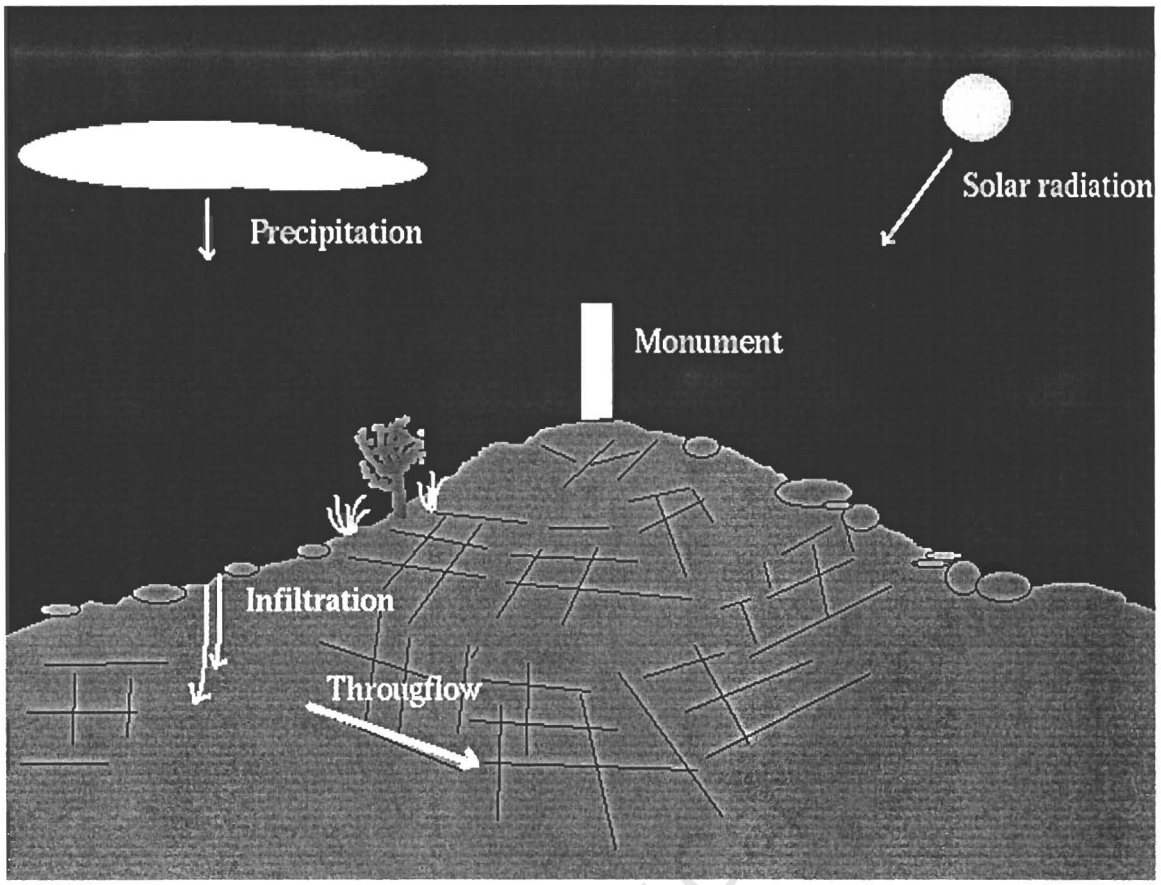

Figure 2.1: Simplified diagram of the footprint surface cycle, indicating some of the factors and processes which will eventually affect monument stability.

(3) A **set of coordinates** which defines the boundaries and focal point. The focal point has fixed coordinates whereas the boundary reference points have dynamic coordinates. For instance, the IGS station HRAO was used as the 'fixed point' in the final adjusted values of the footprint. One could have more than one fixed point, but it is simpler to use one.

(4) **Inputs and outputs** of varying nature such as energy, matter and information (e.g. satellite ephemerides), which crosses the boundaries of the system.

(5) **Processes** within the system which affects measurement accuracy and monument stability.

(6) A **steady state**, in which the footprint shows no signs of instability, it is in dynamic equilibrium.

(7) An **unsteady state**, where one or more reference points show instability, the system will either move towards a new state of equilibrium or return to its previous state.

(8) During the crossover from one steady state to the next, the footprint system is in a **transient state**.

The footprint is mostly a cyclic, dynamic system in which the energy and other factors which constitute the inputs increase and decrease in a cyclic manner. As an example the measurement system is affected by diurnal changes in total electron content and periodic repetition in the geometry of the GPS satellites. The Earth surface, i.e. the crustal component, is affected by diurnal variation in incident solar radiation, which causes possible thermal expansion and contraction. This component is also affected by the drying and wetting cycle of summer rain and winter dry periods. There are of course small random external inputs, a sudden cold period during a normal hot summer, or a rare thunderstorm bringing rain during winter which is not the rain season. The small random effects are normally smoothed out by the more dominating effects, but nevertheless contribute to the complexity of the system.

2.3.2 The Footprint Surface Cycle Concept

The footprint surface cycle can be visualised using the well-known surface cycle of geomorphology and the water cycle of hydrology (see for instance Manning 1987) which envisages that energy and matter cycles through the Earth's upper crust continuously. Adapting these cycles to the problem at hand one can draw a simplified diagram of the footprint surface cycle which is shown in figure 2.1. If one considers the different factors and processes which might affect the stability of our reference monument it becomes apparent that it is a particularly difficult problem in that there are different factors and processes interacting on the foundation of the monument and its immediate area. This approach is of course valid whether the geodetic monument is located on a building or whatever, the surface cycle can and will transform a mountain into a hill and no monument offers immunity against the definite adverse affects which will affect its long and short term stability. One can identify:

Exogenetic factors
- Climate
- Surface temperature
- Precipitation
- Vegetation
- Infiltration
- Weathering
- Run-off

Endogenetic factors

Percolation
Permeability
Porosity
Weathering
Joints and bedding
Rock type and structure
Chemical composition

All these mentioned factors interact in some way, leading to mass movement, groundwater seepage, throughflow, erosion and eventually some form of instability in our surface system. Obviously it would be possible to reduce the effect of some reference site factors by carefully selecting a site for the monument. More often than not, the person setting up the footprint is not a soil scientist or rock engineer and so could make a poor choice. Not one footprint is the same, so in order to make this work useful for the geodetic community, the approach taken here is general enough to make the material presented applicable to most sites. Of course it is impossible to have an in depth investigation of all these mentioned factors and processes, so in this study the effect of surface temperature has been selected. All the other factors should however be kept in mind.

2.4 Conclusions

The geodesist participating in any crustal stability or similar work would benefit from keeping in mind that when a monument is added into the surface cycle, approaching the research using a systems approach could only be beneficial. The systems approach opens the mind to all the other factors and processes which could possible affect the footprint. The monument becomes part of the Earth's surface system and has to be treated and measured as part of this system. The footprint for a specific geodetic site is defined by the operations required to make it scientifically useful and is not determined by any one particular definition set up with special circumstances in mind. Footprints determine geodetic site integrity, identify local instabilities, determine eccentricities between different geodetic techniques, and can vary in scale from very local (tens to hundreds of metres) to several tens of kilometres scale or more, depending on specific local requirements. Footprints are not technique dependent, nor are they bound by particular disciplines and can be regarded as an open dynamic system.

Chapter 3

Footprint Geology

"On the basis of climatic criteria, more than two-thirds of the southern African region is considered to be particularly susceptible to erosion by either wind or water." - **Hudson 1981**

3.1 Introduction

The nature of this study requires that some geological and geomorphological background material be presented to enable the reader to follow the later chapters in coherent fashion, without loss of continuity. Causes and factors involved in site stability are mentioned as these should be taken into account during site selection and during the lifetime of the geodetic monument. For instance, weathering can cause apparent site instability through affecting the stability of a monument by transport of surface material; or weathering of subsurface rock could lead to progressive settlement of a monument. It is often the case that information relating to recent earth movements are subdivided into geological, geomorphological, historical and geodetic (e.g Beloussov 1962, Vita-Finzi 1986) sections but here we briefly overview only geological and geomorphological information pertaining to the HartRAO footprint in general.

3.2 Definition of Neotectonics

The term neotectonics was coined by V. Obruchev (Gorshkov and Yakushova 1967) and several definitions can be found in the literature. The definitions are not quite the same and we adopt the fairly unconstrained definition of an 1978 international commission devoted to the Holocene and published in *Striolae*, the newsletter of the International Association for Quaternary Research, 1982, vol. 4, p.37.:

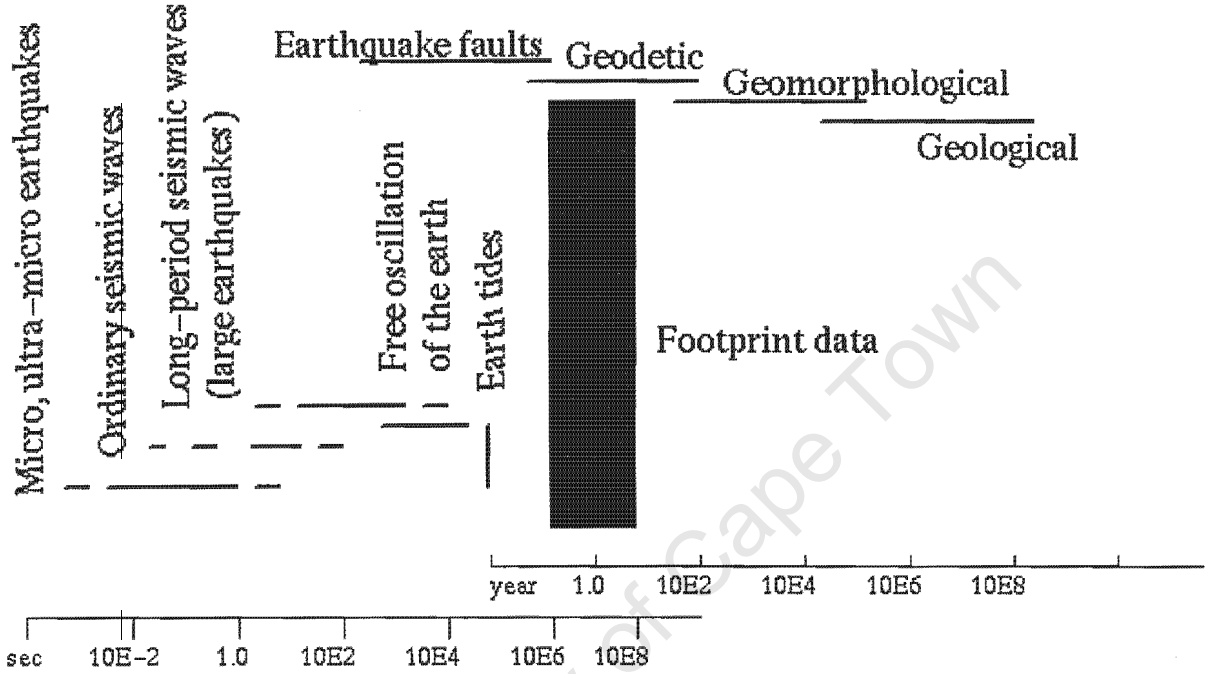

Figure 3.1: Time scales of major sources of evidence which allow determination of recent earth movements. The seismological data are used mainly to interpret movements revealed by other sources. Adapted from Kasahara (1971). The footprint time scale has been added.

> *Any earth movements or deformations of the geodetic reference level, their mechanisms, their geological origin (however old they may be), their implications for various practical purposes and their future extrapolations.*

In this definition the commission uses the term "geodetic reference level" to refer to a geodetic reference point, similar to a reference point of a footprint network. Changes in the coordinates of the reference point (the commission uses "deformation") will indicate earth movement. A simplified diagram of the time scales of major sources of evidence bearing on recent earth movements is shown in figure 3.1. It is obvious from figure 3.1 that the period of time in which geodetic data is collected is but a small fraction of the total period over which movement has or could occur. Nevertheless, repeated measure-

ments using a high precision technique such as GPS is the only way in which quantitative data can be had in such a short period and provides direct evidence of movement, or of stability. In contrast, movement from the evidence of geomorphology and geology can only be inferred.

3.3 HartRAO Geological Setting

Most of the geological history of South Africa is Precambrian and can be traced back in time to a limit of about 3.8 billion years. The crustal development of the southern African region is discussed in detail in the literature (du Toit 1954; Truswell 1977; Tankard et al. 1982) but it is relevant to this work to mention the major crustal evolutionary stages. The crust in southern Africa has passed through a well-defined sequence of evolutionary stages which is summarised by Tankard et al. (1982) as:

Stage 1 A period of Archean crustal development gave rise to crystalline massifs which is represented by the Kaapvaal, Limpopo, and Zimbabwe Provinces. During this stage metamorphism and deformation was common. The granitic basement of the subcontinent was formed, and the period ended at the end of the Archean (2.5 Ga).

Stage 2 A large sedimentary cover buried this ancient basement, the cover is represented by the Pongola Supergroup, the Witwatersrand triad, the Transvaal-Griqualand West Supergroups, and the Waterberg, Soutpansberg, Matsap red beds. During the Early Proterozoic the ancient basement was punctured by massive injections of basic magma in the form of the Bushveld Complex and the largest known Archean body, the Great Dyke in Zimbabwe (2.46 Ga), which has a strike length of 500 km and average width of 6 km. A period of vulcanicity followed the start and end of each period of sedimentation.

Stage 3 Tectonic activity marks this stage. In the southern and western parts of the subcontinent, in several Proterozoic orogens, older crystalline rocks and their supracrustal cover were reworked tectonically. Massive granitoid intrusions were emplaced by partial melting of older crust and by additions from the mantle. Geosynclinal deposits accumulated and geosynclinal opening (about 900 million years ago) and closing of the proto-South Atlantic ocean (between 700 Ma and the Cambrian period) is recorded along the west coast.

Stage 4 The Gondwana Era. A period of abortive rifting and unparalled continental sedimentation throughout the supercontinent of Gondwana, of which southern Africa formed the hub, was ushered in by the Palaeozoic Gondwana era. During the early Palaeozoic southern Africa was at the centre of Gondwanaland, bounded by Antarctica, the Falklands Plateau and South America. The abortive rifting led to the deposition of the

Cape Supergroup succession of shales and quartzitic sandstone. The sedimentary phase gave way to continental glaciation as Gondwana moved across the polar region. This formed the tillites of the Dwyka Formation and gave rise to widespread glaciation and glaciomarine sedimentation. The Karoo basin was subsequently filled with sediments of the Beaufort and Ecca Groups and the Molteno, Elliot and Clarens Formation. This entire sequence was capped by the lavas of the Drakensberg Formation.

Stage 5 The Post-Gondwana era. Continental rift volcanism and the injection of diamondiferous kimberlites, carbonatites, and other alkaline intrusions were followed by Mesozoic fragmentation of Gondwana. Cenozoic and Late Mesozoic sedimentation was restricted to the newly formed margins of the stable subcontinent and depressed areas of the interior.

3.3.1 Precambrian Crustal Provinces: The Kaapvaal

HartRAO's footprint is located on the Kaapvaal province. In general Archean crustal provinces are composed of rocks ranging in age from about 2.5 to 3.8 Ga and when viewed on a map seem to be roughly equidimensional with maximum dimension ranging from less than 500 km to approximately 2000 km. In North America one finds the Superior Province in eastern Canada which is the largest, and in addition, the Wyoming, Slave, Amitsoq and Nain Provinces. In Africa there are at least eight of these provinces. Several can be found in each of the other continents. According to Condie (1981) most of the Archean provinces consists of either or both granite-greenstone or high-grade metamorphic associations. The Kaapvaal Province in southern Africa is one of the major granite-greenstone terranes of the world. Other major terranes occur in the Zimbabwe (southern Africa), Yilgarn and Pilbara Provinces of Western Australia, the Superior and Slave Provinces in North America.

The HartRAO site and inner footprint are located on Andesite. Andesite is the extrusive equivalent of diorite, and is almost totally lacking in potash feldspar and quartzite, but consists mostly of intermediate plagioclase and smaller amounts of the mafic minerals. On site tuffs, breccias and agglomerates are common. Some quartzite is evident in thin layers. Shale is normally only of local evidence with graywacke and associated pelite being the most important sediments (Lowe 1980) but at HartRAO we have more than a statistical share of shale, which was extensively used by early farmers during the late 19th century for house building, of which several ruins are scattered around the site. There is no detailed geological literature on the geology of the HartRAO site, as effort seems to have concentrated on the Bushveld Igneous Complex, just north of Hartrao, on whose southern borders the site is located. This is not surprising, being the world's largest repository of magmatic ore deposits (Willemse 1969).

3.3.2 Faults

From the geodesist's viewpoint, the easiest approach to finding faults in the footprint area would be to consult a geological map. Faults are normally located by identifying suspect areas from an air photograph or satellite image. Prominent features which are unnaturally straight or curve very smoothly, separating contrasting areas are suspect. These suspect areas must then be checked out in the field where conditions are often difficult due to erosion and poor exposure. Rotation, which leads to reverse faulting, grabens and horsts in a multitude of combinations produces misleading and confusing topographic evidence. Identifying the fault by looking at the repetition or omission of strata is only of value in consolidated rocks with stratification which lends itself towards this approach. Morphology or even changes in the vegetation and even pebble rotation is sometimes required for proper identification. Dating faults is also very difficult and requires expertise and equipment the geodesist will have to attain using the assistance of researchers in that field. The footprint area of HartRAO contains several faults, none of which are active according to the local Council of Geosciences, but even then, some seismic noise is not quite explained in an area about 30 km north-east from here, where several faults are situated close to a local dam (G Graham, personal communication). Faults and their possible influence on the footprint stability should therefore be considered as an integral part of the footprint arsenal, as active faults will definitely play a major rule in the design and results of the footprint.

3.4 Geomorphological Evidence

The current outline of the southern African land-mass was established at the time of the Gondwanaland breakup. According to Dingle et al. 1983 the absolute elevation ranged from about 2350 m in Lesotho to 1800 m at Kimberley. Between 133 and 142 million years ago rifting started to form the eastern coastline, and 127 million years ago the South Atlantic ocean resulted as South America separated from Africa. Karoo sequence rocks covered most of southern Africa, with the exception of the Cape fold mountains. Subsequent macro-scale geomorphic development resulted from periods of tectonic uplift, which induced erosion to new base levels (Dardis et al. 1988). The literature seems to abound with conflicting interpretations of the landscape (Moon and Dardis 1988) but an attempt to resolve the confusion was made by Partridge and Maud (1987) in an reinterpretation of the macro-scale evolution of the subcontinent. They indentify the following surfaces:

The African surface. The most widespread, oldest surface, which in general matches the African surface described by King (1967). This surface is rarely in pristine condition. It is quite varied, large areas of the preceding upland surface have not been removed by pedimentation and shows

themselve as partly planed areas. Where the original African surface is preserved on interfluves, lowered and dissected areas are in evidence. They suggest that this surface is the oldest and highest erosion surface, even though there are dissected highlands at greater elevation.

The Post-African surface. The surface below the African in the interior.

Post-African I A surface seaward of the Great Escarpment of Post-African age. This surface is usually present as dissected tablelands, but in pristine form.

Post-African II A surface seaward of the Great Escarpment of Post-African age but younger than Post-African I. This surface is mostly expressed in recent incision.

3.4.1 Natural slopes

The geodesist should be aware of the danger that slope movement presents to his footprint monument stability. This is especially true if the monument is located on a slope and not tied to bedrock. Many footprint areas over the world will be located on terrain which is not perfectly flat and not all sites will have zero slope movement. Slope movement and development is a common, natural occurence in nature and is an important factor in footprint stability. Varnes (1978) classified natural slopes according to activity state. *Active* slopes are moving or have moved in the last seasonal cycle whereas *inactive* slopes exhibit no such evidence. The inactive slopes may be dormant, becoming active when the stabilising factors are dominated by factors causing movement. A *recent* slope movement has occured in recent decades, an *ancient* movement is one for which there is no historical record and a *fossil* movement is a slope movement which occurred in a previous geological age (Zaruba and Mencl 1969).

Giani (1992) mentions some of the principal phenomena which can contribute to an increase in shear stress and/or to a reduction of shear strength, both being causes which determine sliding movement in a slope. Contributions to an increase in shear stress are mainly from the slope surface or toe weakening, or slope surcharging. Natural surcharging result from water percolation in rock discontinuities, rain water or snow weight. Man also plays a role when constructing embankments, heavy buildings and other structures, and of course large water reservoirs.

Slope surface or toe weakening could be the result of:

(1) Erosion by streams, rivers, glaciers, waves, tidal currents, sub-aerial weathering, wetting and drying and frost action.

(2) Subsidence, previous rock fall, toppling, sliding and superficial scaling.

(3) Phenomena connected to human activity such as excavations and mining.

The main causes contributing to a decrease in shear strength, apart from soil texture are:

(1) Rock fabric and structural defects.

(2) Physical and chemical reactions.

(3) Changes in intergranular forces.

A brief description of these causes should be sufficient as an introduction and are listed here to aid the geodesist in adopting an holistic approach. When a geodetic monument is located on rock, one should be aware of the causes which could lead to a decrease in shear strength and subsequent monument instability.

Rock Fabric and Structural Defects.

Rock mass shear resistance are affected by:

(1) Structural discontinuities.

(2) Contrast in stiffness and resistance in nonhomogeneous masses.

(3) Unfavourable orientation of beddings and joints.

(4) Slope orientation.

(5) Cementation degree of semi-coherent rocks, for instance conglomerates and sandstones.

(6) Weathering.

Physical and Chemical Reactions.

These reactions are due to:

(1) Softening in fissured clays.

(2) Physical disintegration of granular rocks (granites or sandstones) under frost action or thermal cycle effects.

(3) Hydration in clay soils leads to a decrease in initial shear strength.

(4) Oversaturation of loess destroys the bonds between the clay particles and large soil particles.

(5) Cement dissolution phenomena in sandstones and conglomerates.

Changes in Intergranular Forces.

The main intergranular force variation depends on:

(1) Water content which determines pore pressure and the water pressure in the rock discontinuities.

(2) Human intervention by diversion of streams, clearing of vegetation and forests.

Slope studies should form part of the footprint systems approach, local movement will in most cases be due to some form of slope movement unless the footprint is situated in active earthquake zone. Even in earthquake zones, slope movement would still be very important as slope activity could be increased by seismic activity.

3.5 Conclusions

Footprints should include some investigation of the geology and geomorpholgy of the area encompassed by the footprint networks as well as a substantial area beyond these networks. Evidence of historical and present/future instability can be had from several sources such as faults, seismics and geomorphology. The main point to be stressed here is that one should approach the footprint study from an holistic viewpoint and one should take into consideration the history, structure and slow evolution of the Earth on which the footprint is located, therefore consider the footprint as a system.

Chapter 4

Monumentation and the Geodesist

"Note that monuments set other than in solid rock or by deep concrete pillars are not adequate for high precision surveys." - **B Hofmann-Wellenhoff et al. 1993**

4.1 Introduction

Monumentation is one of the most important aspects of a geodetic installation, whether it be for VLBI, SLR or a GPS installation. Currently a large number of different monument types, with varying designs, construction, quality and suitability are used in the IGS network. One wishes to achieve the highest possible stability of the monument in each case. Apart from stability, one needs to assess the site for other prerequisites such as low horizon, possible multipathing and vandalism which will determine whether the site is suitable. The nature of the site determines to a large extent the type of monumentation required. This chapter contains some material which was published (Combrinck and Schmidt 1998) as a position paper for the IGS Network Systems Workshop, November 1998, entitled "Physical Site Specifications: Geodetic Site Monumentation". M Schmidt (Natural Resources of Canada) is responsible for the section on multipathing and the horizon mask, which I include here as they are important criteria to consider when selecting a suitable monumentation site. In order to determine crustal stability or measure relative plate motions, conduct a footprint or measure Earth rotation, one needs to fix the geodetic monuments to be used to the Earth's crust.

The more interfaces we have between the geodetic reference point and the solid crust, the more leeway is allowed for indeterminate errors. If data are collected over a long time, local and short term effects which induce positional errors tend to be averaged out, which give some observers confidence in a weak interface. However, as is well known, statistically it is far better practice to

have better data than more but poor data. Therefore it is conceivable to use a floating buoy anchored via a long cable to the seafloor as a geodetic reference point and if one could collect data for a long enough period of time, it would be possible to detect crustal movement. This would however not be quite the way to go about it, as the interface between the reference point and the crust is so weak that the observer would run out of time long before any scientific results materialised. It is obvious that the closer the monument is located to the crust, the better, but even the shortest interface can be weak if made from the wrong material or incorrectly constructed. All of this sounds like common sense but when one inspects some geodetic reference points, it is obvious that more regard has been given to other factors. Resorting under these factors are ease of installation, cost considerations, accessibility, safety and security of equipment and personnel. Before one can design and construct a suitable interface between the reference point and the crust, one must first decide how the crust, in our terms of reference (considering crustal dynamics and footprint networks) can be defined.

4.2 The Earth's Crust from a Monumentation Perspective

It is quite obvious that there are no convenient pre-marked monument locations which the geodesist can happily access and locate his monument upon. The solid crust is elusive and difficult to access directly, so any installation is more or less a compromise. The Earth has a silicate crust, therefore SiO_2 is dominant. The crust is not uniform but different densities of parent material, mixing and different melting points eventually lead to a complicated crust which differs from location to location. Quoting Meissner (1986) some popular definitions of the crust are given here:

(1) crust = outer shell of a terrestrial planet in which the velocity of compressional (P) waves is smaller than about 7.6 km/s or the velocity of shear (S) waves is smaller than about 4.4 km/s.

(2) crust = outer shell in which the density of rocks is below $3.1 g/cm^3$

(3) crust = outer shell which consists predominantly of sediments, gneisses, granite, granodiorite, gabbro, amphibolite, and granulite for the continental crust and of sediments, basalts, gabbros, and some serpentinites for the oceanic crust.

(4) crust = outer shell were the proportion of feldspars to other minerals is more than 50%. It is 50% (Ahrens (1965), as quoted by Meissner (1986)) and consists predominantly of orthoclase $KAlSi_3O_8$ *and albite* $NaAlSi_3O_8$ *(together 31%) and plagioclase (*$NaAlSi_3O_8$ *and* $CaAl_2Si_2O_8$*) (19%).*

(5) crust = outer shell where SiO_2 reaches about 60 wt. % in continental rocks (49% in oceanic), Al_2O_3 about 15% (16% in oceanic rocks), CaO 6% (more than 12% in oceanic rocks), and Fe_2O_3 below 4% (more than 6% in oceanic rocks).

Definition (1) is a seismological definition of the crust given in terms of the seismic velocities. The density definition is given by (2) and (3) is based on different types of rock. Mineralogical and chemical descriptions can also be utilised to define crustal rocks which lead to definitions (4) and (5) respectively. Many other definitions could be had, but the 5 mentioned are unique and quite clear. However not one of them is of much use to the geodesist wishing to install a geodetic monument.

4.2.1 Defining the Monumentation Crust

For our purposes we need a much simpler definition, one that would give us an indication of where the *solid Earth* is, as far as is practical. During the 19th century the Earth's crust was considered to be the outer layer of the Earth, supposedly overlying a molten interior. Taking the outer layer as our "crust" is more often than not an unstable option, as the outer layer is non-uniform and certain parts of it are much more unstable from a positioning point of view than others.

The crust we are interested in is the top layer of bedrock, which in turn is overlaid with fractured and broken rock, normally covered by soil, organic matter, water and in some cases man made structures. The crust in general varies in thickness from less than 20 km in shelf areas to more than 70 km in orogenic areas. The crust at the HartRAO location is about 38 km thick (G Graham, personal communication), with some exposed bedrock in the higher areas, but at the main site where the telescope and the SLR monument are located it is overlaid with deep soil. Drilling indicated a depth of 5 m to more than 36 m.

Clearly a monument located on the soil, or on one of the buildings would be more unsuitable than one that has been built on the bedrock as the interface between the monument and the crust would be strengthened by limiting the material separating the monument and the crust. The upper layer of the crust may not necessarily be that fixed either, as sediments and crystalline basements exhibit the presence of cracks, joints, fractures and fissures for at least the first 10 km of depth, but the topmost 10 m or so is normally the zone where bedrock acts as parent material for soil. This is a zone which should preferably be bypassed when installing a geodetic monument. Using this simple introduction one can create a definition of the crust from a surveying point of view.

This crust varies in composition and physical characteristics. We are however not interested in the depth of the crust, its composition, age or physical

properties. One could therefore (Combrinck 2000) state:

- *Monumentation crust = the layer of the Earth, overlaid by man made structures, water, vegetation and organic matter, soil and regolith. Its depth varies from the surface where it can be exposed, to depths exceeding 100 m. It is the thin layer that separates the soil forming part of the uppermost layer of the Earth from the more stable and subjected to significantly less weathering processes, solid crust and is normally the parent material for the soil.*

The rock close to the monumentation crust could be weathered to such an extent that a residual soil is formed, which could take the form of several layers of rock-like soil or soil-like rock transitions in between. This residual soil, or saprolite, should be bypassed by drilling until true bedrock is reached and not be confused with the monumentation crust. From a stability point of view and its ability to represent the actual crust, the ideal location for a geodetic monument would be on exposed, unweathered bedrock. Geodesy has not reached the stage yet where some point hundreds of metres below the surface can serve as a reference point. This would allow minimisation of the measurement noise introduced by always having some interface between the real crust and the reference point. Regardless of the inaccessibility to the monumentation crust, maximum effort should always be exerted to have the reference point located as close to and connected as strongly as possible to this crust.

4.2.2 Locating the Monumentation Crust

The question looms as to how this elusive monumentation crust should be found. Core drilling will normally provide the answer, especially if an experienced geotechnical engineer is present to describe and log the core. Investigation of the weathering profile will also provide some illumination of the problem. The following discussion is general enough to arm the geodesist with some ideas as what could be encountered or expected. Weathering profiles have been discussed abundantly in the literature and here we present only what is thought to be relevant when considering the installation of a geodetic monument. At the monumentation crust chemical weathering is the dominant weathering process, especially in humid, warm climates. There is normally not a very clean transition between the weathered zone to clean bedrock, which could make pinpointing the monumentation crust somewhat difficult, as a grey area is normally to be expected. Typical weathering profiles are described in Figures 4.1 and 4.2 for intrusive igneous rocks and metamorphic rocks respectively as found at the HartRAO site. The red line indicates the start of fresh, unweathered bedrock. Note that fissures and cracks still progress much deeper, but most of the chemical weathering has ceased or at least is much less at this depth. The line is of course hypothetical, but the concept of a monumentation

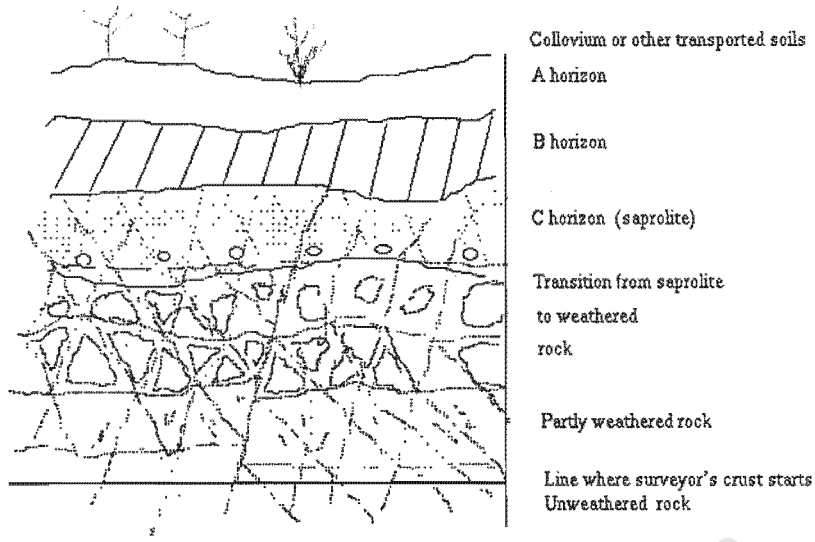

Figure 4.1: Typical weathering profile for intrusive igneous rocks (adapted from Deere and Patton 1971).

crust should be clear. Depending on the geology of the geodetic site, further profiles would include massive intrusive igneous profiles, carbonate profiles and shale profiles.

4.3 Selecting a Monument Site

For a footprint, it would be difficult to build a monument for each reference point in the footprint network which would have comparable or better stability than a site's main geodetic GPS monument, unless unlimited funds were available. However, for the main geodetic monument, you must do your best to ensure that instabilities of any kind have been minimised. If we could build a monument and tie it to bedrock, or be fortunate enough to find exposed bedrock, monument instability would be minimised. Some of the requirements for a good primary monument site are:

- shallow bedrock of high quality
- clear horizon
- safe from vandalism

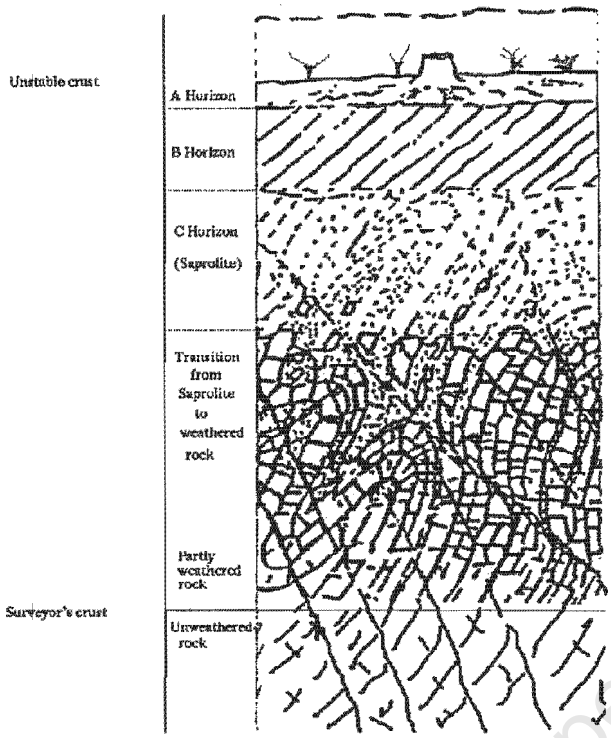

Figure 4.2: Typical weathering profile for metamorphic rocks (adapted from Deere and Patton 1971).

- clear of reflecting surfaces (fences, metal poles etc.)
- not too far from the receiver
- ease of access
- data accessibility
- electric power
- no local crustal instabilities
- controlled vegetation (growing horizon elevators)

Of course not all these site qualities are easily found, nor are they economical or practical to achieve. The type of monument normally depends on the site characteristics, as well as on the investigators eagerness to obtain as stable and durable a monument as possible. Don't build a monument flush with the earth's surface, apart from antenna interaction with (varying) conductive soil, humans and growing vegetation shadowing satellite signals, the antenna is "over-exposed" to its environment. Bugs will crawl into it, ants will nest in it, it might get flooded, trampled on etc. The UNAVCO site has some examples of monument types. Some interesting monuments exist, such as the massive monolith used by the University of Newcastle. To find a good site, one starts

out with an idea as to where the GPS monument should be located, with the above mentioned requirements in mind.

In the geotechnical field, rock and soil stability analyses are used to allow evaluation and prediction of instability, especially those caused by excavation and construction on natural slopes. The analyses are designed to support the safe and functional design of slopes to be cut, and incorporate features such as consolidation works (drainage systems, retaining walls) which can aid in stabilising a slope. Evaluation is made of the role played by design parameters such as excavation height and slope angle, in order to determine their role in the work excavation stability. Unless the researcher is placing his monument on an absolutely flat location, which is not a very likely scenario, it is being placed on a slope. Geotechnical engineering and geomorphology provide us with a lot of useful information which the geodesist can use when selecting a site for a geodetic monument. The purpose of this section is to describe, in a general way, what one should keep in mind when selecting a site from a stability point of view. Many times accessibility is given preference when selecting a site, however this is a poor long-term choice for a geodetic monument.

4.3.1 Field Investigation

Once a decision has been made on the geographical region for the installation and one has studied available geological and geotechnical data, a field reconnaissance should be undertaken to gather information on the proposed site. Note the presence of exposed bedrock, note the strike and dip of the rock, joint spacing and condition. One should draw a map of the site and its immediate surroundings, keeping in mind the requirements of a stable monument. Factors which might influence the stability of the monument on rock are:

- Presence of faults
- Joints, fractures, shear zones
- Varying ground water levels
- Rock slope instability
- Rock which could cause problems due to swelling, dissolving and shrinking
- Presence of cavities due to karstic formations, such as found in dolomitic regions
- Human engineering activity, gas,water and sewer pipes, drainage ditches.
- The type and condition of the rock

The effect of these factors are quite obvious. For instance joints, fractures and shear zones may be filled with compressible soils such as expansive clay. During drying and wetting cycles, expansive minerals, for instance montmorillonite

and anhydrite, shrink and expand, leading to a seasonal signal in your time series. Cavities develop in soluble rocks, especially dolomite, limestone, rock salt and gypsum. This might not have an immediate effect on your monument, but an existing cavity may lead to your monument disappearing into a sinkhole when the cavity roof collapses. Flow of water dissolves gypsum and can cause tilting of your monument. Certain types of rock are less suitable for a stable site, as the density of the rock is normally a factor in the swelling characteristics of the rock. Shales for instance are affected by moisture content, density, weathering and mineral structure.

4.3.2 Boring

Sometimes one can find bedrock which is hidden below the soil by utilizing techniques of geophysics such as resistivity tests and gravimeter measurements. Once a point has been found that will be suitable, boring is the only viable tool which will directly reveal the condition of the subsurface conditions. At HartRAO for instance, during the installation of the SLR reference point, resistivity and gravimetry measurements showed large fluctuations in depth to bedrock. The parent material of the soil is andesite, which often weathers in such a way as to leave large boulders suspended in soil. This could lead to a monument bedded onto a suspended boulder instead of onto real bedrock. Core logging describes a permanent record of the rock mass conditions and is useful in estimating the depth to the weathered zone and fresh bedrock. After finding solid bedrock, one still has to drill through and clear off the weathered and fractured top section until fresh bedrock has been reached. This is the part to which the monument should be fixed. We eventually augered a 1 metre diameter 6 metre deep hole which was cut partially into the andesite to access fresh bedrock. The monument was isolated with foam from the soil and is a massive steel and concrete structure fixed to bedrock.

Of course the number of borings and the depths would be limited if the rock mass conditions are of excellent quality and massive. Rock boring is expensive, so more time spent on locating an approximate position of the bedrock closest to the surface will be worth it. In the case of our IGS GPS station (HRAO) monument we drilled through exposed shale and then into bedrock and grouted a steel monument into the andesite by pressure pumping grouting down the steel tube. The tube had holes drilled in the bottom section, so that the grouting would be forced out into the joints and cracks of the rock, effectively like a tree sprouting roots. The steel was then isolated from the drilled hole via thick wall plastic tube and guided through a steel collar cemented onto a foundation installed on the slate. This allows the shale to breathe as it absorps and loses water, without affecting the stability of the monument.

4.3.3 Horizon Mask

The horizon mask is defined as those areas of the horizon, when viewed from the antenna, that are obstructed so as to impede or block the satellite signal from reaching the antenna. Ideally there would be no obstruction above the horizon; however in a practical world it is rare that this optimum is achieved at the same time as meeting all other siting specifications. Significant blockage below certain elevations or in specific azimuthal quadrants can limit the usefulness of the data collected as well as constrain the user community to a select group rather than meeting the needs of a broader user group.

"Solid" objects such as mountains or buildings as well as trees and structures can cause the blocking of the satellite signal. In the former case the signal will be lost for the duration of time the satellite(s) is/are behind or below the obstructing object. For example in deep valleys or within the boundaries of large cities, this can amount to a considerable amount of lost data. In the case of vegetation and other less "solid" obstructions, the loss may be of a more intermittent nature depending on the transparency of the obstruction to the satellite signal. The obstruction may also vary with time. During the winter months, deciduous trees will provide less obstruction than fully foliated trees. The type of tree cover (thick rain forest vs. sparse needle forest) is important as is the capability of the receiver/antenna that is to be used at the site. Some receiver/antenna combinations are designed to track under tree cover while others are not. Trees will also grow and will thus affect the horizon mask with time. In a similar fashion urban growth or development in the immediate area of the reference station installation may affect the horizon mask with time. Intermittent blockages and site changes may also cause multipath problems.

It is important to select a site with minimal blockage and to ensure that the horizon will not undergo significant change with time. It may be necessary to determine the extent of anticipated development from adjacent landowners. During the site reconnaissance stage, obstructions (current and planned), should be noted and prediction software used to determine the effect of the blockages on the data collection and thus the range of user applications of the data. Changes over time should be noted in the site log.

4.3.4 Multipathing

This can cause errors in GPS measurements, the severity of which is dependent on the extent and type of multipath. As the expression indicates, multipath refers to signals that arrive at the antenna via multiple paths, in this case caused by reflective surfaces in the vicinity of the reference station. Multipath causes interference or distortion and therefore errors, primarily on the code pseudo-ranges but also on the phase pseudo-ranges.

Different types of reflective surfaces can cause a multipath effect on the received signal. Most obvious are highly reflective surfaces such as the sides of

buildings, solar panels and vehicles. Fluctuations in multipath levels can be caused by surfaces such as water whose reflective properties will change with time. Similarly the accumulation of snow or ice on nearby structures or on the surrounding ground can effectively change the properties of the reflected radio signal as a function of time. A diffused scattering of the satellite signal can be expected from metallic structures such as large radio towers and chain link fences.

The siting of the antenna installation and the monitoring of any changes in the surrounding area is very important. Prior to establishing the site, data should be collected using the same type of instrumentation that is to be installed and as close as possible to the exact location of the proposed antenna site. A longer test data set, for example 72 hours, when analysed should provide a good indication of the impact of the site's multipath environment. It may be necessary to test several different antenna heights in order to judge the optimal height for the reference station antenna. The addition of ground planes and use of RF absorbing material may have to be considered. It should also be noted that reflective waves from surfaces below the antenna, such as the ground and the top of a concrete pier can also cause problems and steps may be required to minimise this source of near-field multipath.

4.3.5 Vandalism

Vandalism is of concern to us all and some locations may have serious problems in this regard. It comes in different forms and from different sources as well as in varying degrees of intensity. Some IGS sites are particularly vulnerable in that they are easily accessible, with antenna and receiver a couple of metres apart. The receiver and small UPS may be enclosed in a metal box which is locked. Many times the box is fixed on a steel pipe, so that the casual vandal would not tamper with the equipment. The serious vandal however will saw off the pipe and remove the whole installation intact.

When a site selection and investigation is done, the vandal potential should be estimated amd minimised. Vandalism is normally of human origin (except in South Africa where I have to take baboons into account), but rodents and heavy hoofed animals may wreck havoc with wiring and coaxial cables if exposed; even fire should be considered. During the site selection and monument design phase consider some of these points:

- Is the site visible from public pathways and road ?
- Is your color scheme for the monument and enclosures vandal yellow, or does it blend into the environment, making it less conspicuous ?
- Is the monument constructed in such a way that the antenna is out of reach ?
- Is the reference marker to be a nice, attractive, 2 Kg, beautifully machined and polished brass momento ?

- If you are considering fencing, metal or (sometimes wet) wood, what about multipathing ?
- The very casual vandal might be an innocent visitor, blocking off satellites because your antenna is below human height. Do you need loss of lock ?
- Is your GPS site on the list of things all visitors must see ?
- Are you incorporating some electronic alarm which will warn you if the equipment is being tampered with ?
- Has the radome you are considering using been checked for uniform thickness, rf transparency, does it retain these characteristics out in the sun ?
- Should you consider additional insurance ?
- Will the communication and rf cables be protected ?
- Does the solar panel have reduced reflective surface ?
- Are the equipment boxes really solid and can they be bolted from inside onto rock or buried stakes ?
- Is the site plagued with bush fires ?

There is of course no complete list of what should be taken into account, each investigator will have to carefully assess his options and requirements.

4.4 Monumentation Located on Rock

As the HartRAO footprint reference points are mostly located on rocky outcrops, we first consider the case of monumentation built on a mountain, rocky hill or other point where the monument to Earth-crust interface is rock and there is a slope towards the monument.

4.4.1 The Effect of Rock Mass Strength

Rock mass strength is an important determinant of slope form, especially in the absence of structural controls. Rock properties such as intact strength, spacing of joints and other geological discontinuities determine to some extent the form of the equilibrium slope. Any changes in the slope form over time will affect the stability of the monumentation. Generally the emphasis in the literature has been on processes as controls of rock slope development, (Wood 1942), (King 1953), but more recently rock mass properties has been recognised as controls in rock slope evolution (Terzaghi 1962), (Moon 1985). The study of the properties of materials, although a relative newcomer to the field of geomorphology, emerged in recognisable form with the work of Yatsu (1966) and found its way into the mainstream of geomorphology by Whalley (1976). Compressive strength, the degree of rock weathering and elasticity have been found to effect control on morphometric variables such as valley slope gradients

and drainage density (Cooks 1979, 1981, 1983). A technique to determine rock mass strength was developed by Selby (1980) which allows for the expression of rock mass strength on a scale from 25 to 100. Rock mass strength can be regarded as the resistance of a rock mass to surface processes and it being the foundation of the reference monument, it follows that rock mass strength is directly related to the longterm stability of the monument. Selby's rock mass strength rating is based on the numerical rating of the following rock properties:

- Strength of the intact rock
- Degree of weathering
- Spacing, width, orientation and continuity of joints
- Movement of groundwater out of the rock mass

For the sake of simplicity, joints are geological partings of any description unless otherwise specified. This application of rock mechanics was taken further by Selby (1982) and Moon (1985) and laid the foundation to a better understanding of rock resistance and joint roughness as controls of the stability of different rock slopes. One might not necessarily want to duplicate these procedures for every footprint monument site, but it is nevertheless important to bear in mind the main finding that joint spacing and intact rock strength are some of the prime determinants of slope form. Also the detailed analyses of individual properties of rock masses will enhance the understanding of the development of rock slopes and consequently of long term monument stability. Study of the materials, or at least taking them into account in some way, will aid in evaluating potential stability or instability and has important implications for monument design and site selection. A large number of rock mass classification systems have been developed over the years, most of which were developed for the design of underground excavations. Some of these have been used extensively in correlation with parameters applicable to the design of rock foundations (ASCE 1996) such as the Rock Quality Index (Deere 1964) and the geodesist should be aware of these approaches, as they provide valuable insight as to the possible instabilities, especially in the long term, which could affect a monument's stability.

4.5 Monuments Located on Soil

Classical soil mechanics can be put to use to give one a good indication of the expected stability and movement of a monument located on soil. There are two basic groups of calculations, *settlement calculations* and *stability calculations* which are commonly used in geotechnical engineering. Settlement calculations are of direct importance to us as it is concerned with the stiffness of the soil beneath the monument. Stability calculations are used to model

complete failure of soil masses, where large deformations occur on rupture planes followed by collapse of the geotechnical structure. Useful calculations can be done for a given monument and examples as well as the mathematical theory supporting various approaches can be found in the literature (see for instance Lambe 1964, Bowles 1977).

4.5.1 · Volumetric Variables

A large proportion of the volume occupied by soil consists of voids, normally filled by air or water (pore fluids). When deformed, large and often irreversible changes in volume can occur due to the change of relative positions of the soil particles. In contrast, rock is more homogeneous at the particulate level so it is easier to describe it in terms of stresses and strains. However, the geotechnical structure on which the monument is located is normally much larger than the individual soil particles and as long as we take into account the possibility of large volumetric changes, stresses and strains can be averaged over the soil. The soil particles form a highly redundant skeletal, cellular framework, so any changes in the volume of this particle structure leads to the flow of pore fluid through the soil. The mechanical behaviour of the geomaterial on which a monument is located depends on its state, which in turn is defined by its structure and texture. State parameters are:

- porosity (density)
- water content (consistency)
- stress (stress level, degree of isotropy, stress path)
- strain
- time
- temperature

These parameters are not isolated and act in combination. It is outside the scope of this work to give a detailed description of each parameter, but the geodesist should be aware of the following points:

- The stress fields of porous continuous materials are not homogeneous (Feda 1992) and sources of progressive failures at higher stress levels, different stress gradients, their distribution and intensity, depend on the pore-size curve, as well as the overall porosity and its homogeneity.
- An increase in water content can lead to structural breakdown or decrease in strength and peak shear resistance. Monuments should not be built in a depression where water can accumulate.
- The mechanical response of soils is related to the magnitude of their strain (Ishihara 1981, quoted by Feda 1992). The response is elastic for $\epsilon < 10^{-5}$; elastoplastic for $10^{-2} > \epsilon > 10^{-5}$($\epsilon = 10^{-1}$ representing the

approximate failure strain); loading rate and frequency becomes relevant when $\epsilon > 10^{-3}$. The value $\epsilon > 10^{-3}$ is the threshold for major structural changes before dilatancy and contractancy appear.

4.5.2 Example: Monument Located on Clay

To investigate the long and short term stability of a monument located on expansive clays, a monument (aptly named SINK) was installed about 20 metres from the SLR pad, but was not fixed to bedrock. The data are presented here as an example, but much more data will have to be collected over a period of five to ten years to fully appreciate the magnitude and characteristics of possible settling and tilting. Initially data were sampled continuously in order to detect small order settling. Figure 4.3 contains offset plots (translated and scaled to plot millimetres) ΔX, ΔY, ΔZ, $\Delta Height$ and $\Delta Slope$, in millimetres as a function of MJD. Linear regression values for 81 individual sessions were calculated.

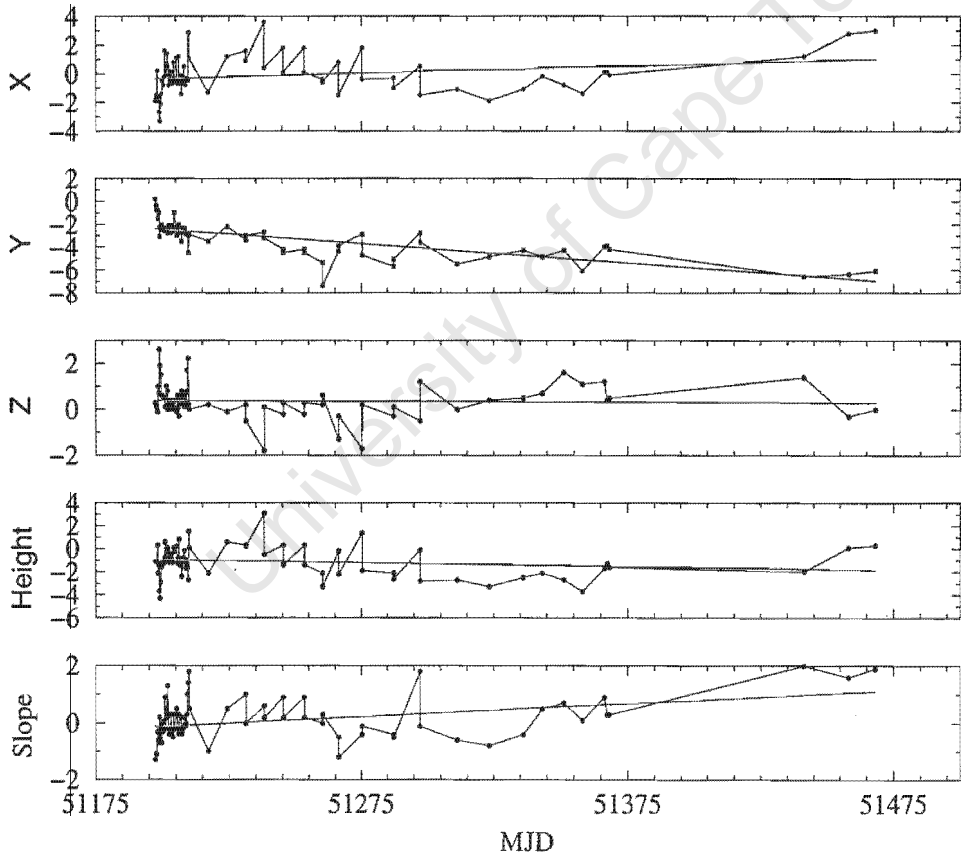

Figure 4.3: Offset plot of baseline vectors, height and baseline (slope distance) changes for a monument located on expansive clay in millimetres as a function of MJD.

A subset of data was used to calculate an approximate value of the noise in an individual measurement. The subset was not arbitrarily selected and will contain some monument instability components, however, the subset should give an indication of individual measurement noise. The first five days of data were excluded (where initial instability would be high) and data beyond MJD 51209 were excluded as the period between sessions lengthens considerably from this day onwards. Eight consecutive days of 6 hour sessions (MJD 51202-51209) were used for the measurement noise determination. The one sigma standard deviations (mm) obtained were $\sigma\Delta X$=0.65, $\sigma\Delta Y$ = 0.56, $\sigma\Delta Z$ = 0.49, $\sigma\Delta Height$ = 0.74 and $\sigma\Delta Slope(distance)$ = 0.48. As an additional check on these standard deviations, some of the 6 hour sessions were processed as three 2 hour sessions, and the standard deviations obtained were consistent.

Very little settlement or heave is present, which is expected as the clay had undergone no drastic changes in moisture content, the data being collected during winter, autumn and early summer. No rain occurred during this period. More data over wet and dry periods are bound to indicate some heave. The calculated slope of the regression for height was -0.003 mm (per day) and the height had a standard deviation of 1.27 mm. This slope is well below the standard deviation of individual measurements, it is therefore not used to indicate any vertical movement. However, a marked tilt is apparent in the Y component, with a regression coefficient of -0.017 mm. This tilt seems to have stabilised towards the latter part of the data. Further monitoring is bound to bring interesting results and it is hoped that eventually a simple numerical settling model could be developed for the soil local to the HartRAO site. The total tilt (about 4 mm) over the measurement period in the y-axis is unacceptable for a geodetic monument. This example underlines the importance of situating monuments on bedrock. The slope distance (baseline) increased by 0.005 mm per day to a total of 1.2 mm. The GPS measurements are not precise enough to identify sub-millimetre movements, but can be used to determine the longer term movements. Therefore, monument instability with the SINK experiment uses the complete data set to describe small movements over a period of 272 days.

4.6 Monuments Located on Buildings

Many geodetic monuments are actually buildings. If one attaches a GPS antenna to a pole which is attached to a building, the pole is not the monument, nor is the antenna mount the monument, the monument is the building. Buildings are not necessarily bad monuments, they often meet requirements in respect of accessibility, safety, power and convenience. Hardly ever are they evaluated in terms of their long-term stability. Buildings don't last long either, maintenance of the structure sometimes requires movement of the GPS

antenna as has been the case with the IGS station HART, which was renamed HARK after being moved. Building foundations suffer from primary consolidation, which results in the porewater pressure being diffused. The theory and calculations can be found in the engineering literature (see for instance Holtz and Kovacs 1981, ASCE 1996) and indicates that even for geodetic monuments, depending on soil type and state, some primary consolidation is to be expected. Secondary consolidation should also be taken into acount. Figure 4.4

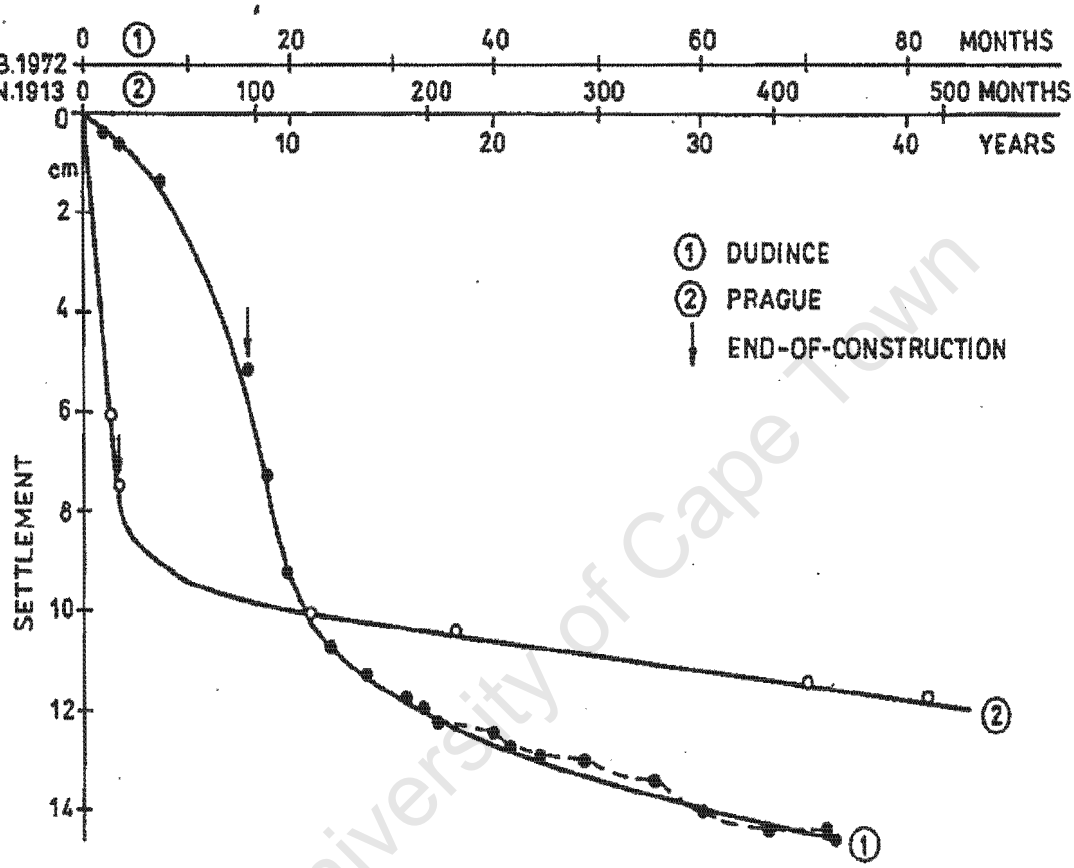

Figure 4.4: Time-settlement relation of two buildings with shallow foundations (from Feda 1992).

describes the settlement of two buildings (Feda 1992) where building No. 1 is located in Dudince (Slovakia) and No. 2 in Prague (Bohemia). Two totally different time scales are applicable, five years in the first case and forty years in the second. Both are within the timeframe of a geodetic monument. The adverse effect on data analysis and interpretation of results if a GPS antenna had been located on either of these buildings are easy to see. All buildings will show some settlement, the best will be those which have had pilings done to bedrock. It is probably good practice to avoid using buildings as monuments. When a building is constructed, its foundations may or may not be fixed to bedrock. The load imposed by the structure at the foundation level will always

be accompanied by strain which results in settlement of structures. This is true for the monument as well to a certain extent. The total settlement of the monument or building foundation in general is given by

$$S = S_e + S_c + S_s \tag{4.1}$$

where S_e = immediate settlement, S_c = primary consolidation settlement and S_s = secondary consolidation settlement. In granular soils the predominant part of the settling is during the immediate settlement phase. In areas where saturated inorganic silts and clays occur the primary consolidation settlement predominates. If your monument is located on highly organic soils or peats the secondary consolidation settlement forms the major part of the settlement.

The expected settlement is not easy to calculate due to the many variables involved such as modulus of elasticity, shear modulus and Poissons ratio obtained from triaxial tests, but reasonable estimates are possible; one can find many different approaches in the literature. If you are installing a monument on a newly constructed building, mortar shrinkage will produce some instabilities, these last about 6 months. Typical primary consolidation over a period of 10 years is on the several cm level. The settlement depends a lot on how close the foundation is to bedrock, the closer, the more stable the monument will be. So within reason, if one has to choose a building for a monument location, it becomes part of the monument and in general older buildings should be more stable.

If a building is being considered for a monument, installation is normally easier as there might be convenient access to power, clear horizon, security and requirements. Stability will to a large extent be dependent on the size of the building, its foundations, its age and nature of the site it on. There might also be other radio frequency (rf) equipment installed on the building, for instance VHF and UHF repeaters, with their accompanying rf harmonics radiating and causing interference in the L band which will degrade the GPS installation's performance. Sometimes there are metal structures which should be taken into account such as airconditioning plants, guard rails, water tanks and antenna towers. A solidly constructed building, with foundations on bedrock can be a good monument/site, but one has to be aware of its stability limitations.

4.7 Monument Types

The University NAVSTAR Consortium (UNAVCO) has an excellent website which contains a large amount of interesting and useful details on monumentation. They have invested a large amount of time on monument stability and is a "must read" for the investigator who is planning to construct and install geodetic monuments. UNAVCO's preferred monument according to their webpage is the deeply anchored/braced monument designed by Wyatt et al. (1995). UNAVCO supports requests for monument consultation and

design with details of some of these to be found on their website, such as the design of a monument using an Invar rod to withstand the climatic extremes of Greenland. Details of the UNAVCO levelling mount, GPS geodetic quality benchmarks and recommendations on sleeve depths for expansive soils can also be obtained on the website.

A very informative monumentation specification table which characterises various monuments in terms of approximate cost, multipath and physical attributes can be found on their website. One common attribute which is conspicuous in the UNAVCO table for most "excellent" monuments is that these installations are difficult and time consuming. Even the stainless steel pin installed in bedrock, although listed as a simple installation, may require a thorough site investigation using geophysical techniques as "bedrock" is sometimes not as it appears to be. The building type monument is not listed, but is currently of a type that should be added to the list. If one attaches a geodetic monument to a building, the building in effect forms part of that monument.

4.8 Antenna Mounts

UNAVCO has done a considerable amount of work on suitable mounts and normally they attempt to address points such as:

- relocation of a replacement antenna
- ease of installation
- stability
- durability
- tampering
- levelling and orientation of antenna
- multipathing
- attachment to monument

UNAVCO has a summary of various antenna mounts on their web page. There are many different versions of the same type and it is often up to the ingenuity of your mechanical workshop as to how the mount is made. There are several good designs available. There is no ultimate mount, but there are some which you may want to throw out after some thought.

For all our installations, HRAO, SUTH, RICH and our new HartRAO/JPL site for Namibia we use a similar design to UNAVCO's "levelling mount". These can be made up easily and are very stable, easy to align and durable. Mounts should use only marine grade stainless steel, marine grade aluminum or other stable and durable material. PVC and other material which do not withstand bushfire or intense solar radiation should be used with caution.

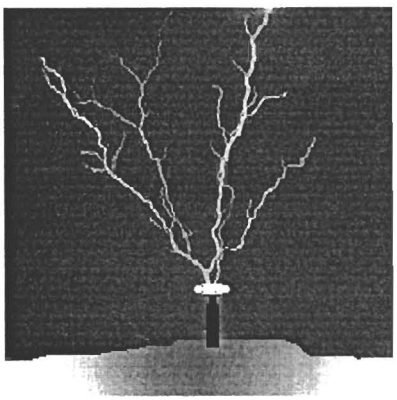

Figure 4.5: Your IGS station ?

4.9 Lightning and the Geodetic Monument

Many IGS and other GPS sites have been damaged by lightning, totally and partially, with damage occurring to the antennas, inline amplifiers, receivers and peripheral equipment. All sites should go to great lengths to ensure that their equipment is protected as best as possible as lightning damage is quite severe.

UNAVCO has done a lot of work on lightning protection for monumentation and the associated equipment attached to the monument and a large amount of useful information and technical details is given on their website. Direct lightning strikes of monuments are in the minority when compared to damage resulting from EMPs (electro-magnetic-pulses). The EMP induces high voltages in unprotected coaxial cables and antennas which allows massive voltage spikes to enter anything else attached to the cables. At HartRAO, we have had several outages of HRAO as a result of lightning, all of the EMP type. We have a more severe problem in this regard compared to most other sites, as this area (Johannesburg) is reputed to have one of the highest counts of lightning strikes per year in the world. Proper grounding rods at the monument and at the other side of the coaxial cable and data lines, inline EMP protectors (Huber+Suhner), surge protection in RS232 lines and power lines are all necessary to reduce the chances of damage. The use of optical fibre links for data communication should be used if possible. One should not use any form of lightning protection unless it has been properly tested and screened, so it would be prudent to check with UNAVCO if your proposed system is suitable. There is a large amount of totally inadequate devices on the market which will not produce the required results.

4.9.1 Surge Protection Devices

Surge protection devices (SPDs) are also known as "surge arrestors", "lightning protection units" and "lightning barriers". The SPDs should ideally operate instantaneously to divert a surge voltage and current to ground, resetting automatically to restore normal operation and be ready for the next surge. Tests done by the IEEE have shown that many cheap types of SPD function only the first time, but still indicate that all is well. Advanced SPDs however combine a number of different surge-supression components to utilize their different characteristics. Data line SPDs make use of high-current, high-voltage gas discharge tubes and low-voltage, low-current surge suppression diodes for rapid and accurate voltage control. UNAVCO is able to advise on suitable units.

4.10 Monumentation at HartRAO

Monumentation for the SLR and HRAO were constructed with stability and durability as the main prerequisites. This discussion excludes the VLBI radio telescope monumentation. The telescope was constructed in the early 1960s, with all three supporting legs bolted down on concrete pillars located on bedrock and forms part of the footprint and the global geodetic network, but its monumentation design falls outside the scope of this work. The monumentation for the footprint consisted basically of standard trig survey beacons, selected for good network geometry, stability, accessibility and security. These beacons are all located on or very close to exposed bedrock as they were built on the surrounding outcrops of the Witwatersberg and the hills which surround the HartRAO site. The beacons were equipped with stainless-steel self-centring plates which allows very accurate re-occupation of a monument.

4.10.1 SLR Pad

Introduction

The SLR pad is included here, as the main pier to which the brass reference marker for the SLR is attached, is centred inside a self-centring plate for GPS and is used during footprint surveys as a reference point.

Monumentation Design Considerations

As with any geodetic installation we were primarily concerned about the stability of the monument. Drawings supplied by NASA of the platform on which the SLR would be located specified a reinforced concrete slab, 7.62m square and 300 mm deep, founded in stable soil. The HartRAO site however does not

have stable soil, but is mostly potentially active residual Hekpoort Andesite clays. The presence of clays meant that a thorough geotechnical investigation would be necessary and a very specific founding solution would be required.

Geotechnical Investigation

Lacking the necessary instrumentation and expertise, contact was made with the South African Geological Survey (Dr E.H. Stettler and Mr C. Crail) who proceeded to conduct a micro-gravity survey (Stettler and Crail 1993) and A.B.A. Brink & Associates, Consulting Engineering Geologists, who led the geotechnical investigation (Brink and Associates 1993). The survey would give us a good indication as to where bedrock was shallowest beneath the site. In this short summary of the geotechnical investigation I concentrate on aspects which affects or pertains to the monumentation and not on SLR specific requirements and I freely use the information supplied in the geotechnical reports. We had specified an area inside the fenced-in perimeter of the facility, a decision mainly based not only on security and convenience reasons, but on the requirement to have adequate open sky access, so that no obstructions would be at an elevation higher than about 12°. The geotechnical investigation finally involved geophysical surveys to determine depth to bedrock, followed by auger drilling, percussion drilling and the drilling of one diamond-drill borehole.

Geophysical Survey

Due to the fact that the site is underlaid by Hekpoort Andesite it was decided to use the gravity method instead of seismics to determine the variation in bedrock topography. The area demarcated for possible site location for the SLR, described as a depth to bedrock contour map is depicted in figure 4.6. The area allocated for the proposed installation measured 72 x 30 m and a 3 m grid was established on this area. Gravity measurements were conducted using a Sodin gravimeter with hourly tie-ins at a base station. The gravity measurements were reduced to Bouguer anomaly values, after performing gravimeter drift corrections, free air and Bouguer slab corrections. Repeatability was to 0.03 mgal. Four auger holes were used to determine the depth to bedrock and allowed calculation of the residual gravity field which is indicative of the overburden thickness. A frequency domain electromagnetic survey with a GEONICS EM-34 was conducted to locate possible power lines, pipes or natural conductive features. We had a rough idea where power lines and a water pipe to an existing borehole equipped with an electric pump had been installed, which was subsequently confirmed by the electromagnetic survey. Borehole positions on the area where bedrock was indicated to be shallow is described in figure 4.7. Six vertical rotary percussion boreholes were drilled on the 30th and 31st of March 1993, in the area where the gravity survey

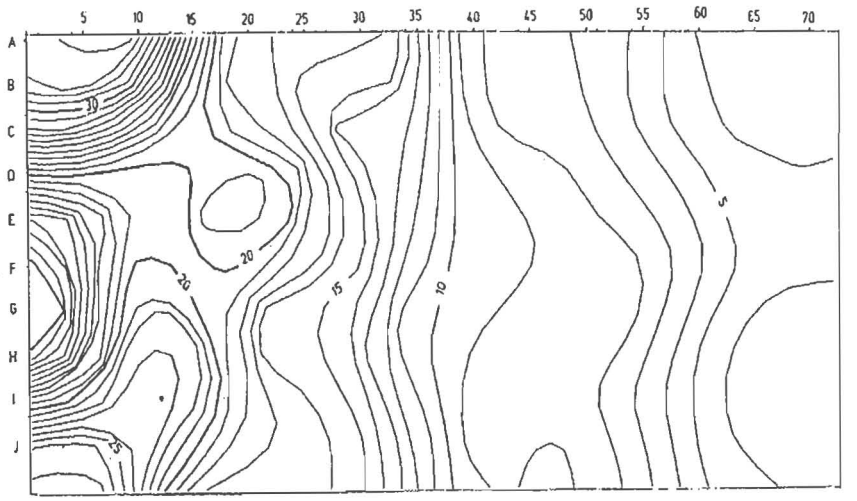

Figure 4.6: SLR location: Depth to bedrock contour map. Scale indicated is metres. The map is oriented east (top), west (bottom), with north on the left. SLR monument site is C60 to D60 (Stettler and Crail 1993).

had indicated bedrock to be shallowest. The drill bit size was 135 mm, minimum depth of the boreholes 8 m, with each hole penetrating at least 7 m into bedrock. The position of the SLR pad was finally determined using the depth to bedrock information obtained from the percussion boreholes. During the 1st and 2nd of April 1993 a single vertical diamond drill (DH1) was drilled where we were planning to install the main reference marker(see figure 4.6). The core size of this diamond drill was 54 mm, the borehole 15 m deep with 11.2 m penetrating into bedrock. The cuttings obtained from the percussion and diamond-drill core were logged by Mr N.C. Jackson.

Geology and Soils

Bedrock is fine-grained, widely jointed, dark grey, very soft to hard rock lava of the Hekpoort Andesite Formation of the Pretoria Group, Transvaal sequence. The percussion boreholes in the immediate vicinity of the proposed SLR pad indicated that the depth to bedrock varied between 4 m and 5.5 m. The gravity survey clearly showed an increase in depth to bedrock (figure 4.7) northwards to the edge of the fenced-in area. Depth to bedrock was in excess of 30 m in the north-east corner. According to Brink 1979 the varying degree of decomposition of the andesite and subsequently the varying depth to bedrock, depends to a large degree on the joint spacing which in itself is variable in this area. We were also concerned about siting the SLR reference pier on a corestone, which is common to the area. It was decided to drill at least 7 m into rock to prove that we were indeed drilling into bedrock and not

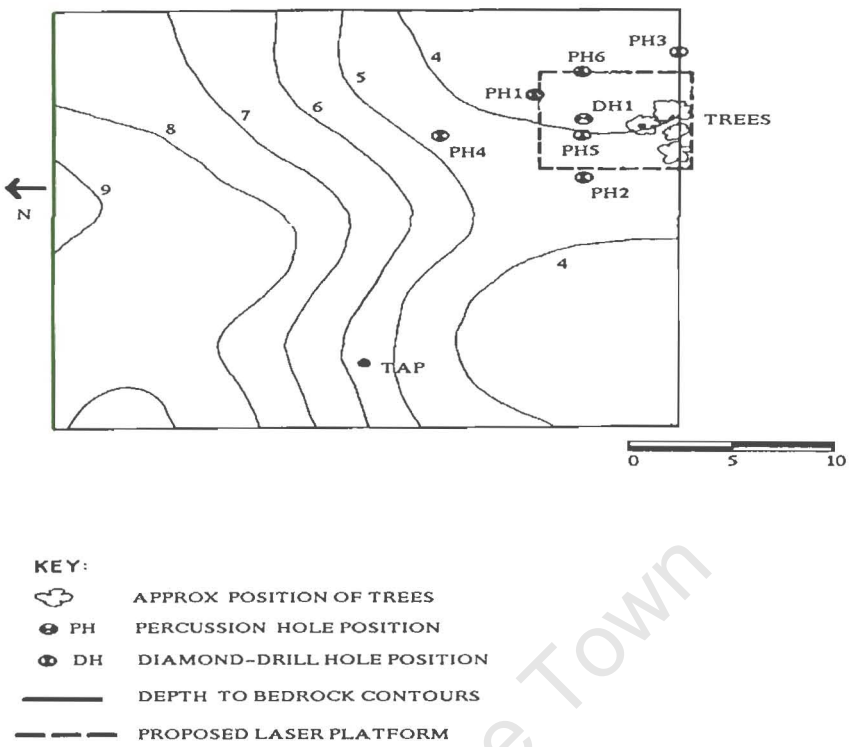

Figure 4.7: SLR pad: borehole positions (adapted from A.B.A. Brink & Associates 1993).

into a corestone. At a depth of between 4.99 m and 5.23 m, below the selected position for the main reference marker, an horizon of highly weathered soft rock was encountered. This rock has a very stiff consistency and is not expected to contain any expansive clay minerals, or be compressible to such an extent that it would lead to instability problems.

Reference Pier

The reference pier, a 1 m by 1 m square steel reinforced pillar is keyed to bedrock through its being located on the bedrock, furthermore we used a steel rod extending from the pier, grouted into the bedrock down the additional 7 m percussion borehole. This steel rod passed through the weathered zone encountered at a depth of about 5 m and will aid in the overall stability of the pier. The pier is isolated from the surrounding platform by expansive foam. The main reference point (a brass marker with centred punchhole) was fixed onto the reference pier and for GPS use, was located inside a stainless steel self-centring plate. This point was used as a reference point in the footprint surveys.

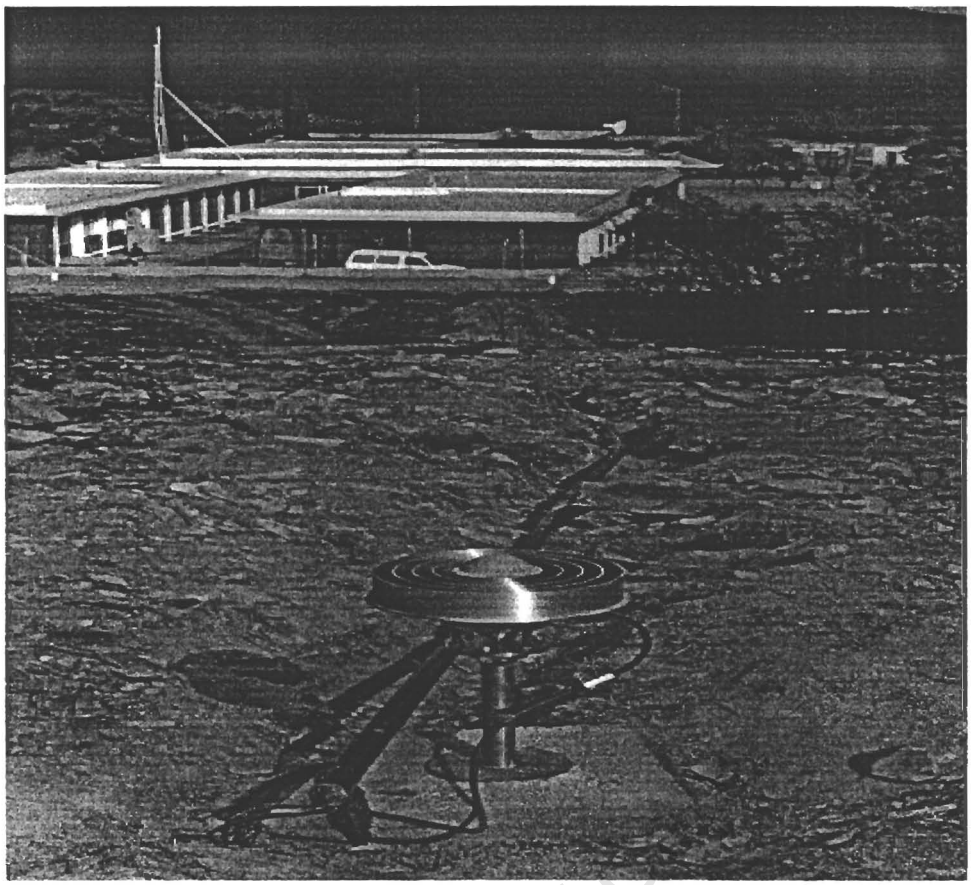

Figure 4.8: Main IGS monument at HartRAO; HRAO, located on a shale outcrop fixed to andesite.

4.10.2 IGS GPS Station HRAO

HartRAO's main IGS GPS monument is shown here as Figure 4.8. The monument has just been installed and at that stage was not quite completed. The 26 m radio telescope is situated in the background and the the view is roughly towards the west. The site has a desert-like appearance due to a veld fire which occurred during the installation. The site geology of the HRAO site is described in Figure 4.9. Figure 4.10 describes the interpreted geological sections A-A and B-B. The site selected for the monument is located outside the fenced perimeter of HartRAO, about 130 metres west of the main-building. This was done to minimise human and other traffic around the antenna, as visitors and casual investigators block satellite signals, causing loss of lock when their inquisitiveness leads them to

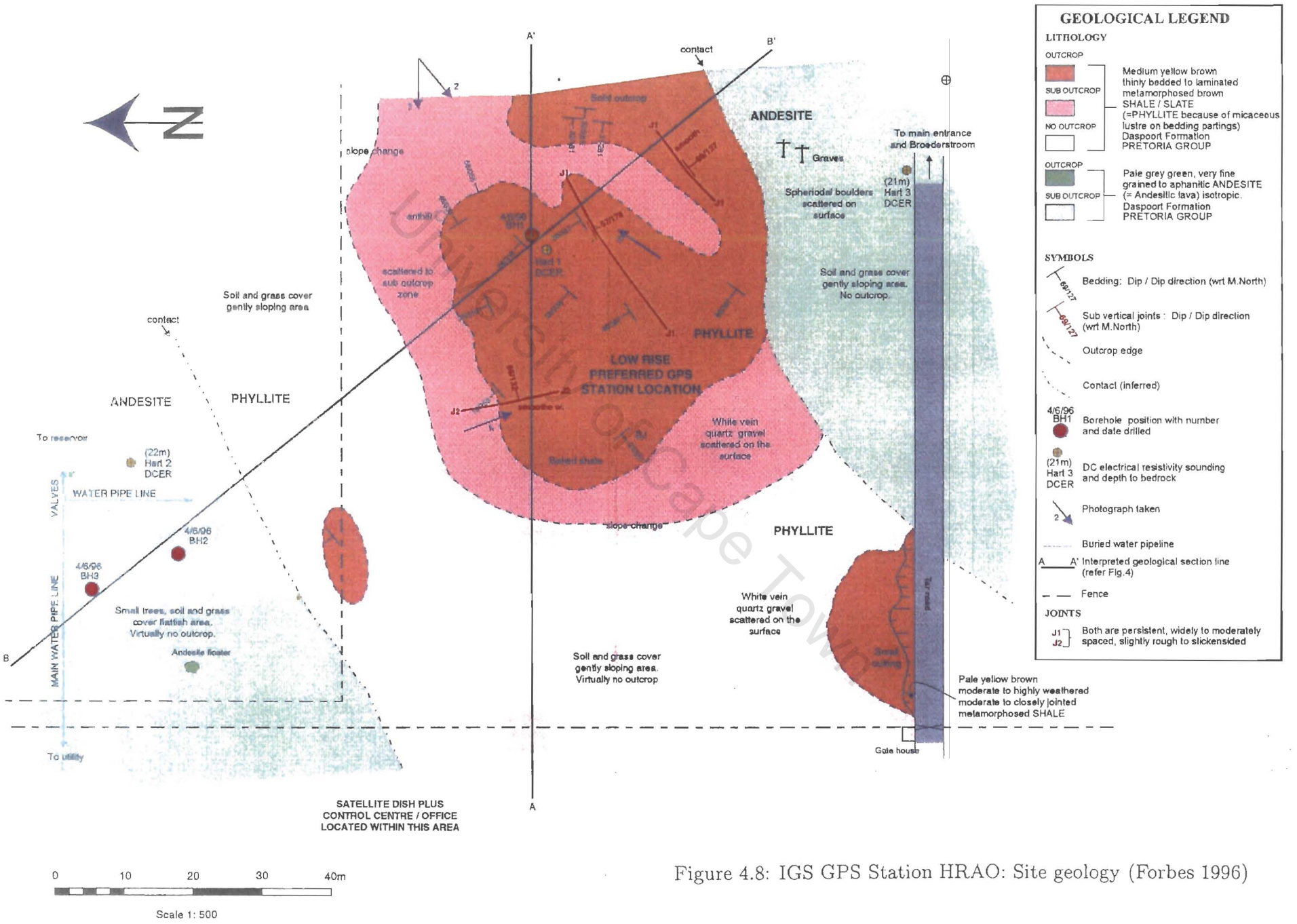

Figure 4.8: IGS GPS Station HRAO: Site geology (Forbes 1996)

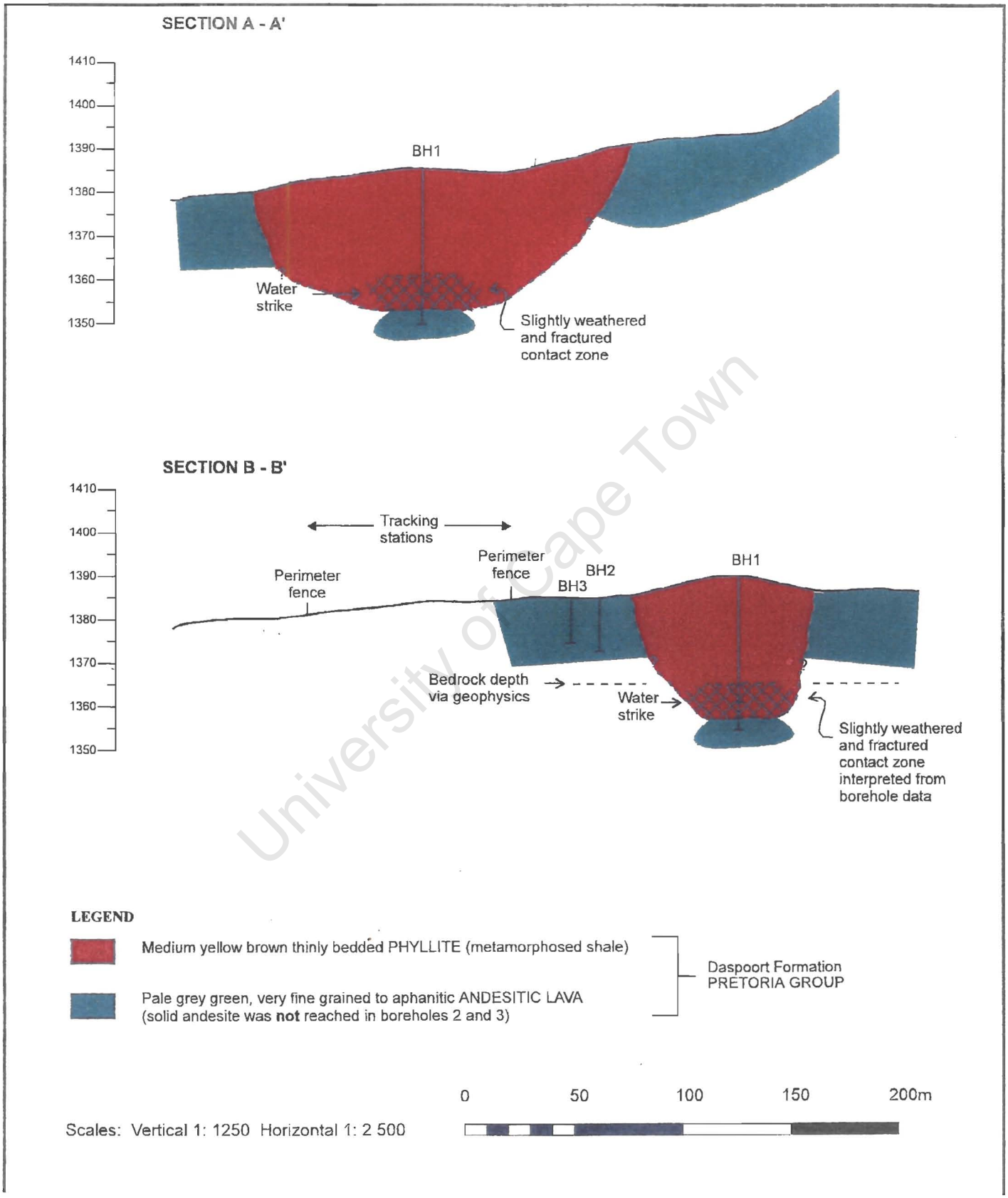

Figure 4.9: IGS GPS Station HRAO: Geological sections A-A and B-B (Forbes 1996)

the antenna. Another good reason to select this spot was that the point is a small hill, offering the antenna some additional elevation over trees, grass and fencing. The hill is a shale pocket located on the andesite. As there was concern about the possibility of a weathered contact zone between the shale and the andesite, I decided to have a hole drilled through the shale, into the andesite, and had a steel pipe grouted into the andesite. The steel pipe was isolated from the shale with plastic pipe and fixed to the shale surface via a steel collar, which in turn was fixed to a cement block. This isolates the steel pipe from any vertical movement the shale might have, as shale could expand slightly due to changing water content. Due to the severe lightning we experience during the summer thunderstorm period, adequate lightning protection was provided by buried copper rod and inline gas discharge tube protectors at the antenna, as well as at the receiver side.

4.11 Footprint Monument Site Descriptions

This section briefly describes one footprint monument as a typical example of the monuments used for the outer, inner and intermediate networks. The footprint monuments are all similar to monument 413. Figure 4.11 is a photograph of 413 which is occupied with a L1/L2 Geodetic antenna with a groundplane. This monument is located on exposed andesite. The cactus in the lower left corner is real and has been the source of discomfort in the past. This monument is typical of the trig beacons adapted with self-centring plates as used for the HartRAO footprint. The self-centring plates allow sub-millimetre antenna relocation.

4.12 Conclusions

Monumentation for the geodesist is extremely important. The equipment which occupies a monument, for instance a GPS antenna, will be upgraded and replaced as time passes but the monumentation is final once constructed. It should therefore be the best possible which the geodesist can afford. The location of the monument should be investigated and the geological structure and factors such as security and accessibility should be included in the selection process. Final results of a footprint or any other geodetic network depends to a large extent on the stability and suitability of the monumentation used. Variable parameters enter the stability equation and one must take into account those which may influence the error budget of the footprint. The approach finally decided upon should also be practical and expedient, to optimise use of existing monumentation, without sacrificing stability for a quick and easy solution. Long term stability should not be traded easily, as this is the geodetic monument's main function.

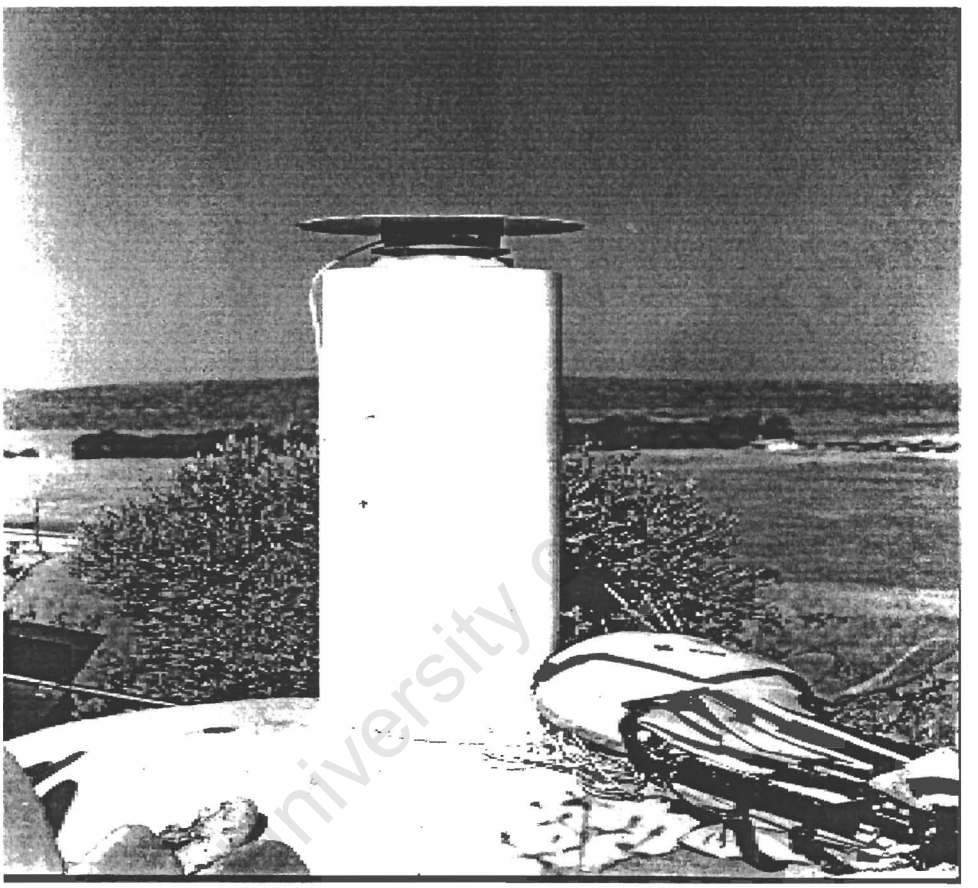

Figure 4.11: Inner network: Monument 413, typical of all the footprint monuments.

Chapter 5

GPS Error Sources

"When the effect of an incorrect choice of the mathematical model, deviations of standardisation and identification, is of a regular and consistent character it will be called systematic." - **P Richardus 1984**

5.1 Introduction

The purpose of this chapter is to describe GPS as a high precision geodetic tool as far as regional networks and footprint surveys are concerned. Although the approach is general to some extent it is largely biased towards systematic errors which could be introduced by using single frequency receivers on short baselines, processed using the double-differences technique. Many of the arguments are however applicable to dual frequency receivers. General introduction, overviews, system description and operational details can be found in the literature, see for instance STANAG 4294 (1990), Leick (1990), Hofmann-Wellenhof et al. (1993) and Kaplan et al. (1996). In this work we are particularly interested in sources of error which show or could show diurnal fluctuation in one way or another. These diurnal fluctations affect relatively short time-series data, as one would encounter during footprint surveys where sessions might be of some hours duration but which will not have the benefit of averaging over several weeks or even years of data. This chapter also have the additional objective of showing that ionospheric, tropospheric and satellite geometry changes could not be the major source of the diurnal, cyclical position changes which have been ascribed to thermal expansion of Hill 411 in the relevant chapters (7 and 8) of this work.

5.2 Ionosphere

The effect of the ionosphere on standalone GPS is described in detail by Leva, Uijt de Haag and Van Dyke (1996) based on a description by Hofmann-

Wellenhof, Lichtenegger and Collins (1993) so the reader is referred to these publications for the development of the mathematical background. When dual frequency receivers are used, the frequency dependent ionospheric delay can mostly be eliminated, but with single frequency receivers some ionospheric model will have to be used such as the Klobuchar model. This model (Leva, Uijt de Haag and Van Dyke 1996) is able to remove approximately 50% of the ionospheric delay at mid-latitudes, by modelling the vertical ionospheric delay with a half cosine function of local daytime and by a constant level during nighttime. The coefficients to be used in mathematical series expressions for the ionospheric model are transmitted by the GPS satellites and are used by processing software on a routine basis (Leick 1990).

The approach in this work was to process single frequency data using a minimum of two receivers, so that in effect relative positioning is done, one receiver being given fixed and known coordinates. Two receivers were used when obtaining data for the SINK (name given to the monument) experiment (Section 4.5.1) and when obtaining data to determine the baseline between 411 and SLR (Section 7.5). These results were not part of or included in the footprint proper, for which a minimum of 3 receivers were used for all the sessions. Double differences are used to cancel the effect of clock biases by assuming simultaneous observations and satellite signals of equal frequencies. It is normally assumed that this approach, used in conjunction with short baselines, say up to 2 km, will provide good results. The residual effects of tropospheric and ionospheric refraction, as well as errors in the GPS broadcast ephemeris for small aperture networks are so small that they can be neglected (Bock and Shimada 1989). The short baselines as used in the inner network of the footprint survey should therefore ensure that, due to the fact that the GPS receivers are practically receiving signals via the same signal paths, the effects of ionosphere and troposhere should be negligible. For short baselines such as in the footprint inner network, it is suggested that it might be more appropriate to use single frequency phases, as the single frequency measurement is less noisy than the corresponding ionosphere-free phase. This advantage must however be very small, as previous measurements at HartRAO using dual frequency receivers on a short baseline of about 60 m, over a period of several days and a later set of observations using single frequency receivers did not show any improvement in positional repeatability. In any event, there must be some effect as the paths are not exactly the same, leading to greater decorrelation and unacceptable (and varying in magnitude) errors the longer the baseline. The possible magnitudes of these effects will be investigated in this section. The Total Electron Content (TEC) degrade GPS signals by advancing the carrier phase and by retarding the group velocity (e.g. NAV data and PRN code). The TEC depends on the location of the GPS receiver, time, satellite elevation angle, season, ionizing flux, magnetic activity, sunspot cycle and scintillation (Leva, Uijt de Haag and Van Dyke 1996).

These effects in terms of diurnal, seasonal and annual variations are also very relevant in satellite communications (Dabas, He and Zhang, 1996) as along the propagation path the TEC introduces Faraday rotation on linearly polarised waves, which leads to a rotation of the plane of polarisation as wel as time delay effects on rf signals which result in polarisation mismatches and dispersion. The maxima of these effects coincide with that of the TEC. TEC is normally expressed in units of electrons/m^2 and electron peak densities in electrons/cm^3 at some specified height. Two extremes occur for the TEC, midnight (minima) and midafternoon (maxima). If maxima at midafternoon coincides with maximum temperature, there is the question whether one is in fact seeing the effect of thermal expansion or the effect of TEC on positioning accuracy. It is possible to compute the change in TEC using a single frequency receiver if pseudo ranges and carrier phases are observed between epochs (Leick 1990) and this has been applied by Threthewey et al. (1993) who has used single frequency measurements to provide a real-time estimate of ionospheric delays. One of the experimental monitor sites was set up at HartRAO (the author was responsible for the data collection at HartRAO) and results from this data clearly illustrates the temporal and spatial non-uniformity of the ionosphere, where a "text book" type plot of phase-code difference in metres are plotted as a function of obliquity, indicating a delay of 9 metres.

This approach was not taken here, but use was made of the near linear relationship between the TEC and maximum electron density to provide an estimate of the variation of the TEC on a diurnal basis as a function of time. This variation is not fixed and maxima and minima points can vary by up to 20 % (private communication A Poole). An international project entitled the International Reference Ionosphere (IRI), sponsored by the Committee on Space Research (COSPAR) and the International Union of Radio Science (URSI) was developed by a Working Group in the late sixties to produce an empirical standard model of the ionosphere. This model is based on all available data sources and improved editions of the model have been released from time to time. For any given location, time and date, IRI describes the electron density, electron temperature, ion temperature, and ion composition in the altitude range from about 50 km to about 2000 km as well as the electron content. Using the IRI-95 model, available online at the National Space Science Data Center (NSSDC) at GSFC, the model was used to calculate electron densities for the time period that GPS data was acquired during the Hill 411 experiment (see Chapter 6, Thermally Induced Instabilities). Figure 5.1 contains plots of the IRI-95 model of peak electron densities for the F2 layer. Peak densities occurred during early evening (17H00 to 18H30 local time), at which time surface temperatures were already declining. Chapter 6 indicates that surface temperature and elongation of the hill in the southern direction are out of phase by 180°, which is explained by the fact that thermal expansion of the hill brings about a decrease in distance between the reference (411) on

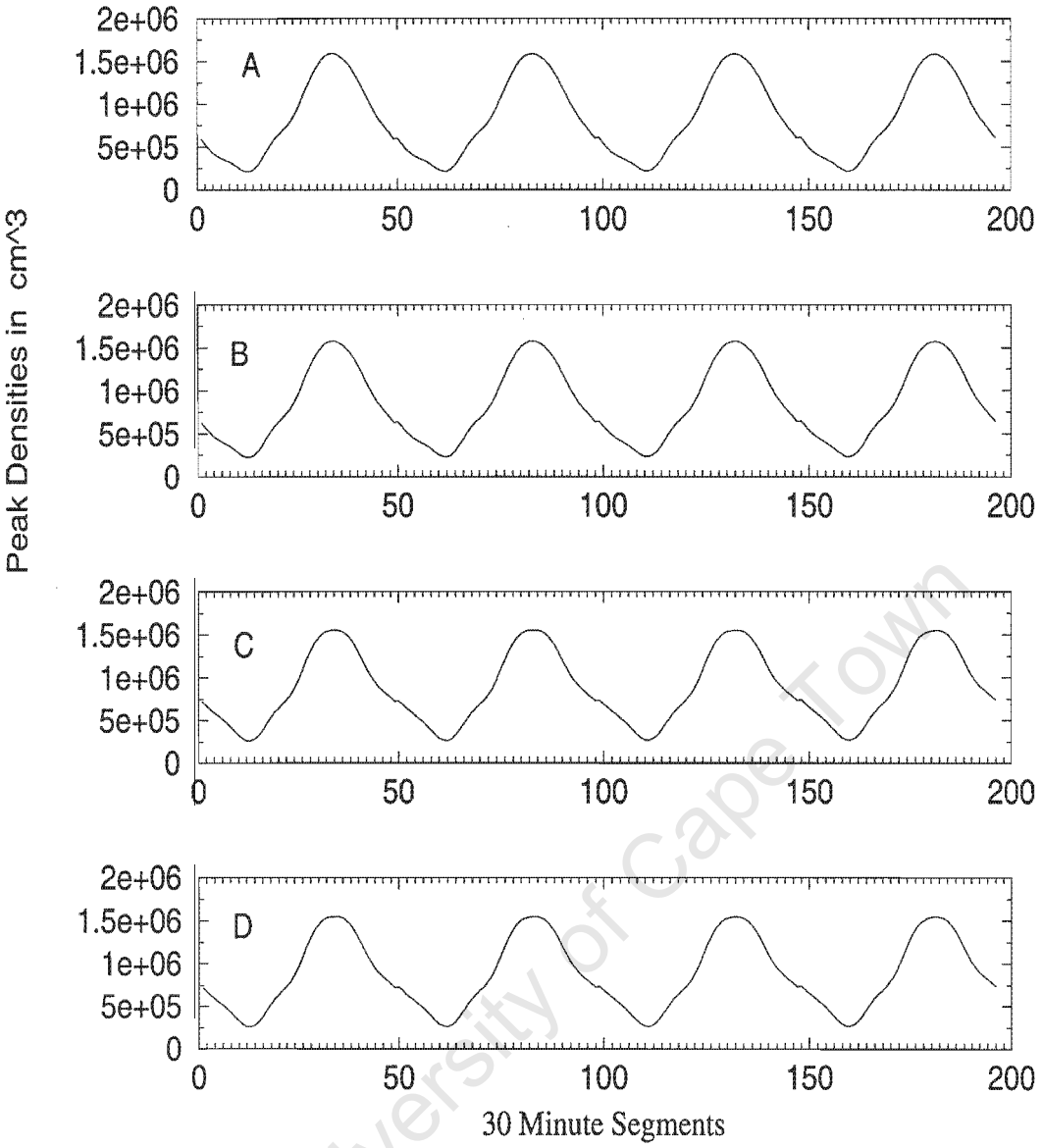

Figure 5.1: Electron peak density of F2 layer as a function of 30 minute segments, 0H00 UT to 24H00 UT for 4 days. (A) 21-24 October 1997, maxima at 17H00 (B) 27-30 October 1997, maxima at 17H30 UT (C) 4-7 November 1997, maxima at 18H00, (D) 11-14 November 1997, maxima at 18H30

the hill and the fixed reference (SLR). The peak electron density is however phase shifted from this theoretically ideal situation by several hours, thus lags behind by 4-5 hours and it therefore does not seem plausible that TEC could be taken as the primary cause of the positional variation. One could approximate the difference in delay caused by the horizontal distance between 411 and SLR. This is given by (Cosentino and Diggle 1996) in their discussion of differential

GPS as:

$$\epsilon_u^{Iono} - \epsilon_m^{Iono} = \frac{1}{\sin \phi\prime} \cdot \frac{40.3}{f^2} \cdot TEC - \frac{1}{\sin \phi\prime_m} \frac{40.3}{f^2} \cdot TEC \tag{5.1}$$

where ϵ^{Iono} is the delay due to the ionosphere expressed in units of length, f is the frequency of the signal, TEC the total electron content and $\phi\prime$ the elevation angle at the ionospheric pierce point. Equation 5.1 can be simplified to

$$\epsilon_u^{Iono} - \epsilon_m^{Iono} = \left(\frac{1}{\sin \phi\prime} - \frac{1}{\sin \phi\prime_m} \right) \cdot \frac{40.3}{f^2} \cdot TEC \tag{5.2}$$

so that

$$\epsilon_u^{Iono} - \epsilon_m^{Iono} = \frac{p}{d_m} \cdot \left(\frac{p}{d_m} - \cos \phi_m\prime \right) \cdot \frac{40.3}{f^2} \cdot TEC \tag{5.3}$$

where p is the distance between the two stations, ϕ_m the elevation angle of the satellite from the fixed reference and $\phi_m\prime$ the elevation angle at the fixed reference station's ionospheric pierce point. For the baseline between 411 and SLR (1485 m) and $\phi_m\prime = 45°$, the difference in delays is about 0.5 mm. Considering the varying geometry of the satellites, worst case scenario would be a satellite at 15° elevation, the cutoff used during the processing of the data. This would lead to a difference in delay of 0.7 mm. At this baseline length, the horizontal positioning error due to the ionosphere would be negligible and can therefore not be possible for the 3 to 4 mm (peak to peak) amplitude variation seen in Chapter 6. Firstly the TEC is out of phase and secondly the possible error introduced is smaller than the measured variation in baseline length. It does however add to the noise in the signal and will influence the thermal expansion signal by superimposing a phase shifted sinusoidal signal on the thermal expansion signal.

5.2.1 Troposphere

Local atmospheric conditions normally lead to a more rapid decorrelation in the delays at two receivers than for the delays caused by the ionosphere. The physics which support tropospheric delay is adequately described by the literature and here the discussion concentrates on the calculation of possible errors introduced by the troposphere for baseline lengths of the inner network, in particular for the baseline 411 to SLR. There is a diurnal component in the delays experienced by two receivers separated by some distance. This is due to the fact that the phase and group velocities experience an equal delay which is a function of the tropospheric refractive index.

This index depends on local atmospheric conditions such as cloud cover, pressure, relative humidity and temperature. Relative humidity also depends on temperature, so one would expect these two components to make up most

of the cyclical diurnal component. The relative humidity, f (as a fraction) is related to the temperature, T and dewpoint Td by:

$$f = \exp(17.27(Td/(Td + 237.3) - T/(T + 237.3))) \tag{5.4}$$

This equation is derived from an empirical fit to the saturation vapor pressure of water due to O. Tetens in Zeitschrift für Geophysik, Vol VI (1930), quoted by Saucier (1983). At HartRAO the pressure remains fairly stable over periods much longer than 24 hours and variations are at the mBar level, centred around 860 mBar. Pressure variations would not be an important variable in determining errors. Cosentino and Diggle (1996) uses a model developed by Altshuler (1971) to estimate the kind of delay difference to be expected due to the troposphere and here we use the same approach:

$$\epsilon_u^{Tropo} = \csc\phi(1.4588 + 0.0029611 \cdot N_s) - 0.3048[0.00586(N_s - 360)^2 + 294] \cdot \phi^{-2.30} \tag{5.5}$$

here ϵ_u^{Tropo} is the tropospheric delay experienced by the user in meters, ϕ the elevation angle from the user to the satellite in degrees and N_s is the surface refractivity. The difference in delay between the reference and a distant receiver can be determined in terms of the horizontal distance p between the two stations and the height d of the satellite by calculating

$$\csc\phi - \csc\phi_m = \frac{d_u}{d_s} - \frac{d_m}{d_s} \approx p \cdot \frac{\cos\phi_m}{d_s} \tag{5.6}$$

where d_u and d_m is the distance from the distant receiver and reference receiver to the satellite respectively. Assuming the surface refractivity N_s is constant (< 1.5 mm) and neglecting data at elevation angles less than 15°;

$$\epsilon_u^{Tropo} - \epsilon_m^{Tropo} = p \cdot \frac{\cos\phi_m}{d_s} \cdot (1.4588 + 0.0029611 \cdot N_s). \tag{5.7}$$

Taking as example the distance between SLR and 411 and choosing a midrange value of 360 for N_s, one finds the difference in tropospheric correction at 411 and SLR, for an angle of 45°, to be less than 0.2 mm. The error in assuming that the signal path through the troposphere is virtually identical for both reference and distant receiver is therefore negligible for the inner network and is certainly not the main source of error in or the reason for the diurnal positional variation as discussed in Chapter 6.

5.2.2 Satellite Geometry and Multipathing

Satellite geometry is especially important for point positioning and kinematic surveying and a measure commonly used is the Dilution of Precision (DOP) factor (Hofmann-Wellenhof, Lichtenegger and Collins 1993). DOP has a direct correlation with obtained accuracy therefore it is advantageous to make

measurements when many satellites are visible and they have a good geometrical distribution in the visible sky. The GPS satellites are in 12 hour orbits, therefore the satellite geometry repeats approximately every 24 hours. The satellites are earlier by 4 minutes per day, as the orbital period of the satellites is about 11h58m. This near diurnal geometry could lead to some diurnal positional change. Horizontal Dilution of Precision (HDOP) and Geometrical Dilution of Precision (GDOP) plots were made for the periods at which thermal and GPS data were sampled to ascertain whether there was a daily cycle of GDOP or HDOP. No significant diurnal signature was found which could influence measured position. Leva, de Haag and van Dyke (1996) describe in detail the formulations of DOP in terms of the components of the covariance of the position and time solution and the pseudorange measurement accuracy for standalone GPS. Vertical accuracy is affected more than horizontal accuracy. It is difficult to see whether a change in satellite geometry would significantly influence short baseline, single differenced results. Judging from the plots of the various DOP distributions as a function of time, it would not be unreasonable to expect some effect which would have a large random component, it will however not have a diurnal cycle which would influence the results as obtained for Hill 411.

The data sampled at Hill 411 each had a session length of 2 hours, which allowed a substantial change in geometry per data point. This change in geometry reduces the adverse effect of possible multipathing. A random selection of the data was processed at shorter time intervals and no large deviations were obtained. This indicates that multipathing was not a major contributor to the possible positional errors. Elósegui et al. (1995) showed that carrier phase multipathing affects the vertical coordinate to a much larger degree than the horizontal coordinates. Errors in the estimated vertical coordinate become large for reflective objects placed near the antenna phase centre, depends on the elevation angle cutoff, and becomes enlarged when a correction to the zenith atmosphere propogation delay is estimated at the same time. Therefore, if multipathing was present and resulted in a diurnal effect, the vertical component would be more affected than the horizontal and this is not seen in the results.

Zero Baseline Test

In order to test the two receivers used for the Hill 411 measurements, a zero baseline test was done. The purpose of this test was to ensure that the two receivers functioned normally and within specifications. It is possible that an electronic instability could cause some error. A dc blocking capacitor and signal splitter was used to allow both receivers to be connected to the same antenna with only one receiver delivering power to the antenna. Three sessions of one hour each were measured, each of which produced very acceptable

results. Baseline lengths were all sub-millimetre. It is assumed therefore that independent receiver errors cannot be responsible for the measured diurnal positional changes as measured on Hill 411.

5.2.3 Antenna Dependent Errors

Antenna phase-center variations result from the nonsphericity of the antenna phase pattern and this could influence the positional accuracy, especially as the satellite geometry changes. However, if the two antennae are identical, then according to Schupler et al. (1994) short baselines should be insensitive to this error. Work done by Elósegui et al. (1996) indicates no diurnal cycle in the movement of a GPS antenna located on a moving platform. Their results show a larger scatter for the vertical component than for the horizontal component, but neither contains a cyclical component. Two identical GPS antennae were used to reduce phase-centre variations. The two antennae used in the Hill 411 experiment have unfortunately not been checked for phase pattern but the biggest antenna pattern related effect would probably be from a change in the elevation angle distribution of the satellites over time (Schupler personal communication). The vertical location of the phase center for a given antenna is very sensitive to the elevation angle range over which the antenna is sampled. It is therefore assumed that as two identical antennae were used, phase-center variations cannot be the major source of the diurnal change in baseline length seen in the data from Hill 411. The antennae were not moved during each of the data sets to reduce possible re-location or orientation errors.

5.3 Conclusions

Considering the discussions above, the total error due to ionosphere, troposhere, multipathing and satellite geometry could in the worst case scenario be in the 1-2 mm region for Hill 411 experiment baseline length. Most of this should be in the vertical component, with some cyclical component due to the ionosphere. The cyclical component should be less than 1 mm and should be phase shifted with that of the thermal expansion effect. No doubt the contributions of these errors are present in the positional data as determined for the Hill 411 experiment and are partially responsible for the noise in the data. It is quite reasonable to assume that on some days these errors would mask the presence or seriously complicate the structure of a thermal signature present.

Chapter 6

Footprint Network

"foot'print n. mark left by foot in ground." - **Collins Gem, English Dictionary, 1963**

6.1 Introduction

In a way, footprints are like fingerprints, not one is alike and each footprint will show the influence of its owner. The smaller inner network should possibly be called the fingerprint, as it is usually given much more attention. During the planning stages, fair consideration was given to network geometry and accessibility to reference points. One major consideration however was that no new reference points could be built, although they could be equipped with self-centring plates. This in itself required a fair amount of energy as having no assistant at that stage, the author had to drag water, cement, steel plates, electric drill and so on up the hills. Using self-centring plates and existing standard trig beacons did lead to a suitable geometrical configuration and practical network which was cost effective. During the construction of the 26 m radio telescope and the years following, several beacons were constructed surrounding the telescope and some of these were very suitable for the inner network. The outer and intermediate networks were designed by using as starting point, a topographical map on which the trig beacons have been marked. Some apparently suitable beacons were selected from the map. This was followed by a field investigation to ascertain their overall suitability, leading to a final selection of the existing footprint network. This chapter presents sonme general equipment issues, network description, the different epochs, processing strategy and final results. Most of the tables, plots and error ellipses are contained in Appendices D to H. These are discussed briefly but are mostly self-explanatory. Plots and tables referred to which are not located in the appendices in the text are mostly located at the end of the chapter.

6.2 General Equipment Issues

After the initial identification of beacons which allowed a suitable network geometry and which met reasonable accessibility criteria, fieldwork consisted mainly of equipping the beacons and SLR pad with stainless steel self-centring plates. These are essential for high accuracy in relocating GPS antennas. Three types of receiver and antennae were used, HRAO is equipped with a Dorne Margolin choke ring antennna and TurboRogue SNR12RM, 12 channel receiver using a Hydrogen MASER (5 MHz) frequency standard as external clock reference. The SLR pad was initially occupied with a Trimble 4000 SSE receiver (dual frequency), equipped with a Geodetic L1/L2 antenna and the first epoch of measurements was done with these type of receivers. After purchasing our own Trimble 4000 SE receivers equipped with L1 compact dome antennae, all subsequent epochs were conducted with only the L1 equipment. The epoch descriptions which follow later in this chapter specifies which equipment was used.

6.3 Network Description

The footprint network consists of three networks of reference points, centred around the inner main reference points (HRAO, SLR and VLBI), an outer, intermediate and inner network. The outer network consists of three reference points, the intermediate has four and the inner five reference points. The geometry of the networks are depicted in Figures 6.1 and 6.2. The outer network reference points are located in the areas Lyttelton (LYT), Rustenburg (RUS) and Potchefstroom (POT). Baseline lengths from the SLR pad (HRAO was not functional yet) are 53.5 Km, 67.8 Km and 45.5 Km respectively; dual frequency GPS receivers are essential. The intermediate network reference points are located on rocky outcrops at Syferfontein (SYF), Tweefontein (TWE), Broederstroom (B16) and on the Magaliesberg (MAG). Baseline lengths are 26.5 Km, 14.7 Km, 19.9 Km and 16.4 Km respectively. The inner network reference points are located on hills surrounding the radio telescope, one of which (BRIT 44) abbreviated to B44 in this work, is the beacon which was used by Chief Directorate: Surveys and Mapping, to tie the national network of trig beacons to the VLBI reference point, to establish the Hartebeesthoek94 Datum. These points are B44, 411, 413, 414 and 415, which roughly speaking form points on a circle centred on the telescope and are listed clockwise from B44 when viewed from above. Baseline lengths are approximately 1364.7 m, 1485.0 m, 1488.0 m, 846.6 m and 1306.5 m respectively.

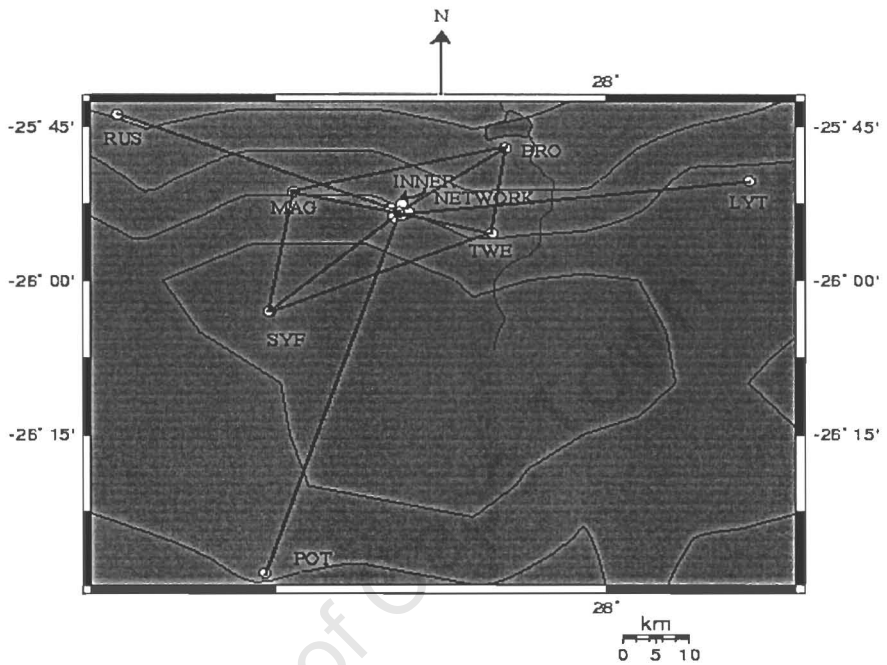

Figure 6.1: Geometry of the HartRAO footprint network.

6.3.1 First Epoch: Outer, Intermediate and Inner Network, April/May 1997

In this work the different "epochs" refer to an epoch of the network and not to an epoch of a sub-network, each epoch has dates assigned to it in any case to avoid any confusion. The equipment used for the first epoch was borrowed from the University of Pretoria (courtesy of Fritz van der Merwe). Due to the lack of suitable equipment, the outer network will only be measured again when HartRAO has its own dual frequency GPS equipment. Ideally one should occupy the sites for several days, which was not possible with borrowed equipment. Nevertheless, the first epoch (April/May 97) was measured using

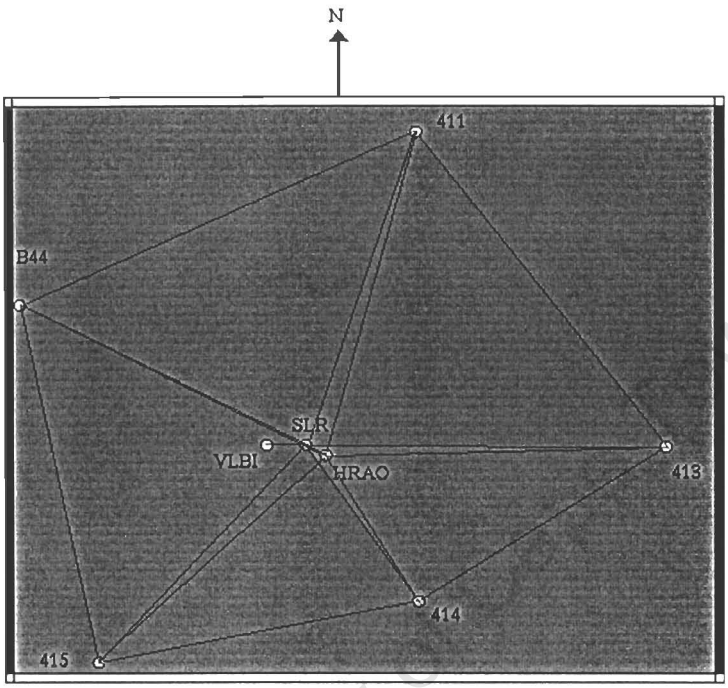

Figure 6.2: Geometry of the HartRAO footprint inner network.

2 Trimble 4000 SSIs, equipped with L1/L2 geodetic antennas and the results were acceptable. The results for the outer network adjusted individual sessions and final adjusted values are given in Table D.1 and Table D.2. Sessions lasted about 3 hours. Comparison of the 2 SLR-LYT sessions show agreement on the several millimetre level, which gives an indication of the repeatability. No statistics were done on these sessions, the formal errors would be too optimistic so proper Gaussian statistics will have to wait for more independent measurements once dual frequency GPS receivers are obtained. Formal stan-

dard deviations on these final adjusted values are on the several millimetre level with the height component being about twice as weak. Results for the adjusted individual sessions of the intermediate network are given in Table D.3 and the final adjusted values are given in Table D.4. Formal standard deviations are also in the several millimetres region with the height component being weaker by a factor of two. Sessions are also of about 3 hours duration. The results of the inner network are summarised in Table D.5 and Table D.6. Duration of sessions vary between about 45 minutes and 6 hours. One of the main factors which adversely affected occupation time during the whole of this first epoch of measurements was concern about the safety of the equipment. The equipment could not be left functioning overnight and had to be attended all the time. The final values show formal standard deviations on millimetre and sub-millimetre level, with the normal factor of 2-3 affecting the vertical component. These formal errors should just be regarded as an indication of the error sizes, as repeated measurements have shown that real Gaussian statistics to determine positional errors, are at least twice as large as the *GPSURVEY* formal errors. This is also the case with other software (Ashtec) as reported by C Merry (personal communication). Most of the plots describing footprint results in this work therefore do not have error bars, errors are only quoted when some reasonable statistics could be used to provide indications of standard deviation. No attempt is made here to support small number statistics or to be over optimistic about errors. In the final adjustment, the SLR is kept fixed, using the ITRF96, epoch 97 coordinates as determined from HRAO to SLR with GPS during 1999. This is done so that the epochs which use the SLR as fixed (before HRAO was operational) tie in with the later surveys using HRAO as fixed point.

Error Ellipses

Standard or error ellipses are described in detail by Richardus (1984) and Leick (1990) and the reader should consult these references for the mathematical development which is not repeated here. Standard ellipses are useful in that they provide information on the directional precision and add some insight into the precision of the network after adjustment. It is important to summarise some useful characteristics of the standard ellipse (Leick 1990):

- Narrow ellipses are not desirable as the standard deviation increases rapidly
- The centre of the ellipse coincides with the adjusted position, the ellipse delimits the probability area for the true position
- The positional error is directly related to the standard ellipse
- The shape of the ellipses depends on the geometry of the network
- The positional error is the standard deviation of the distance to a fixed

station as determined from the linearised distance equation and variance-covariance propagation, in a certain direction

Figures G.1 to G.3 depicts the standard ellipses for the first epoch. All the ellipses have reasonable shapes and there are no obvious outliers.

6.3.2 Second Epoch: Inner network, September 1997

Only the inner network was re-occupied during September 1997. Duration of sessions were much longer than that of the first epoch, varying between about 4 and 24 hours. This epoch of the inner network was done with two 4000 SSIs equipped with geodetic L1/L2 antennas as used for the first epoch. Individually adjusted sessions and final adjusted values are summarised in Table D.7 and Table D.8 respectively. The SLR was again the fixed point for the adjustment. Formal errors are on the millimetre level, with B44 showing the largest errors.

Standard Ellipses

Figures G.4 to G.5 depicts the standard ellipses for this epoch. B44 and 415 indicates larger errors than the previous epoch.

6.3.3 Third Epoch: Inner Network, January 1998

Only the inner network was re-occupied, this time using 1 borrowed 4000 SSI located on the SLR pad and 2 borrowed (courtesy OPTRON) 4000 SEs. During this epoch the repeatability between sessions were investigated for some of the baselines. Beacon 606 was added in order to give a good solution for a reference point for the Satellite Applications Centre (SAC) of the CSIR. Table D.9 contains the adjusted individual sessions and Table D.10 the final adjusted values. Most of the sessions were of 2 hour duration, except SLR-415 on 12 March 1998 which was longer (3:30), SLR-415 on 5 February 1998 was shorter (1:13) as well as SLR-414 on 2 February 1998 (1:13). Repeatability between individual sessions was not very good. A statistical summary of the baseline vector components (x, y and z) as well as height and slope distance between SLR and 411 are given in Table 6.1. In this table and all other summary statistics tables in this work, the correlation coefficient is with time, regression coefficient (SLOPE) indicates the slope of the fitted line and the column labelled *Slope distance* refers to baseline length. The vector components are plotted in Figure 6.3. Height and slope distance are plotted in Figure H.1 and Figure H.2 respectively.

A statistical summary of the baseline vector components (x, y and z) as well as height and slope distance between SLR and 414 are given in Table 6.2. The

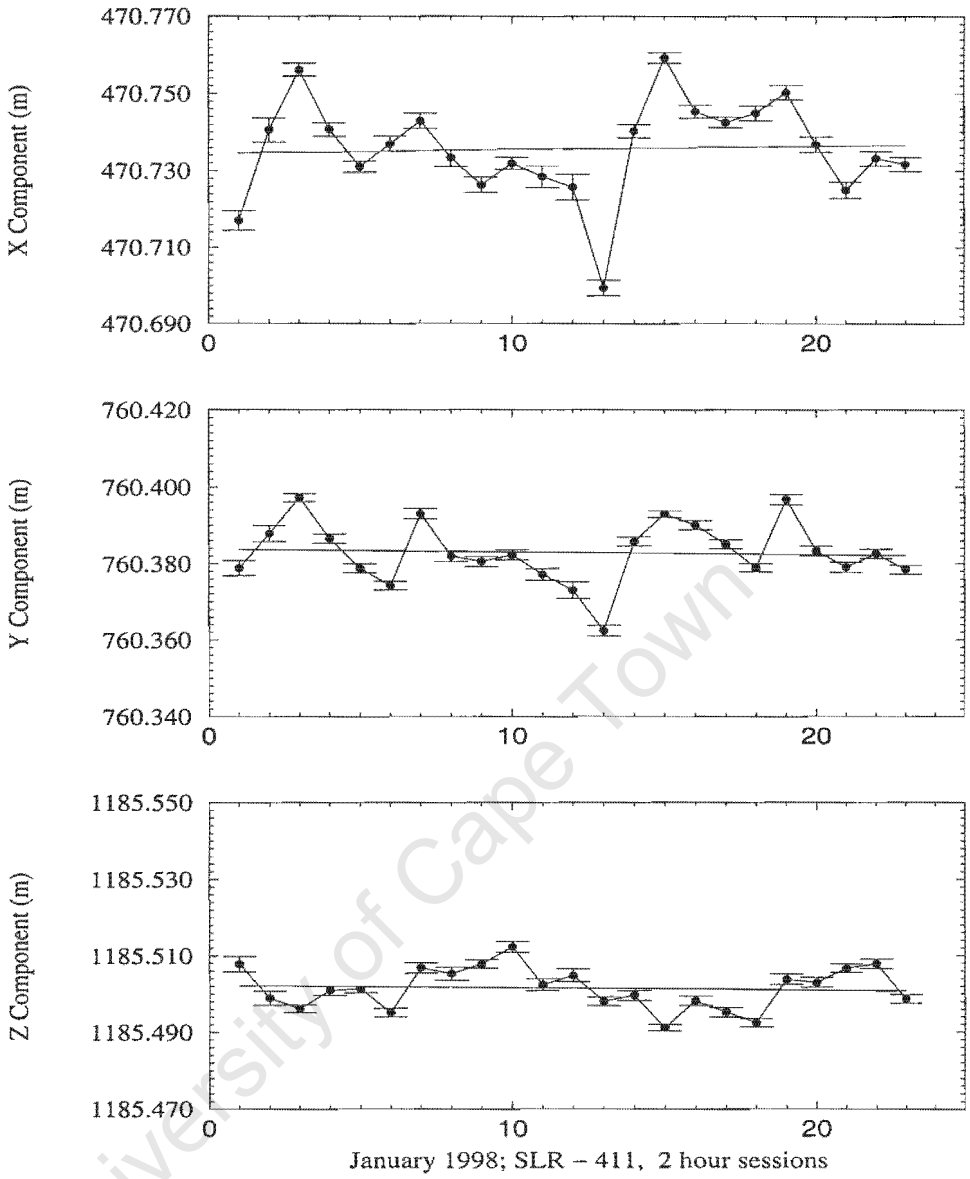

Figure 6.3: Inner network January 1998, 23 two hour duration sessions. Baseline SLR to 411, X, Y and Z components, linear regression. Error bars are included as example of optimistic (2-3 times) formal errors.

vector components are plotted in Figure H.3. Height and slope distance are plotted in Figure H.4. Similarly, a statistical summary of the baseline vector components (x, y and z) as well as height and slope distance between SLR and 415 are given in Table 6.3. The vector components are plotted in Figure H.5. Height and slope distance are plotted in Figure H.6.

Table 6.1: Summary statistics: SLR - 411, 23 two hour sessions, January 98;

Statistic	x component	y component	z component	Height	Slope Distance
Mean of dependent variable (m)	470.7356	760.3829	1185.5010	175.3745	1484.988
Standard dev. of dep. variable	0.0128	0.0080	0.0055	0.0143	0.0079
Correlation coefficient	0.049	-0.058	-0.078	0.035	-0.049
Regression coefficient (SLOPE)	9.269e-05	-6.897e-05	-6.304e-05	7.292e-05	-5.682e-05
Standard error of coefficient	0.0004	0.0002	0.0002	0.0005	0.0003
Regression constant (INTERCEPT)	470.7345	760.3837	1185.502	175.3736	1484.988

Table 6.2: Summary statistics: SLR - 414, 5 sessions, January 98;

Statistic	x component	y component	z component	Height	Slope Distance
Mean of dependent variable (m)	-421.1310	302.0763	-669.4782	83.1569	846.6419
Standard dev. of dep. variable	0.0059	0.0049	0.0025	0.0074	0.0019
Correlation coefficient	0.131	0.054	-0.064	0.112	-0.089
Regression coefficient (SLOPE)	0.0049	0.0002	-0.0001	0.00052	-0.0001
Standard error of coefficient	0.0021	0.0018	0.0009	0.0027	0.0007
Regression constant (INTERCEPT)	421.1324	302.0758	-669.4779	83.15538	846.6422

Table 6.3: Summary statistics: SLR - 415, 7 sessions, January 98;

Statistic	x component	y component	z component	Height	Slope Distance
Mean of dependent variable (m)	41.6877	-956.5502	-888.9745	21.6712	1306.5230
Standard dev. of dep. variable	0.0056	0.0038	0.0017	0.0062	0.0025
Correlation coefficient	0.171	0.339	0.565	0.138	-0.636
Regression coefficient (SLOPE)	0.0004	0.0006	0.0004	0.0004	-0.0007
Standard error of coefficient	0.0011	0.0007	0.0003	0.0013	0.0004
Regression constant (INTERCEPT)	41.6859	-956.5526	-888.9763	21.6696	1306.5260

Standard Ellipses

Figures G.6 to G.7 depicts the standard ellipses for this epoch. B44 has the largest errors.

6.3.4 Fourth Epoch: April 1998, Inner Network

The fourth epoch included the IGS station (HRAO) installed by the author on the HartRAO site. Trimble 4000SEs equipped with compact dome antennae were used to occupy the SLR pad and footprint reference points. Ajusted individual sessions are contained in Table D.11 to Table D.13. Standard deviations are in millimetres. The final adjusted values are listed in Table D.14. Most of the sessions during this epoch was of one hour duration. HRAO was used as the fixed reference. The vector components, height and slope distance are plotted in Figures H.7, H.8, H.9, H.10, H.11 and H.12 being plots for monuments 411,413,414,415,B44 and SLR respectively.

Standard Ellipses

Figures G.8 to G.9 depicts the standard ellipses for this epoch. Errors are larger than those of the previous epochs.

6.3.5 Fifth Epoch: July 1998, Intermediate Network

The intermediate network was measured with single frequency GPS receivers. In general, the session durations were made as long as possible and vary in duration between 3 and 16 hours. TRIMBLE 4000 SEs were used and with a baseline of about 20 km for the intermediate network, careful selection of horizon limit (15 degrees) and observing hours were made to reduce the influence of ionosphere and troposphere. Some of the baselines were measured between sunset and sunrise in an effort to minimise the influence of the ionosphere, but no improvement could be had. Finally, several sessions had to be discarded as they exceeded the cutoff ratio for Trimble 'fixed' solutions. It would seem that 10-15 km baseline lengths are about the maximum lengths that can be used with high confidence, as longer baselines easily lead to weak solutions. This is depicted in Figure 6.4 where the crossover of the *GPSURVEY* ratio test and reference variance test occurs at about 12.7 Km. The ratio is between the next smallest and smallest variance as computed from two different fixed-integer groups. The ratio cut-off was set to 1.5, any solution which has a ratio of less than 1.5 is a 'float' solution and is discarded. The reference variance test is based on the Chi-squared distribution at some specified level of confidence, which in this work was set at 0.95. The degrees of freedom are equal to the processed number of measurements less the number of estimated

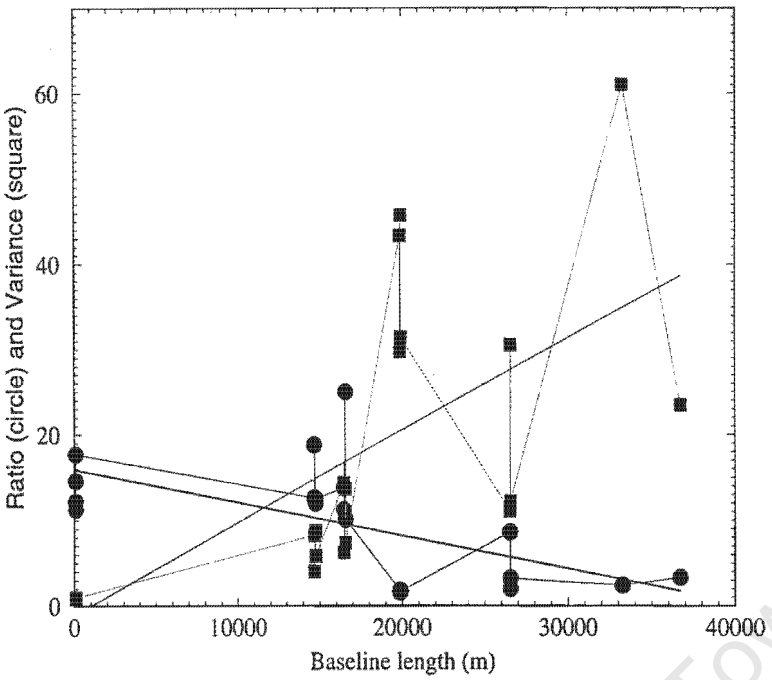

Figure 6.4: Intermediate network July 1998. Reference variance test and ratio test as a function of baseline length, single frequency data only. Baseline lengths longer than $\approx$ 15 Km show large variance and small ratios. Dual frequency data would have been preferable.

states (Trimble 1996). Although not a large amount of data is available, this plot is representative of what one would expect with more data. For final adjustment of this network, all weaker (float) solutions were discarded and the stations then received the same weighting. Dual frequency receivers should have been used but were unavailable. The results for the individual adjusted sessions are presented in Table D.15 and the final adjusted solutions are listed in Table D.16.

Baseline: HRAO-SLR

The baseline between SLR and HRAO was also measured at this epoch, with four sessions on four different days, with session durations of 12 to 24 hours. The adjusted individual sessions are plotted in Figure 6.5. In this plot the formal errors (one sigma) are included as error bars. The first session shows larger formal errors than the other sessions, especially in the z component. It is in the x component where the value actually differs by about 5 mm from the 3 other sessions, although here the formal error is at the same level as the last 3 sessions. This is one reason why, the *Trimble* formal errors are not used to determine repeatability in this work. Repeatability is more accurately represented by actual repeatablity between individual sessions. Formal errors

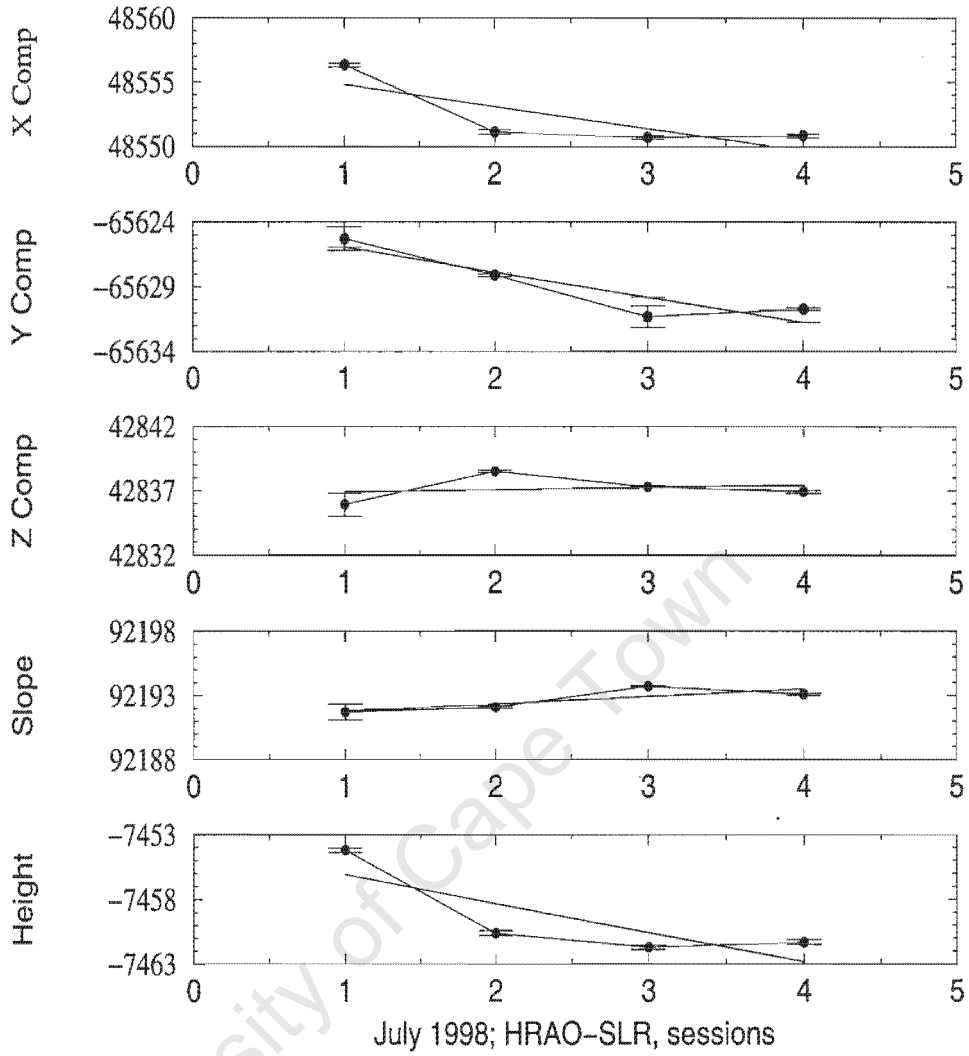

Figure 6.5: July 1998, 4 sessions, 16, 13, 24 and 12 hour duration respectively. Baseline HRAO to SLR, X, Y, Z components, slope distance and height (mm), linear regression.

should however not be ignored, as they could indicate problems with a specific session. Summary statistics are presented in Table 6.4.

Standard Ellipses

Figures G.10 to G.11 depicts the standard ellipses for this epoch. Errors are acceptable and the ellipse shapes are not elongated.

Table 6.4: Summary statistics: HRAO-SLR, 4 sessions, July 1998;

Statistic	x component	y component	z component	Height	Slope Distance
Mean of dependent variable (mm)	48552.22	-65628.85	42837.15	-7459.45	92192.65
Standard dev. of dep. variable	2.72	2.74	1.08	3.53	0.91
Correlation coefficient	-0.80	-0.91	0.22	-0.82	0.82
Regression coefficient (SLOPE)	-1.69	-1.94	0.18	-2.24	0.58
Standard error of coefficient	0.89	0.61	0.58	1.11	0.29
Regression constant (INTERCEPT)	48556.45	-65624.00	42836.70	-7453.85	92191.20

Table 6.5: Summary statistics: HRAO-SLR, 6 sessions, June 1999;

Statistic	x component	y component	z component	Height	Slope Distance
Mean of dependent variable (mm)	48556.17	-65626.35	42834.72	-7454.18	92191.83
Standard dev. of dep. variable	0.30	0.26	0.33	0.41	0.18
Correlation coefficient	0.43	0.02	-0.47	0.38	-0.06
Regression coefficient (SLOPE)	0.07	0.00	-0.08	0.08	-0.01
Standard error of coefficient	0.07	0.07	0.08	0.10	0.05
Regression constant (INTERCEPT)	48555.93	-65626.36	42835.01	-7454.47	92191.85

6.3.6 Sixth Epoch: June 99, Inner Network

The inner network was re-occupied during June 1999. Individual adjusted results are tabled in Table D.17 (standard deviations in millimetres) and the final results are given in Table D.18. Most of the sessions were of 4 to 6 hours duration. The session on 24 June 1999, for baseline HRAO-B44 was rejected for inclusion in the final adjusted results. Although the formal errors are of similar value to the other sessions for this baseline, all components show large deviations (tens of mm) from the other and expected results. It was therefore treated as an outlier. For comparison purposes with the previous epoch, the baseline HRAO-SLR is analysed in some detail. The adjusted individual sessions are plotted in Figure H.13. Formal errors are all on the sub-millimetre level and repeatability between individual sessions are bordering on sub-millimetre levels. Summary statistics are presented in Table 6.5.

Standard Ellipses

Figures G.12 to G.13 depicts the standard ellipses for this epoch. Errors and shapes of the ellipses are acceptable.

6.4 Processing Strategy

6.4.1 Processing Software

The processing software used for the footprint was Trimble's GPSurvey software version 2.2. Initially SLR was used as the fixed reference, but when HRAO became available, it was the primary fixed reference. The reason for this is that during 2000 the SLR MOBLAS6 will occupy the SLR reference point; this occupation is permanent and the reference point will no longer be directly accessible to a GPS antenna. The position of HRAO and SLR are both in ITRF96 epoch 97 so no translations or rotations are required. During any stage of the processing, at least one station had to be fixed using ITRF96 epoch 97 coordinates. This is required as a 10 metre error in reference position could lead to a 1 ppm error in computed baselines. Fixed control values for the SLR and HRAO were set in *TRIMNET PLus*, the network adjustment program to ensure that the coordinate precision type was carried over. Coordinate seeding (propagation of precise coordinates) from the fixed reference was ensured by always, in any given session, having a full set of data available from the fixed reference. Therefore no session was conducted without any fixed reference data. Broadcast ephemeris was used for the inner network but precise ephemeris was used for the intermediate and outer network. During a test run with precise ephemeris on some of the inner network data, no improvement on the solutions was found. The Hopfield tropospheric model was used for all processing. There seemed to be no adverse effect or any improvement at the baseline lengths of the inner network if the tropospheric model was included. There was a marked effect at the longer baselines of the intermediate and outer network, therefore it was decided to use the model as default. Ionospheric modelling could only be used during the first epoch when dual frequency receivers were available. Using single frequency receivers could lead to a scale factor in the adjusted results (Beutler et al. 1987). This scale factor causes single frequency baselines to be shorter than the true baseline (Georgiadou 1990). The effect of the ionosphere on short baselines are discussed in Chapter 5, section 5.2. As only single frequency receivers were available for most of the footprint, this scale effect (maximum ≤ 0.7 mm for inner network) will only become a problem when dual frequency receivers are obtained. One will then have to investigate a small scale adjustment if required. Elevation mask was set to 15°, for all sessions, except when a test was done to ascertain whether an improvement could be had by decreasing or increasing the mask elevation. No conclusive improvements were found for higher elevation settings, but lower elevation settings indicated problems due to the fact that the fixed (SLR or HRAO) had a physical horizon setting anyway, being located in a valley. Therefore all data were processed using a setting of 15°.

6.4.2 Least Squares Network Adjustment

The network adjustment is done using the baseline approach, which consists of two consecutive stages of data processing. Firstly, the sessions are processed to obtain baselines between the reference points. With four receivers (using HRAO and the three 4000SSEs) only three baselines can be considered as being quasi-independent, the fourth being a trivial baseline. An independent session is required to make the fourth baseline quasi-independent (Leick 1990), therefore more than one session per baseline was usually planned for in a survey.

Secondly, the derived baselines are combined in a network and then adjusted. All occupied reference points received the same weighting, although for the intermediate baselines measured in July 1998, all weak solutions were discarded before final adjustment. Following a discussion by Kuang (1996), the basic Gauss-Markov model for the three-dimensional network adjustment can be written as:

$$E\{\Delta \mathbf{r}\} = \mathbf{A}\mathbf{x} \tag{6.1}$$

$$D\{\Delta \mathbf{r}\} = \mathbf{C}_{\Delta r}. \tag{6.2}$$

The parameter configuration matrix $\mathbf{A}$ consists of plus/minus ones or zeros. The vector of corrections to the approximate coordinates of the reference points are denoted as $\mathbf{x}$, whereas the observational vector $\Delta\mathbf{r}$ is given as:

$$\Delta \mathbf{r} = \left(\Delta \mathbf{r}_1^T \Delta \mathbf{r}_2^T \ldots \Delta \mathbf{r}_n^T\right)^T \tag{6.3}$$

where $\Delta\mathbf{r}_i$ is the quasi-observed vector of the coordinate differences between the reference points j and the fixed (SLR) point k, so that

$$\Delta \mathbf{r}_i = \mathbf{r}_j - \mathbf{r}_k (i = 1, \ldots, n) \tag{6.4}$$

6.5 Final Results

Tables 6.6 (epochs April 1997 and July 1998) and 6.7 summarise the consecutive epochs adjusted results for the intermediate and inner network respectively. No consistent scale adjustment (see section 6.4.1) seem present in the results of the inner network, the scale adjustment due to using double frequency (April 1997) and single frequency (July 1998) is lost in the measurement noise. The dual frequency results will be more accurate at this baseline length and will be used as the starting point in a time series once dual frequency receivers are available. The expected error limits are based on the much larger data set obtained for 411 and approximately indicates an average one sigma error to be expected asssuming equal weight to all error sources for each reference point. It will require another 10 years of footprint data before one moves out of the small number statistics, therefore statistics here are assumed

(but may not be) to be based on Gaussian distribution of data. Fortunately the larger data set of 411 allows one to make reasonable assumptions about the real and expected repeatability between different epochs. The results are not quite consistent with the expected error limits (x: $\sigma \approx 3.5$, y: $\sigma \approx 2.5$, z: $\sigma \approx 2.5$, height: $\sigma \approx 4.1$). The technical specifications of the Trimble 4000SEs expect an accuracy of 1 cm + (2 parts per million times baseline length) in the horizontal and 2 cm + (2 parts per million times baseline length) in the vertical. Much of the difference between the standard deviations of the 4 epochs and the expected values can be ascribed to small number statistics, so the discrepancies should reduce as more epochs are included. Monument 411 has an x component standard deviation about twice the expected value (7.7 opposed to 3.5), the y component agrees well (2.6 opposed to 2.5), the z component is better at 1.7 to 2.5 and the height is 7.9 opposed to 4.1. Monument 413 is consistently weaker, Monument 414, 415 and B44 agrees fairly well although all are weaker in the x component and therefore the height component. It would therefore at this stage of the footprint surveys be futile and unscientific to generate a velocity field or make serious assumptions about site instability. It is clear however, that no marked site instability exists.

Epoch January 1998, which utilised two different receiver types as well as different antenna types is an obvious outlier and is excluded from the final results. This is the only difference which somehow would be able to account for the deviations in the results. During processing, the correct models for the different antennas were selected, so incorrect antenna phase centre should not be the problem. The solution would probably be not to mix antenna or receiver types. This type of problem has been investigated by other researchers, and specifically on Trimble equipment, Brunner and Tregoning (1994) and results by J. Braun and C. Rocken as presented on the UNAVCO web page

`http://www.unavco.ucar.edu/dev_test/publications/sst_sse_mix/`

indicate that mixing of the Trimble 4000 SST with the Trimble 4000 SSE and Trimble 4000 SSI receivers over observation times of less than a few hours can cause vertical height errors of up to five centimeters. One can assume that the problem in this work must be related as the errors are of the same order, even though this work mixed Trimble 4000 SSE and 4000 SSEs. The mixing of different receivers tend to average out with an increase in session duration and Braun and Rocken show that for an observation session of sixteen hours, the scatter of the solutions falls to the several millimeter level. Mixing antennas also produces problems vertical height errors of the order of several millimetres to a centimetre. The UNAVCO Academic Research Infrastructure (ARI) Receiver and Antenna Test Report, which can be found at

`http://www.unavco.ucar.edu/dev_test/publications/ari_test.pdf`

Table 6.6: Intermediate Network, Summary of Final Adjusted Values; April 1997 and July 1998

Station	X (m)	Y (m)	Z (m)	Height (m)
SYF	5087912.0152	2647390.8163	-2784754.9430	1724.7960
	5087912.0255	2647390.8097	-2784754.9300	1724.7957
MAG	5094604.2140	2655029.0501	-2765594.0532	1848.4156
	5094604.2360	2655029.0698	-2765594.0668	1848.4472
TWE	5077436.6740	2680240.8243	-2772191.7106	1587.2350
	5077436.6921	2680240.8227	-2772191.7085	1587.2478
B16	5082290.3645	2685062.6944	-2758359.7619	1443.8410
	5082290.3804	2685062.6826	-2758359.7720	1443.8531

contains an analysis of tests done on different antennae and receivers.

Figure 6.6 to Figure 6.15 depicts the offset plotted geocentric coordinates as well as height, including and excluding the January 1998 epoch. All offset Plots were translated and scaled to indicate millimetre deviation from the mean value. Excluding the January 1998 epoch represents a much more acceptable solution. The January 1998 epoch is therefore treated as an outlier. Similar reasoning follows for the other inner network reference points. Table 6.8 summarises the final results which include the the four epochs (January 1998 is excluded) for all the inner reference points.

6.6 Conclusions

No attempts are made here to pretend that a velocity field can be estimated for the different reference points. Generating a velocity field which has a true scientific basis will require a time-series of at least ten years. The results here cannot be used to determine deformation as the measurement errors are larger than the deformation. A much longer period of time will have to elapse,

Table 6.7: Inner Network, Summary of Final Adjusted Values

Station	Epoch	X (m)	Y (m)	Z (m)	Height (m)
SLR	April 1998	5085401.0551	2668330.0531	-2768688.8565	1406.7317
SLR	June 1999	5085401.0587	2668330.0559	-2768688.8585	1406.7366
411	April 1997	5085871.9006	2669090.4991	-2767503.4179	1582.2476
411	September 1997	5085871.9192	2669090.5052	-2767503.4214	1582.2665
411	January 1998	5085871.7990	2669090.4413	-2767503.3592	1582.1169
411	April 1998	5085871.9088	2669090.5010	-2767503.4177	1582.2548
411	June 1999	5085871.9123	2669090.5020	-2767503.4197	1582.2589
413	April 1997	5084842.4384	2669707.1442	-2768765.2104	1570.8490
413	September 1997	5084842.4441	2669707.1478	-2768765.2140	1570.8566
413	January 1998	5084842.3252	2669707.0790	-2768765.1472	1570.7040
413	April 1998	5084842.4330	2669707.1368	-2768765.2014	1570.8377
413	June 1999	5084842.4404	2669707.1401	-2768765.2065	1570.84725
B44	April 1997	5086361.0408	2667483.8006	-2768214.7243	1610.8751
B44	September 1997	5086361.0490	2667483.8030	-2768214.7295	1610.8849
B44	January 1998	5086360.9537	2667483.7482	-2768214.6772	1610.7632
B44	April 1998	5086361.0544	2667483.8034	-2768214.7298	1610.8895
B44	June 1999	5086361.0534	2667483.8061	-2768214.7280	1610.8890
414	April 1997	5084979.9704	2668632.1571	-2769358.3578	1489.9471
414	September 1997	5084979.9753	2668632.1619	-2769358.3588	1489.9535
414	January 1998	5084979.9283	2668632.1318	-2769358.3365	1489.8937
414	April 1998	5084979.9797	2668632.1607	-2769358.3597	1489.9569
414	June 1999	5084979.9827	2668632.1625	-2769358.3618	1489.9610
415	April 1997	5085442.7570	2667373.5132	-2769577.8374	1428.4214
415	September 1997	5085442.7601	2667373.5163	-2769577.8397	1428.4261
415	January 19998	5085442.7503	2667373.5074	-2769577.8342	1428.4122
415	April 1998	5085442.7521	2667373.5113	-2769577.8329	1428.4147
415	June 1999	5085442.7519	2667373.5123	-2769577.8314	1428.4143

with footprint surveys conducted at regular, perhaps twice a year, intervals to obtain adequate and meaningful data for possible deformation analyses. There are however several worthwhile deductions which can be made from these results:

- Each reference point will exhibit measurement errors which might not necessarily be of the same order as others, even during the same campaign, using the same instrumentation and techniques.
- Errors in the x component, which in our case is the strongest component of height, in general are 2 to 3 times larger than in the y and z component.
- Some reference points may be subject to local effects which influences short term (several hours) stability, such as the thermal expansion measured on Hill 411. These effects should not be misinterpreted as crustal instability, or be used to generate a velocity field.
- Mixing receivers and/or antennas can lead to unpredictable results, even if it is supposed to be accounted for in the processing software.
- Determining geodetic site stability using GPS is feasible, as long as one realises that it is a long term project and that final results of an epoch is but one result. Several epochs will indicate the real repeatability of the measurements.
- Deformation analysis will only be feasible once real deformation exceeds the errors in repeatability. It would seem that at least five years of data at HartRAO would be required before an attempt at deformation analysis can be made.
- Given the expected error limits as calculated using the relatively large data set of reference point 411, as well as the standard deviations obtained from the final results, reference points 414 and B44 indicate some possible instability in the x component. Further measurements will indicate whether this unsteady state will progress to a steady state.
- No large systematic deviations from the mean values, or sudden anomalous deviations are present, which indicate that the HartRAO site is stable.

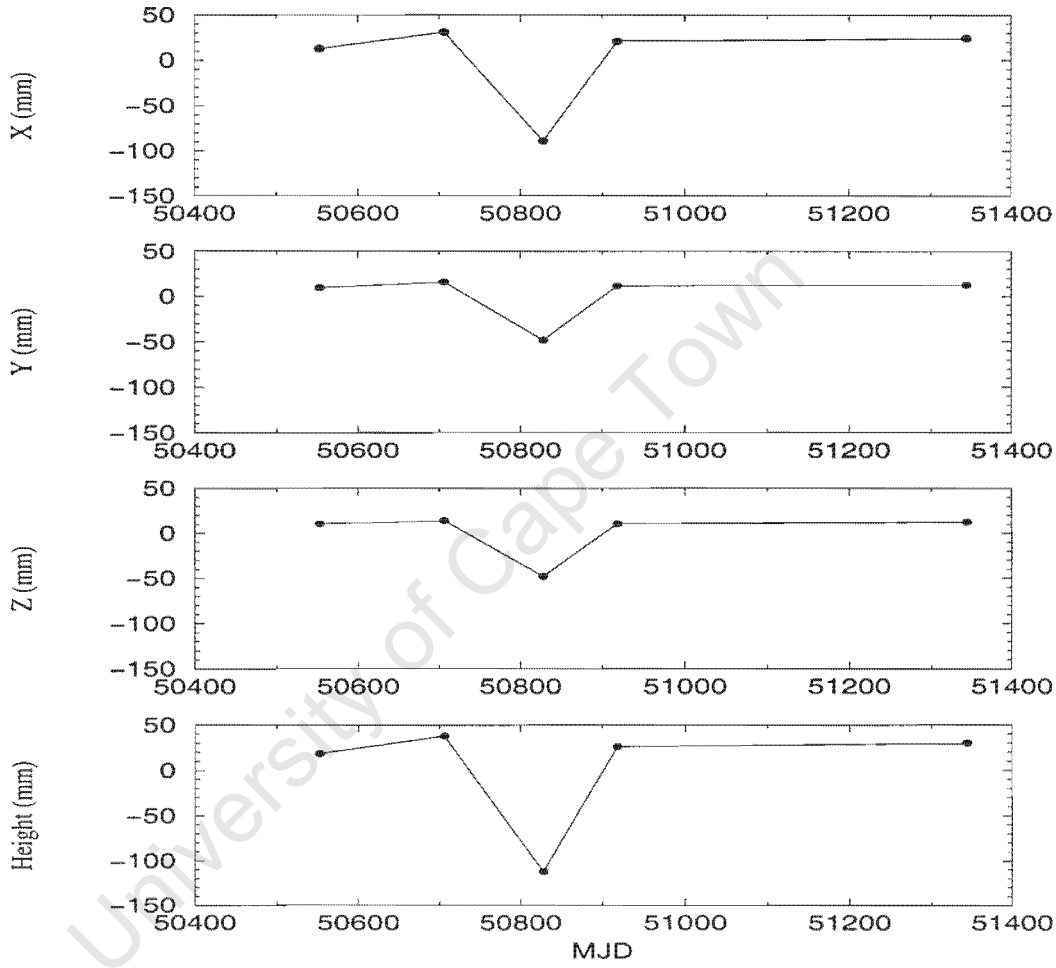

Figure 6.6: Reference point 411: Final adjusted offset plotted geocentric coordinates and offset plotted height. The January 1998 epoch measurements show an unacceptably large deviation.

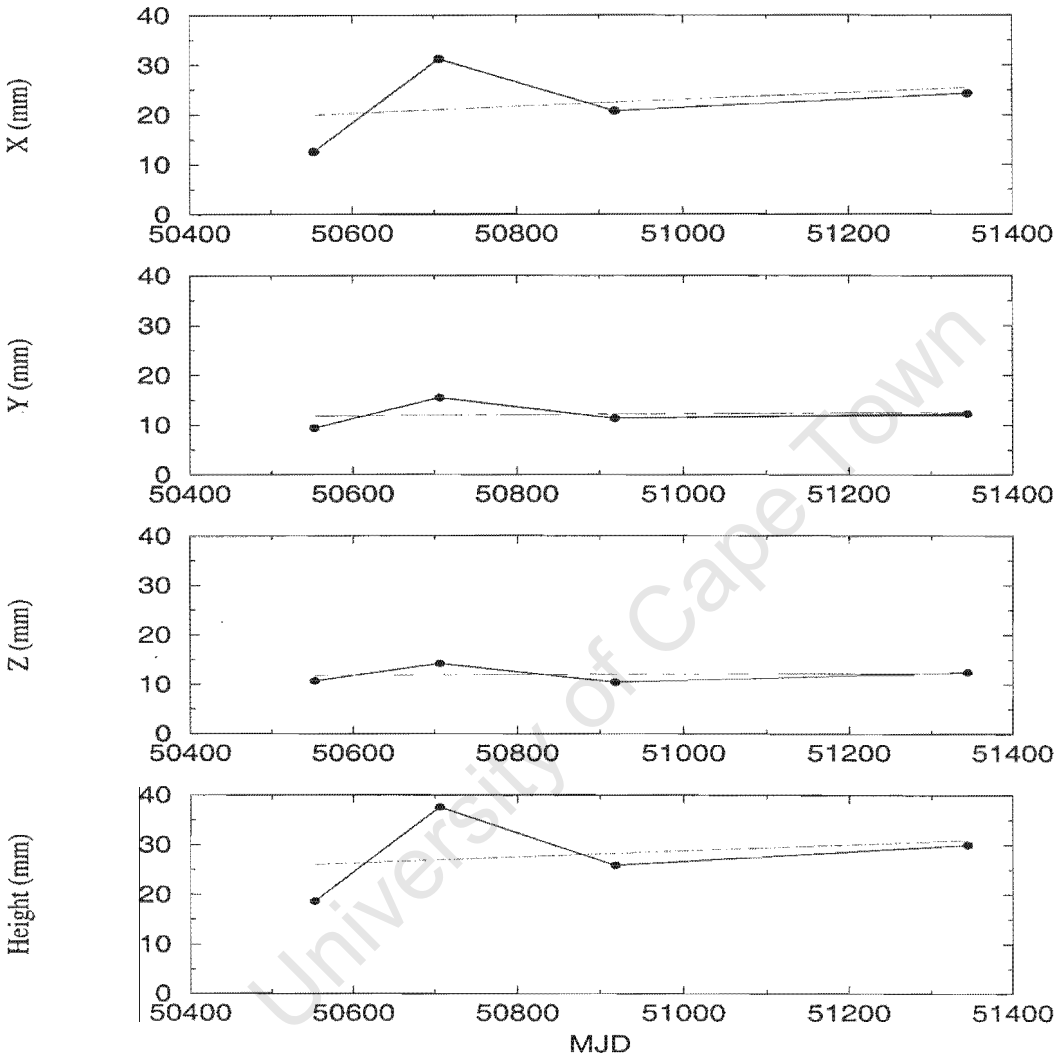

Figure 6.7: Reference point 411: Final adjusted offset plotted geocentric coordinates and offset plotted height. The January 1998 epoch measurements are not included, linear regression indicates expected behaviour of a stable site within measurement limits.

Table 6.8: Final summary statistics: Inner network, geocentric coordinates and height, 4 epochs;

Statistic	x component	y component	z component	Height
411				
Mean of dependent variable (m)	5085871.9102	2669090.5018	-2767503.4192	1582.25695
Standard dev. of dep. variable (mm)	7.736	2.551	1.735	7.896
Slope (mm/day)	0.007	0.001	0.0006	0.006
413				
Mean of dependent variable (m)	5084842.4390	2669707.1422	-2768765.2081	1570.8476
Standard dev. of dep. variable (mm)	4.631	4.793	5.402	7.769
Slope (mm/day)	-0.0008	-0.008	-0.008	-0.007
414				
Mean of dependent variable (m)	5084979.9770	2668632.1606	-2769358.3595	1489.9546
Standard dev. of dep. variable (mm)	5.361	2.419	1.704	5.880
Slope (mm/day)	0.015	0.005	0.005	0.016
415				
Mean of dependent variable (m)	5085442.7553	2667373.5133	-2769577.8354	1428.4191
Standard dev. of dep. variable (mm)	3.989	2.161	3.861	5.677
Slope (mm/day)	-0.009	-0.003	-0.009	-0.012
B44				
Mean of dependent variable (m)	5086361.0494	2667483.8033	-2768214.7279	1610.8846
Standard dev. of dep. variable (mm)	6.195	2.253	2.526	6.676
Slope (mm/day)	0.014	0.006	0.003	0.015

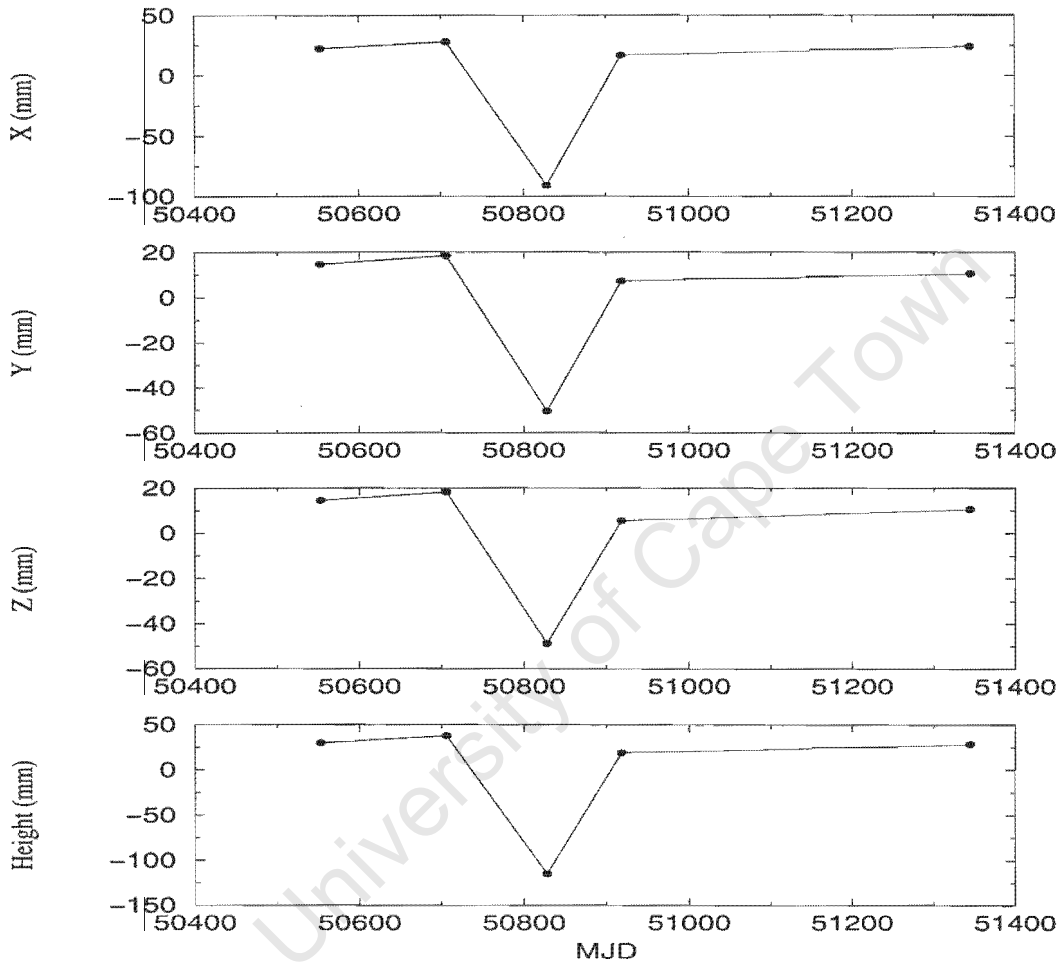

Figure 6.8: Reference point 413: Final adjusted offset plotted geocentric coordinates and offset plotted height. The January 1998 epoch measurements show an unacceptably large deviation.

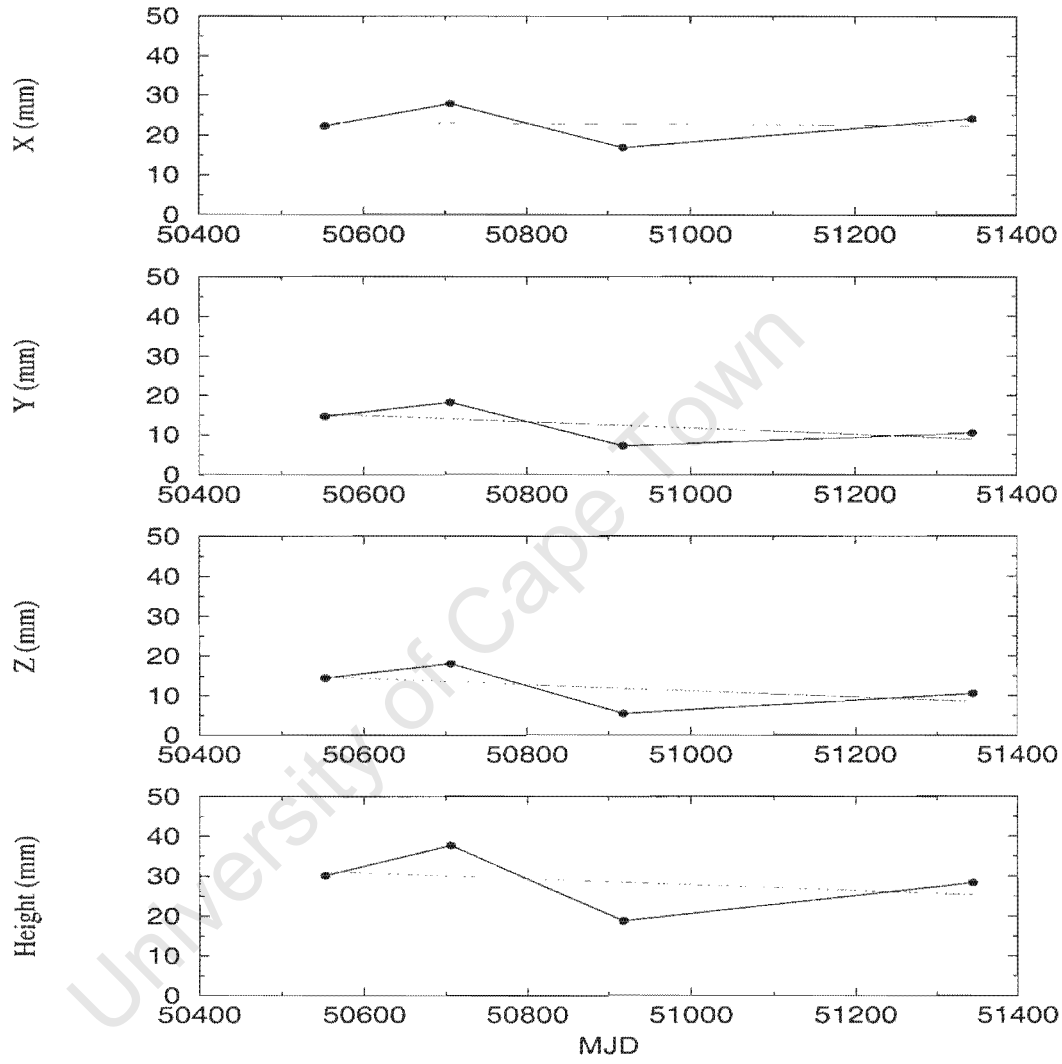

Figure 6.9: Reference point 413: Final adjusted offset plotted geocentric coordinates and offset plotted height. The January 1998 epoch measurements are not included, linear regression indicates expected behaviour of a stable site within measurement limits.

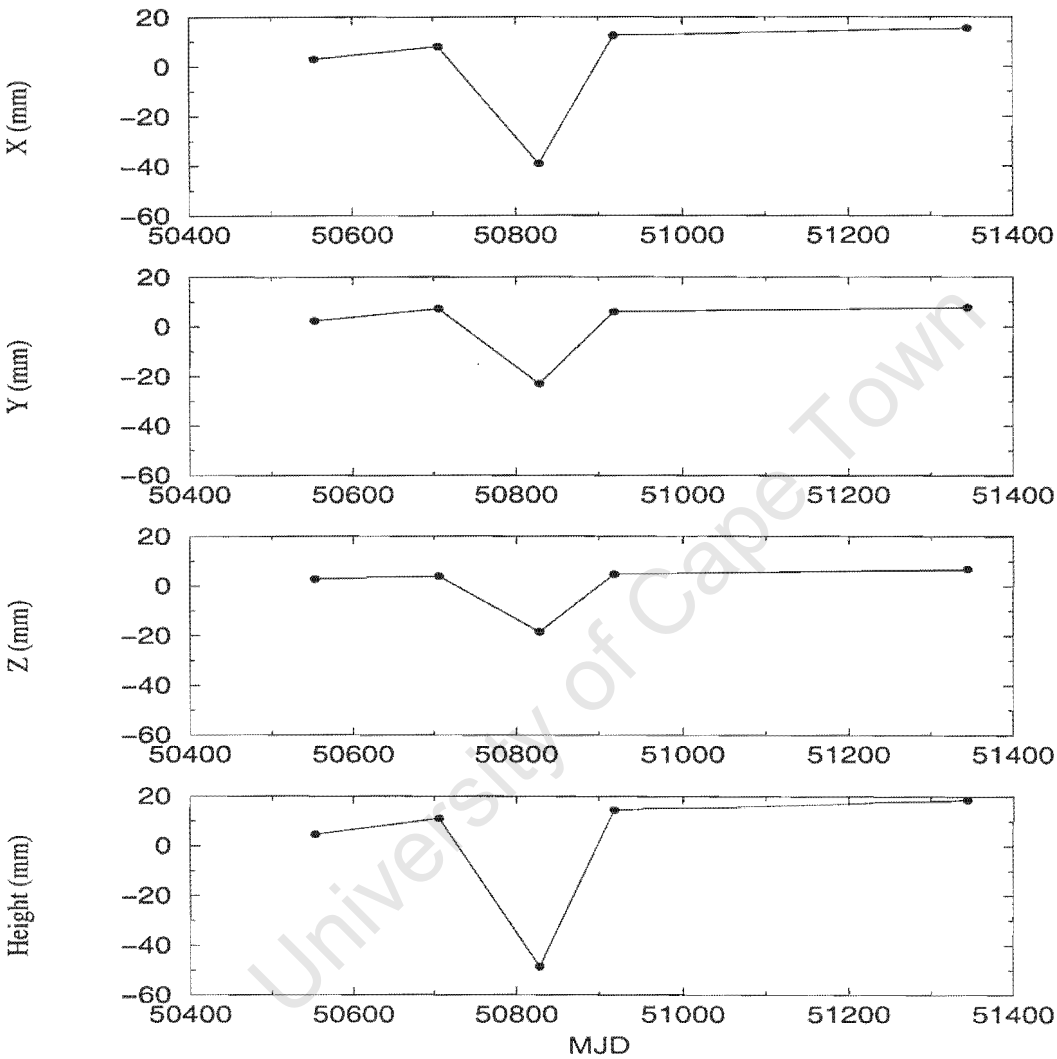

Figure 6.10: Reference point 414: Final adjusted offset plotted geocentric coordinates and offset plotted height. The January 1998 epoch measurements show an unacceptably large deviation.

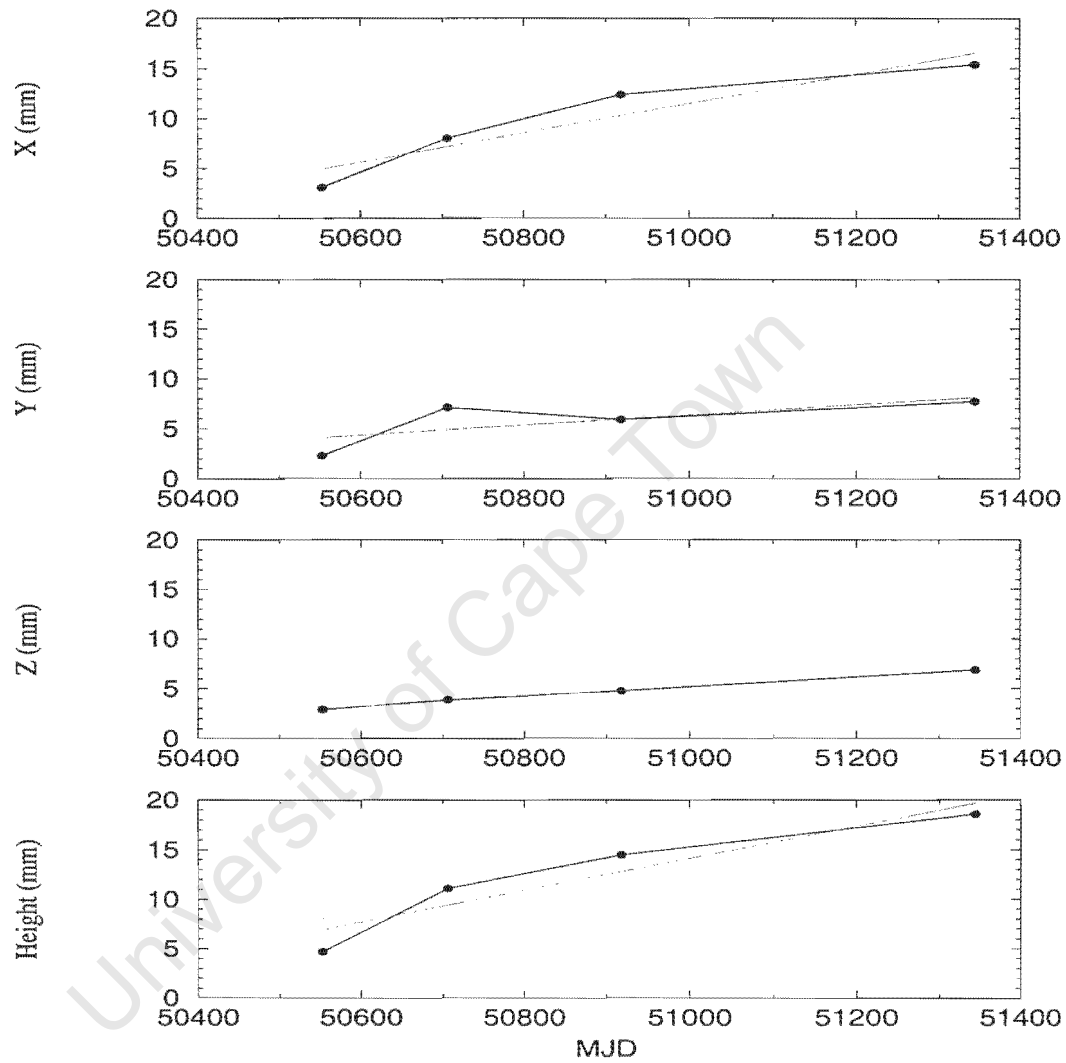

Figure 6.11: Reference point 414: Final adjusted offset plotted geocentric coordinates and offset plotted height. The January 1998 epoch measurements are not included, linear regression indicates expected behaviour of a stable site within measurement limits.

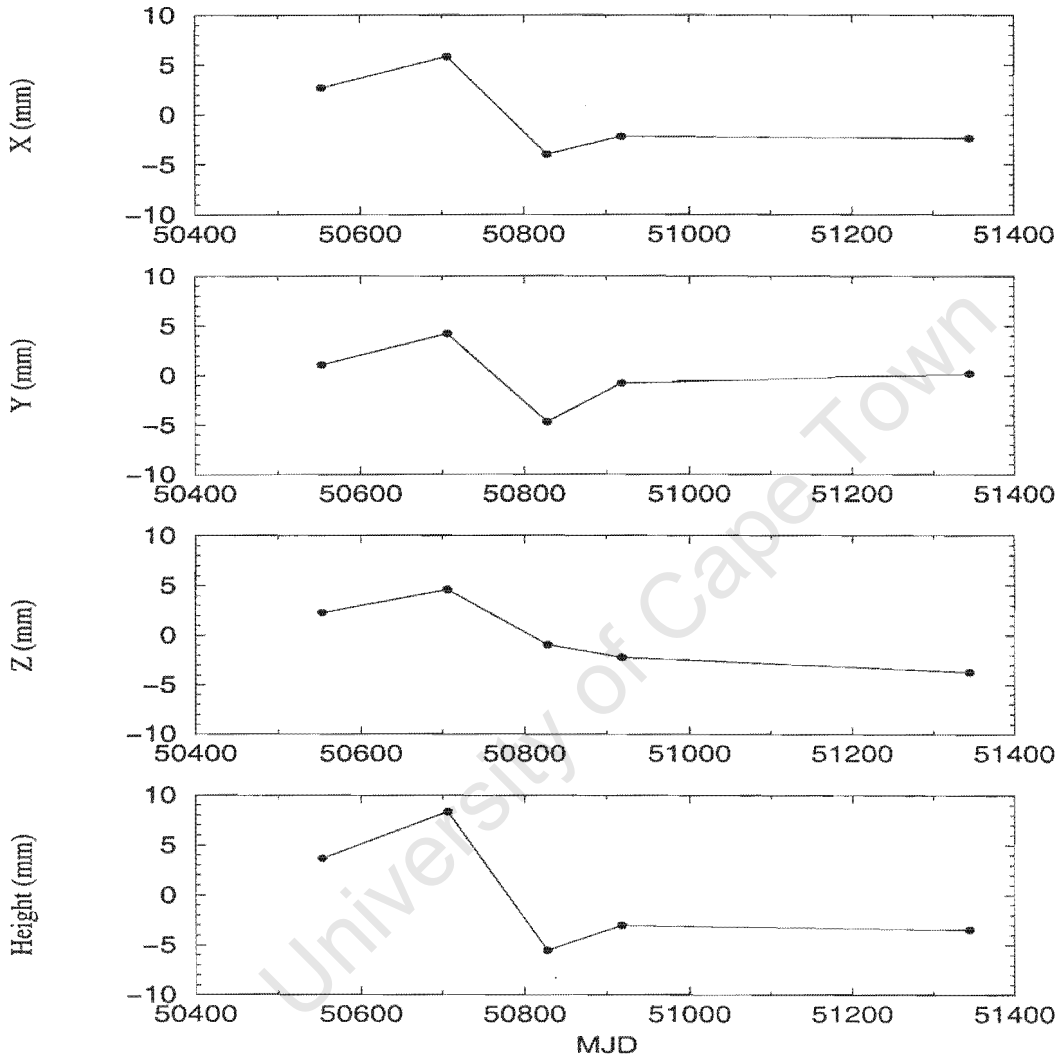

Figure 6.12: Reference point 415: Final adjusted offset plotted geocentric coordinates and offset plotted height. The January 1998 epoch measurements show an unacceptably large deviation.

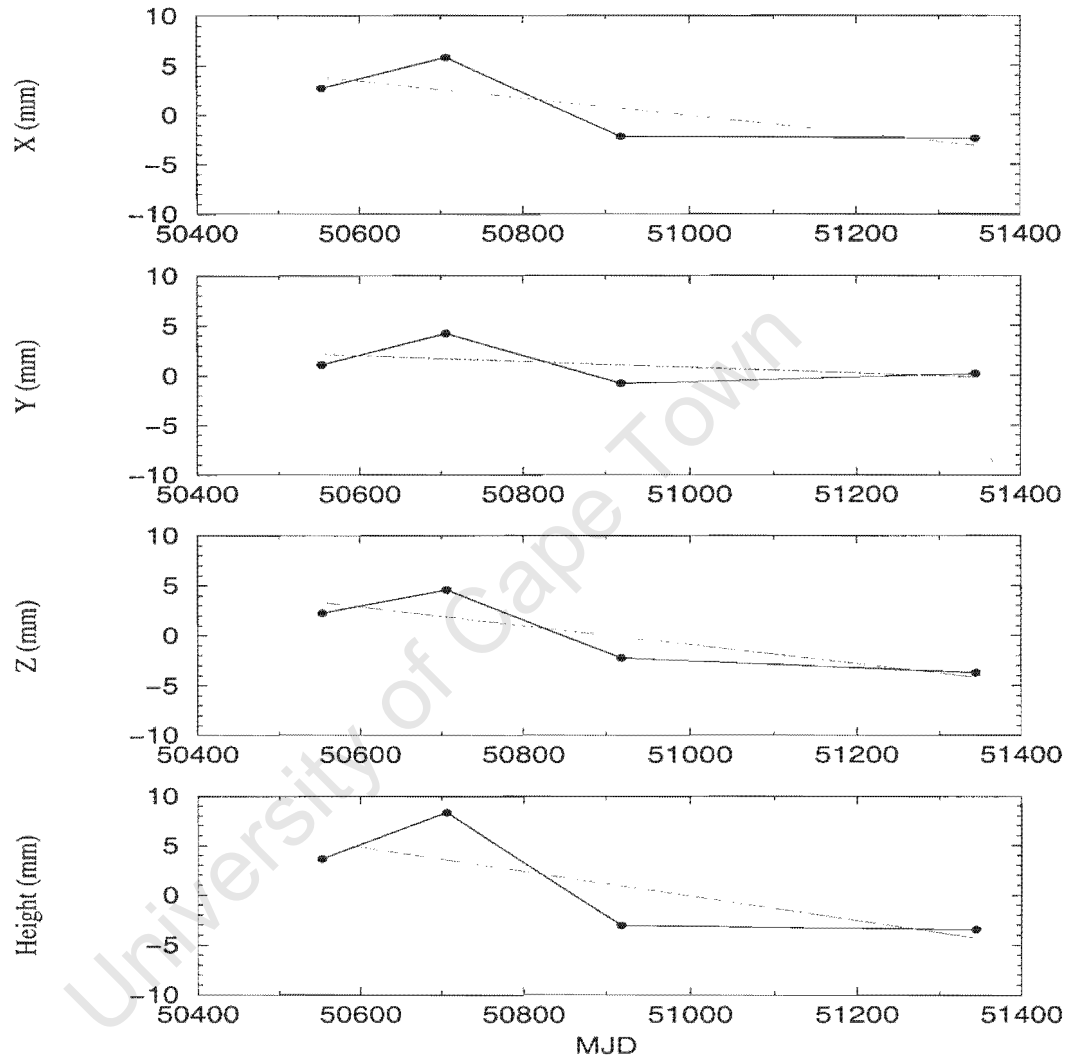

Figure 6.13: Reference point 415: Final adjusted offset plotted geocentric coordinates and offset plotted height. The January 1998 epoch measurements are not included, linear regression indicates expected behaviour of a stable site within measurement limits.

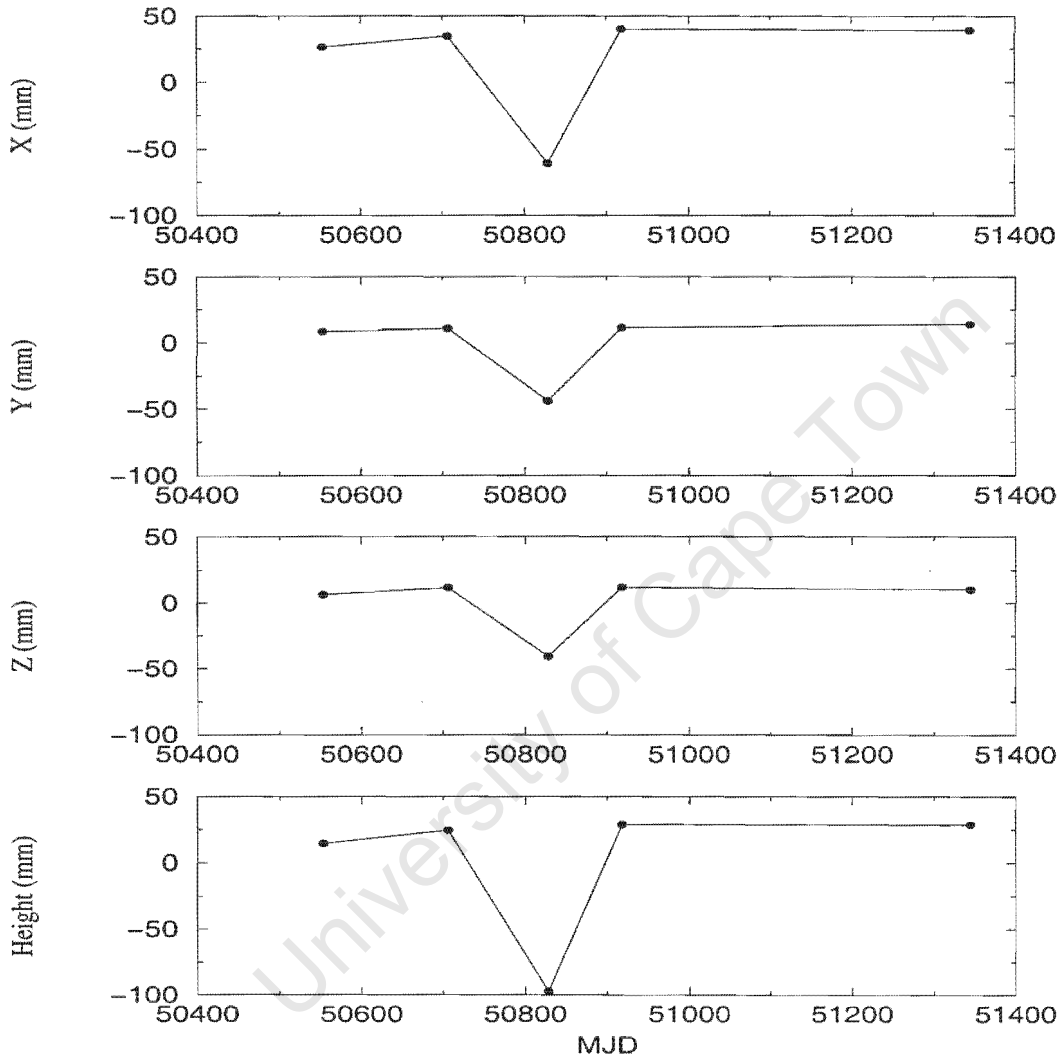

Figure 6.14: Reference point B44: Final adjusted offset plotted geocentric coordinates and offset plotted height. The January 1998 epoch measurements show an unacceptably large deviation.

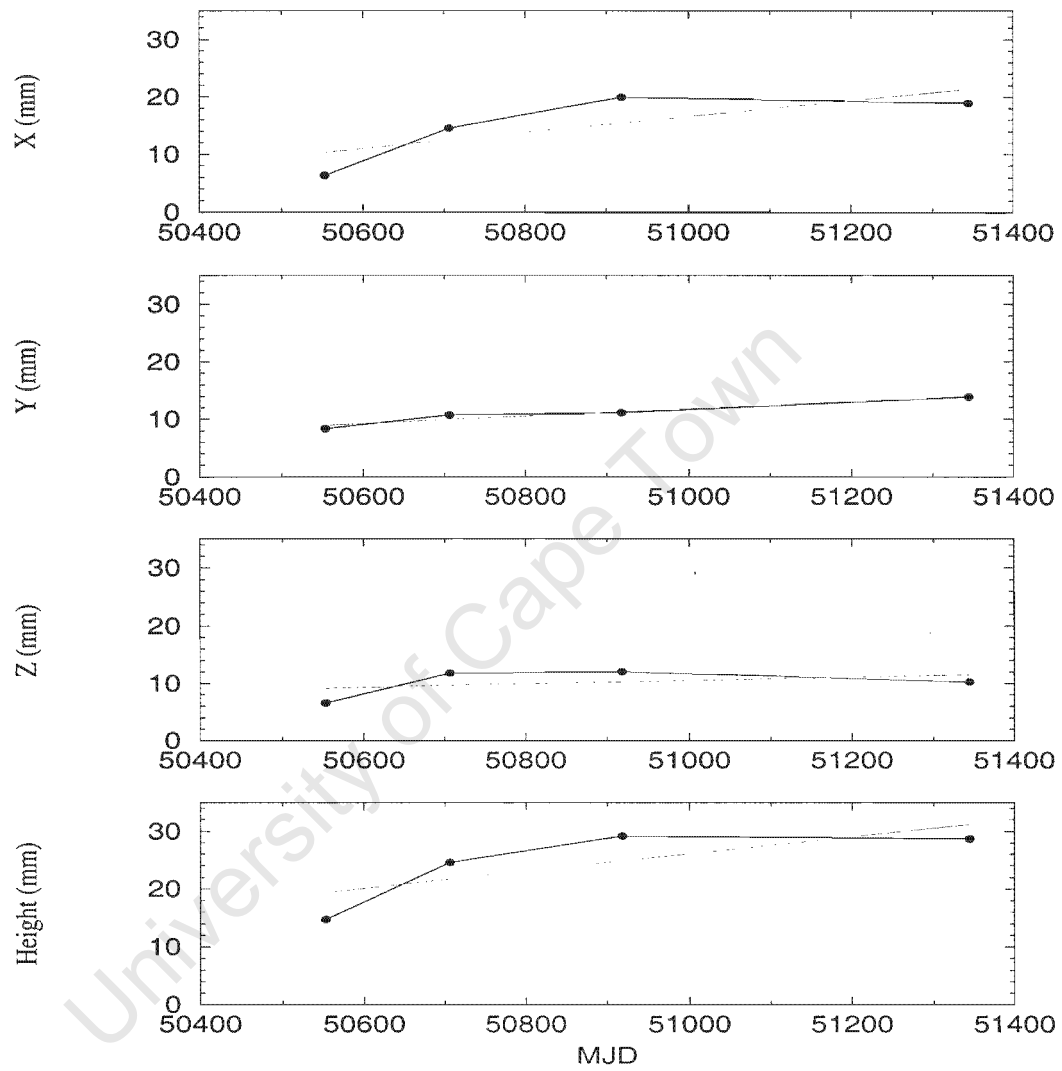

Figure 6.15: Reference point B44: Final adjusted offset plotted geocentric coordinates and offset plotted height. The January 1998 epoch measurements are not included, linear regression indicates expected behaviour of a stable site within measurement limits, although the smooth slopes might be indicative of a local instability.

Chapter 7

Thermally Induced Instabilities

"When different parts of a body are at different temperatures heat flows from the hotter parts to the cooler" - **Carslaw and Jaeger (1959)**

7.1 Introduction

The uppermost layer of the Earth's crust is subject to temperature variations of a periodic nature. Rotation of the Earth on its axis produces daily temperature variation due to the rise and set of the Sun, changes of season produce an annual cycle and longer term thermal cycles such as ice ages are also present. Short period changes result from hot or cold weather fronts, which bring wind, cloud or rain that affects the surface temperature. At any given time, the temperature of the geodetic monument and the surrounding Earth surface is therefore subjected to a combination of these factors which produce thermal variations. In order to verify the results of the thermal and GPS measurements theoretically, a simple distinct element method (DEM) numerical thermal model (NTM) is developed in the Chapter 8 to model the effect of diurnal surface temperature variation and its effect on monument stability. The questions to be answered here is:

- Whether the thermal variations of the Earth's surface are of a large enough magnitude to influence both the short and long term stability of a geodetic monument. Here the approach has been for a monument located on a large (1000 m) diameter rocky outcrop referred to as "Hill 411", 411 being the number of the monument.
- What the magnitude of possible monument movement would be for a given temperature range.
- Whether any permanent geodetic monument position changes are possible due to extreme temperature variations.
- Is it possible to measure these monument positional changes using GPS ?

- What are the implications for footprint and campaign type surveys where individual sessions are of the order of hours, or perhaps several days ?

In this chapter the general setting is described keeping in mind the footprint system approach, followed by a description of instrumentation, data collection, reduction and results. The approach is systematic and is structured as follows:

- The system exogenic input is described, this being solar radiation, and the various processes and factors involved which will determine its overall influence.
- The Earth surface temperature variation is discussed. This has important consequences for geodetic monument stability, as temperature changes have a large effect on horizontal stress, especially if one assumes a uniaxial-strain reference state.
- Sources of stress at the surface is introduced, with emphasis on thermal variations as a source of stress.
- Thermal monitoring of a geodetic monument located on a rocky outcrop is described, including brief overview of instrumentation and software developed to obtain the data.
- Thermal data reduction and GPS data reduction are described.
- Results of thermal and GPS measurements are discussed.
- The implications for footprint and campaign type surveys are discussed.

7.2 Solar Radiation

About half the solar energy that enters the atmosphere consists of light, followed by infrared radiation and a small fraction of ultraviolet radiation. The amount of solar radiation which finally reaches the surface to which our geodetic monument is tied to, is considerably less than the amount per unit area (the solar constant $= 0.135\ W\ cm^{-2}$) which impinges on the outer boundary of the atmosphere. This is mainly due to absorption and scattering as the radiation passes through about 140 km of air, water vapour, dust, and in some areas large amounts of air pollution. More than 70% of incident solar radiation can be reflected by dense clouds. The total solar radiation received by the surface therefore depends on its location, the weather and atmospheric conditions, the inclination of the surface, the time of day and the time of the year, as well as on the variable distance between the Sun and the Earth ($\pm 3.5\%$). The length of the path through which the solar radiation must reach the monument location determines the attenuation of the incident solar radiation, which is in turn determined by the position of the Sun.

The incident radiation upon a surface placed normal to the direction of the radiation from the Sun G_n can then be estimated (Heywood 1956) by

$$G_n = H_{sh}^{top}(0)\tau_a^m \tag{7.1}$$

where $H_{sh}^{top}(0)$ is the solar constant, m the relative air mass (the ratio of the actual path length to the shortest possible path length) and τ_a is the transmission coefficient for unit air mass.

The presence of more water vapour in the air, such as HartRAO experiences during summer, decreases the value of τ_a slightly. A mean value of 0.7 is acceptable for most purposes but could vary from about 0.81 on a clear day to 0.62 when it is overcast (Kreith 1965). The position of the Sun in terms of the zenith distance z (angle between zenith and the direction of the Sun) determines the value of m. As the thickness of the atmosphere is much less than the radius of the Earth, m can be given by secant z, an approximation which is sufficiently accurate for $0 \geq z \leq 80°$. When the surface is horizontal, the incident radiation per unit area G_i is reduced by the cosine of the angle between the direction of the solar radiation (ϑ) and the surface normal, so that

$$G_i = G_n \cos\vartheta \tag{7.2}$$

In terms of time t measured in hours, rotation period of the Earth $T = 24hr$, geographical latitude ϕ, the Sun's declination δ and assuming a non-varying solar constant $H_{sh}^{top}(0)$ as well as a completely transparent atmosphere, one can write (van Wijk and Scholte Ubing, 1966)

$$H_{sh}^{top}(\vartheta) = H_{sh}^{top}(0)[\sin\phi\sin\delta + \cos\phi\cos\delta\cos 2\pi(t - t_0)/T]. \tag{7.3}$$

Here t_0 is a constant which should be chosen so that $H_{sh}^{top}(0)$ has its highest value at true noon, therefore if the difference between true and average noon is neglected $t_0 = 12hr$. Alisow et al. (1956) as quoted by van Wijk and Scholte Ubing (1966) used the following semi-empirical equation which relates irradiancy of the Earth's surface by direct solar radiation ${}_{dir}H_{sh}(\vartheta)$ to optical airmass

$${}_{dir}H_{sh}(\vartheta) = H_{sh}^{top}(\vartheta) \cdot (1 + Cm)^{-1}. \tag{7.4}$$

The state of the atmosphere determines the constant C and is determined experimentally. A value of 0.106 was used in an example by Alisow et al. (1956).

A turbidity factor is often used to account for atmospheric pollution and the influence of the variable atmospheric constituents. The product of this factor and the actual optical air mass results in the apparent optical air mass, which is an atmosphere devoid of pollution and water vapour which would cause the same depletion. This factor's moderate insensitivity to solar altitude makes it suitable for characterising atmospheric conditions.

Table 7.1: Short-wave radiation received on a horizontal surface ($cal\ cm^{-2}\ day^{-1}$ for various latitudes, months and atmospheric conditions. (Bernhardt and Phillips (1958))

	N. Lat.				S. Lat.			
	0	30	60	90	30	60	90	
January	600	350	50	-	715	685	730	
April	605	610	460	350	450	170	-	At the top of
July	560	670	640	690	320	40	-	the atmosphere
October	595	365	70	-	685	630	630	
January	520	290	30	-	630	580	580	Direct radiation
April	535	530	380	225	385	130	-	after correction
July	490	585	545	555	265	25	-	for Raleigh
October	525	305	50	-	605	530	485	scattering
January	360	215	20	-	480	510	-	Direct radiation
April	365	420	320	-	280	110	-	for a turbid,
July	335	430	440	-	195	15	-	cloudless
October	360	220	25	-	470	470	-	atmosphere
January	160	120	10	-	255	130	-	Direct radiation
April	160	230	130	-	140	30	-	for a turbid,
July	145	240	155	-	90	10	-	atmosphere
October	170	130	10	-	225	130	-	and clouds
January	260	160	10	-	350	270	-	
April	260	310	150	-	210	70	-	Total global
July	240	340	275	-	150	20	-	radiation
October	270	230	60	-	290	190	-	

Ranges of turbidity factors used by Alisow et al. (1956) are:

- equatorial latitudes 3.4 - 6.7
- 8 metropolitan areas 3.1- 4.3
- low country in Europe and the U.S.S.R. 2.1 - 3.5
- mountains 1.8 - 2.7

Some of the results obtained by Bernhardt and Phillips (1958) as quoted by van Wijk and Scholte Ubing (1966) are given here in Table 7.1. The total global radiation is the sum of the irradiancy of a unit of horizontal surface due to direct solar radiation and diffuse short wave radiation due to dust, clouds and molecular scattering from all parts of the sky. Optical air mass and the state of the atmosphere, especially its cloud content, dust, pollutants and water vapour causes the ratio of diffuse to direct radiation to vary greatly. The values given

Table 7.2: Reflection factors of natural surfaces likely to be found at a geodetic site (adapted from van Wijk and Scholte Ubing (1966))

Surface	Percentage reflection
granite	15
fresh snow	80-85
compressed snow	70
melting snow	30-65
quartz sand	35
wet sand	9
dry sand	18
bare fields	12-25
green grass	16-27
dry grass	16-19
wet prairie	22
dry prairie	32
desert, midday	15
desert, low solar altitude	35

in Table 7.1 immediately indicates implications for the thermal environment of a geodetic monument, based on its location and assuming all other factors (reflection and absorption factors) being equal. In general, over any given year, we would expect smaller temperature excursions from the mean at the lower latitudes. The larger variation in radiation received by higher latitudes indicate a possible higher difference in minimum and maximum temperatures. This is just a general indication, as other factors at the geodetic site will influence the Earth's surface temperature, but nevertheless, lower latitudes should tend towards higher thermal stability.

7.2.1 Reflection at the Earth's Surface

One factor which will influence surface temperature to a certain extent is reflection. Reflection of incident solar radiation varies greatly with the type of rock or other surface material exposed to the Sun. Reflection can even affect the local climate, for instance the low reflection factor of a water surface and absorption of short wave radiation in a deep water layer results in a large amount of solar energy being stored in the water which acts as a moderating influence on local climate. The portion of energy not reflected by the surface is absorbed and converted to thermal energy, leading to an increase in temperature of the surface. Seasonal changes of the reflection factor can lead to aggravation of the expected temperature changes, for instance the reflection off dry dark clay is at least twice that of wet dark clay. At the HartRAO site for instance, this will decrease the temperature of some of the site surface which is devoid of vegetation and contains a high percentage of a dark clay which is

bound to be dry, as the site has none or very little ($< 5\ mm$) winter rainfall. Table 7.2 lists reflection factors for various natural surfaces likely to be found at a geodetic site. On Hill 411, rock surface temperatures are quite different depending on the albedo of the rock, with very dark rock having surface temperatures up to ten degrees warmer than adjacent, but lighter coloured rock. The reflection factor for the Earth as a whole is its albedo, with a value of about 0.43. The Earth's emission characteristics allows it to be considered as a black body with surface temperature of approximately 280 K and emits radiation of much longer wavelength than the incident solar radiation.

7.2.2 Absorption at the Earth's Surface

It is to be expected therefore that the natural surfaces of the Earth should have high values of absorption factor, which is listed in Table 7.3. The absorptivity α of a surface depends on the factors which affect its emissivity and on the quality of the incident radiation, measured by its distribution in the spectrum. Kirchhoff's law shows that the emissivity of a surface at temperature T is equal to the absorptivity α exhibited by the surface for black radiation from a source at the same temperature. Therefore a surface which is a poor absorber will also be a poor emitter. The emissivities of most nonmetals are above 0.8 at low (non-furnace) temperatures and if α is a constant independent of the spectral energy distribution of the incident radiation, emissivity ϵ can be substituted for α (McAdams 1954). This is applicable even if there is a temperature difference between the incident radiation and the surface. One can therefore expect that surface surrounding the geodetic monument will have high emission and absorption characteristics, which will lead to temperature variations upon removal of or variations of the source of heat. The atmosphere is not highly transparent to radiation from the Earth, in contrast to solar radiation, but radiation from the Earth is mostly absorbed by water vapour, clouds and CO_2. Water vapour leads to a window of partial transparency (at 10 μ) which is largely responsible for the radiant heat loss which results in cooling of the Earth during clear nights. CO_2 absorbs less long wave radiation than water vapour and is partially transparent at 10μ. Absorption by clouds is the strongest, a cloud of 50 m thickness being basically opaque for long wave radiation, even if it contains only 1 gram of liquid water per cubic metre, which gives a total water thickness of only 0.05 mm (van Wijk and Scholte Ubing, 1966).

7.3 Earth Surface Temperature Variation

In order to understand the periodic nature of surface temperature variation, we can approach the problem from a physicist's viewpoint. This approach also allows the step by step explanation of terms and concepts which might not

Table 7.3: Absorption factors α of natural surfaces for long wave radiation: After van Wijk and Scholte Ubing (1966)

Surface	α
sand(dry-wet)	0.95-0.98
mineral soil (dry-wet)	0.95-0.97
peat (dry-wet)	0.97 -0.98
firs	0.97
trees	0.96
grass	0.96-0.98
leaves	0.94-0.98
water	0.95
snow	0.97

necessarily be in the field of geodesy. It is therefore convenient to consider a model system as a starting point. This system possesses properties which are required for vibrational behaviour, and no others. Starting with this simple model, we shall be able to model the more complicated physical system of Earth surface temperature variation. One typical approach in physics text books (see for instance Bickley and Talbot 1961; and Main 1978) is to use a model system consisting of a mass m attached to one end of a helical spring, the other end of the spring is fixed. Appendix (A) describes the basics of harmonic motion and methodically develops the equation which we will use as a starting point for our thermal model.

7.3.1 Periodic Variation of the Earth's Surface Temperature

Kelvin's classical work (Kelvin 1861) describes the analysis of 18 years of data and resulted in the harmonical analyses of the yearly mean temperature curves. The following section is based on an example by Fowler (1990) which we adopt and freely modify and expand to suit the requirements of our model. Similar examples can be found in (Carslaw and Jaeger 1947), (Ingersoll et al. 1955) and (Carslaw and Jaeger 1959) using slightly different mathematical approaches. Using the solution for harmonic motion in the form as derived in Appendix A, section (A.21) one can model the periodic variation in the surface temperature of the Earth as $T_0 e^{i\omega t}$. Here T_0 is the maximum variation of the mean surface temperature, i is the square root of -1, ω is the product of 2π and the frequency of the temperature variation. The temperature is a function only of time t and depth z so our starting point is the Fourier conduction equation

$$\frac{\partial T}{\partial t} = \kappa \nabla^2 T \tag{7.5}$$

The constant κ is the thermal diffusivity. The Fourier conduction equation can be written in one dimension as the one-dimensional heat conduction equation

$$\frac{\partial T}{\partial t} = \frac{k}{\rho c_p}\frac{\partial^2 T}{\partial z^2} + \frac{A}{\rho c_p} \tag{7.6}$$

to determine the temperature $T(z,t)$. We can set A to zero, which is the rate per unit volume per unit time of heat generated. The Earth surface density is ρ and has specific heat c_p, T is the surface temperature and t is time. The thermal conductivity is denoted by k. In order to use equation (7.6) we define two boundary conditions:

(1) $T(0,t) = T_0 e^{i\omega t}$ and
(2) $T(z,t) \to 0$ as $z \to \infty$.

The separation of variables technique can be used to solve this problem and we assume that the variables z and t can be separated so that one can write

$$T(z,t) = V(z)W(t) \tag{7.7}$$

We presuppose that the periodic nature of the temperature variation will be the same for different depths below the surface as it is at the surface. The magnitude and phase of the temperature variation however is dependent on the depth below the surface. After substituting (7.7) into equation (7.6), with A set to zero, one has

$$V\frac{dW}{dt} = \frac{k}{\rho c_p}W\frac{d^2V}{dz^2} \tag{7.8}$$

which one can rearrange to

$$\frac{1}{W}\frac{dW}{dt} = \frac{k}{\rho c_p}\frac{1}{V}\frac{d^2V}{dz^2} \tag{7.9}$$

If one substitutes equation (7.7) into the boundary condition (1) and (2), one finds for condition (1); $W(t) = e^{i\omega t}$ which shows that c_2 is T_0, and for condition (2); $V(z) \to 0$ as $z \to \infty$ which shows that the positive exponential solution is not permitted. The left-hand side of equation (7.9) is only a function of z and the right-hand side only of t and therefore both sides must equal a constant c. Considering boundary condition (1) the constant c must equal $i\omega$ and substituting $W(t) = e^{i\omega t}$ into equation (7.9) results in

$$\frac{d^2V}{dz^2} = \frac{i\omega\rho c_p V}{k} \tag{7.10}$$

which is the equation to be solved for $V(z)$. Equation (7.10) has two solutions:

$$V(z) = c_2 e^{-qz} + c_3 e^{qz} \tag{7.11}$$

where $q = (1+i)\sqrt{\omega\rho c_p/2k}$ and c_2 and c_3 are constants. Therefore $T(z,t)$ is given by

$$T(z,t) = T_0 e^{i\omega t} e^{(-(1+i)\sqrt{\frac{\omega\rho c_p}{2k}}Z)} \tag{7.12}$$

thus

$$T(z,t) = T_0 e^{(-\sqrt{\frac{\omega\rho c_p}{2k}}z)} e^{(i(\omega t - \sqrt{\frac{\omega\rho c_p}{2k}}z))} \tag{7.13}$$

It is obvious that the greater the depth the more the periodic variation is dampened. At a depth (called the *skin depth*) of

$$L = \sqrt{\frac{2k}{\omega\rho c_p}} \tag{7.14}$$

the amplitude of the periodic variation is $1/e$ of the amplitude at the surface. The maximum variation of the temperature at any point z below the surface will be the peak-to-peak amplitude (twice the amplitude). One can therefore write

$$T_r(z,t) = T_0 e^{(-\sqrt{\frac{\omega\rho c_p}{2k}}z)} \tag{7.15}$$

where T_0 is the amplitude (or half the total range) at the surface. There is a phase lag ϕ between the temperature at the surface and the temperature at depth z which from equation (7.13) can be seen to be

$$\phi = \sqrt{\frac{\omega\rho c_p}{2k}}z \tag{7.16}$$

The phase lag is one radian at skin depth and when the phase lag is π, the temperature at depth z is in anti-phase with the surface temperature. The phase lag can for the sake of convenience be written in another form as described by Ingersoll et al. (1955). We have $\kappa = K/\rho c$ defined by Kelvin as the diffusivity and use the definition here for mathematical convenience. The time of maxima or minima temperature at any depth z is given by (Ingersoll et al. 1955)

$$\omega t - z\sqrt{\frac{\omega}{2\kappa}} = (2n+1)\frac{\pi}{2} \tag{7.17}$$

which can be rewritten as

$$t = \frac{z\sqrt{\omega/2\kappa} + (2n+1)\pi/2}{\omega} \tag{7.18}$$

where odd values and even values of n gives minima and maxima respectively. If the surface minima occurs at $\omega t = 3\pi/2$ then if z and t are both supposed to increase so that

$$\omega t - z\sqrt{\frac{\omega}{2\kappa}} = \frac{3\pi}{2} \tag{7.19}$$

this minimum will be propagated into the Earth's surface to reach any depth z at the time determined by this equation. This is at some time t_1 later than its occurrence at the surface. The lag is then described by

$$t_1 = z\frac{1}{2\kappa\omega} \tag{7.20}$$

therefore

$$t_1 = \frac{z}{2}\sqrt{\frac{P}{\pi\kappa}} \tag{7.21}$$

where P is the period. This same approach is valid for maximum, zero or any other phase. The apparent velocity of such a wave in the surface of the Earth is derived from equation (7.21) so that

$$V = \frac{z}{t_1} \tag{7.22}$$

so that

$$V = 2\sqrt{\frac{\pi\kappa}{P}} \tag{7.23}$$

This has obviously nothing to do with the actual speed with which the heat energy is transmitted but describes the rate at which a given maxima or minima may be said to travel. It (equation 7.23) does however aid in deducing a further useful expression for the wave length of such a wave which can be written as

$$\lambda = VP = 2\sqrt{\pi\kappa P} \tag{7.24}$$

The equations for lag, apparent velocity and wavelength can be used to determine the diffusivity of the surface below our geodetic reference point. A diffusivity of $\kappa = 0.01$, a typical value for rock material, will result in a wavelength of about 2.7 cm for a frequency of 1 cycle/min, 1 m for 1 cycle/day and 20 m for 1 cycle/year (Carslaw and Jaeger 1959).

7.4 Sources of Stress Near the Surface

There are four major sources of stress in rock close to the surface which might affect geodetic monument stability. The components of the in situ stress field which leads to deviation from a reference state due to natural processes include near-surface thermal stresses induced by the diurnal thermal cycle, residual, tectonic and gravitational stresses. In this work the research concentrated on thermal stresses and its effect on monument stability, however a short introduction is given to residual, gravitational, and tectonic stresses as they should not be ignored in certain instances. More in depth detail can be had from Coates (1964), Artyushkov (1973), Greiner and Illies (1977), Holtzhausen and Johnson (1979), McNutt (1980), Fleitout and Froidevaux (1983), Bott and Kusznir (1984), Engelder and Sbar (1984) and Zoback et al. (1989).

- **Residual stresses**
  In a rock body, a metastable stress condition in absence of external stresses is created during plastic deformation resulting from overburden weight, original crystallisation, thermal gradients and tectonic pressures. These residual stresses may cause instability, buckling and fracture propagation when the metastable state is disturbed by removal of overburden or confining stresses.

- **Gravitational stresses**
  The weight of a column of rock above a specific point in the rock induces gravitational stress at that point. Vertical stresses due to gravity could lead to horizontal stresses as rock expands in directions perpendicular in response to applied compressive stress, as described by Poisson's ratio.
- **Tectonic stresses**
  Tectonic stress in general consists of the horizontal components of the in situ stress field which are a deviation from a reference state due to natural processes from local to platewide scales. The literature seems to have different approaches to what exactly should be regarded as tectonic stress. The near-surface thermal stress, stress due to topographic loading and unloading due to erosion, as well as thermoelastic loading processes resulting in local stresses, are not tectonic and tectonic stresses should probably be seen as those stresses which result from plate-scale boundary tractions. Tectonic stresses are important in areas of converging and diverging lithospheric plates.

7.4.1 Thermally Induced Stresses

The rocks near the surface undergo large variations in thermal stress due to the diurnal and annual temperature cycles. As discussed the temperature and therefore the thermal stresses are periodic and are related to surface temperature by the function (Carslaw and Jaeger 1959)

$$T_z = T_s \exp(-\frac{z\sqrt{\pi}}{kt}) \tag{7.25}$$

where T_z is the temperature variation ($^\circ C$) at depth z (cm), T_s is the total temperature variation about the mean at the surface ($^\circ C$), k is the diffusivity constant (cm^2/sec) and t is the period in seconds. If the boundaries of the rock mass behave in uniaxial strain then the horizontal stress induced by the temperature variation is given by Hooker and Duvall (1971)

$$\Delta S_h^T = \frac{\alpha_t E(T_1 - T_0)}{1 - \nu} \tag{7.26}$$

where ΔS_h^T represents the horizontal stress due to the temperature variation (MPa) and $T_1 - T_0$ is the change in temperature. E is Young's modulus (Appendix A, Equation A.31) and ν is Poisson's ratio (Appendix A, Equation A.33). If a rock body is in a uniform state of stress, existing joints will not open nor will new joints develop. Far below the surface unbalanced compressive stressses will also not lead to joint development due to confinement experienced by the rock. However, unbalanced compresssive stresses near the surface of a rock body could result in areas of tension. Apart from compressive stress, other factors such as dehydration and tectonic processes, or as in the main focus of this discussion, thermal processes, could lead to stresses which could

Table 7.4: Rock properties determined in uniaxial compression and indirect tensile tests (after Wuerker (1955),D'Andrea et al. (1965), CRC Handbook of Chemistry and Physics (1993)

Rock type	Density $\rho\ (kg/m^3)$	Thermal conductivity $(W/m \cdot K)$	$E(10^5\ (MPa)$	ν	$\sigma_c\ (MPa)$	Tensile strength (MPa)
Granite	2640-2760	2.79	0.55-0.9	0.21-0.28	210	9-13
Gabbro	-	-	1.05	0.34	200	22
Basalt	2400-3100	-	1	0.28	290	16
Marble	2600-2840	2.80	1.1	0.28	250	15
Limestone	2680-2760	2.15	0.2-0.9	0.23-0.20	30-180	2.1-10
Sandstone	2140-2360	2.90	0.02-0.7	0.3-0.4	10-42	0.3-1.1
Chalk	1900-2800	-	0.05-0.7	0.4	15-19	0.5-0.9

exceed the tensile strength of the rock. Fracture propagation could then lead to joint formation. Typical rock properties determined in uniaxial compression and indirect tensile tests are given in Table 7.4.

During a project to improve their understanding of thermal stresses, Hooker and Duvall(1971) installed temperature transducers in granite quarries and found a diurnal temperature variation of 12.1 $^\circ C$ was measureable to a depth of 65 cm. Very similar results were obtained in thermal measurements obtained on the exposed andesite of Hill 411 at HartRAO. These temperature changes can result in a thermal stress of several MPa. If the tensile strength of the rock is exceeded this will facilitate crack propagation, especially close to the rock surface where the temperature variation is larger. Hooker and Duvall (1971) found that the annual thermal stress at depth $z = 30\ cm$ was 7.9 MPa, in close agreement with values obtained determined using equation 7.26.

Some rocks have a tensile strength of only 10 MPa, which indicates that crack propagation, and consequent geodetic monument instability due to thermal variations is not a matter to discard. A complete mathematical treatment of crack propagation under thermal stress is given by Kassir and Sih (1975). Although beyond the scope of this work, it is worth noting that having a free boundary on the surface, causes local stresses to be greater than those of a crack in an infinite medium. Local stresses increase with a decrease in distance between the free boundary and the crack.

Vertical stress components with depth determined over a range from the surface to a depth of 2400 m show a magnitude change of between zero to 100

MPa and the vertical stress component has a spread about a mean value given by Herget (1988) as

$$\sigma_V = (1.87 \pm 1.23\ MPa + (0.026 \pm 0.00278)\ Mpa/m \qquad (7.27)$$

Horizontal stress components are much more scattered, with cases where the horizontal stress component is larger than, or in some cases less than the vertical stress component. Herget (1988) used a typical population of stress components based on world data, to obtain sub-populations, which indicates three relationships:

(1) $\sigma_H < \sigma_V$, e.g. Scandinavia

(2) $\sigma_H = \sigma_V$, e.g. South Africa

(3) $\sigma_H > \sigma_V$, prevailing, with

$$\sigma_H = (8.17 \pm 0.54\ MPa + (0.0417 \pm 0.00229)\ Mpa/m \qquad (7.28)$$

Herget (1988) indicates that, in general, horizontal stresses are higher than vertical stresses. What concerns us most, is that horizontal stresses are markedly high ($\approx 10\ MPa$) at the surface. If additional stress is added due to thermal stress, the near-surface layer of rock is definitely subjected to de-stabilising forces, which will either attempt to cause periodic movement of the rock and the monument attached to it, or in some cases permanent movement due to crack propagation or even failure.

7.5 Thermal Monitoring of Geodetic Monument Site

The site chosen for thermal measurements is a typical rocky outcrop on the Witwatersberg, equipped with a standard trig beacon on its highest point. A total of 12 thermal transducers were installed at this site (Figure E.5, Appendix E). Most of the transducers were located in the rock, just below the surface, at a depth of approximately 7 cm. The transducers were located in a rough circle centred on the trig beacon as it was thought that differential heating would lead to monument tilt which might be noticed in the data; this was not found. If there is such a signal present, it was below the threshold of detection. One transducer was located at the surface of the rock, but not exposed to direct sunlight. This transducer was used to provide the ambient surface temperature used in this study. The monument 411 is located on the southern edge of the hill, therefore it should exhibit lateral movement towards the south if thermal expansion is present. The monument should exhibit very little and probably immeasurable vertical motion resulting from thermal expansion, especially on a daily basis as the damping depth is not much more than 70 cm

for a diurnal thermal cycle at the location of 411. If the hill was solid rock, with no cracks and fissures, a diurnal rock temperature variation of $20°C$, assuming an expansion coefficient of 1×10^{-6}, would lead to expansion values with an amplitude of 10 mm. However, the adjacent rock blocks are not always in contact, or have a softer filler occupying the space between rocks. To complicate matters further, different rock blocks, even if they are adjacent exhibited different surface temperatures. This is expected as their albedo and inclination as well as size differs. The rock surface temperature achieves much higher values than the ambient temperature, $20°C$ higher not being uncommon. Considering the complexity of a real hill, the ambient temperature close to the surface was used to investigate the GPS results for possible thermal expansion. The expected amplitude in slope distance, i.e. the distance to SLR was therefore not possible to calculate numerically unless a large number of assumptions were made. These assumptions are discussed in Chapter 8.

7.5.1 Instrumentation

Thermal Transducers

The interaction of a thermal transducer with the surrounding rock is strongly governed by its properties and construction. The design of its packaging therefore needs careful consideration as some of the thermal interaction between the sensor and its packaging, as well as with the attached signal line could result in errors in the temperature measurement. The sensitivity and accuracy has to be maximised while the influence of other effects has to be minimised. In a temperature transducer the thermal signal is the transducer temperature induced in the transducer material by the package in which the sensor is mounted. This package material could create problems and these have to be minimised. The main problems are:

(1) Self-heating

(2) Good thermal contact with the rock

(3) Isolation from the environment

Self-heating This occurs if the transducer requires electrical power to function. This power is converted to heat and affects the temperature of the transducer leading to an artificial signal. This effect can be reduced if there is sufficient thermal contact between the transducer, its packaging and the surrounding rock.

Thermal contact Good thermal contact with the rock is important as any impurities in the hole in which the transducer is to be located, will provide thermal insulation of some sort. The drilled hole must therefore be cleaned of

any debris that has fallen into the hole during the drilling process, so that when the transducer is inserted, there will be good contact between the packaging material and the rock. The drill size must be chosen so that the sensor must fit fairly tightly in the hole, but one must still be able to push the sensor to refusal which allows the tip of the sensor to have contact with the rock as well as the sides.

Isolation from the environment The transducers close to the surface of the rock are mounted in holes only 7 cm deep. If there is inadequate heat conduction between the transducer and its packaging, there could be errors resulting from temperature changes in the atmosphere leaking along the signal line. This effect can be reduced by specifying a minimum depth in the rock. The complete sensor (transducer mounted in package) must have a minimum length and a thermal conducting paste, such as aluminium oxide (Al_2O_3) should be used between the transducer and its packaging. The signal line itself can be chosen to minimise its heat absorbing properties and thermal conductance. In this study we used electrical cable which is very well insulated, consisting of a white outer plastic wrapping, followed by an aluminium sheath, a plastic foam layer and then two lines of plastic clad solid copper wire. The top of the hole must be sealed after installation of the sensor with silicon or other suitable sealant to avoid the ingress of water. A general technical description of the telemetry equipment is presented in Appendix I.

7.5.2 Decoding and Data Capture Software

Software was written in the course of this study to allow the transmitted frequency shift keyed (fsk) temperature data to be logged on a computer. Only a brief description is given of the software and then only of its main functions. The code was written using C++. The main functions of the program (aptly named DECODER) are:

- File handling functions for data storage.
- Interface PC and PC14B I/O card.
- Interface between I/O card and decoder hardware.
- Interpret encoded data from bitstream to temperature values and channel number.
- Graphically display incoming data on 8 simultaneously displayed plots.
- Filter each channel received data through a median filter.
- Control an audio tape recorder for backup purposes if required.
- Time tag data with MJD.
- Monitor transmitter battery voltage, sound alarm if voltage drops below preset value.

7.5.3 Thermal Data Reduction

A procedure had to be developed to generate $\Delta x, \Delta y, \Delta z$, slope distance, height, and temperature as a function of MJD for GPS and the simultaneous thermal measurements. Some of this was very laborious as the GPS software package was not versatile enough in its output specifications. The steps are documented in Appendix B. Basically the measured temperature and time data is fitted using a nonlinear regression algorithm, which determines parameters such as phase, amplitude, period and other parameters required to uniquely describe thermal data as a function of time. The parameters are optimised by sweeping through a range of some of the parameters, in a least squares approach. Using the optimised parameters, the temperature is predicted to match the time series of the GPS observations, which then allows further processing and correlation. The procedure is documented in the appendix for the sake of having a record of the steps involved, any other similar approach using other, suitable software should deliver the same results.

7.5.4 Results of Thermal and GPS Measurements

Four separate sets of GPS data were accumulated in order to investigate possible reference point instability resulting from thermal expansion of Hill 411. These data sets were named A, B, C and D and are discussed in chronological sequence and are located in Appendix E as Table E.1 to Table E.4. Appendix E also contains plots of the x, y and z vector components, fitted sinusoidals and residuals for all four data sets, as Figure E.6 to Figure E.17. All the data sets were collected using the same antenna and receivers at each reference point. One receiver occupied the SLR pad and one receiver occupied the monument 411. Data was processed using broadcast ephemeris. The antennae were not disturbed during the sessions to reduce possible re-occupation errors. Receivers were Trimble 4000SEs and the antennae Trimble compact dome. Elevation masks were set at 15 degrees and sampling rate at 30 seconds interval. Only two receivers were available so processing was similar for a radial survey using GPSurvey. In order to make the text reasonably easy to read, figures not contained in Appendix E, relating to the different data sets are located at the end of this chapter.

Table 7.5: Data set A; 411, statistical summary, 38 two hour sessions

Variable	Minimum value	Maximum value	Mean value	σ
X (m)	470.8482	470.8644	470.8575	0.0039
Y (m)	760.4411	760.4505	760.4472	0.0027
Z (m)	1185.436	1185.442	1185.438	0.0017
Height (m)	175.515	175.5331	175.526	0.0047
Distance (m)	1485.005	1485.012	1485.009	0.0018
Temperature (deg C)	17.09138	34.4172	25.79512	5.662

Data set A

Figure E.1 (Appendix E) contains plots (A) of the surface temperature as a function of time (days), (B) a sinusoid as fitted to the thermal data, and (C) the residuals of the fit for data set A. The amplitude for this data set is $7.6°C$ and the period 1.0005 days. Although the period here is very close to 24 hours, thermal data can vary in such a way that especially for short data spans, the thermal period can swing either side of 24 hours. When several days are fitted in succession, the fitted period rapidly converges to a 24 hour period as would be expected. The proportion of variance explained by a simple sinusoidal fit for data set A is 0.87, indicating that although not exact, a simple sinusoid is a fair approximation to the diurnal thermal cycle. The simple sinusoid is useful in determining the period and phase of the thermal signal, no attempt is made to fit any amplitude. Here we only use the sinusoidal (with linear trend) fit to detect a possible thermal signature. Figure 7.3 clearly shows that the repeatability between data points are fairly good, but the sinusoidal signal is hidden in the noise to a large extent. Maximum deviation for any distance observation is 3.4 mm. The proportion of variance explained is $R^2 = 0.3966$ (39.66%), which on its own is not sufficient to support the postulate that a sinusoidal signal which represents thermal expansion is present. What we will have to ascertain is whether for a significant number of the datasets, the correlation between distance and diurnal temperature variation indicates a thermal signature.

It is clear however that there is some signature present, as the data is not distributed in a random way centred on a straight line. The fitted amplitude is 1.18 mm and the period 0.9 days. The distance shows a negative correlation (-0.27) with temperature, which even if the thermal signature is small indicates a diurnal expansion effect. A statistical summary of the variables are given in Table 7.5. Table 7.6 contains the correlations between the variables (raw data) and Table 7.7 contains the correlations between the sinusoidal fitted data and temperature. The z component has mostly the same negative correlation value as the distance, which is expected, the other variables show very little

correlation with the surface temperature. Figure 7.4 indicates some sinusoidal effect, but this is probably due to the approximately 24 hour repetition of the satellite geometry, which can markedly affect the vertical component.

Table 7.6: Data set A; 411, raw data correlations, 38 two hour sessions

Variable	X	Y	Z	Height	Distance	Temp.
X	1.000	0.901	-0.740	0.988	0.816	-0.065
Y	0.901	1.000	-0.679	0.938	0.870	-0.042
Z	-0.740	-0.679	1.000	-0.806	-0.286	-0.270
Height	0.988	0.938	-0.806	1.000	0.789	-0.008
Distance	0.816	0.870	-0.286	0.789	1.000	-0.270
Temperature	-0.065	-0.042	-0.270	-0.008	-0.270	1.00

Table 7.7: Data set A; 411, fitted correlations, 38 two hour sessions

Variable	X	Y	Z	Height	Distance	Temp.
X	1.000	0.411	-0.227	0.991	0.893	-0.302
Y	0.411	1.000	-0.872	0.496	0.503	0.223
Z	-0.227	-0.872	1.000	-0.281	-0.238	-0.458
Height	0.991	0.496	-0.281	1.000	0.902	-0.258
Distance	0.893	0.503	-0.238	0.902	1.000	-0.545
Temperature	-0.302	-0.223	-0.458	-0.-0.258	-0.545	1.00

Data Set B

Data set B has 32 observations and the proportion of variance explained by the sinusoidal fit to the distance data is $R^2 = 0.4008$ (40.08%). Maximum deviation for any data point is 3.4 mm. The fitted amplitude is 1.3 mm and the period 1.0007 days. A statistical summary of the variables are given in Table 7.8 and Table 7.9 contain the correlations between the variables and Table 7.10 the correlations between the sinusoidal fitted and temperature data. Figure E.2 (Appendix E) contains plots (A) of the surface temperature as a function of time (days), (B) a sinusoid as fitted to the thermal data, and (C) the residuals of the fit for data set B.

Table 7.8: Data set B; 411, statistical summary, 32 two hour sessions

Variable	Minimum value	Maximum value	Mean value	σ
X (m)	470.8424	470.853	470.8468	0.0029
Y (m)	760.4384	760.4461	760.4417	0.0018
Z (m)	1185.441	1185.448	1185.445	0.0017
Height (m)	175.5072	175.5198	175.5123	0.0034
Distance (m)	1485.005	1485.012	1485.008	0.0016
Temperature (deg C)	11.926	26.851	18.763	4.9

Table 7.9: Data set B; 411, correlations, 32 two hour sessions

Variable	X	Y	Z	Height	Distance	Temp.
X	1.000	0.762	-0.479	0.965	0.606	-0.286
Y	0.762	1.000	-0.459	0.848	0.624	-0.389
Z	-0.479	-0.459	1.000	-0.656	0.327	-0.236
Height	0.965	0.848	-0.656	1.000	0.481	-0.229
Distance	0.606	0.624	0.327	0.481	1.000	-0.604
Temperature	-0.286	-0.389	-0.236	-0.229	-0.604	1.00

Table 7.10: Data set B; 411, fitted correlations, 32 two hour sessions

Variable	X	Y	Z	Height	Distance	Temp.
X	1.000	0.887	-0.677	0.990	0.445	-0.240
Y	0.887	1.000	-0.383	0.841	0.729	-0.598
Z	-0.677	-0.383	1.000	-0.771	0.290	-0.471
Height	0.990	0.841	-0.771	1.000	0.330	-0.124
Distance	0.445	0.729	0.290	0.330	1.000	-0.949
Temperature	-0.240	-0.598	-0.471	-0.124	-0.949	1.00

Table 7.11: Data set C; 411, statistical summary, 25 two hour sessions

Variable	Minimum value	Maximum value	Mean value	σ
X (m)	470.843	470.856	470.8478	0.0032
Y (m)	760.4389	760.4463	760.4425	0.0018
Z (m)	1185.439	1185.446	1185.443	0.0024
Height (m)	175.508	175.5239	175.5143	0.0039
Distance (m)	1485.003	1485.011	1485.007	0.0019
Temperature (deg C)	17.85886	37.96152	28.52683	6.58

Data Set C

Data set C has fewer observations than sets A, C and D at 25, and the proportion of variance explained by the sinusoidal fit to the distance data is $R^2 = 0.4317$ (43.17%). Maximum deviation for any data point is 3.3 mm. The fitted amplitude is 1.7 mm and the period 0.9959 days. A statistical summary of the variables is given in Table 7.11. Table 7.12 contains the correlations between the variables and Table 7.13 the correlations between the sinusoidal fitted and temperature data. Figure E.3 (Appendix E) contains plots (A) of the surface temperature as a function of time (days), (B) a sinusoid as fitted to the thermal data, and (C) the residuals of the fit for data set C.

Table 7.12: Data set C; 411, correlations, 25 two hour sessions

Variable	X	Y	Z	Height	Distance	Temp.
X	1.000	0.823	-0.548	0.971	0.377	0.002
Y	0.823	1.000	-0.377	0.844	0.538	0.058
Z	-0.548	-0.377	1.000	-0.707	0.536	-0.444
Height	0.971	0.844	-0.707	1.000	0.210	0.135
Distance	0.377	0.538	0.536	0.210	1.000	-0.415
Temperature	0.002	0.058	-0.444	0.135	-0.415	1.00

Table 7.13: Data set C; 411, fitted correlations, 25 two hour sessions

Variable	X	Y	Z	Height	Distance	Temp.
X	1.000	0.961	-0.268	0.699	-0.046	0.148
Y	0.961	1.000	-0.202	0.649	0.045	0.217
Z	-0.268	-0.202	1.000	-0.370	0.887	-0.648
Height	0.699	0.649	-0.370	1.000	0.001	-0.073
Distance	-0.046	0.045	0.887	0.001	1.000	-0.714
Temperature	0.148	0.217	-0.646	-0.073	-0.714	1.00

Data Set D

Table 7.14: Data set D; 411, statistical summary, 25 two hour sessions

Variable	Minimum value	Maximum value	Mean value	σ
X (m)	470.8376	470.8543	470.8453	0.0036
Y (m)	760.435	760.4452	760.4405	0.0027
Z (m)	1185.442	1185.45	1185.446	0.0019
Height (m)	175.5014	175.5209	175.5101	0.0042
Distance (m)	1485.004	1485.012	1485.008	0.0021
Temperature (deg C)	15.6041	29.65367	22.4815	4.69

Data set D has 36 observations, the proportion of variance explained by the sinusoidal fit to the distance data is $R^2 = 0.5721$ (57.21%). Maximum deviation for any data point is 3.7 mm. The fitted amplitude is 2.2 mm and the period 1.0000 days. A statistical summary of the variables are given in Table 7.14. Table 7.15 contains the correlations between the variables and Table 7.16 the correlations between the sinusoidal fitted and temperature data. Figure E.4 (Appendix E) contains plots (A) of the surface temperature as a function of time (days), (B) a sinusoid as fitted to the thermal data, and (C) the residuals of the fit for data set A.

7.6 Final Results and Conclusions

Figure 7.1 contains plots of the correlation with temperature of all the vector components (SLR to 411) including height and distance. Figure 7.1 is based on correlation of the raw data with temperature. Although the z component should be highly correlated with distance, data sets B and D shows a deviation from the expected. This is partially due to the fact that this correlation is between the raw GPS data point vectors, which is noisy. Figure 7.2 similarly

Table 7.15: Data set D; 411, correlations, 25 two hour sessions

Variable	X	Y	Z	Height	Distance	Temp.
X	1.000	0.654	-0.470	0.961	0.614	-0.530
Y	0.654	1.000	-0.341	0.789	0.745	-0.418
Z	-0.470	-0.341	1.000	-0.619	0.260	-0.178
Height	0.961	0.789	-0.619	1.000	0.571	-0.440
Distance	0.614	0.745	0.260	0.571	1.000	-0.680
Temperature	-0.530	-0.418	-0.178	-0.440	-0.680	1.00

Table 7.16: Data set D; 411, fitted correlations, 25 two hour sessions

Variable	X	Y	Z	Height	Distance	Temp.
X	1.000	0.519	0.079	0.895	0.767	-0.966
Y	0.519	1.000	0.075	0.763	0.724	-0.587
Z	0.079	0.075	1.000	-0.016	0.528	-0.284
Height	0.895	0.763	-0.016	1.000	0.784	-0.854
Distance	0.767	0.724	0.528	0.784	1.000	-0.886
Temperature	-0.966	-0.587	-0.284	-0.854	-0.886	1.00

contains plots of the correlation with temperature of all the vector components (SLR to 411) including height and distance but is based on the fitted data. All vector components, height and distance were fitted with sinusoids with a linear trend, using non-linear regression. The data fits were done in a least squares sense with some of parameters set to sweep recursively through a window to ensure the best possible fits. This shows a marked improvement in the anti-correlation between distance variation and diurnal temperature variation. The correlation between the z component and distance also improves, but the basic results are the same. The x and y components as well as height are in general less correlated with temperature than the z component and distance. Distance has a negative correlation with temperature as expansion of the hill decreases the distance between SLR and 411. There is a slight phase lag between expansion and the surface temperature, the exact amount of phase lag is difficult to estimate however due to the noise in the data. This phase lag is due to the fact that the rock blocks are not perfectly square and have rounded and broken edges, therefore physical contact between adjacent rocks occur at levels below the actual rock surface. The phase lag at deeper depths, in combination with temperature variation at the surface, could produce complicated expansion patterns. Data set A is particularly noisy, the other data sets are better though, especially data set D where the raw distance data clearly reflects a sinusoidal type variation, even without the aid of a sinusoidal fit. With data set D, as shown in Figure 7.2, even components x,y as well as height shows

Table 7.17: Data set A,B,C,D; 411, Table of thermal signature amplitude in distance

Data set	Amplitude (mm)	Average deviation (fit)	Period (days)	Δ T (deg C)	Correlation with distance
A	1.2	1.2	0.90	17.3	-0.27
B	1.3	0.9	1.01	14.9	-0.60
C	1.7	1.2	0.99	20.1	-0.42
D	2.2	1.1	1.00	14.0	-0.68

better correlation with temperature. This is not unexpected, as monument movement in three axes would result from thermal expansion due to the geometry of the rock blocks. The basic result are consistent for all four data sets, distance consistently shows a anti-correlation with temperature.

Additional data should allow one to determine the phase lag, which will depend on the geometry and structure of the upper rock layer. Table 7.17 lists the approximate amplitudes of the thermal signature in the distance. The small amplitude values (1-2 mm) (2-4 mm peak to peak) are not unexpected. Further measurements over longer time periods will improve the results and should allow one to develop a general model which could be applied to similar sites. It is important to note that even if data for a footprint is collected over periods longer than a full thermal cycle, the displacement of the monument will still be present in seasonal cycles, as well as diurnal cycles which exceeds the temperature deviations during geodetic measurements. The positional error of 411 during a session lasting only part of a day for example, must be seen to be in the 2-4 mm range (peak to peak is twice the amplitude), during normal daily temperature variations. This figure could possibly be more during certain conditions. To this inherent error must be added measurement errors and possibly errors resulting from other local effects. It is normally not possible to occupy a footprint monument for weeks at a time, which would allow the diurnal thermal cycle to be averaged out to a large extent, on the other hand it would seem that a session of several hours might lead to some result, and a further session at some other epoch might indicate (falsely) that site instabilities exist. One cannot interpret normal thermal 'breathing' of a hill as site instability, but it must be taken into account.

Considering the objectives stated at the introduction to this chapter, one can say with reasonable certainty that:

- Thermal variations of the Earth's surface are of large enough magnitude to influence the short term and long term stability of a geodetic monument.
- The magnitude of possible monument movement for a 1000 m diameter

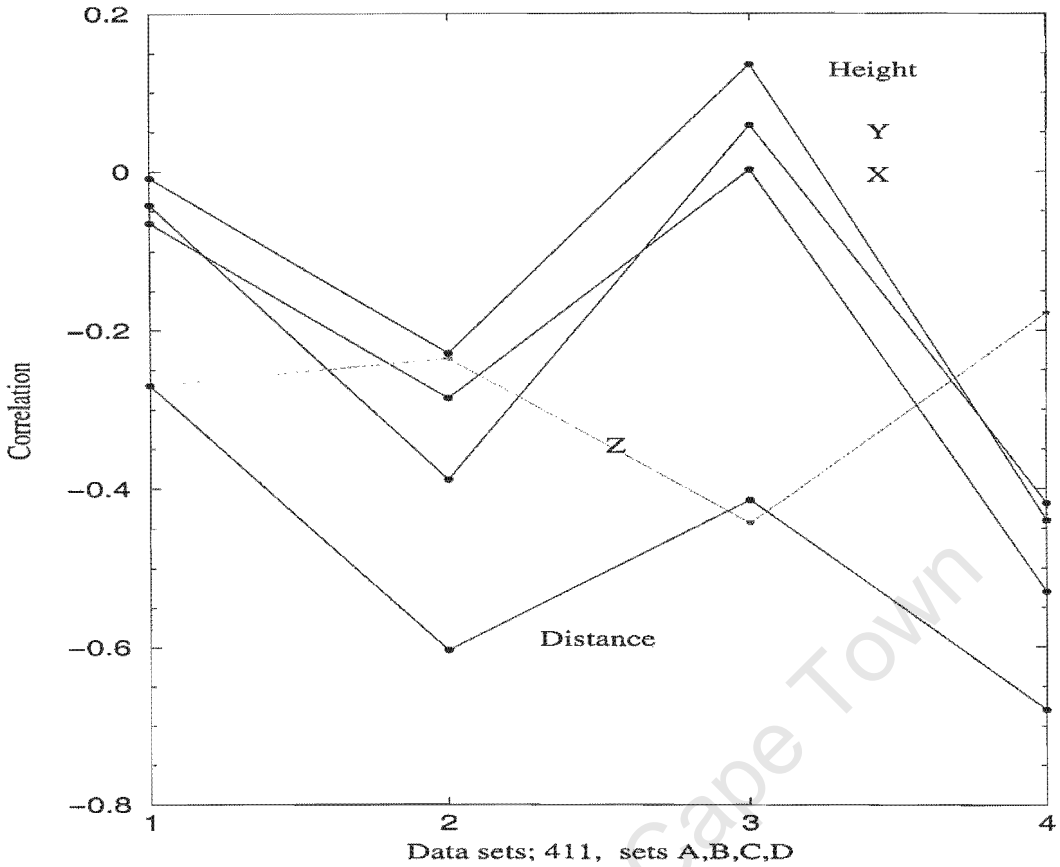

Figure 7.1: Hill 411, correlations of all vector components, height and distance with diurnal temperature variation. The z component and distance clearly shows the highest correlation, indicative of a thermal signature in the position of 411.

hill, as found in this study is in the 2-4 mm range for $\approx 20°C$ temperature range.

- Permanent geodetic monument position changes are possible due to extreme temperature variations, as thermal expansion could physically relocate a rock block.
- It is possible to measure these monument positional changes using GPS.
- Implications for footprint and campaign type surveys where individual sessions are of the order of hours, or perhaps several days, can vary from the deduction that site instabilities exist to the publication of velocity fields ~~which are factually incorrect. For instance, collecting data sequen~~tially during a cold winter, a mild winter, a mild summer and then a hot summer, even if the sessions are of several days, will lead to a velocity field which contains incorrect assumptions about crustal movement, which in fact would be thermal expansion.
- Geodetic monuments located at lower latitudes should, in general, exhibit

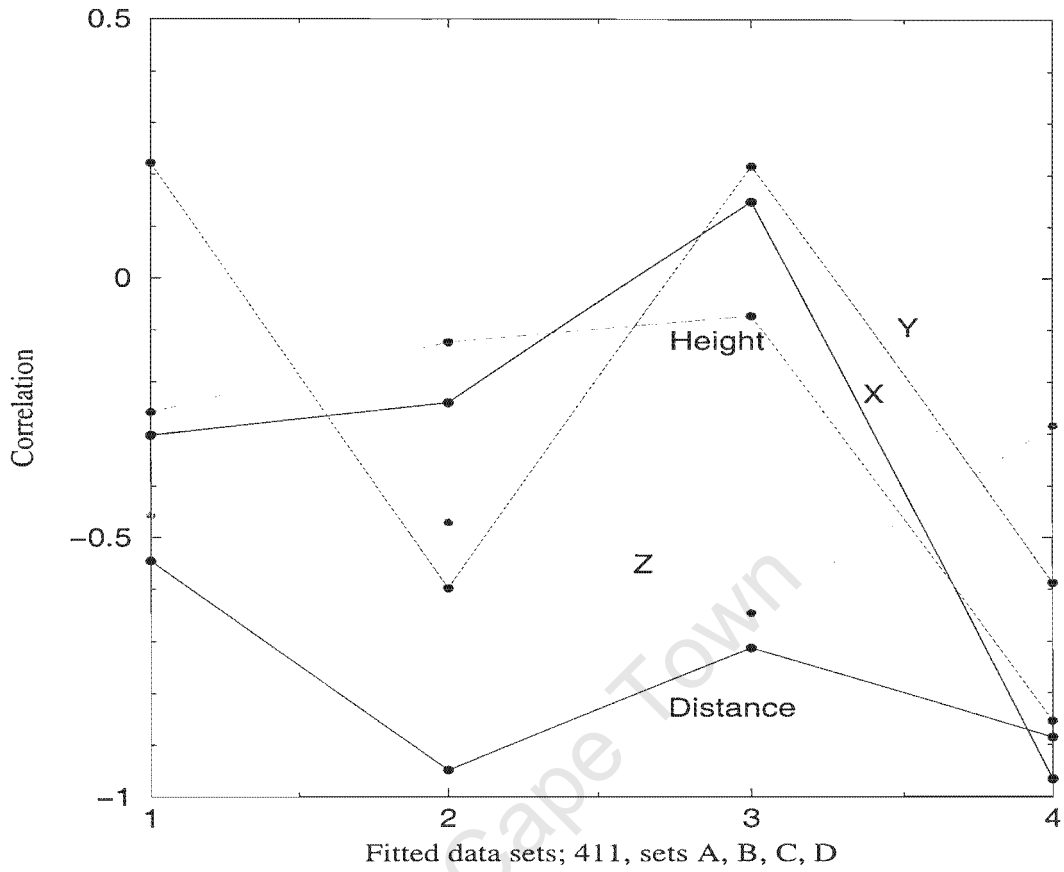

Figure 7.2: Hill 411, correlations of all fitted vector components, height and distance with diurnal temperature variation. The z component and distance clearly shows the highest correlation, indicative of a thermal signature in the position of 411.

less relative thermal instabilities than monumentation installed at higher latitudes, all variables apart from latitude being equal.

- Rock which has a low tensile strength could lead to sudden monument instability, displayed as an actual displacement due to crack propagation.

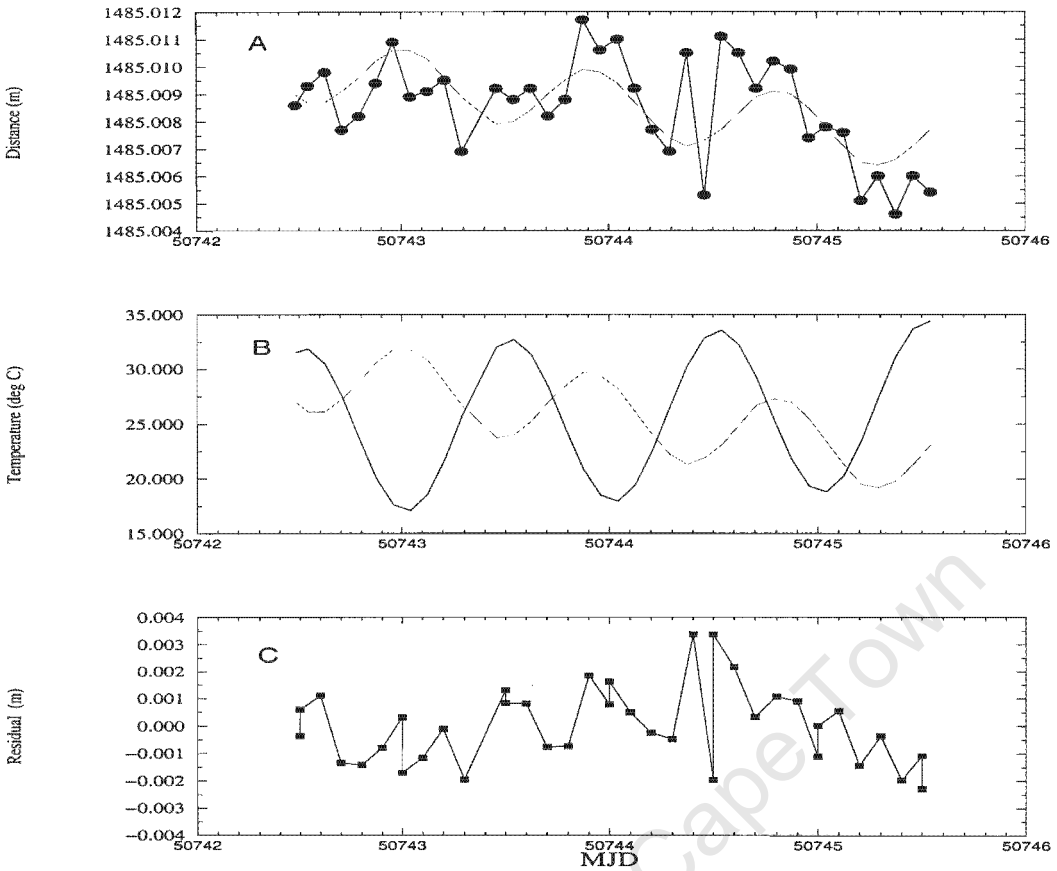

Figure 7.3: Data set A: (A) Measured distance data points, SLR to 411 and sinusoid with linear trend fitted to the distance data. (B) Sinusoidal fit to surface temperature data, overlaid with sinusoidal fit (red) to distance data points. (C) Residuals of (A).

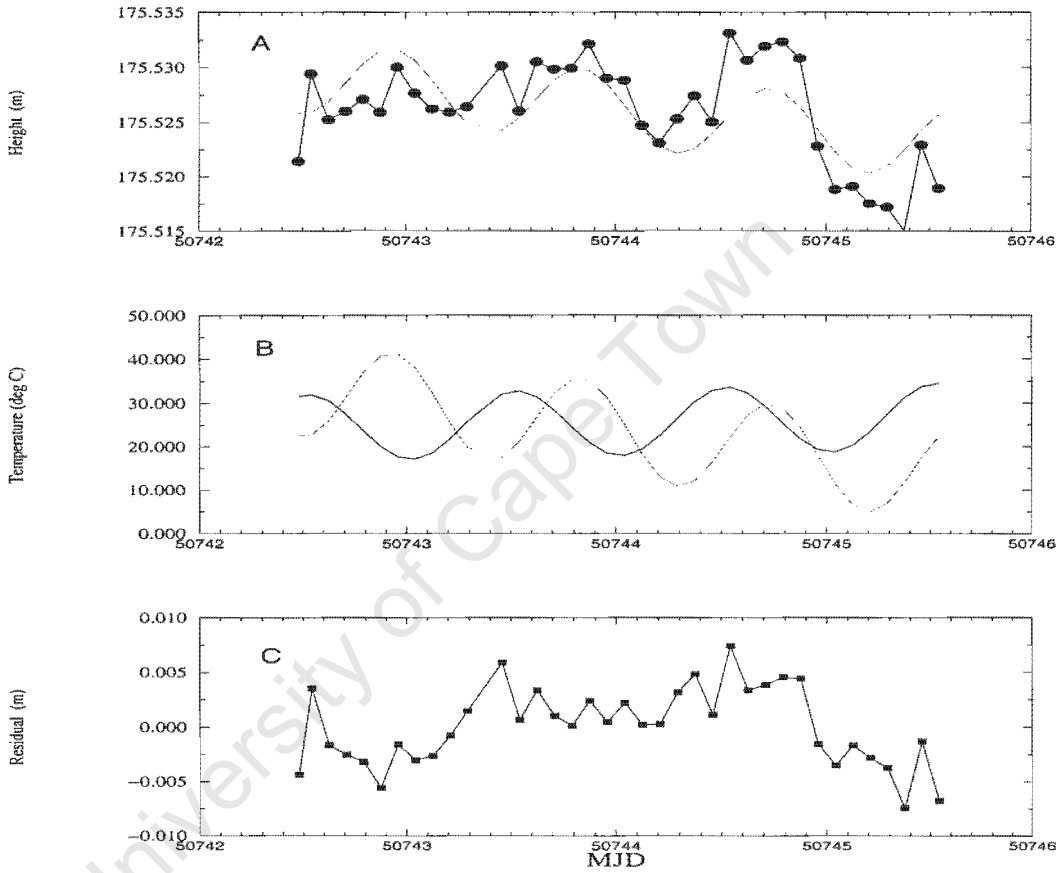

Figure 7.4: Data set A: (A) Measured height data points, SLR to 411 and sinusoid with linear trend fitted to the distance data. (B) Sinusoidal fit to surface temperature data, overlaid with sinusoidal fit (red) to distance data points. (C) Residuals of (A).

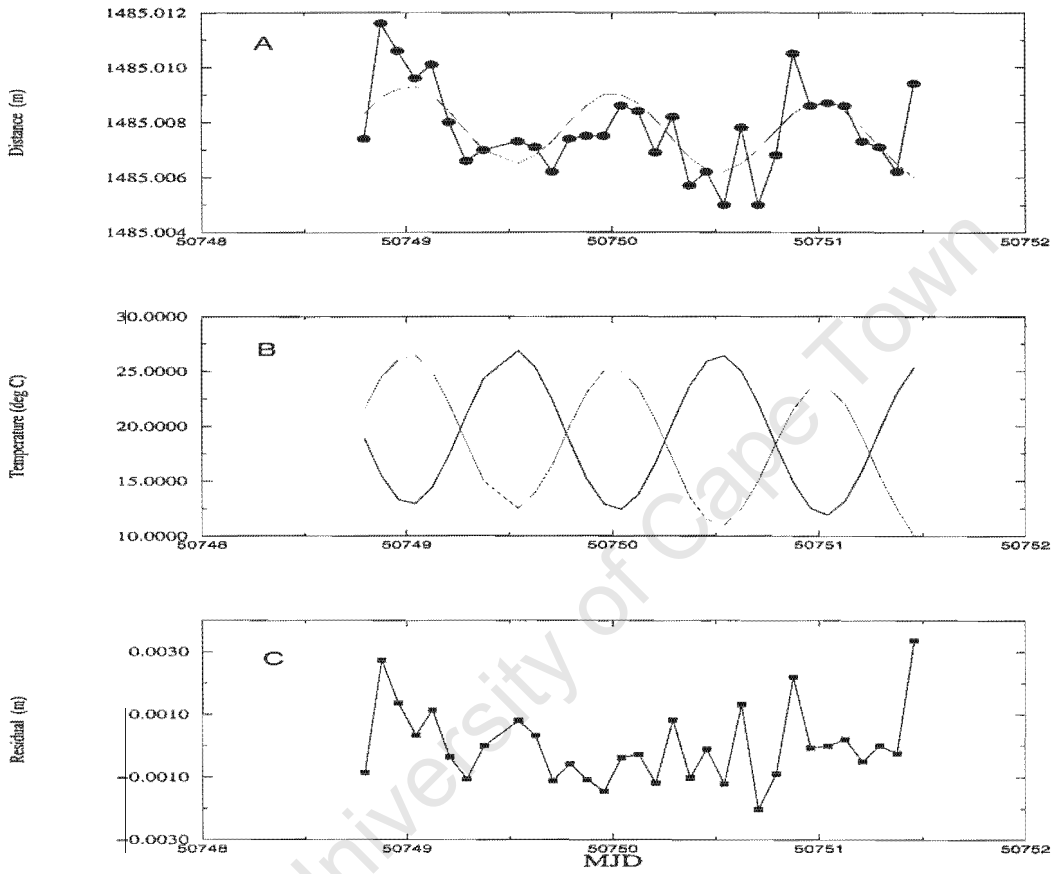

Figure 7.5: Data set B: (A) Measured distance data points, SLR to 411 and sinusoid with linear trend fitted to the distance data. (B) Sinusoidal fit to surface temperature data, overlaid with sinusoidal fit (red) to distance data points. (C) Residuals of (A).

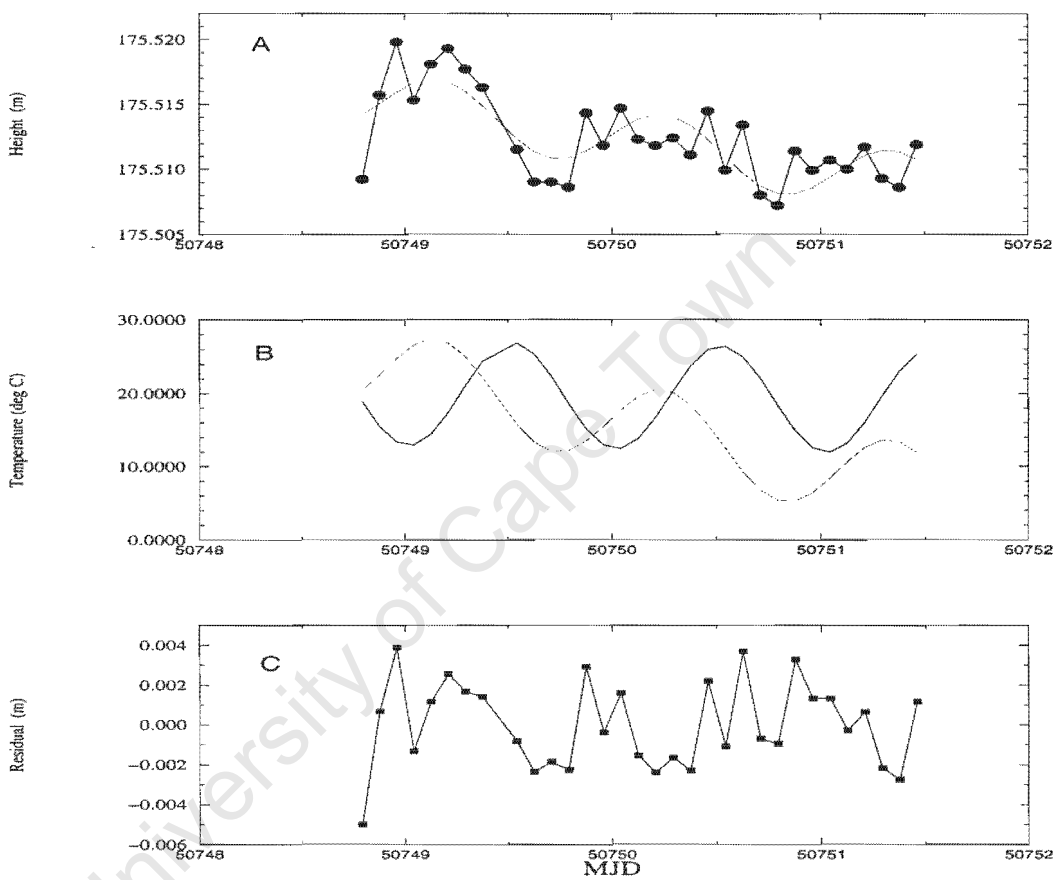

Figure 7.6: Data set B: (A) Measured height data points, SLR to 411 and sinusoid with linear trend fitted to the distance data. (B) Sinusoidal fit to surface temperature data, overlaid with sinusoidal fit (red) to distance data points. (C) Residuals of (A).

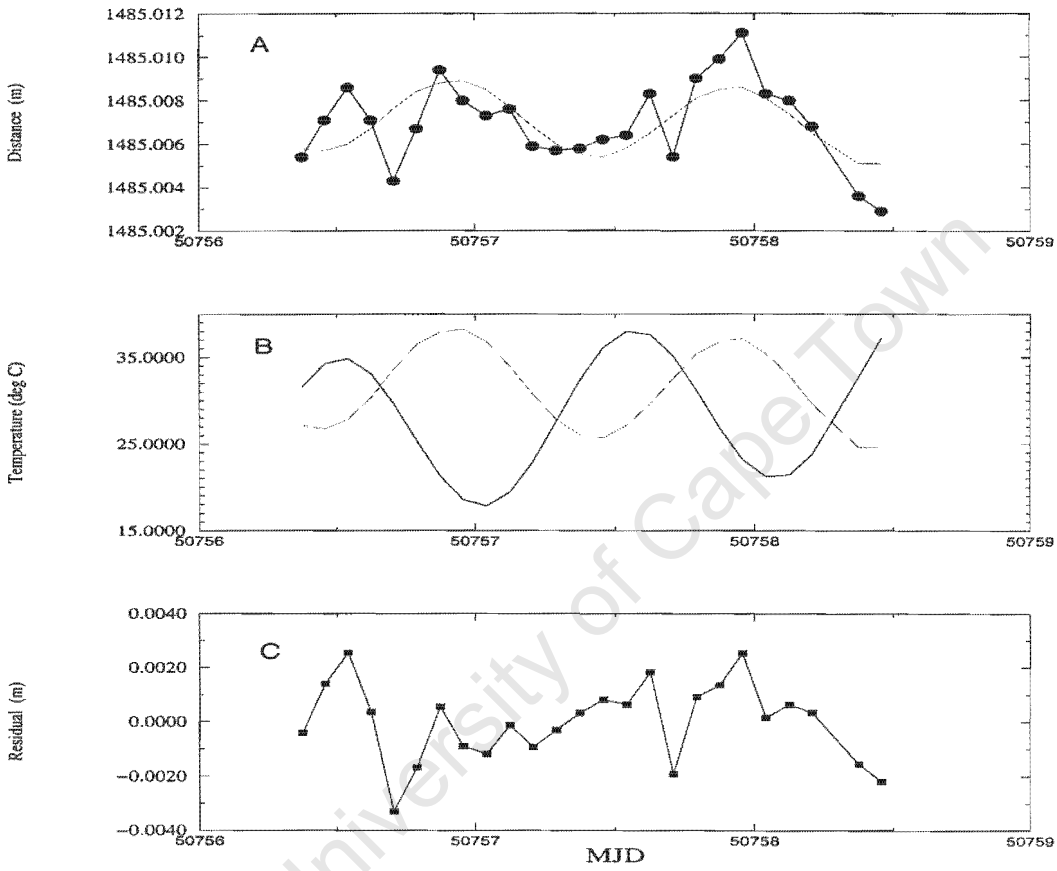

Figure 7.7: Data set C: (A) Measured distance data points, SLR to 411 and sinusoid with linear trend fitted to the distance data. (B) Sinusoidal fit to surface temperature data, overlaid with sinusoidal fit (red) to distance data points. (C) Residuals of (A).

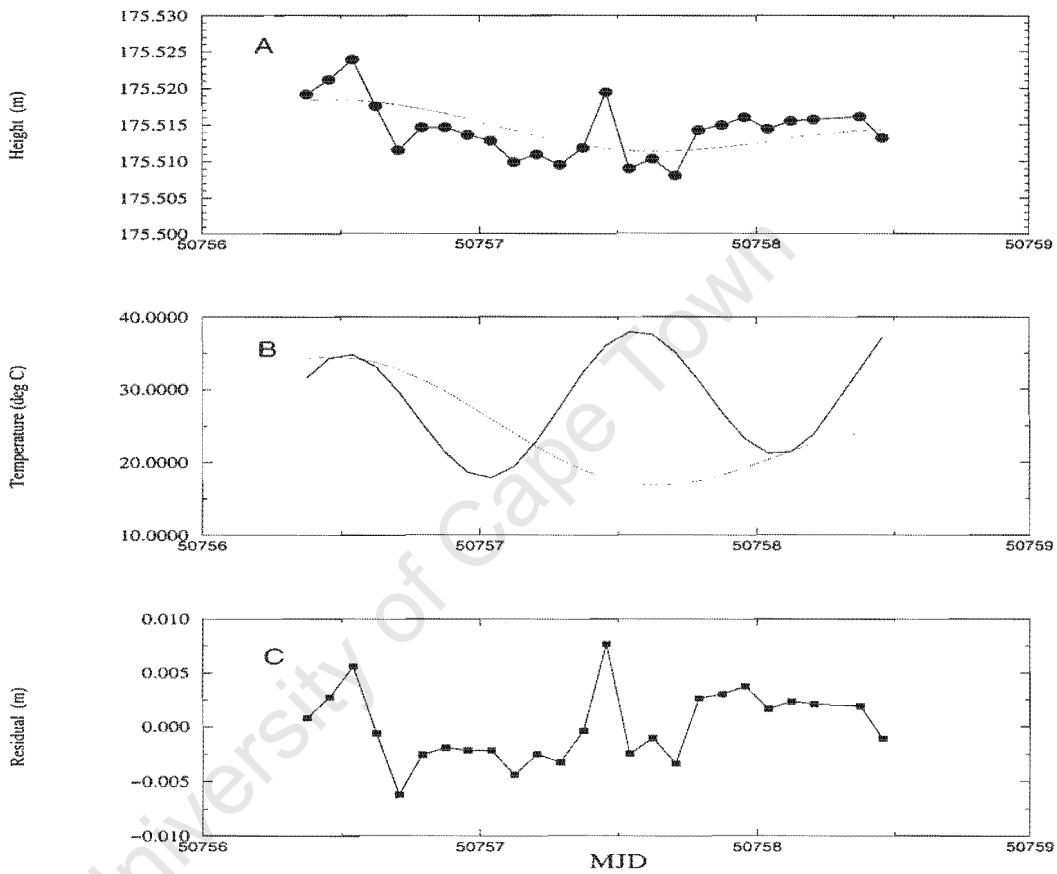

Figure 7.8: Data set C: (A) Measured height data points, SLR to 411 and sinusoid with linear trend fitted to the distance data. (B) Sinusoidal fit to surface temperature data, overlaid with sinusoidal fit (red) to distance data points. (C) Residuals of (A).

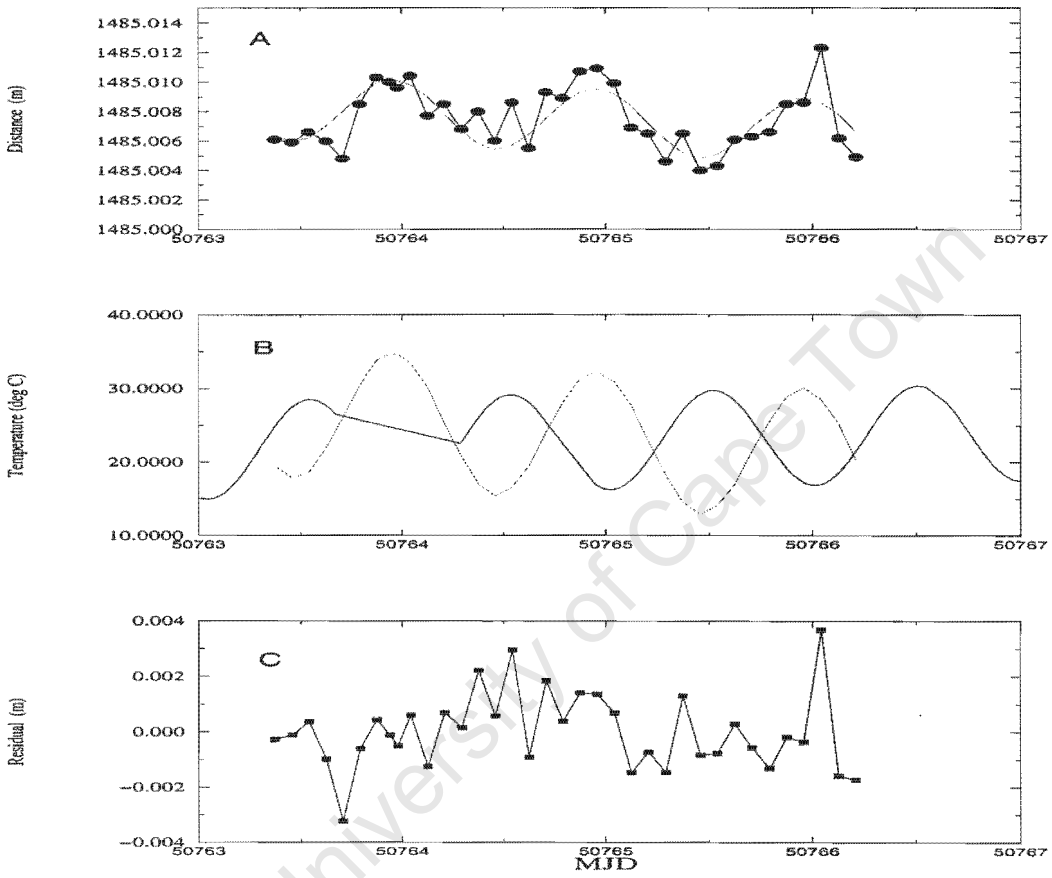

Figure 7.9: Data set D: (A) Measured distance data points, SLR to 411 and sinusoid with linear trend fitted to the distance data. (B) Sinusoidal fit to surface temperature data, overlaid with sinusoidal fit (red) to distance data points. (C) Residuals of (A).

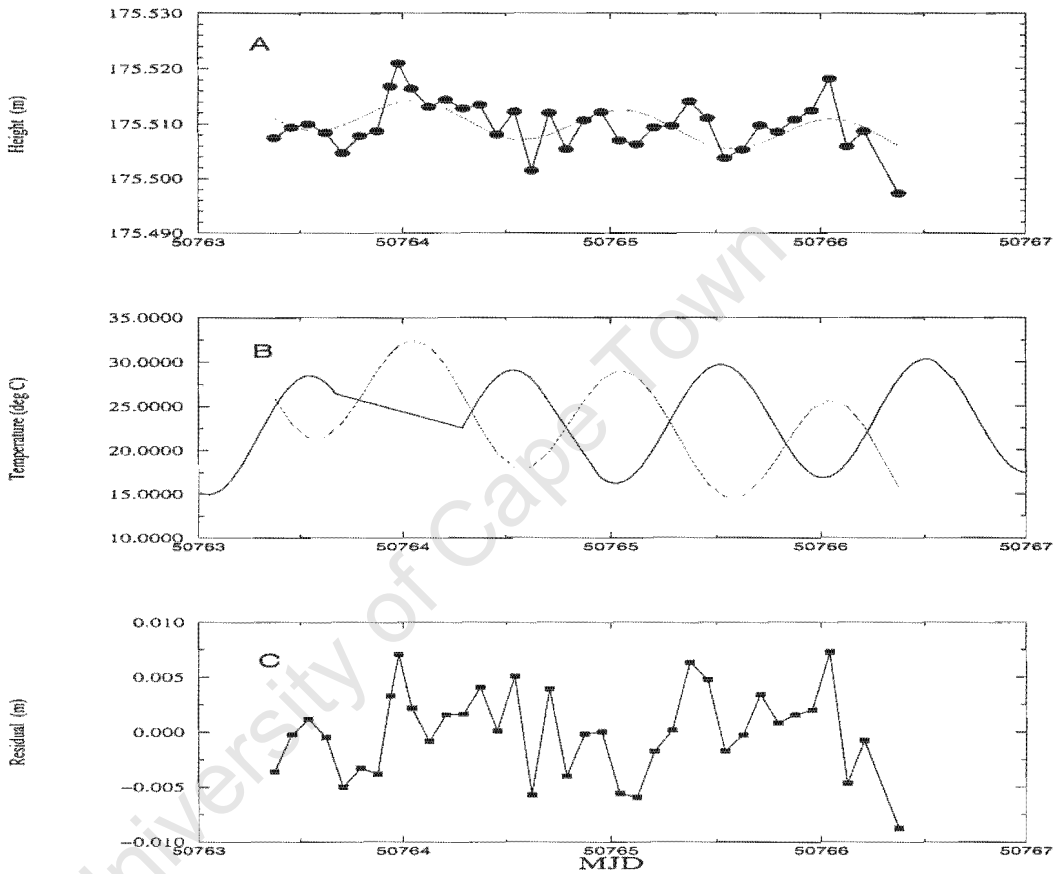

Figure 7.10: Data set D: (A) Measured height data points, SLR to 411 and sinusoid with linear trend fitted to the distance data. (B) Sinusoidal fit to surface temperature data, overlaid with sinusoidal fit (red) to distance data points. (C) Residuals of (A).

Chapter 8

Thermal Modelling

"The new construct which we invent to explain the wondered-about observations is thus called an analogy or model. I prefer to use the latter term." - **G Kale 1979**

8.1 Introduction

In order to investigate the stability of the Hill 411 from a theoretical viewpoint, a simple numerical thermal model (NTM) was developed. The model uses the Distinct Element Method (DEM) (Cundall, 1971) approach, which is freely modified and adapted to include thermal expansion of a system of rock blocks. Examples of original source code for using the DEM approach were not available, but enough descriptive literature could be found to enable the development of source code which uses the DEM approach. This provided the opportunity to add whatever features was thought to be necessary for the development of a reasonable numerical model within the scope of this work.

8.2 Development of a Thermal Model

A complete model for a geodetic monument located on a rocky outcrop would include appropriate elements of:

(1) Time

(2) Interface of monument to crust

(3) Monument

(4) Antenna mount

(5) Geological structure

(6) Geometry of rocky outcrop

(7) Climatic conditions

(8) Rock characteristics

(9) Stresses and strains

(10) Groundwater

(11) Plantgrowth

8.2.1 Distinct Element Method

The main differences between a DEM model and other discontinuous medium approaches is given by Hart et al. (1988) as:

(1) The solutions are in the time domain.

(2) The interacting forces between the blocks leads to a blocky system geometry modification.

(3) The movements of individual blocks are relative to each other and the blocks can undergo rotations and displacements.

The design criteria and required features for the NTM in this work were:

(1) It should utilise the principles of the DEM.

(2) Cartesian differences between two reference points should be available at any point in the model process.

(3) It must be able to accept diurnal and seasonal thermal variations as part of the system input.

(4) It should be a graphical as well as opposed to a numerical only system. This allows the user to visualise the model and creates a friendly interface.

(5) The model should be 2D to reduce complexity.

(6) The solution should provide insight into the dynamic behaviour of a large rocky hill, occupied by a geodetic monument tied to its surface. The final solution should provide a detailed analysis of the relative movement of the monument to another specified fixed point, which is regarded as being fixed in space.

In the application of the model to thermal expansion of the hill, it is essential that the blocks behave as close as possible to reality. Each block must thus be able to rotate and move according to the laws of motion, be subjected to gravity, sliding friction as well as other parameters determined by the rock type and geometry of the hill. In order to determine a specific block's motion, we therefore need to know the magnitudes and positions of the forces acting on this block, these are due to the motion of the blocks surrounding this particular block. It is therefore a requirement that the motion parameters of each block in the model cross-section be known, for each instance of model-time. Only

relevant material required to describe the model is discussed here as there is an abundance of literature available on dynamics. The NTM models a single layer of blocks located on a rocky hill. Although blocks can be stacked, the NTM was designed for a single layer affected by thermal expansion.

8.2.2 Block Motion

Translation and rotation of each block around its centroid describes its motion. The motion depends on the direction and magnitude of the off balance moment and forces acting on the block. As it was decided to have a two dimensional model, each block must move parallel to a fixed plane. The fixed plane is the cross-section through the hill. Two coordinates are required to find the centroid position and an angular coordinate is necessary to determine the orientation of the block. The instantaneous motion of a block is therefore given by the two linear velocity components of its centroid and the angular velocity of the block. A single block is regarded as a detached block in a sense and is allowed to undergo :

- Sliding
- Free falling
- Bouncing
- Rolling

Analytical methods for rock slope stability analysis methods were divided into rigorous methods or lumped mass methods by Hungr and Evans (1988) and the NTM could be considered as a rigorous method as opposed to a lumped mass method as the size and shape of the blocks are known a priori and all block movements (rotation and translation, ballistic trajectory). Additionally continuous thermal expansion of the block is included in this work, which implies a continuous change in shape and size. During expansion, blocks in contact transfer rotational and translational moments. The NTM is simple in that it does not allow block deformation or fracturing resulting from contact. The relatively slow process of thermal expansion does not normally lead to violent impact, such as resulting from rock toppling or rockface failure, so this simplistic approach should still be acceptable. Angular block velocity as well as X and Y velocity vectors are initially set to zero. This is set by the program as soon as the go ahead is given for the modelling to start. Before the modelling starts, blocks will be moved to some required position by the modeller and many will have achieved some movement. The monument is regarded as a block in itself, but has the special characteristic that it does not undergo thermal expansion, which if made properly should be very minimal and well below the detection threshold of a GPS survey. In order to fix the monument block to a standard surface block, either any standard block could have been selected as the monument block, or the monument block could be

fixed to a standard block. The latter option is used, which requires some operator intervention as the monument must be carried (using the cursor) to the block on the edge of the model hill. Care must be taken not to upset other blocks while constructing the hill. All blocks have a top and a bottom, blocks should not be turned upside down. The block on the side of the hill and the monument are bonded to each other, but are not one, bumping the monument even after it has been located on its foundation will lead to it being moved or toppled.

The following motion equations follow the description of Giani 1992. Consider a varying with time force $F(t)$ acting on a single mass, Newton's second law of motion can be written as:

$$\vartheta \dot{u}/\vartheta t = F/m \tag{8.1}$$

At time t, using the central difference scheme (see for instance, Wylie 1960), the left-hand side of Equation 8.1 can be written as

$$\frac{\vartheta \dot{u}}{\vartheta t} = \frac{\dot{u}^{(t+\Delta t/2)} - \dot{u}^{(t-\Delta t/2)}}{\Delta t} \tag{8.2}$$

and substitution of the corresponding terms of Equation 8.2 to the left-hand side of Equation 8.1,

$$\dot{u}^{(t+\Delta t/2)} = \dot{u}^{(t-\Delta t/2)} + F(t)/m \cdot \Delta t. \tag{8.3}$$

Following the central difference scheme, velocities are stored at half-time step so that the time $t + \Delta t$ displacement can be written as

$$u^{t+\Delta t} = u^t + \dot{u}^{(t+\Delta t/2)} \Delta t \tag{8.4}$$

where $u(t)$ is the known displacement from the previous step. In the case of several forces acting on the blocks (including gravity) the velocity equations can be written as

$$\dot{u}_i^{(t+\Delta t/2)} = \dot{u}_i^{(t-\Delta t/2)} + \left[\frac{\sum F_i^{(t)}}{m} + g_i \right] \Delta t \tag{8.5}$$

and

$$\dot{\theta}^{(t+\Delta t/2)} = \dot{\theta}_i^{(t-\Delta t/2)} + \frac{\sum M^t(l)}{m} \Delta t \tag{8.6}$$

where the angular velocity of the block about its centroid is denoted by $\dot{\theta}$, the moment of inertia of the block by I and the block centroid velocity components denoted by $\dot{u}_i$. Equation 8.5 and Equation 8.6 produce updated velocities which are used to determine the new block location,

$$x_i^{(t+\Delta t/2)} = x_i^{(t)} + \dot{u}^{(t+\Delta t/2)} \Delta t \tag{8.7}$$

and

$$\Theta_i^{(t+\Delta t/2)} = \Theta_i^{(t)} + \dot{\Theta}^{(t+\Delta t/2)} \Delta t \tag{8.8}$$

where x_i are the coordinates of the block centroid and Θ_i the rotation of the block around its centroid.

8.2.3 Plane Sliding

Sliding surfaces are not stepped or irregular, but are made up of a block side which occupies the same line as another block side, or a block side resting on the underlying hill blocks, the underlying hill blocks are not modelled as they undergo no short-term thermal expansion. Sliding friction can be set during or before modelling.

8.2.4 Block Mass and Gravity

Block mass is proportional to block size, and gravitational force is proportional to the block mass and is directed vertically downwards. The value of gravity can be altered during or before modelling commences, as it enhances downward block movement which might be very slow when using a large amount of blocks. The value should be reset to unity once the hill has been constructed and the monument properly located otherwise unpredictable instabilities could result.

8.2.5 Elastic Impact

The elastic impact parameter (coefficient of restitution, see Appendix A) is allowed to be set to some desired value between 0 and 1. The loss of kinetic energy during impact is determined by the interface between adjacent blocks, block destruction, rolling and sliding resistance and elastic wave generation. No attempt is made to separate the coefficient of restitution into normal and tangential to the impact surface components, although Giani (1992) reports that such an approach could lead to a better definition of bouncing rocks. Although for our NTM purpose, the blocks do not move large distances, nor bounce down the slope, the blocks are in fact subjected on a smaller, much slower scale to the same block bouncing behaviour. It is feasible, that for a given hill geometry, some of the blocks may become unstable enough (over time) to move rapidly down a slope surface, so the NTM makes provision for this event.

8.2.6 Observed and NTM Approximations of Rock Block Deformation

Condensing and applying the findings of Giani (1992), this section describes observed rock deformation tendencies, followed by a description of how the NTM approximates these characteristics for parallelepiped block motion:

Block shape. In nature softer blocks tend to become more rounded with travel due to sharp corners breaking off. Rough block surfaces become smoother. For almost cubic and parallelepiped shapes the size and shape

of the block surface in contact with the slope determines block bounce mode and its subsequent movement. If a block impacts with its face towards the impact surface, the impact surface absorbs most of the energy and sliding becomes the principal movement. This sliding continues until the movement ceases or a rough slope surface section forces toppling and accompanying bouncing and rolling movements. In contrast, when a block falls on one of its corners, the impact produces transfer of its translational movement to a rotational moment so that bouncing is dominant over sliding. Giani (1992) found that when determining the coefficient of restitution, considerable scattering of values are obtained. Restitution coefficients become very high when a block becomes or is, rounded, rolling friction angles are also very low, which result in unexpectedly large travel distances for the blocks.

• In the NTM block shape is normally set up to approximate the average block shape of the hill under investigation. A typical setup used blocks 70 cm deep (Y axis) and 3.5 m long (X axis). Blocks can be parallelepiped or cubic, but no more complicated as proper thermal expansion modelling rapidly complicates for other shapes. The block shapes are deformable, but only resulting from thermal expansion or contraction, not due to weathering or fracturing due to impact.

Block size. Block rolling prevails when the falling block is larger than the average particles on which it is impacting. Bouncing and rock to rock impacts are the dominant block motion type when the falling block is smaller than the particles on which it falls. The block can stop when its rebound height is insufficient to clear the local roughness of the slope.

• In the NTM blocks are all of the same size. Rolling and bouncing is allowed.

Block strength. When block failure occurs after impact, the point of impact becomes the initial travelling point for the rock fragments. The initial velocity of each fragment is therefore randomly orientated.

• The NTM does not make provison for block failure, as impact due to thermal expansion does not normally lead to block failure.

It is not unreasonable to expect that thermal expansion of parallelepiped blocks will also lead to slow rounding of sharp corners and smoothing of rough sides due to the abrasion which will occur. Over a long period of time, this abrasion, which is just another weathering mechanism, will slowly change the shape and size of the blocks, leading to a change in the shape of the hill and the abraded material will form the parent material for soil. The NTM does not make provision for this mechanical weathering effect. It would seem that the most reliable way to obtain coefficients of restitution is through experimental observation. In the NTM the option was therefore included to select different values for the coefficient of restitution. The values are not broken up into separate parameters, the normal K_n and tangential K_t coefficients which for some applications (such as rock fall modelling) may be more accurate, but

a single value K is used to predict bouncing and blockfall behaviour. Values between 0.2 and 0.5 seem to be fairly realistic for the NTM. Values for K_n and K_t by Barbieri et al. (1988) as quoted by Giani (1992) ranges from 0.25 to 0.5, which indicates the typical large range of values obtained through experimental means, depending on the type of outcropping material.

8.2.7 Volumetric Strain

Thermal stresses are a result of the heating and cooling of the rock and occur close to the Earth's surface. As example, a typical linear coefficient of thermal expansion α for sandstone is 10.8×10^{-8} m per $1°C$ change in temperature. A block subjected to a set of stresses can undergo deformation due to the change in length of a straight line or a change of angle between two straight lines (shear strain). The straight line length change is the longitudinal or normal strain ϵ which is defined as:

$$\epsilon = \frac{l_b - l_a}{l_b} = \frac{\Delta l}{l} \tag{8.9}$$

where l_b and l_a is the length before and after, Δl is the change in length and l is the original length. A reduction in length corresponds to a positive strain (ϵ) and results from a compressive (positive) stress. An increase in length is due to negative strain. Due to the geometry of the blocks on the hill and the fact that the hill surface is heated rather evenly, shear strain is not taken into account in the model.

The volume dilation e expressed as negative strain for each block is defined (Herget 1988) as

$$e = \frac{\Delta V}{V} = \frac{V_f - V}{V} \tag{8.10}$$

where V_f is the final volume, V the original volume. One has

$$V = l_x \times l_y \times l_z \tag{8.11}$$

where l_x, l_y, l_z are the lengths in the x, y and z directions. The final volume can therefore be written as:

$$V_f = (l_x + \Delta l_x)(l_y + \Delta l_y)(l_z + \Delta l_z) \tag{8.12}$$

The normal strains can then be written as

$$\epsilon_x = \frac{\Delta l_x}{l_x} \tag{8.13}$$

$$\epsilon_y = \frac{\Delta l_y}{l_y} \tag{8.14}$$

$$\epsilon_z = \frac{\Delta l_z}{l_z} \tag{8.15}$$

Therefore one has for the volume dilation

$$e = \frac{\Delta V}{V} = \frac{(l_x + \Delta l_x)(l_y + \Delta l_y)(l_z + \Delta l_z)}{l_x \times l_y \times l_z} \tag{8.16}$$

which is the same as

$$e = \epsilon_x + \epsilon_y + \epsilon_z \tag{8.17}$$

so that the volumetric strain is the sum of the three orthogonal strains. The model uses only two dimensions, where the x and y coordinates represent the coordinate in length and height respectively. The model further assumes that the strains are directly proportional to the applied stress, which leads to a linear relationship between the applied stress and resulting strain and makes Hooke's law applicable. Hooke's law can be written as

$$\sigma_z = E \times \epsilon_z, \tag{8.18}$$

where σ is the normal stress (force/area), E is the elastic modulus (force/area) and ϵ the dimensionless strain. The software is written in such a way that the top of the block (i.e. the surface) expands at a rate determined by the model surface temperature, whereas the foot of the block expands at the phase lagged, dampened, temperature which would be present at that depth. The theory to determine these phase lagged temperatures were discussed in Chapter 7. Both parameters are written to an output file and presented graphically.

8.2.8 Software Description

The software is fully windowed to allow easy access to all functions and features. Parameters such as expansion coefficient and time interval between data points written to file are chosen using scroll bars. Time compression is allowed within certain limits. Careful selection of time compression and time interval between the writing of data sets to an output file needs to be made as a run of say 2 to 3 days; oversampled it can lead to very large files and consequent problems. Block parameters can be viewed during the modelling process, or plots of the following parameters can be displayed:

- ΔX
- ΔY
- ΔZ
- Surface temperature
- Temperature at depth z
- Height
- Slope distance
- Monument inclination (in degrees)

The plots are updated at the selected file output rate.

8.3 NTM Assumptions and Approximations

The nature of construction of any hill, no matter what size it is, is very complex. The spacing of the joints vary, the material filling the joints vary in consistency and moisture content, the surface temperature varies and the surface cover (soil, vegetation, broken rock etc.) varies, and one is confronted by a visualisation of a discontinuous, nonhomogeneous texture and structure. It is thus necessary to make some assumptions.

For instance, some of the expansion is taken up by the material filling the joints and this has to be considered. This filling could act as a cement, keeping blocks locked together. Plastic organic alluvial clay for instance is very compressible. One should therefore visualise a hill to be like a sponge, but made of non-similar material so that when compressed or stretched, will exhibit non-uniform behaviour. In general, the higher the compressibility and deformability of the filler material, the less evidence there will be of thermal expansion. For small stress levels, volumetric compression takes precedence over dilatancy but if subjected to shear, dilatancy (volume increase) could result leading to a negative volumetric strain. Filling material is normally weaker than the parent rock; typical filling material being clay, silt, sand, breccia, mylonite and gouge. These discontinuities will exhibit a lower shear strength than closed dicontinuities. In some cases the filled discontinuities contain high strength deformation type minerals such as pyrite, calcium and quartz, the last of which can be found scattered all over the HartRAO site in thin veins from some millimetres to about a centimetre in diameter. The behaviour of the adjacent rock blocks as influenced by the filling material is therefore very difficult to take into account in the NTM.

To account for the discontinuity (joints) filler material, the following assumptions were made:

- The daily geological history of the hill is being repeated on a daily basis, therefore no or very little structural collapse occurs and no irreversible deformation occurs.
- No crushing, breaking down, destruction of internal bonds, or changes in size, shape or composition of structural elements are allowed.
- Axial deformation (in the x plane) is completely reversible.
- Cyclical loading has allowed the joint filler material to harden, allowing greater elasticity and near perfect reversibility.
- No allowance is made for water content.
- No allowance is made for low friction material such as chlorite.
- Swelling potential and particle size are ignored.

As far as the rock blocks which make up the model hill is concerned, the following assumptions are made:

- The relatively low stress levels of normal diurnal heating lead to reversible, time-independent behaviour. The rock blocks are regarded as hard, intact and indestructable.
- The rock blocks behave in an ideally elastic way and during the period of modelling do not undergo any irreversible or irrecoverable deformation.
- Linear stress-strain relationships are assumed.
- A small amount of inherited strain is present, individual blocks may or may not reoccupy exactly the same point as before during cyclic loading resulting from the diurnal temperature variation, therefore a small heredity part is present.

8.3.1 Results and Conclusions

Modelling a full-size hill proved to be too much for the available computing power, therefore simulations were run on a hill which had a diameter of about 200 metres. Assuming a linear relationship between the expansion characteristics of the modelled hill and the real hill, the output of the NTM was not unrealistic.

The output of the NTM on a PC screen was captured with a digital camera and are reproduced in Appendix I (Section I). The quality of the screen-photos are not the best but do illustrate in sufficient clarity some of the results. The individual graphs (as displayed on the PC screen) are labelled from 0 to 7 where

- 0 = X vector (mm)
- 1 = Y vector (mm)
- 2 = Distance (mm)
- 3 = Surface temperature (deg C)
- 4 = Phase lagged, dampened temperature at bottom of rock block (deg C)
- 5 = Inclination of block (degrees)
- 6 = Expansion and contraction of block top face (microns)
- 7 = Expansion and contraction of block bottom face (microns)

For greater clarity, Figure 8.1 contains plots of the variation of slope distance for the three different coefficients of expansion as determined by the NTM, the data are the same used for Figures I.2 to Figures I.4. Figure 8.1 depicts typical NTM output examples for a temperature variation of 20 degrees. Figure 8.1 (A), (B) and (C) has the linear coefficient of thermal expansion α set to 1×10^{-5}, 1×10^{-6} and 1×10^{-7} respectively. The output values are translated and scaled (an offset plot) to improve their descriptive value. Figure 8.1 (A) is a

bit unrealistic due to the large thermal expansion coefficient used. The data produced on the block inclination indicated some Y vector instability. Even though the inclination plots seem to indicate no tilting, close scrutiny shows some tilt (several millidegree level) on short time scales due to noise resulting from relative block movement. Figure 8.1 (B) indicates an amplitude (peak to peak) of about 1.5 mm, which if scaled to full hill size of about 1000 metres, would result in an amplitude (p-p) of about 7.5 mm. A slight amount of heredity is also seen. It can be seen from Figure 8.1 (C) that the diurnal variation in the X vector is lost in the noise.

In general about 66% of the possible hill expansion is lost in the elastic behaviour of the filling material which absorbs adjacent rock block movement.

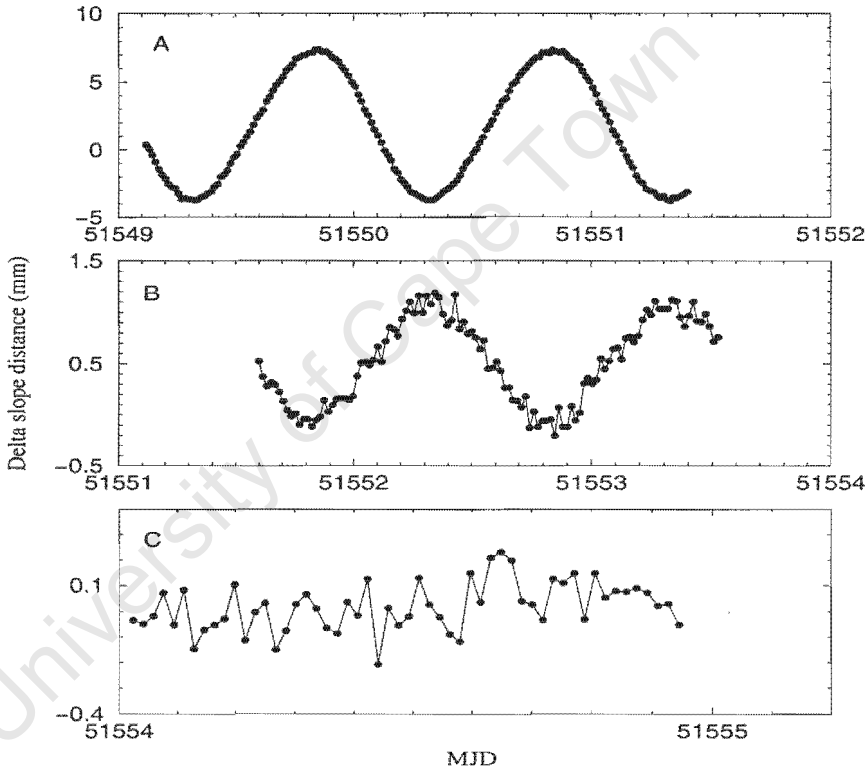

Figure 8.1: Thermal expansion of a 200 metre diameter hill as produced by the NTM, coefficient of expansion set to (A): 1×10^{-5}, (B): 1×10^{-6} and (c): 1×10^{-7}.

Using an expansion coefficient of 5×10^{-7}, a peak to peak amplitude of about 1.7 mm is obtained for a hill with a diameter of about 1000 m. This is a scaled value using a 200 m model hill, where results showed a peak to peak amplitude of $\approx$ 0.35 mm. The change in slope distance as obtained by the NTM is presented in Figure 8.2.

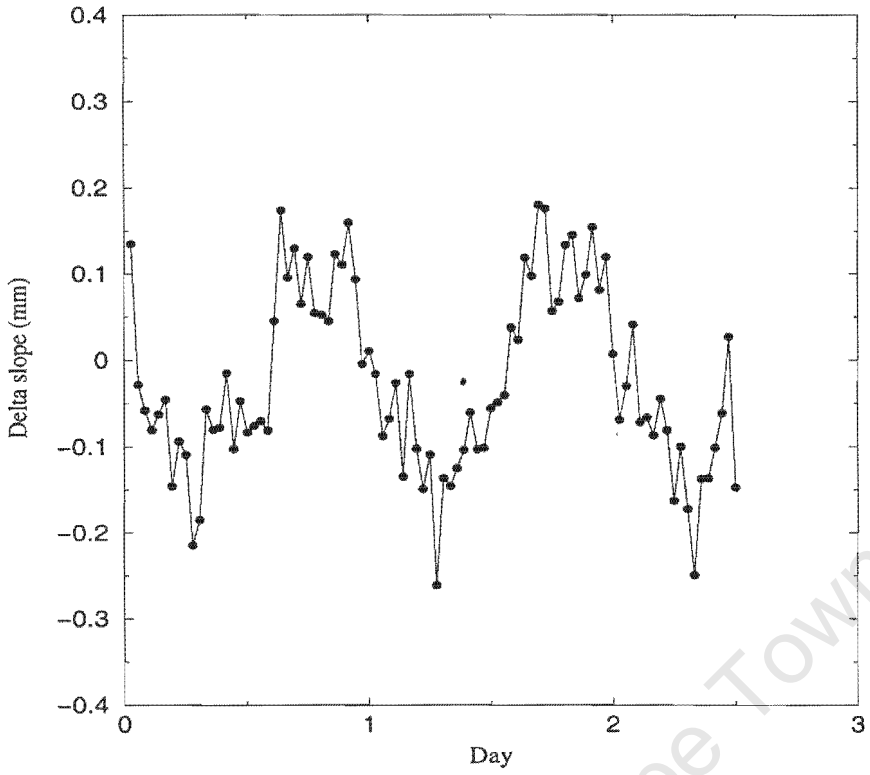

Figure 8.2: Thermal expansion of a 200 metre diameter hill as produced by the NTM, coefficient of expansion set to 5×10^{-7}. Peak to peak amplitude is ≈ 0.35 mm. Linearly scaled to the size of Hill 411, this result shows good agreement with the results as determined by GPS ($\approx 2 - 4$ mm).

Final conclusion This NTM value is sufficiently close to the values obtained by GPS to allow one to make the statement that:

It is possible for an outcrop or hill of a certain geological structure to exhibit thermal expansion due to diurnal heating. This diurnal heating could affect the short term stability of a geodetic monument, inferring that longer term (seasonal) thermal changes will lead to longer term monument instabilities.

Chapter 9

Regional Network

"A geodetic network is also an invaluable tool for deformation monitoring."
- S. Kuang 1996

9.1 Introduction

During the course of this work, several IGS and regional permanent GPS stations were installed. HartRAO was set up as the IGS Regional Data Centre for Africa and a server allowed access to RINEX data and IGS products such as precise ephemeris to users. The stations that are archived are processed in a regional network and the results are published weekly on our web page.

9.2 Network description

At the time of writing, the regional network consists of 15 IGS stations and 1 regional station, with one station in the process of being installed. The network is graphically presented in Chapter 1, Figure 1.6. The regional network is not static in the sense that stations are added whenever possible, some stations therefore have a relatively longer time series than others. The archive commences from January 1998 and older data than that must be retrieved from the global data centres if available. The network is basically centred around HartRAO, but there are more stations to the south (Antarctica) than to the north. The northern region would include the African continent, which is a problematic region for IGS installations, mainly due to political instability, lack of adequate infrastructure and supporting logistics. However there are functioning stations in Malindi (Kenya) and the Ivory coast on the continent and stations on the Seychelles (Indian Ocean) and Ascension (Atlantic Ocean). The number of stations in the southern African region has increased as a result of the efforts of this work, with the addition of HRAO (Hartebeesthoek), SUTH (Sutherland), NAMI (Windhoek, Namibia) and RICH (Richardsbay)

Table 9.1: HartRAO regional GPS network, baselines are to HRAO. SA=South Africa. Adapted from *http://igscb.jpl.nasa.gov/network/list.html*

Station	Location	Long(E)	Lat(N)	Height (m)	Baseline (m)	Agency
asc1	Ascension Island	-14.4120	-7.9512	105.1508	4757316	NASA/JPL
dav1	Davis (Antarctica)	77.9726	-68.5773	44.5000	5584964	AUSLIG
goug	Gough Island	-9.8667	-40.3488	81.3000	3761982	AWI
hark	Hartebeesthoek (SA)	27.7077	-25.8871	1555.0000	2114	CNES
hrao	Hartebeesthoek (SA)	27.6870	-25.8901	1414.1877	0	HRAO-JPL
kerg	Port Aux Francais (Kerguelen)	70.2555	-49.3515	74.0583	4391931	CNES
mali	Malindi (Kenya)	40.1944	-2.9959	22.7200	2840895	ESA
maw1	Mawson (Antarctica)	62.8707	-67.6048	59.1840	5068376	AUSLIG
nami	Windhoek (Namibia)	17.0894	-22.5749	1736.6765	1135585	HRAO
ohig	O'higgins (Antarctic Peninsula)	-57.9003	-63.3207	30.6210	6865996	IfAG
palm	Palmer (Antarctic Penisula)	-64.0511	-64.7751	31.0896	7087360	
rich	Richardsbay (SA)					HRAO/JPL/UCT
sey1	La Misere (Seychelles)	55.4794	-4.6737	538.2248	3724926	JPL-IDA
suth	Sutherland (SA)	20.8105	-32.3802	1799.7960	981212	HRAO/JPL
syog	East Ongle Island (Antarctica)	39.5837	-69.0070	50.0902		GSI
vesl	Sanae IV (Antarctica)	-2.8417	-71.6738	862.4000	5270767	AWI
ykro	Yamoussoukro (Cote D'ivorie)	-5.2401	6.8706	270.4983		NASA/JPL

in comparison to only one station before (HART/HARK) at Hartebeesthoek. Table 9.1 lists appoximate coordinates and baseline lengths to HRAO.

9.3 Processing methodology

The software package used to process the GPS regional data is the GAMIT package, developed at the Massachusetts Institute of Technology (MIT) and Scripps Orbit and Permanent Array Center (SOPAC). We are using the LINUX implementation of GAMIT (currently version 9.82) and compile the latest release using the GNU C compiler. The GAMIT GPS analysis package is comprehensively documented (see for instance *Documentation for the GAMIT GPS Analysis Software* Release 9.7, June 1998 and *Global Kalman filter VLBI and GPS analysis program* Version 4.1, June 1998) and here only a very brief summary of GAMIT processing and use of the *globk* (Global Kalman Filter) is given, concentrating on our specific implementation of the package. As the analysis software is modular, but tied by a specific sequence of data flow, processing is done by shell scripts. The modules perform such tasks as data preparation for processing, reference orbit generation, computing residual observations and partial derivatives from a geometrical model, data breaks and outlier detection, and a weighted least squares analysis. The least squares analysis estimate the relative position of the stations in the network, Earth-rotation and orbital parameters, zenith delays, and phase ambiguities. Doubly differenced phase observations are used for parameter estimation and triple differences in editing. GAMIT is used to generate station position estimates and an associated covariance matrix.

The GAMIT solution is loosely constrained and the reference frame is defined by further processing of the GAMIT solution by *globk*. In order to define the reference frame GAMIT users normally include h-files (GAMIT output file) from a global network such as the SOPAC *igs1* and *igs2* h-files resulting from their global analysis which include station coordinates, orbital parameters and Earth orientation parameters. Unfortunately these files are too bulky to download on a daily basis and the reference frame had to be defined using a different strategy. In these analyses therefore only regional data is used and the reference frame is maintained through the IGS orbit and IERS Earth orientation values. The solution is therefore in the NUVEL-1A No-net-rotation (NNR) frame. The stations HRAO, HARK and SUTH define the origin by having their positions constrained. HRAO and HARK are constrained to 1 cm horizontal and 10 cm vertical whereas SUTH is constrained to 5 cm horizontal and 10 cm vertical. Satellite orbital positions are constrained at the 10 cm level and satellite velocities to .01 mm/s, all non-gravitational force parameters are kept fixed. Polar motion apriori values are set to 0.25 mas, 0.1 mas/day. In this approach *glred* (similar to *globk* but treats the daily h-files independently) is used to generate a loose solution and subsequently *glorg* generates a constrained solution. The constrained solution is used as the final result.

9.4 Results

9.4.1 Baseline repeatability

Using the *ofiles* produced by SOLVE one can examine the baseline repeatabilities of the network. The output for baseline vectors are given in local coordinates (north, east and up) tangent to a sphere as well as in a geocentric (XYZ) reference frame. The vectors are given as second station - first station. A typical example of baseline repeatablity is given in Table C.1 to Table C.3 where baselines determined from day 1 to 69 (1999) are summarised. Baseline repeatability is given by the standard deviation (RMS) which is also expressed as parts per billion (PPB), the standard error of the mean is denoted by SIG. In order to keep the table size reasonable, Table C.1 to Table C.3 does not reflect individual day deviation from the weighted means, with their respective uncertainties, although this is available in the *ofile*. The effect of the ionosphere can be reduced (Dong and Bock 1989) by forming the linear combination (LC) of the L1 and L2 phase measurements

$$\Phi_{LC} = 2.546\Phi_{LI} - 1.984\Phi_{L2} \tag{9.1}$$

The solution components are from the 'bias-fixed solution', where the narrow-lane biases are held fixed, and the LC observations are used to estimate geodetic parameters. If phase ambiguities have been solved correctly, the estimates

from biases-free and biases-fixed solutions for all components should agree within the larger biases-free uncertainties. A further check on the results is whether large quantities of data has been discarded by AUTCLN, which is the program that automatically cleans (fixes) cycle slips. This can be done by checking the normalised rms (nrms) which with the default weighting scheme should be about 0.25 for a good solution. Values of nrms larger than 0.5 indicates incorrect station coordinates or cycle slips that were not removed. This nrms value is available in the Q-file. The nrms is the square root of chi-square per degree of freedom. More details about chi-square and the probability distribution functions of the chi-square distribution with n degrees of freedom can be had from Meyer (1975). Table 9.2 contains a sample of typical nrms values for the network. The number of stations can vary from day to day depending whether station data is available. At this point in the processing (before defining a reference frame), the number of stations available does not seem to affect results.

9.4.2 Results in the ITRF

In order to obtain station positions in the ITRF, the output files from GAMIT h- are converted to binary input files for the *globk* Kalman filter. The *globk* command file controls options for the program which are very important as the settings determine the approach taken in defining a reference frame for the analysis. Input data is filtered to some extent by setting the maximum allowable increment in the χ^2 value to 10. Daily runs which contain corrupted data or for some reason are not good are therefore not included in the solution. Although not using h-files from a global network, the use of the final IGS orbits (assuming 0.1 m in position, 0.01 mm/s in velocity accuracy) result in negligible errors for the HartRAO regional network. The recommended conservative orbital constraints in the *globk* manual of 10 cm for orbital position and 0.01 mm/s for velocity is used. Non-gravitational force parameters are kept fixed. A priori values for polar motion tables are set to 0.25 mas, 0.1 mas/day and the Markov values are set to similar variations per day. The earth orientation parameters are therefore constrained so that the network orientation is defined by the polar motion and UT1 tables provided as input to *globk*. The shell scripts are set up in such a way as to use *glred* to estimate coordinates for each daily session, with *glorg* maintaining the reference frame. Final results are posted on the web site

`http:\\www.hartrao.ac.za\geodesy\geodesy_index.html`

and are updated as soon as new data have been processed. Timeseries images are available in either GIF or postscript format. The shorter baseline (SUTH, NAMI, HRAO, HARK) stations have the axes of the timeseries plots fixed to 50 mm for the North and East components and the up component fixed to 100 mm. The other longer baseline plots are not constrained in either axis. Here

Table 9.2: Extract of HartRAO regional GPS network normalised rms values; 1999

Day number	Number of stations	nrms
1	11	0.30405
2	11	0.27567
3	10	0.26099
4	9	0.28379
5	10	0.29778
6	10	0.22521
7	9	0.25196
8	11	0.26610
9	9	0.24681
10	9	0.23034
11	10	0.29663
12	12	0.25641
13	10	0.25869
14	12	0.25210
15	11	0.26294
16	12	0.25601
17	12	0.25502
18	10	0.23242
19	11	0.22905
20	12	0.25001
21	12	0.21903
22	11	0.22887
23	12	0.25116
24	11	0.26296
25	11	0.23052
26	12	0.22284
27	11	0.24654
28	12	0.21581
29	13	0.22865
30	13	0.21742

we include timeseries plots for a subset of the network, HRAO, SUTH, VESL, GOUG and MALI. Results are in ITRF97.

9.4.3 Preliminary Interpretation

The following discussion is based on a subset of the data processed up to day 66 of 2000. The results do of course change slowly as more data are added and so cannot be seen as final in any way.

HRAO

The time-series for the regional network is still relatively short compared to that of VLBI; but for HRAO (Figure 9.1), which is collocated with the VLBI antenna, agreement is within millimetres. The motion vectors are smaller (Vn=18.1 mm/yr, Ve=13.8 mm/yr) than those predicted for African plate motion in the NUVEL-1A no-net-rotation (NNR) reference frame (Vn=20.05 mm/yr ,Ve=20.66 mm/yr). In comparison to the same data independently processed by SOPAC (Figure 9.2) as available from the SOPAC web page:

`http://lox.ucsd.edu`

the north and east components agree very well, but the vertical component determined by SOPAC is about twice as large at Vu=13.5 mm against Vu=6.7 mm (HartRAO). The smaller vertical component agrees better with the VLBI results (north$\approx$ 16.6, east$\approx$ 17.4, up$\approx -.29$) (Figure 1.3) (Ma and Ryan 1998). HartRAO's solution has shown a gradual improvement of the vertical component, it would however require several years of data before very detailed comparisons could be made. The SOPAC results are as processed by GAMIT, but as an independent global solution. The sudden increase in error bar sizes are due to a change in processing strategy, moving from weekly to daily solutions (private communication M van Domselaar). The HartRAO solutions are daily. This comparison does indicate that the processing strategy and choice of parameters for the GAMIT package as used at HartRAO allows solutions that do not deviate substantially from the SOPAC solutions.

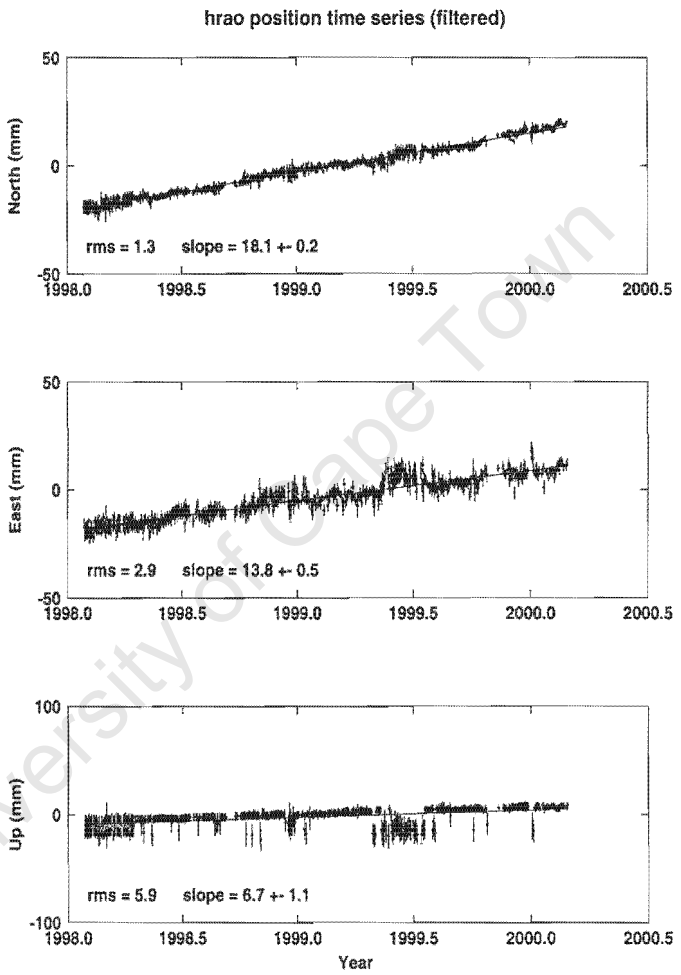

Figure 9.1: IGS station HRAO, filtered time series

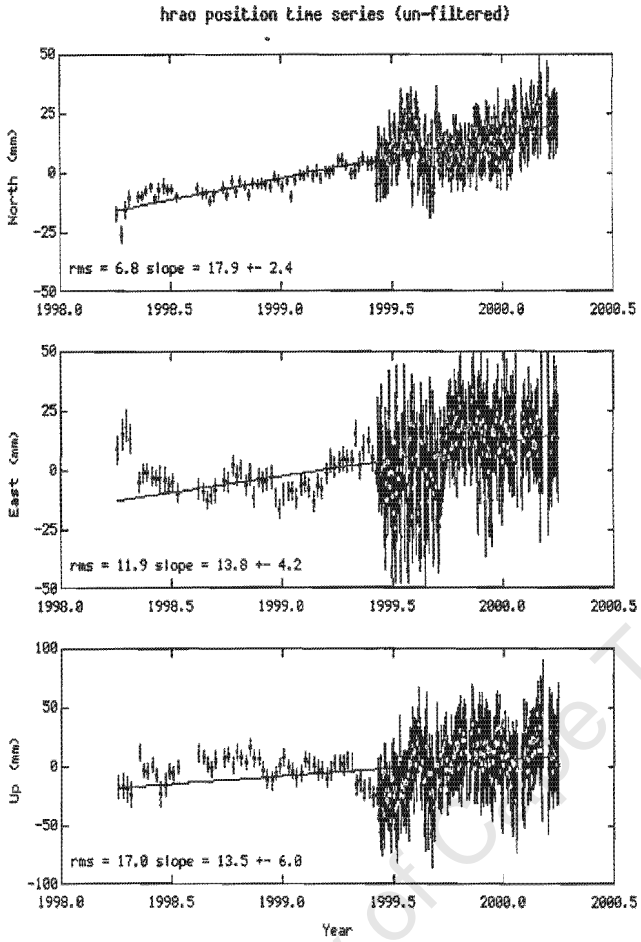

Figure 9.2: IGS station HRAO, unfiltered time series as processed by SOPAC

HARK

Similar to the HRAO comparison, the same data independently processed by SOPAC (Figure 9.4) as available from the SOPAC web page indicate an acceptable agreement between the north and east components. The vertical component is also (as in the HRAO comparison) about twice as large at Vu=17.8 mm (SOPAC) against Vu=8.4 mm (HartRAO). The two stations, HARK and HRAO should in fact exhibit the same motion, as they are located only 2113.8 metres from each other. This would however only be true if everything else was the same, GPS equipment, external references, monumentation, crustal interface and time of data coverage. In fact HARK shows several large data gaps in its time series and has an inferior monument being located on a steel pole attached to a building, which in turn is located on expansive clays. At the time of writing, the HARK installation is to be relocated during mid 2000 and the antenna will be fixed to a monument located on soil (not bedrock). If this difference in motion vector components still persists it would require

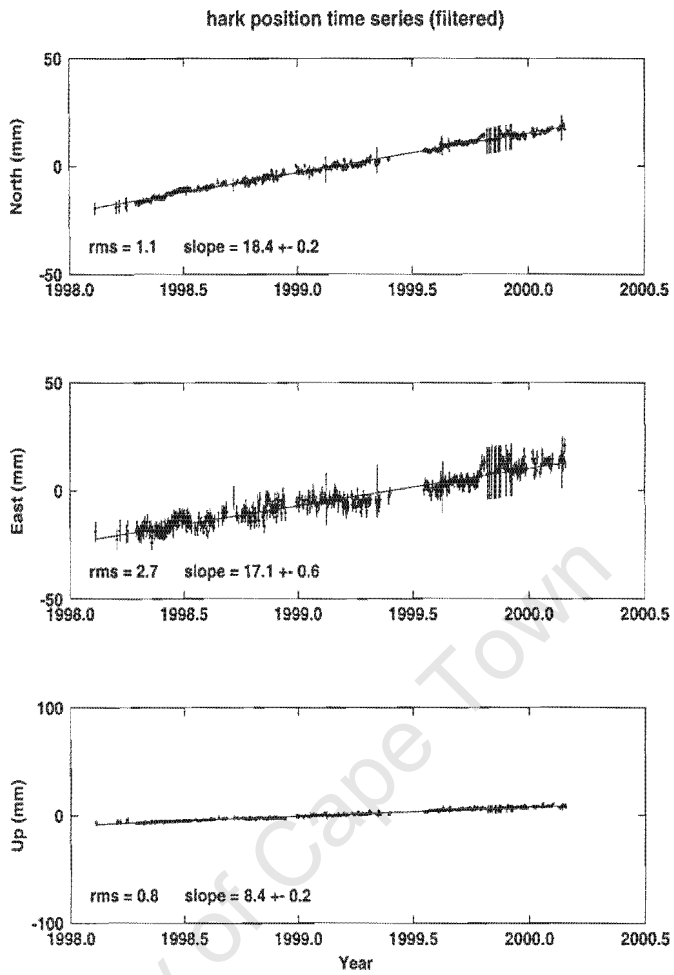

Figure 9.3: IGS station HARK, filtered time series

investigation as to the source and reasons for not being more similar.

SUTH

An interesting preliminary result is to be seen from the SUTH (Sutherland) data as shown in Figure 9.5. The Vn, Ve results for SUTH (Vn=18.7, Ve=17.3 mm/yr), however, are slighly slower than but much closer to the NUVEL-1A NNR prediction (Vn=20.41, Ve=20.17 mm/yr). The HRAO-SUTH relative motion (in the east component Ve=13.8 mm/yr (HRAO) and Ve=17.3 mm/yr (SUTH)) is somewhat disconcerting, but at the moment is being viewed as preliminary, as a longer time-series as well as more IGS stations are required to improve the results and strengthen the network. A preliminary interpretation of the HRAO-SUTH motion by C Hartnady (UCT) (private communication) indicates that the HRAO-SUTH motion results could have major implications for earthquake hazard along the Senqu Seismic Belt which stretches across South Africa and Lesotho from the east coast near Port Shepstone to the west

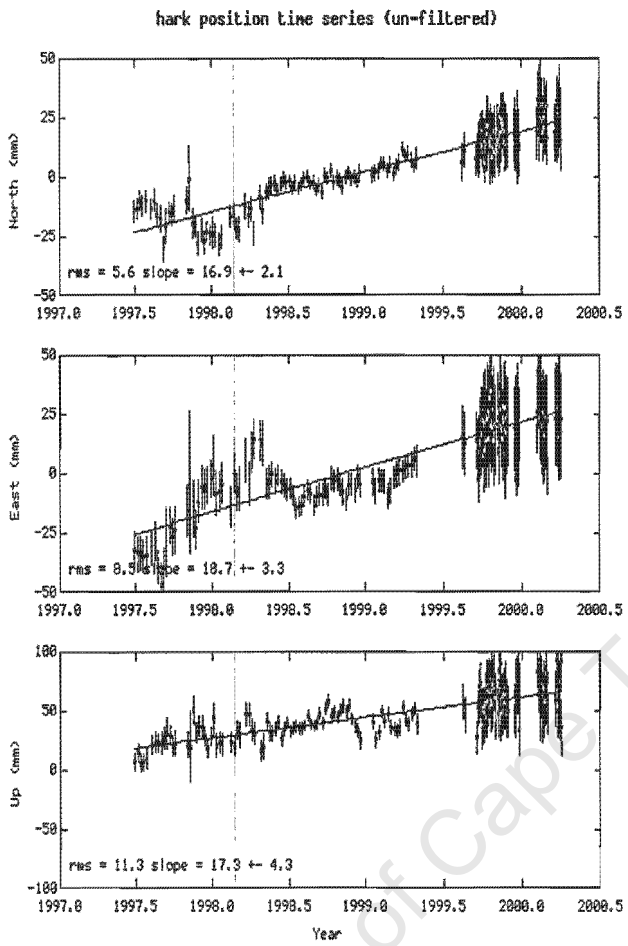

Figure 9.4: IGS station HARK, unfiltered time series as processed by SOPAC

coast near Port Nolloth. It is therefore important to add more stations and maintain the network in order to improve these results. Fair agreement exists between the HartRAO (Figure 9.5) and SOPAC (Figure 9.6) results. The velocity components Vn=18.7, Ve=17.3 (HartRAO) and Vn=19.7, Ve=21.1 (SOPAC) differ with about 1 mm and 4 mm on the north and east components respectively. The SOPAC vertical component (Vu=41.1) is however much higher (and more unrealistic) than the HartRAO vertical component (Vu=4.8). It is expected that the SOPAC determined vertical component will reduce in value as the time series is lengthened.

No attempt is made to interpret the results of the other stations in the network as their baselines (relative to HRAO and each other) are much longer and a longer time-series is required before any interpretation can take place. Their timeseries are however available on the HartRAO Geodesy Programme web page:

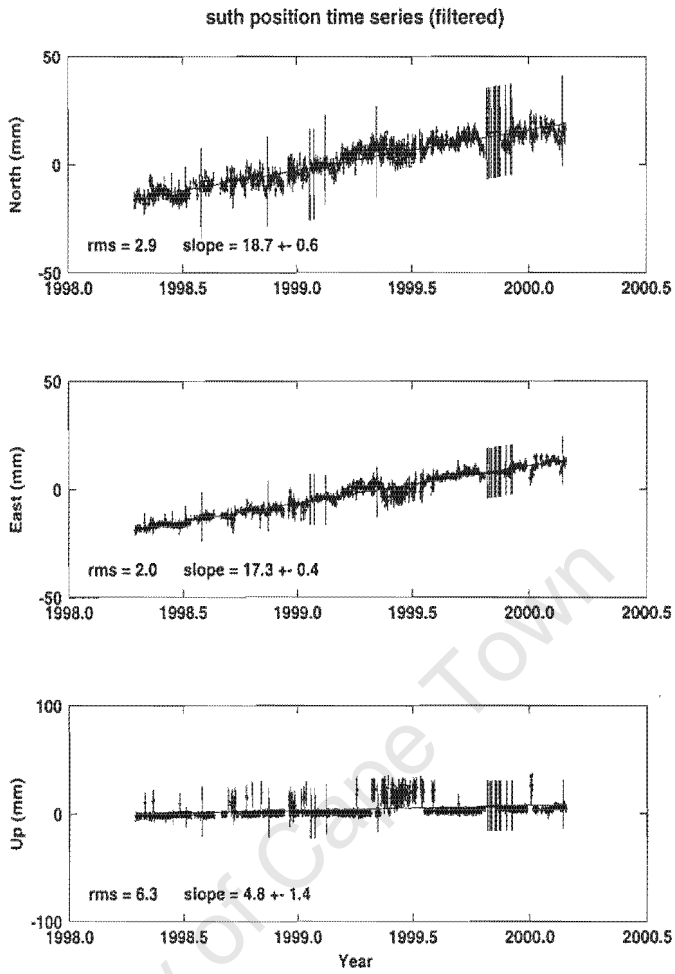

Figure 9.5: IGS station SUTH, filtered time series

`http:\\www.hartrao.ac.za\geodesy\geodesy_index.html`

9.5 Conclusions

During the course of this work, the author has colloborated with JPL and the IGS in order to densify the IGS network and therefore the ITRF in southern Africa. Using GAMIT, a regional network has been processed which has started showing preliminary results which might yet prove to be of scientific value, especially if the results could be used by the IGS as a regional analysis centre contribution. The results for the IGS stations in the southern Africa region compares favourably with independent results determined by SOPAC. The collocated VLBI and HRAO results shows reasonable agreement. It would be useful however to strengthen the network geometry by having at least one

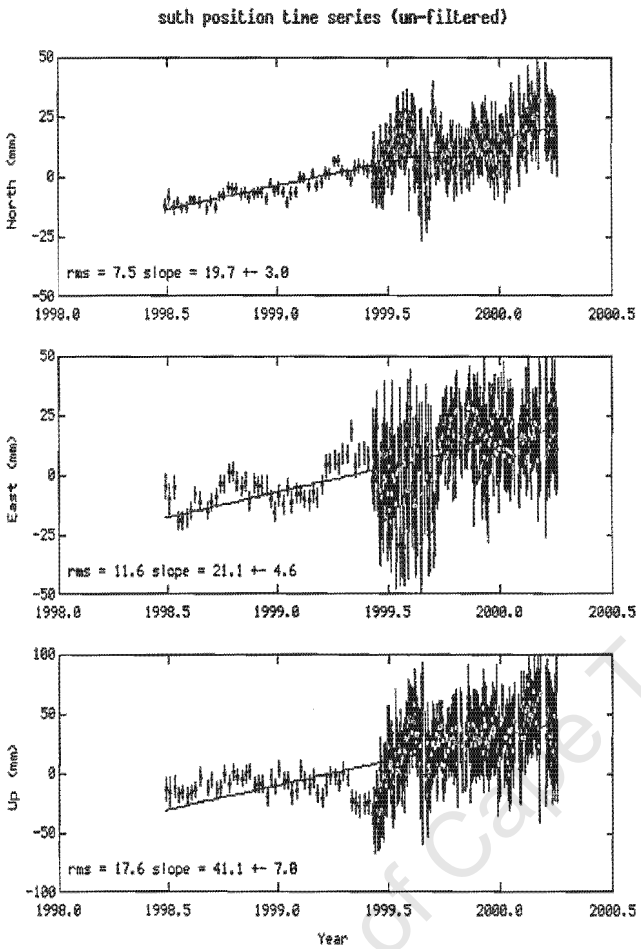

Figure 9.6: IGS station SUTH, unfiltered time series as processed by SOPAC

more IGS station towards the north of HRAO. The establishment of an IGS regional data centre at HartRAO has brought IGS products and data closer home and this has sparked growth in the local use of IGS products. Collaboration with neighbouring countries such as Namibia, will help these countries to adopt the WGS84 datum as their national datum. This has already been the case in Namibia where the ITRF coordinates of the site NAMI has been used as independent check on the new Namibian ITRF based network (private communication Walter Volkmann). The stations HRAO and SUTH also provided critical data for this project.

Chapter 10

Summary, Conclusions and Recommendations

10.1 Summary and Conclusions

Conducting footprint surveys at HartRAO maintain local site integrity through the monitoring of the relative positions of reference points on site and provide necessary high accuracy ties between the different space geodetic techniques. By using a novel approach to the HartRAO footprint, the footprint is seen as a system and the multitude of factors which could affect the local stability and baseline measurement accuracy are considered. This work shows that local effects are imbedded in all global data to a larger or lesser degree, therefore global solutions and regional solutions are contaminated to some extent with local movements. These local movements, if not accounted for or even acknowledged to exist, influence global and regional geodetic results. Local effects could in particular, adversely affect campaign type surveys as the occupation period of reference points are seldom long enough to average out diurnal and seasonal signals.

This work shows that a footprint does not only consist of baseline measurements, but encompasses an appreciation and consideration of local site geological structure, soil conditions and factors which affect local monument stability. Approaching the footprint, or any geodetic monument and its location using a systems approach makes one aware of the fact that the monument and the measurement technique is open to influence from other processes and factors. These processes and factors determine monument stability and measurement accuracy. When viewed holistically one starts to question the traditional approach to footprints and it is clear that in order to eventually achieve millimetre and submillimetre accuracy on the local and global scale, footprints must be able to determine the magnitude and influence of local movements. Although difficult to quantify, selecting and investigating thermal effects on

monument position in this work has shown that it is possible to put numbers to these local movements.

Monument stability depends on a strong interface between the monument and the earth's crust, the crust is defined in this work from the geodesist or surveyor's perspective. Typical weathering profiles will assist the geodesist in assessing the nature of the underlying material on a prospective geodetic monument site. Although many types of monumentation exist, the choice should not be at random or based on cost alone, but stability should be the primary objective. Preceding monument construction, a field investigation is required to determine the size and nature of factors such as faults, joints, fractures, varying ground water levels, slope instability and human engineering, all which could influence a monument's stability. Several other factors should also be kept in mind, amongst these are the techniques and cost of locating bedrock, horizon mask, multipathing and possible vandalism.

Long term monument stability is related to rock mass strength, which in turn depends to some extent on the strength of the intact rock, degree of weathering, joint spacing and groundwater movement out of the rock. The application of rock mechanics will lead to a better understanding of monument instabilities. Classical soil mechanics can be utilised to predict expected stability or evaluate the suitability of a particular location for a monument if it has to be located on soil. Settlement studies as used in engineering can be utilised to determine possible monument instability for stations using buildings as a monument.

By selecting possible thermal expansion as a local effect which should be considered, GPS measurements indicate monumentation instability due to thermal expansion. These measurements are supported by an error analysis and a numerical thermal model. It is shown that diurnal errors due to changing GPS satellite geometry, the ionosphere as well as troposphere can only contribute in some way but are not responsible for the diurnal baseline variation due to thermal expansion. The thermal model is based on the distinct element method and allows various parameters such as coefficient of thermal expansion and hill size to be set by the modeller. Expansion coefficients typical for rock as found on the HartRAO site are in the range 1×10^{-6} to 5×10^{-7} and produce results which are comparable to the GPS measured results. Based on the GPS and the thermal model results, one can state with certainty that it is possible for a hill of a certain geological structure to exhibit thermal expansion due to diurnal heating. This diurnal heating could affect the short term stability of a geodetic monument, inferring that longer term (seasonal) thermal changes will lead to longer term monument instabilities.

The footprint results show an acceptable degree of stability, within the errors of the measurement technique. It would take several years more of footprint surveys before a deformation analysis would be possible. Any anomalous movement of either the radio telescope, SLR or IGS station HRAO, as well as any of the footprint reference points should now be detectable. Dual frequency GPS receivers would improve accuracy and are a necessity on the longer baselines of the footprint.

Using the software suite GAMIT, a regional network is processed weekly. The reference frame is maintained through the IGS orbit and IERS Earth orientation values. The solution is in the NUVEL-1A No-net-rotation (NNR) frame. The stations HRAO, HARK and SUTH define the origin by having their positions constrained. Baseline repeatabilities are 10-15 parts per billion. Although the baseline timeseries is yet too short to produce unequivocal results, results for HRAO compare favourably with VLBI results for HartRAO. Comparison with independent global solutions done at SOPAC indicate that the HartRAO regional solutions would be able to make valuable contributions to the IGS. Densification of the regional network will allow determination of local crustal instabilities on a sub-continental scale, such as is required to monitor the extension of the East African Rift into southern Africa. Using the results of the regional network will allow collaboration with neighbouring countries. The regional network will help these countries to adopt the WGS84 datum as their national datum. This has already been the case in Namibia where the site NAMI has been used as additional control and ITRF reference. Ideally one should have at least one IGS station in each of the southern African countries, this will allow these countries to have a primary ITRF reference point.

10.2 Recommendations

As the nature of this work requires as long a time-series as possible, some recommendations for further work is mentioned:

- The footprint surveys to be continued on a regular basis.
- At least two dual frequency GPS receivers should be acquired to enable the outer and intermediate networks to be surveyed on a regular basis.
- More support be canvassed from the IGN/IGS to enable densification of IGS GPS stations in southern Africa.
- Continuation and upscaling of HartRAO's contribution and involvement in the IGS, IVS and ILRS. In particular we should aim towards being established as an IGS Regional Network Associate Analysis Center (RNAAC).

- Further investigation and numerical modelling of thermal expansion effects on monument installation and their environment should be done.
- Models should be developed to ascertain the stability of geodetic monuments depending on different site locations. It should be possible to infer the stability of a monument by using certain parameters (such as rock structure, degree of weathering, filling material, temperature variations, monument construction) as controlling factors.
- Advanced modelling should lead to a quality factor for geodetic monuments, enabling some sort of weighting to be included in, as example, all IGS monuments. All IGS monuments are not equally stable, therefore a suitable system is required to make allowance for local effects and monumentation instabilities. This would effect the global solutions, which currently regard most monuments as being perfect.

Chapter 11

References

Ackoff, R. L., Gupta, S.K. and Minas, J.S. 1962. *Scientific Method: Optimizing Applied Research Decisions* (New York).

Ahrens, L. H. 1965. *Distribution of the Elements in Our Planet.* McGraw-Hill. New York.

Allisow, B.P., Drosdow, O.A. and Rubinstein, E. S. 1956. *Lehrbuch der Klimatologie.* German translation from the Russian. Deutscher Verlag der Wissenschaften. Berlin.

Altshuler, E. E. 1971 *Corrections for Tropospheric Range Error.* Report AFCRL-71-0419, Air Force Cambridge Research Laboratory. Bedford MA. USA.

Artyushkov, E. V. 1973. Stresses in the lithosphere caused by crustal thickness inhomogeneities. *Journal of Geophysical Research.* **78**. 7675-7708.

ASCE 1996. *Rock Foundations.* Technical engineering and design guides as adapted from the U.S. Army Corps of Engineers, by the American Society of Civil Engineers. Series TA775. R63. ASCE. USA.

Barbieri, G., Giani, G.P., Uras, G. and Vernier, A. 1988. Modellizzazione della frana di crollo di Monte Oili in agro di Baunei (Nuoro). Presentato alla Riunione Plenaria delle Unitá Operative del CNR (gruppo Nazionale Difesa Catastrofi Idrogeologiche) a Roma.

Bell, L., Bryant, M., Nelson, V. and Allenby, R. 1994. *NASA's Space Geodesy Project: A Summary of GPS Footprint Results.* Unpublished report provided by C Noll of the NASA Crustal Dynamics Data Information System (CDDIS).

Bernhardt, F. and Phillips, H. 1958. *Die räumliche und zeitliche Verteillung der Einstrahlung, der Asusstrahlung und der Strahlungsbilanz im Meeresniveau.* Akademie Verlag. Berlin.

Beutler, G., Abell, M.D., Bauersima, I., Gurtner, W., Mader, G.L. Rothacher, M. and Schildknecht, T. 1987. Evaluation of the 1984-Alaska-GPS-Campaign

with the Bernese GPS software. *Journal of Geophysical Research*, Vol. 92, NO. B2. pp 1295-1303.

Bickley, W.G. and Talbot, A. 1961. *An Introduction to the Theory of Vibrating Systems.* Oxford University Press. London. UK.

Braddick, H.J.J. 1965. *Vibrations, Waves, and Diffraction.* McGraw-Hill. Berkshire. UK.

Bock, Y. and Shimada, S. 1989. Continously Monitoring GPS Networks for Deformation Measurements. JPL Geodesy and Geophysics Preprint No. 193.

Bock, Y., Wdowinski, S., Fang, P., Zhang, J., Williams, S., Johnson, H., Behr, J., Genrich, J., Dean, J., van Domselaar, M., Agnew, D., Wyatt, F., Stark, K., Oral, B., Hudnut, K., King, R., Herring, T., Dinardo, S., Young, W., Jackson, D. and Gurtner, W. 1997. Southern California Permanent GPS Geodetic Array: Continuous measurements of regional crustal deformation between the 1992 Landers and 1994 Northridge earthquakes. *Journal of Geophysical Research - Solid Earth* Vol.102, No. B8. 18013-18034.

Bott, M. H. P. and Kusznir, N.J. 1984. The origin of tectonic stress in the lithosphere. *Tectonophysics.* **105**,1-13.

Bowles, J.E. 1977. *Foundation Analysis and Design.* McGraw-Hill. New York.

Brink, A.B.A. 1979. *Engineering Geology of Southern Africa.* Vol. 1, Building Publications, Pretoria.

Brink, A.B.A. & Associates. 1993. Unpublished report entitled Report to the Directorate Hartebeesthoek Radio Astronomy Observatory on Geotechnical Investigation for Satellite Laser Ranging Pad at HartRAO.

Brunner, F. and Tregoning, P. 1994. Investigation of Height Repeatability from GPS Measurements. *Australian Journal of Geodetic and Photogrammetric Surveying*, **60**, pp. 33-48.

Carslaw, H.S. and Jaeger, J.C. 1947. *Conduction of Heat in Solids.* First Edition. Oxford University Press. Oxford. UK.

Carslaw, H.S. and Jaeger, J.C. 1959. *Conduction of Heat in Solids.* Second Edition. Oxford University Press. Oxford. UK.

Chorlton, F. 1983. *Textbook of Dynamics.* 2nd ed. Ellis Horwood series in mathematics and its applications. Ellis Horwood Ltd. West Sussex. England.

Combrinck, W.L. and Schmidt, M. 1998. Position Paper, Physical Site Specifications: Geodetic Site Monumentation. In: *IGS Workshop Proceedings:1998 Network Systems Workshop.* C.E. Noll, K.T. Gowey, R.E. Neilan, eds. Pasadena, CA: Jet Propulsion Laboratory, 1998

Combrinck, W.L. and Merry, C.L. 1997. Very long baseline interferometry antenna axis offset and intersection determination using GPS. *Journal of Geophysical Research*, Vol. 102, NO. B11. pp 24,741-24,743.

Combrinck, W.L. 2000. Local surveys of VLBI telescopes. In: Proceedings of the First IVS General Meeting, ed. N. R. Vandenberg. NASA/CP-2000-209893.

Coates, D.F. 1964. Residual stress in rocks. In: *State of stress in the Earth's crust.* ed. W.R Judd. Elsevier. New York.

Cooks, J. 1979. Die verband tussen litologie en landvorme. *South African Geographer*, **7**, 127-135.

Cooks, J. 1981. Rock quality measured by seismic wave velocity as a factor in landform development. *South African Journal of Science*, **77**, 517-521.

Cooks, J. 1983. Geomorphic response to rock strength and elasticity, *Zeitschrift für Geomorphologie* , **27**, 483-493.

Cosentino, R.J. and Diggle, D.W. 1996. Differential GPS. In: *Understanding GPS: principles and applications.* E.D Kaplan ed. Artech House. USA.

CRC Handbook of Chemistry and Physics. 1993. Ed. David R. Lide. CRC Press. Florida. USA.

Cundal, P.A. 1971. A computer model for simulating progressive large scale movements in blocky rock systems. *Rock fracture.* Proc. int. symp. Nancy. Paper 2-8.

Dabas, R.S., He, Y.W. and Zhang, M.G. 1996. Ionospheric effects on space communication systems. In *Handbook on Radiopropagation Related to Satellite Communications in Tropical and Subtropical Countries.* ed. G.O. Ajayi. International Centre for Theoretical Physics, Trieste, Italy.

D'Andrea, D.V., Fischer,R.L. and Fogelson, D.E. 1965. Prediction of compressive strength from other rock properties. *U.S. Bureau of Mines R.I.* **6702**.

Dardis, G.F., Beckedahl, H.R. and Stone, A.W. 1988. Fluvial Sytems. In *The Geomorphology of Southern Africa.* eds. B.P.Moon and M.J. Selby. Southern Book Publishers (Pty) Ltd. Johannesburg.

Dietrich R (editor). 1996. The Geodetic Antarctic Project GAP95. German Contributions to the SCAR 95 Epoch Campaign. Deutsche Geodatische Kommission. Munchen.

Dingle, R.V., Siesser, W.G. and Newton, A.R. 1983. *Mesozoic and Tertiary Geology of Southern Africa.* Balkema. Rotterdam.

Deere, D.U. 1964. Technical description of rock cores for engineering purposes. *Rock Mechanics and Engineering Geology*, **1**,No. 1, 17-22.

Dong, D.N. and Bock, Y. 1989. GPS network analysis with phase ambiguity resolution applied to crustal deformation studies in California. *Journal of Geophysical Research*, Vol. 94, pp 3949-3966.

Elósegui,. Davis, J.L., Jaldehag, R.T.K., Johansson, J.M., Niell, A.E. and Shapiro, I.I. 1995. Geodesy using the Global Positioning System: The effects of signal scattering on estimates of site position. *Journal of Geophysical Research*, Vol. 100, NO. B7. pp 9921-9934.

Elósegui,. Davis, J.L., Johansson, J.M., and Shapiro, I.I. 1996. Detection of transient motions with the Global Positioning System. *Journal of Geophysical Research*, Vol. 101, NO. B5. pp 11249-11261.

Engelder, T. 1993. *Stress Regimes in the Lithosphere.* Princeton University Press. Princeton, New Jersey. USA.

Engelder, T. and Sbar, M.L. 1984. Near-surface in situ stress. *Journal of Geophysical Research.* **89**. 9321-22.

Feda, J. 1992. *Creep of Soils and Related Phenomena.* Elsevier. Amsterdam.

Fleitout, L. and Froidevaux, C. 1983. Tectonic stress in the lithosphere. *Tectonics.* **2**. 315-24.

Forbes, C. 1996. Geological Survey Report No. 1996-0138. Geological Survey, Pretoria, South Africa.

Foth, H.D. 1984. *Fundamentals of Soil Science.* John Wiley & Sons. New York. USA.

Fowler, C.M.R. 1990. *The Solid Earth.* An introduction to global geophysics. Cambridge University Press. Cambridge.

Georgiadou, Y. 1990. Ionospheric delay modelling for GPS relative positioning. GPS'90 Proceedings. In: *Second International Symposium on Precise Positioning with the Global Positioning System.* Canadian Institute of Surveying and Mapping. Ottawa. Canada.

Giani, G.P. 1992. *Rock Slope Stability Analysis.* A. A. Balkema. Rotterdam.

Greiner, G. and Illies, J.H. 1977. Central Europe: Active or residual tectonic stresses. *Pure and Applied Geophysics.* **115.** 11-26.

Hart, R., Cundall, P.A. and Lemos. L. 1988. Formulation of a three-dimensional distinct element model-part II. Mechanical calculation fro motion and interaction of a system composed of many polyhedral blocks. *Int. J. Rock Mech. Min. Sci.*, **25(3)**, 117-125.

Harvey, D. 1969. *Explanation in Geography.* Edward Arnold. London.

Herget, G. 1988. *Stresses in Rock.* A.A. Balkema. Rotterdam. Netherlands.

Heywood, H. 1956. Solar Energy: Past, Present and Future Applications. *Engineering*, **176**. 377-380.

Hofmann-Wellenhof, B., Lichtenegger, H, and Collins, J. 1993. *Global Positioning System.* Theory and Practice. Springer-Verlag. Wien.

Holtzhausen, G.R. and Johnson, A.M. 1979. The concept of residual stress in rock. *Tectonophysics.* **58**. 237-67.

Holtz, G.T and Kovacs, W.D. 1981. *An Introduction to Geotechnical Engineering.* Prentice-Hall. New Jersey.

Hooker, V.E. and Duvall, W.I. 1971. In situ rock temperature: Stress investigations in rock quarries: Report of Investigations 7224, Washington, D.C., U.S. Bureau of Mines.

Hudson, N.W. 1981. Non-technical constraints on soil conservation. In: Tingsanchali, T. and Eggers, H. (eds.), *Southeast Asian Regional Symposium on Problems of Soil Erosion and Sedimentation.* Asian Institute of technology, 15-26.

Hungr, O. and Evans, S. G. 1988. Notes on dynamic analysis of flowslides. In C.H. Bonnard (ed.) *Landslides, Proc. 5th int. symp., Lausanne.*

Ingersoll, L.R., Zobel, O.J. and Ingersoll, A.C. 1955. *Heat Conduction with Engineering, Geological and Other Applications.* Thames and Hudson. London.

Ishihara, K. 1981. Strength of cohesive coils under transient and cyclic loading conditions. State-of-the-art in earthquake engineering. In: Ergunay O. and Erdik M. (eds), *Turkish National Committee on Earthquake Engineering.*

Jaeger, J.C and Cook, N.G.W. 1963. Pinching-off and disking of rocks. *Journal of Geophysical Research*, **68**, 1759-1765.

Kale, G. 1979. *Theory of Science.* An Introduction to the History, Logic, and Philosophy of Science. McGraw-Hill. New York.

Kaplan et al. 1996. *Understanding GPS: principles and applications.* E.D Kaplan ed. Artech House. USA.

Kassir, M.K. and Sih, G.C. 1975. *Three-dimensional crack problems.* Noordhoff International Publishing. Leyden.

Kelvin Lord. 1861. *Trans.Roy.Soc.Edin.* **22**, 405.

King, L.C. 1953. Canons of landscape evolution. *Bulletin of the Geological Society of America*, **64**, 721-751.

King, L.C. 1967. *Morphology of the Earth.* Oliver and Boyd. Edinburgh.

Kreith, F. *Principles of Heat Transfer.* International Textbook Company. Scranton. Pennsylvania.

Kuang, S. 1996. *Geodetic Network Analysis and Optimal Design: Concepts and Applications.* Ann arbor Press, Inc. Chelsea, Michigan.

Lambe, T.W. 1964. Methods of estimating settlement. *J. Soil Mech. Found. Div. Am. Soc. Civ. Eng.*, **90**, no. SM5.

Leick, A. 1990. *GPS Satellite Surveying.* John Wiley & Sons. New York. USA.

Leva, J.L, de Haag, Uijt de Haag, M. and Van Dyke K. 1996. Performance of Standalone GPS. In *Understanding GPS: principles and applications.* E.D Kaplan ed. Artech House. USA.

Lowe, D. R. 1980. Archean sedimentation. *Ann. Rev. Earth Planet. Sci.* **8**, 1245-167.

Ma, C., Watkins, M.M. and Heflin M. 1994. Global Reference Frame: Intercomparison of Results (SLR, VLBI and GPS). NASA Conference Publication 3283, Satellite Laser Ranging in the 1990s. Report of the 1994 Belmont Workshop. NASA. USA.

Ma, C. and J. W. Ryan. 1998 . NASA Space Geodesy Program – GSFC DATA Analysis – 1998, VLBI Geodetic Results 1979-1998, August, 1998.

Main, I.G. 1978. *Vibrations and Waves in Physics.* Cambridge University Press. Cambridge. UK.

Manning, J.C. 1987. *Applied Principles of Hydrology.* Merrill Publishing Company. Ohio. USA.

McAdams, W.H. 1954. *Heat Transmission.* 3rd ed. McGraw-Hill. New York.

McNutt, M. 1980. Implications of regional gravity for state of stress in the earth's crust and upper mantle. *Journal of Geophysical Research.* **85.** 6377-96.

Meissner, R. 1986. *The Continental Crust. A Geophysical Approach.* Academic Press, Inc. London.

Meyer, S.L. 1975. *Data Analysis for Scientists and Engineers.* John Wiley & Sons. USA.

Moon, B.P. and Selby, M.J. 1983. Rock mass strength and scarp forms in southern Africa. *Geografiska Annaler*, **65A**, 135-145.

Moon, B.P. 1985. Controls on the form and development of rock slopes in fold terrane, in *Hillslope Processes*, ed. A.D Abrahams. Allen & Unwin. Boston. USA.

Moon, B.P. and Dardis, G.F. 1988. eds. In the introduction to *The Geomorphology of Southern Africa.* Southern Book Publishers (Pty) Ltd. Johannesburg.

NASA Technical Paper 2147. 1983. *The NASA Geodynamics Program: An Overview.* Scientific and Technical Information Branch. Office of Space Science and Aplications. NASA. Washington. USA.

Partridge, T.C. and Maud, R.R. 1987. Geomorphic evolution of southern Africa since the Mesozoic. *South African Journal of Geology*, **77**, 207-9.

Richardus, P. 1984. *Project Surveying.* General adjustment and optimization techniques with applications to engineering surveying. 2nd ed. A. A. Balkema, Boston.

Selby, M.J. 1980. A rock mass strength classification for geomorphological purposes: with tests from Antarctica and New Zealand, *Zeitschrift fur Geomorphologie*, **24**, 31-51.

Selby, M.J. 1982. Controls on the stability and inclinations of hillslopes formed on hard rock. *Earth Surface Processes and Landforms*, **7**,449-467.

STANAG 4294. 1990. NAVSTAR Global Positioning System (GPS) System Characteristics, Preliminary Draft. NATO Unclassified Document. Prepared by ARINC Research Corporation for the Joint Program Office, Headquarters Space System Division (AFSC), Los Angeles Air Force Base.

Stettler, E.H. and Craill, C. 1993. Geological Survey Report No. 1993-0051. Geological Survey, Pretoria, South Africa.

Tankard, A.J., Jackson, M.P.A., Eriksson, K.A., Hobday, D.K., Hunter, D.R., and Minter, W.E.L. 1982. *Crustal Evolution of Southern Africa.* 3.8 Billion Years of Earth History. Springer-Verlag. New York.

Terzaghi, K. 1962. Stability of steep slopes in hard unweathered rock. *Geotechnique*, **12**, 251-270.

Trethewey, M.L., Catchpole, I. and Hansla, A. 1993. Single Frequency Ionosphere Determination using GPS *Proceedings of the Institute of Navigation GPS-93 Vol II*, Sixth International Technical Meeting of the Satellite Division of the Institute of Navigation, Salt Lake City, Utah.

Trimble. 1996. *GPSurvey software, WAVE Software User's Guide.* Revision A. Trimble Navigation Limited. USA.

Vaníček, P. and Krakiwsky, J. 1986. *Geodesy: the Concepts.* 2nd ed. Elsevier Science Publishers. The Netherlands.

van Wijk, W.R. and Scholte Ubing, D.W. 1966. Radiation. In *Physics of Plant Environment* ed. W.R.van Wijk. North-Holland Publishing Company. Amsterdam.

Varnes D.J. 1978. Slope movement types and processes. In Schuster R.L. & Krizek R.J. (eds), *Landslides: Analysis and Control.* Special Report, 176. Transportation Research Board, National Academy of Sciences, Washington, pp. 11-33.

Whalley, B.W. 1976. *Properties of materials and geomorphological explanation.* Oxford University Press. Oxford.

Willemse, J. 1969. The geology of the Bushveld Igneous complex: The largest repository of magmatic ore deposits in the world. *Econ. Geol. Monogr.* **4**, 1-22.

Wood, A. 1942. The development of hillslide slopes. *Proceedings of the Geological Association*, **53**, 128-140.

Wuerker, R.G. 1955. Annotated tables of strength and elastic properties of rock. *Transactions of the Australian Institute of Mining Engineers,* **202**,157.

Wyatt, F., Johnson, H. and Agnew, D. 1995. Improved stability of a deeply anchored geodetic monument for deformation monitoring. *Geophysical Research Letters*, **22**, No. 24, 3533-3536.

Wylie, C.R. 1960. *Advanced Engineering Mathematics.* McGraw-Hill. New York. USA.

Yatsu, E. 1966. *Rock control in geomorphology.* Sozosha. Tokyo.

Zaruba Q. and Mencl V. 1969. *Landslides and their control.* Elsevier, New York, USA.

Zoback, M.L. et al. 1989. Global patterns of tectonic stress. *Nature.* **341.** 291-98.

Zumberge J.F., Fulton D.E. and Neilan R.E. (editors). 1997. International GPS Service for Geodynamics 1996 Annual Report. JPL, Pasadena, U.S.A.

Zumberge J.F., Webb F.H. and Watkins M.M. 1998. Efficient Estimation of Precise High-Rate GPS Clocks. In IGS 1998 Analysis Center Workshop. Eds. J.M.Dow, J.Kouba and T.Springer. European Space Centre of the ESA. Darmstadt.

Appendix A

Clarification of Certain Concepts

Introduction

This appendix has been included to allow additional clarification of certain concepts if required. It is structured to follow the reasoning in the main text from where reference to it is made and has not been structured to be read as a separate chapter. Each section therefore does not necessarily follow on from the previous. A list of the topics discussed is included in the contents (page viii).

A.1 Equation describing thermal variation at the Earth's surface

In general we follow the discussion of Main (1978) in order to keep notation uniform. All other forces not due to the elasticity of the spring are ignored; there are no friction, viscosity or gravity in this model system. Suppose the mass is at some position a distance ψ to the right of its equilibrium position. The spring will exert a force towards the left and in a similar way, if the displacement is towards the left, the force will act to the right. In both cases the magnitude of the force will increase as the size of the displacement increases. The mass always experiences a return force which tends to alter the displacement ψ towards its zero value.

The free motion of this system therefore takes the form of a vibration and the mass is given an acceleration

$$\ddot{\psi} \equiv \frac{d^2\psi}{dt^2} \tag{A.1}$$

which is determined by Newton's second law

$$m\ddot{\psi} = F_s. \tag{A.2}$$

Here F_s is the spring force. The mass will have acquired some momentum due to its velocity and will overshoot its equilibrium position. After passing its equilibrium position, the mass will decelerate, be brought to rest and accelerate back to its equilibrium position where it will overshoot again. The direction of the displacement ψ therefore continually alternates. Both elasticity and the inertial property of the mass are necessary for vibrational motion. The elasticity tends to return the mass to its equilibrium position whereas the inertia makes it overshoot. All vibrational phenomena depend on the existence of parameters analogous to inertia and elasticity.

Harmonic Motion

Using the second-order differential equation of motion (A.2) we can find an expression giving ψ as a function of the time t. The equation can only be solved if it is known exactly how F_s varies with ψ. To enable us to get quantitative results we make the simple assumption that F_s is proportional to ψ for the spring in our model. Therefore

$$F_s = -s\psi \tag{A.3}$$

where the positive constant s is the spring constant or stiffness. Our model now has all the properties of the imaginary object known to physics as the Harmonic Oscillator.

The equation of motion (A.2) can now be written as

$$m\ddot{\psi} = -s\psi \tag{A.4}$$

Rewritten in standard form this becomes

$$\ddot{\psi} + \omega_0^2\psi = 0 \tag{A.5}$$

The angular frequency or radian frequency,(a positive quantity) ω_0 introduced in equation (A.5) can be written as

$$\omega_0 \equiv |(s/m)^{\frac{1}{2}}| \tag{A.6}$$

Equation (A.5) is satisfied by

$$\psi(t) = A\cos(\omega_0 t + \phi) \tag{A.7}$$

where A is any constant length and ϕ is any constant angle. A quantity which depends on time this way varies harmonically. If ψ varies harmonically the

vibration is known as harmonic motion. An important quantity in (A.7) is the phase angle of the oscillation which is defined as $\omega_0 t + \phi$. The phase angle depends on the choice of the time origin and is especially useful when the phases of two oscillations are to be compared. Harmonic motion is periodic and repeats itself in cycles, the phase increases uniformly with time so that values of any angle which differ by an integral multiple of 2π are physically indistinguishable. When the phase increases by 2π the interval τ given by $\omega_0 \tau = 2\pi$ has occurred. This time interval is called the period of the vibration. The period is defined as $f^{-1} = 2\pi/\omega_0$. During a full cycle, ψ takes on all values of the amplitude A. The frequency is the number of cycles per unit time, so that

$$\nu_0 = \omega_0/2\pi \tag{A.8}$$

Boundary conditions

Equation (A.7) contains two arbitrary constants. Any pair of values of A and ψ will describe an oscillation which can be performed by the spring and mass. However, in practice one deals with a vibration whose parameters have been determined by other physical conditions such as the method used to get the vibration going in the first place. These boundary conditions sets the values of A and ψ for the particular vibration. As an example, if the mass was originally held at a distance A_1 to the right of its equilibrium position, and thereafter released at time $t = 0$, one could say that

$$\psi(0) = A\cos\phi = A_1 \tag{A.9}$$

and

$$\dot{\psi}(0) = -\omega_0 A\sin\phi = 0 \tag{A.10}$$

where $\dot{\psi}$ means $d\psi/dt$. These two boundary conditions will fix A and ϕ. The second condition shows that ϕ is 0 or π. The first condition makes $\cos\phi$ positive so we reject the last alternative. Therefore $A = A_1$ and (A.7) can be written as

$$\psi(t) = A_1\cos\omega_0 t \tag{A.11}$$

Phase differences

In the example just discussed, the vibration started at $t = 0$, this conveniently makes ϕ zero. If one had a different starting time t_0, then having a different value for ϕ would advance or retard the action by the same amount in time. However, when one wants to compare two or more oscillations of the same frequency the phase constant ϕ assumes new importance. If the amplitudes of the oscillations vary in step, so that they are always in the ratio A_2/A_1 the two oscillations are in phase. If one oscillation happens to reach the peak of its amplitude before the other, it leads in phase and has a phase advance of

ϕ relative to the second oscillation. The second oscillation has a phase lag of $|\phi|$. A phase lag greater than 180° is equivalent to a phase lead of less than 180° and it is normally convenient to use the smaller value. When there is a phase difference of exactly 180° the oscillations are in antiphase.

Alternative solutions for harmonic motion

The solution (A.7) can be written in different forms. Main (1978) for instance derives four alternative ways of writing the solution. For our purposes we need a form which can be easily differentiated and integrated. Following the reasoning of Main (1978) we substitute a trial expression of the form

$$\psi = Ce^{pt} \tag{A.12}$$

in order to try and solve the differential equation (A.5). The substitution is acceptable if the relation

$$p^2 = -\omega_0^2 \tag{A.13}$$

is satisfied. We do this as we require a function that when differentiated twice produces itself multiplied by a negative constant. This is true for p being equal to two values, $\pm i\omega_0$ so that the general solution could be written as the linear combination

$$\psi(t) = Ce^{i\omega_0 t} + C'e^{-\omega_0 t} \tag{A.14}$$

where C and C' are complex constants (Braddick 1965, Main 1978). This solution has four arbitrary constants (Re C, Im C, Re C' and Im C'), but the boundary conditions can only manage two. A single physical displacement can only be represented if ψ is either real or imaginary but not complex. By insisting that the two terms are complex conjugates of each other, the expression on the right of (A.14) can be made real so that

$$(C'e^{-i\omega_0 t})^* = Ce^{i\omega_0 t} \tag{A.15}$$

As the complex conjugate of a product of two quantities equals the product of their complex conjugates, we have

$$C'e^{i\omega_0 t} = Ce^{i\omega_0 t} \tag{A.16}$$

therefore

$$C' = C^* \tag{A.17}$$

We can therefore write

$$\psi(t) = Ce^{i\omega_0 t} + C^*e^{-i\omega_0 t} \tag{A.18}$$

which has only two arbitrary constants (Re C and Im C). The expression on the right of (A.18) is real so one can write

$$\psi(t) = Re(Ce^{i\omega_0 t}) + Re(C^*e^{-i\omega_0 t}) \tag{A.19}$$

and so

$$\psi(t) = 2Re(Ce^{i\omega_0 t}) \tag{A.20}$$

If a new complex constant $T_0 \equiv 2C$ is defined one reaches the form

$$\psi(t) = Re(T_0 e^{i\omega_0 t}) \tag{A.21}$$

the right hand side which will from this point be written as $T_0 e^{i\omega_0 t}$ leaving implicit the instruction to take the real part. For many purposes, although not for all, the imaginary component can be dropped since equation (A.21) contains the information which we require, namely the phase and amplitude (Bickley & Talbot 1961).

A.2 Elasticity and Stress in the Upper Crust

It is often convenient to assume that the upper crust behaves as a linear elastic body. On the scale of the footprint, say a circular area with a radius of 20 km, the earth is approximately isotropic and has elastic properties which are independent of direction. On the assumption that the crust suffers from small strains as found for elastic behaviour, the principal stress axes should coincide with the principal strain axes. In this case the elastic behaviour of the crust and lithosphere can be represented by three equations of linear elasticity. These equations define the principal stresses of the three-dimensional stress tensor as linear functions of the principal strains (Jaeger and Cook,1969):

$$\sigma_1 = (\lambda + 2\zeta)\epsilon_1 + \lambda\epsilon_2 + \lambda\epsilon_3 \tag{A.22}$$

$$\sigma_2 = \lambda\epsilon_1 + (\lambda + 2\zeta)\epsilon_2 + \lambda\epsilon_3 \tag{A.23}$$

$$\sigma_3 = \lambda\epsilon_1 + \lambda\epsilon_2 + (\lambda + 2\zeta)\epsilon_3 \tag{A.24}$$

where λ and ζ are elastic properties of the rock (Lame's constants). The ratio of shear stress to shear strain ζ is known as the modulus of rigidity. The elastic property λ relates stress with strain in two perpendicular directions and $\lambda + 2\zeta$ relates stress and strain in the same direction.

Volumetric strain is defined as

$$\Delta\epsilon = \epsilon_1 + \epsilon_2 + \epsilon_3 \tag{A.25}$$

so that one can combine equations (A.22, A.23, A.24) as

$$\sigma_i = \lambda\Delta\epsilon + 2\zeta\epsilon_i. \tag{A.26}$$

To discuss the two elastic constants, Young's modulus (E) and Poisson's ratio (ν), the uniaxial stress state which is a state for which only one component of principal stress is not zero, should first be introduced.

For uniaxial stress $\sigma_1 \neq 0, \sigma_2 = \sigma_3 = 0$, and the three equations of elasticity can be written as

$$\sigma_1 = (\lambda + 2\zeta)\epsilon_1 + \lambda\epsilon_2 + \lambda\epsilon_3 \tag{A.27}$$

$$0 = \lambda\epsilon_1 + (\lambda + 2\zeta)\epsilon_2 + \lambda\epsilon_3 \tag{A.28}$$

$$0 = \lambda\epsilon_1 + \lambda\epsilon_2 + (\lambda + 2\zeta)\epsilon_3 \tag{A.29}$$

To obtain the relationship between the strain parallel to the applied stress ϵ_1 and strain in the directions of zero stress, ϵ_2 and ϵ_3 one can use equations (A.28) and (A.29) so that

$$\epsilon_2 = \epsilon_3 = -(\frac{\lambda}{2(\lambda + \zeta)})\epsilon_1. \tag{A.30}$$

If we substitute values for ϵ_2 and ϵ_3 back into equation (A.27) we find the ratio between stress and strain for uniaxial stress (Engelder 1993). This ratio is Young's modulus,

$$E = \frac{\sigma_1}{\epsilon_1} = \frac{\zeta(3\lambda + 2\zeta)}{\lambda + \zeta}. \tag{A.31}$$

Equation (A.31) is Hooke's law in simplified form,

$$\sigma_{ij} = C_{ijkl}\epsilon_{kl} \tag{A.32}$$

where the stiffness tensor is denoted by C_{ijkl}. When an elastic rock is under uniaxial stress, there will be shortening in one direction and lengthening in orthogonal directions. Poisson's ratio describes the ratio of the lateral expansion to the longitudinal shortening:

$$\nu = -\frac{\epsilon_2}{\epsilon_1} = (\frac{\lambda}{2(\lambda + \zeta)}). \tag{A.33}$$

Typical values for rocks of ν is in the range 0.15 to 0.30.

A.3 NTM elastic parameter

The parameter is based on Newton's law of restitution, which states that *when two particles impinge, their relative velocity component along the common normal after impact, bears a constant ratio $-K$ to that before impact, where K is a constant for given materials and* $0 \leq K \leq 1$.
The coefficient of restitution is set as $K = 1$ for a perfectly elastic impact and for an inelastic impact $K = 0$. Following an example by Chorlton (1983) adapted for our purpose we consider two adjacent two dimensional blocks Bm_1 and Bm_2. These blocks each have velocity components $[u_1, v_1]$ and $[u_2, v_2]$ respectively. If relative motion between the two blocks leads to impact, an impulsive action occurs at the point of contact, resulting in a change of the line-of-centre components to values u_1', u_2' immediately after impact, while the

components at right angles to these, v_1, v_2, remain unchanged. Considering the conservation of linear momentum along the line of centres one has

$$Bm_1u_1 + Bm_2u_2 = Bm_1u_1' + Bm_2u_2'. \tag{A.34}$$

Using Newton's law of restitution,

$$u_1' - u_2' = -K(u_1 - u_2). \tag{A.35}$$

The kinetic energy lost ΔKE at impact is given by

$$\Delta KE = \frac{1}{2}Bm_1(u_1^2+v_1^2)+\frac{1}{2}Bm_2(u_2^2+v_2^2)-\frac{1}{2}Bm_1(u_1'^2+v_1^2)-\frac{1}{2}Bm_2(u_2'^2+v_2^2), \tag{A.36}$$

i.e.

$$\Delta KE = \frac{1}{2}Bm_1(u_1^2 - u_1'^2)+\frac{1}{2}Bm_2(u_2^2 - u_2'^2). \tag{A.37}$$

Using equations (A.34) and (A.35) one finds

$$u_1 - u_1' = Bm_2(1+K)(u_1 - u_2)/(Bm_1 + Bm_2), \tag{A.38}$$

$$u_2 - u_2' = -Bm_1(1+K)(u_1 - u_2)/(Bm_1 + Bm_2), \tag{A.39}$$

$$u_1+u_1' = ([2Bm_1 + (1-K)Bm_2]\,u_1+Bm_2(1+K)u_2)/(Bm_1+Bm_2), \tag{A.40}$$

$$u_2'+u_2 = (Bm_1(1+K)u_1+[2Bm_2 + (1-K)Bm_1]\,u_2)/(Bm_1+Bm_2). \tag{A.41}$$

Sustitution into equation (A.37) gives

$$\Delta KE = \frac{1}{2}Bm_1Bm_2(1-K^2)(u_1 - u_2)^2/(Bm_1 + Bm_2), \tag{A.42}$$

which shows there is no loss of energy for a perfectly elastic impact. For the NTM this never occurs, as rock impacts are not perfectly elastic.

Appendix B

Certain Procedures

B.1 Thermal data reduction procedures

- Edit GPSurvey output files to the format; station no., day, month, year, hour, minute, second, $\Delta x, \Delta y, \Delta z$, slope, height.
- A program was written (thermal.c) to convert the date and time to MJD. Example input line:

  thermal (executable) threed.nlr (input file) thermal.xyz (output file) -toMJD (command)

  Example input file line:

  1 21 10 1997 11 30 00 470.8526 760.4472 1185.4401 175.5214 1485.0086

  Resulting output for this line:

  1 50742.479167 470.8526 760.4472 1185.4401 175.5214 1485.0086

- Use the program thermal.c to convert the output of the decoder program (DECODER) to MJD, temperature for a selected channel.
  Example command parameters:

  thermal nov9704.dat nov9704.ax0 -ax -nofit -skip

  Example output:

  50765.292465 24.1200

  If the input file is too large, divide the file into subfiles.
- In order to find the correlation between, say Δx and temperature, one

has to apply curve fitting to the Δx data and the temperature data. A direct interpretation of the data is not possible as there is a phase lag between (surface) temperature and Δx variation. Noise in the the GPS measured Δx values preclude direct correlation, i.e. the spread in the data is too large for direct correlation. In order to match the GPS data to the thermal data file, so that they cover the same time period, edit the file thermal.xyz to a new file temp. This file must cover the only the period of data of interest, so that the thermal data and GPS data time coverage are roughly the same. Use separate directories for different data sets. In this work for instance, the following structure was used:

Directory A covers MJD 50742.47-50745.54 (38 sessions)
Directory B covers MJD 50748.79-50751.45 (32 sessions)
Directory C covers MJD 50756.38-50758.45 (25 sessions)
Directory D covers MJD 50763.37-50766.38 (37 sessions)

Directories A,B,D was processed in two stages as the non-linear least squares software used to fit the data (NLREG) could only manage 24 equations for the fitted line. Before processing can be done one needs in the directory, say C, the following files;

chan7.nlr (NLREG command file)
temp (copied from thermal.xyz)
thermal.xyz (master file, output from program THERMAL)

Copy the file temp to xyz.dat. Always stay in this working directory as other files of the same name exist in the other (A,B,D) directories. Delete temp.

- Find the MJD needed for the period of interest. Take the MJD column in xyz.dat and copy it to file mjd (if using PCWrite use Ctrl-F7 for blocking, copy it to the bottom of the file,use Ctrl-F6to mark and copy to a file mjd). Delete the copied column in xyz.dat, leave the original part. Note the start and stop times. For example, say for data set C it is 50756.375000-50758.458333. Find the thermal data which covers this. For ambient temperature data, go to C:/thermal/channel7. This is covered by NOV9701.ax7 (50756.347-50757.540) and NOV9702.ax7 (50758.308-50758.46), note that some data is missing between the two files. Copy the two files to the working directory. Combine them into one file and cut to the required period. Move it to a file NOV976.ax7. Delete the lines you don't need.
- Edit chan7.nlr to include NOV976.ax7. Run NLREG chan7. Check that the fit is acceptable. Optimise the parameters in the parameter file. Make a note of the parameters. In this example, initial is followed by final parameters;

p0 = -108829.703;-15444.8215
p1 = 2.14465667; 0.304813871
Amplitude = 9.0703458; 8.96398788
Period = 0.995066789; 0.995039831
Phase = -219.992791; -218.574405

- Copy predb7.nlr to pred7.nlr. Edit the parameters to the new values. Edit the MJD values in the t1,t2 etc. equations. To do this, read in the MJD file and insert the values using the copy command. Having the exact MJD will allow the predicted temperaure to be calculated, based on the fitted parameters. Copy them one by one as they might not follow in sequence if a data point was lost. In this case there are 25 observations, NLREG just manages this so it does not have to be split into two files. Take out the variable 'predictval', add it after predicted values have been found for plotting purposes. Edit the predc7.lst file, the output data is what we require, delete redundant data lines and edit predicted temperatures into a column. Copy the column to file predtemp. Insert column as 2nd variable, i.e. 'predictval' in predc7.nlr. Run nlreg and check that the run is acceptable.
- Add the file predtemp column to xyz.dat as the last column. Copy an existing x.nlr to the directory. Delete the data, add new xyz.dat in its place. Do the same for y, z, distance and height. Optimise fits throughout all these procedures. You now have a time matched thermal data file, based on a least squares fit to the original thermal data, which matches the GPS observations time series. This needs to be done for all the data sets, but before continuing, go and have a cup of tea.

Appendix C

HartRAO Regional GPS Network

This appendix contains an extract of the GAMIT solutions of the HartRAO regional GPS network. Baselines for which only a short timeseries of data are available are not included. The extract covers the first 2 months of 1999. Repeatabilities for any other period do not differ significantly from that given here, so these values are fairly typical.

Table C.1: HartRAO regional GPS network, baseline repeatability.

Stations		Days	N	±	E	±	U	±	Length	±
ASC1-DAV1	RMS	59	-5872197.8395	0.0503	2334364.0583	0.0209	-5661286.4156	0.0512	8484228.1265	0.0498
ASC1-DAV1	PPB	59	-5872197.8395	5.9243	2334364.0583	2.4624	-5661286.4156	6.0361	8484228.1265	5.8741
ASC1-DAV1	SIG	59	-5872197.8395	0.0050	2334364.0583	0.0029	-5661286.4156	0.0061	8484228.1265	0.0050
ASC1-GOUG	RMS	50	-3401817.1925	0.0221	384577.3146	0.0291	-1006831.0686	0.0613	3568468.6804	0.0147
ASC1-GOUG	PPB	50	-3401817.1925	6.1896	384577.3146	8.1526	-1006831.0686	17.1794	3568468.6804	4.1112
ASC1-GOUG	SIG	50	-3401817.1925	0.0028	384577.3146	0.0038	-1006831.0686	0.0089	3568468.6804	0.0029
ASC1-HARK	RMS	56	-2156816.8145	0.0164	3851864.3588	0.0327	-1777823.8452	0.0515	4759135.9967	0.0294
ASC1-HARK	PPB	56	-2156816.8145	3.4363	3851864.3588	6.8657	-1777823.8452	10.8223	4759135.9967	6.1679
ASC1-HARK	SIG	56	-2156816.8145	0.0024	3851864.3588	0.0035	-1777823.8452	0.0072	4759135.9967	0.0038
ASC1-HRAO	RMS	61	-2156887.5137	0.0163	3850136.8013	0.0330	-1776607.8303	0.0502	4757315.6841	0.0327
ASC1-HRAO	PPB	61	-2156887.5137	3.4305	3850136.8013	6.9275	-1776607.8303	10.5569	4757315.6841	6.8634
ASC1-HRAO	SIG	61	-2156887.5137	0.0023	3850136.8013	0.0033	-1776607.8303	0.0070	4757315.6841	0.0038
ASC1-KERG	RMS	27	-4717310.0349	0.0383	4144888.3446	0.0352	-5332788.0325	0.0483	8238430.7702	0.0530
ASC1-KERG	PPB	27	-4717310.0349	4.6452	4144888.3446	4.2787	-5332788.0325	5.8646	8238430.7702	6.4342
ASC1-KERG	SIG	27	-4717310.0349	0.0051	4144888.3446	0.0049	-5332788.0325	0.0116	8238430.7702	0.0080
ASC1-MALI	RMS	58	178983.6839	0.0091	5192335.9404	0.0723	-2678213.7913	0.0699	5845101.9485	0.0482
ASC1-MALI	PPB	58	178983.6839	1.5576	5192335.9404	12.3715	-2678213.7913	11.9653	5845101.9485	8.2487
ASC1-MALI	SIG	58	178983.6839	0.0026	5192335.9404	0.0067	-2678213.7913	0.0085	5845101.9485	0.0058
ASC1-MAW1	RMS	55	-5745035.6028	0.0430	2377249.8977	0.0221	-5039158.1990	0.0536	8003116.0499	0.0418
ASC1-MAW1	PPB	55	-5745035.6028	5.3688	2377249.8977	2.7646	-5039158.1990	6.6992	8003116.0499	5.2279
ASC1-MAW1	SIG	55	-5745035.6028	0.0046	2377249.8977	0.0030	-5039158.1990	0.0068	8003116.0499	0.0049
ASC1-NAMI	RMS	45	-1720306.4003	0.0221	3079709.3500	0.0442	-1065698.4196	0.0575	3685074.8857	0.0539
ASC1-NAMI	PPB	45	-1720306.4003	6.0053	3079709.3500	12.0041	-1065698.4196	15.6021	3685074.8857	14.6239
ASC1-NAMI	SIG	45	-1720306.4003	0.0034	3079709.3500	0.0057	-1065698.4196	0.0110	3685074.8857	0.0057
ASC1-OHIG	RMS	37	-5336006.8152	0.0399	-1976152.4726	0.0159	-3534292.9061	0.0609	6698460.5449	0.0279
ASC1-OHIG	PPB	37	-5336006.8152	5.9552	-1976152.4726	2.3775	-3534292.9061	9.0919	6698460.5449	4.1614
ASC1-OHIG	SIG	37	-5336006.8152	0.0045	-1976152.4726	0.0032	-3534292.9061	0.0090	6698460.5449	0.0050
ASC1-PALM	RMS	60	-5450002.0755	0.0607	-2076911.1704	0.0244	-3839658.5106	0.0773	6982768.7997	0.0394
ASC1-PALM	PPB	60	-5450002.0755	8.6948	-2076911.1704	3.4926	-3839658.5106	11.0654	6982768.7997	5.6391
ASC1-PALM	SIG	60	-5450002.0755	0.0056	-2076911.1704	0.0040	-3839658.5106	0.0106	6982768.7997	0.0059
ASC1-SUTH	RMS	61	-2759404.5885	0.0179	3110500.0841	0.0303	-1547068.6639	0.0497	4436546.6194	0.0293
ASC1-SUTH	PPB	61	-2759404.5885	4.0332	3110500.0841	6.8314	-1547068.6639	11.2116	4436546.6194	6.5972
ASC1-SUTH	SIG	61	-2759404.5885	0.0023	3110500.0841	0.0032	-1547068.6639	0.0072	4436546.6194	0.0035
ASC1-VESL	RMS	60	-5705073.0129	0.0503	403507.3526	0.0237	-3596527.4021	0.0758	6756159.0878	0.0288
ASC1-VESL	PPB	60	-5705073.0129	7.4412	403507.3526	3.5121	-3596527.4021	11.2167	6756159.0878	4.2677

Table C.2: HartRAO regional GPS network, baseline repeatability; continued

Stations		Days	N	±	E	±	U	±	Length	±
DAV1-GOUG	RMS	52	-1339458.8261	0.0355	-4864365.7096	0.0457	-2472286.3454	0.0417	5618576.6415	0.0531
DAV1-GOUG	PPB	52	-1339458.8261	6.3146	-4864365.7096	8.1286	-2472286.3454	7.4130	5618576.6415	9.4530
DAV1-GOUG	SIG	52	-1339458.8261	0.0047	-4864365.7096	0.0053	-2472286.3454	0.0114	5618576.6415	0.0063
DAV1-HARK	RMS	55	2397477.1463	0.0314	-4416559.4270	0.0287	-2436031.8062	0.0512	5584634.7061	0.0397
DAV1-HARK	PPB	55	2397477.1463	5.6277	-4416559.4270	5.1307	-2436031.8062	9.1751	5584634.7061	7.1015
DAV1-HARK	SIG	55	2397477.1463	0.0033	-4416559.4270	0.0046	-2436031.8062	0.0095	5584634.7061	0.0048
DAV1-HRAO	RMS	61	2395738.4288	0.0350	-4417681.2778	0.0282	-2436463.6328	0.0482	5584964.2368	0.0392
DAV1-HRAO	PPB	61	2395738.4288	6.2659	-4417681.2778	5.0407	-2436463.6328	8.6232	5584964.2368	7.0216
DAV1-HRAO	SIG	61	2395738.4288	0.0034	-4417681.2778	0.0044	-2436463.6328	0.0092	5584964.2368	0.0047
DAV1-KERG	RMS	26	2067395.1161	0.0156	-559002.2691	0.0081	-364786.4245	0.0490	2172481.3551	0.0173
DAV1-KERG	PPB	26	2067395.1161	7.1712	-559002.2691	3.7257	-364786.4245	22.5673	2172481.3551	7.9433
DAV1-KERG	SIG	26	2067395.1161	0.0022	-559002.2691	0.0019	-364786.4245	0.0108	2172481.3551	0.0026
DAV1-MALI	RMS	58	4560656.3325	0.0762	-3901970.2664	0.0603	-4202209.5752	0.0468	7326904.0841	0.0796
DAV1-MALI	PPB	58	4560656.3325	10.3970	-3901970.2664	8.2292	-4202209.5752	6.3827	7326904.0841	10.8612
DAV1-MALI	SIG	58	4560656.3325	0.0075	-3901970.2664	0.0065	-4202209.5752	0.0098	7326904.0841	0.0075
DAV1-MAW1	RMS	58	30193.5870	0.0088	-634936.3232	0.0138	-31577.8498	0.0225	636437.7014	0.0139
DAV1-MAW1	PPB	58	30193.5870	13.7771	-634936.3232	21.6679	-31577.8498	35.4170	636437.7014	21.8917
DAV1-MAW1	SIG	58	30193.5870	0.0010	-634936.3232	0.0017	-31577.8498	0.0056	636437.7014	0.0017
DAV1-NAMI	RMS	44	1773210.2814	0.0468	-5149123.5569	0.0690	-3042272.7803	0.0602	6238042.3032	0.0727
DAV1-NAMI	PPB	44	1773210.2814	7.4975	-5149123.5569	11.0667	-3042272.7803	9.6467	6238042.3032	11.6468
DAV1-NAMI	SIG	44	1773210.2814	0.0071	-5149123.5569	0.0085	-3042272.7803	0.0195	6238042.3032	0.0106
DAV1-OHIG	RMS	38	-4002272.1106	0.0274	-1999255.2558	0.0160	-1837648.2892	0.0497	4836543.6894	0.0332
DAV1-OHIG	PPB	38	-4002272.1106	5.6558	-1999255.2558	3.3122	-1837648.2892	10.2774	4836543.6894	6.8714
DAV1-OHIG	SIG	38	-4002272.1106	0.0030	-1999255.2558	0.0020	-1837648.2892	0.0086	4836543.6894	0.0040
DAV1-PALM	RMS	60	-4109657.6781	0.0325	-1677204.4294	0.0366	-1803780.9107	0.0621	4791234.3402	0.0506
DAV1-PALM	PPB	60	-4109657.6781	6.7778	-1677204.4294	7.6428	-1803780.9107	12.9512	4791234.3402	10.5573
DAV1-PALM	SIG	60	-4109657.6781	0.0039	-1677204.4294	0.0034	-1803780.9107	0.0114	4791234.3402	0.0053
DAV1-SUTH	RMS	61	1471985.4589	0.0319	-4531343.5512	0.0257	-2125756.5849	0.0454	5217150.2401	0.0359
DAV1-SUTH	PPB	61	1471985.4589	6.1086	-4531343.5512	4.9201	-2125756.5849	8.7039	5217150.2401	6.8841
DAV1-SUTH	SIG	61	1471985.4589	0.0031	-4531343.5512	0.0041	-2125756.5849	0.0091	5217150.2401	0.0045
DAV1-VESL	RMS	60	-1917741.5535	0.0215	-1986005.2238	0.0403	-630411.5278	0.0415	2831848.8853	0.0390
DAV1-VESL	PPB	60	-1917741.5535	7.5840	-1986005.2238	14.2423	-630411.5278	14.6486	2831848.8853	13.7813
DAV1-VESL	SIG	60	-1917741.5535	0.0033	-1986005.2238	0.0037	-630411.5278	0.0104	2831848.8853	0.0043
GOUG-HARK	RMS	46	819136.2027	0.0203	3503266.3969	0.0418	-1105746.6671	0.0526	3763845.8069	0.0443
GOUG-HARK	PPB	46	819136.2027	5.3835	3503266.3969	11.1056	-1105746.6671	13.9738	3763845.8069	11.7756

Table C.3: HartRAO regional GPS network, baseline repeatability; continued

Stations		Days	N	±	E	±	U	±	Length	±
GOUG-HRAO	RMS	52	819635.0600	0.0197	3501449.8446	0.0405	-1104787.7945	0.0496	3761982.0198	0.0428
GOUG-HRAO	PPB	52	819635.0600	5.2349	3501449.8446	10.7660	-1104787.7945	13.1873	3761982.0198	11.3892
GOUG-HRAO	SIG	52	819635.0600	0.0033	3501449.8446	0.0052	-1104787.7945	0.0073	3761982.0198	0.0047
GOUG-KERG	RMS	24	-3220884.4846	0.0392	4101367.5963	0.0358	-2718280.9231	0.0568	5880847.2349	0.0581
GOUG-KERG	PPB	24	-3220884.4846	6.6719	4101367.5963	6.0951	-2718280.9231	9.6542	5880847.2349	9.8846
GOUG-KERG	SIG	24	-3220884.4846	0.0069	4101367.5963	0.0086	-2718280.9231	0.0107	5880847.2349	0.0079
GOUG-MALI	RMS	51	2383211.6701	0.0436	4884648.4862	0.0900	-3031618.3025	0.0620	6223359.0793	0.0764
GOUG-MALI	PPB	51	2383211.6701	6.9994	4884648.4862	14.4673	-3031618.3025	9.9674	6223359.0793	12.2820
GOUG-MALI	SIG	51	2383211.6701	0.0066	4884648.4862	0.0128	-3031618.3025	0.0108	6223359.0793	0.0095
GOUG-MAW1	RMS	47	-4023595.5701	0.0329	2327434.2611	0.0204	-2028498.7475	0.0494	5071595.2835	0.0452
GOUG-MAW1	PPB	47	-4023595.5701	6.4899	2327434.2611	4.0274	-2028498.7475	9.7454	5071595.2835	8.9035
GOUG-MAW1	SIG	47	-4023595.5701	0.0055	2327434.2611	0.0049	-2028498.7475	0.0073	5071595.2835	0.0049
GOUG-NAMI	RMS	39	1527487.7199	0.0467	2673058.3592	0.0537	-784997.3889	0.0707	3177212.7135	0.0432
GOUG-NAMI	PPB	39	1527487.7199	14.6906	2673058.3592	16.8889	-784997.3889	22.2619	3177212.7135	13.5837
GOUG-NAMI	SIG	39	1527487.7199	0.0065	2673058.3592	0.0095	-784997.3889	0.0141	3177212.7135	0.0078
GOUG-OHIG	RMS	33	-3099387.7603	0.0244	-2134564.6229	0.0163	-1240817.1589	0.0580	3962599.8839	0.0252
GOUG-OHIG	PPB	33	-3099387.7603	6.1462	-2134564.6229	4.1250	-1240817.1589	14.6355	3962599.8839	6.3532
GOUG-OHIG	SIG	33	-3099387.7603	0.0041	-2134564.6229	0.0047	-1240817.1589	0.0076	3962599.8839	0.0043
GOUG-PALM	RMS	53	-3363272.4810	0.0362	-2209874.3238	0.0257	-1443520.6441	0.0558	4275382.8084	0.0306
GOUG-PALM	PPB	53	-3363272.4810	8.4562	-2209874.3238	6.0066	-1443520.6441	13.0398	4275382.8084	7.1471
GOUG-PALM	SIG	53	-3363272.4810	0.0041	-2209874.3238	0.0045	-1443520.6441	0.0074	4275382.8084	0.0040
GOUG-SEY1	RMS	2	1314817.3900	0.0216	5778721.7410	0.0449	-4010627.0772	0.0299	7155941.5371	0.0156
GOUG-SEY1	PPB	2	1314817.3900	3.0242	5778721.7410	6.2753	-4010627.0772	4.1808	7155941.5371	2.1738
GOUG-SEY1	SIG	2	1314817.3900	0.0171	5778721.7410	0.0315	-4010627.0772	0.0256	7155941.5371	0.0247
GOUG-SUTH	RMS	52	394671.8651	0.0157	2752703.9263	0.0302	-634082.6206	0.0392	2852228.1740	0.0327
GOUG-SUTH	PPB	52	394671.8651	5.5114	2752703.9263	10.5841	-634082.6206	13.7308	2852228.1740	11.4673
GOUG-SUTH	SIG	52	394671.8651	0.0024	2752703.9263	0.0038	-634082.6206	0.0060	2852228.1740	0.0036
GOUG-VESL	RMS	51	-3323227.8285	0.0219	246534.0700	0.0161	-952497.0194	0.0454	3465814.8854	0.0201
GOUG-VESL	PPB	51	-3323227.8285	6.3106	246534.0700	4.6497	-952497.0194	13.0927	3465814.8854	5.7860
GOUG-VESL	SIG	51	-3323227.8285	0.0028	246534.0700	0.0031	-952497.0194	0.0055	3465814.8854	0.0025
HARK-HRAO	RMS	57	-331.9109	0.0031	-2082.7154	0.0057	-142.4427	0.0103	2113.8019	0.0056
HARK-HRAO	PPB	57	-331.9109	********	-2082.7154	********	-142.4427	********	2113.8019	********
HARK-HRAO	SIG	57	-331.9109	0.0003	-2082.7154	0.0009	-142.4427	0.0019	2113.8019	0.0009
HARK-KERG	RMS	24	-3006687.7804	0.0258	2814974.9212	0.0284	-1521677.9238	0.0511	4390872.2276	0.0312
HARK-KERG	PPB	24	-3006687.7804	5.8671	2814974.9212	6.4695	-1521677.9238	11.6365	4390872.2276	7.0994

Table C.4: HartRAO regional GPS network, baseline repeatability; continued

Stations		Days	N	±	E	±	U	±	Length	±
HARK-MALI	RMS	54	2402110.8374	0.0394	1377151.8619	0.0233	-629957.4171	0.0703	2839635.5529	0.0272
HARK-MALI	PPB	54	2402110.8374	13.8579	1377151.8619	8.2215	-629957.4171	24.7722	2839635.5529	9.5930
HARK-MALI	SIG	54	2402110.8374	0.0041	1377151.8619	0.0040	-629957.4171	0.0105	2839635.5529	0.0033
HARK-MAW1	RMS	51	-4426632.5851	0.0339	1403497.4536	0.0132	-2030079.4240	0.0440	5068145.9739	0.0305
HARK-MAW1	PPB	51	-4426632.5851	6.6866	1403497.4536	2.6029	-2030079.4240	8.6734	5068145.9739	6.0143
HARK-MAW1	SIG	51	-4426632.5851	0.0044	1403497.4536	0.0029	-2030079.4240	0.0064	5068145.9739	0.0033
HARK-NAMI	RMS	45	322961.2447	0.0156	-1086052.1318	0.0654	-100369.9928	0.0392	1137491.6852	0.0643
HARK-NAMI	PPB	45	322961.2447	13.6793	-1086052.1318	57.4848	-100369.9928	34.4774	1137491.6852	56.5493
HARK-NAMI	SIG	45	322961.2447	0.0030	-1086052.1318	0.0066	-100369.9928	0.0113	1137491.6852	0.0062
HARK-OHIG	RMS	39	-5017601.4601	0.0437	-2863022.9470	0.0276	-3712814.0080	0.0565	6867183.7507	0.0486
HARK-OHIG	PPB	39	-5017601.4601	6.3658	-2863022.9470	4.0127	-3712814.0080	8.2236	6867183.7507	7.0724
HARK-OHIG	SIG	39	-5017601.4601	0.0057	-2863022.9470	0.0046	-3712814.0080	0.0076	6867183.7507	0.0057
HARK-PALM	RMS	57	-5213324.2547	0.0543	-2724392.9708	0.0442	-3955444.8198	0.0663	7088484.3632	0.0527
HARK-PALM	PPB	57	-5213324.2547	7.6635	-2724392.9708	6.2289	-3955444.8198	9.3491	7088484.3632	7.4324
HARK-PALM	SIG	57	-5213324.2547	0.0062	-2724392.9708	0.0052	-3955444.8198	0.0090	7088484.3632	0.0061
HARK-SUTH	RMS	58	-735188.9969	0.0075	-647659.4477	0.0134	-77558.6725	0.0226	982843.3084	0.0124
HARK-SUTH	PPB	58	-735188.9969	7.5983	-647659.4477	13.6464	-77558.6725	22.9548	982843.3084	12.6348
HARK-SUTH	SIG	58	-735188.9969	0.0008	-647659.4477	0.0018	-77558.6725	0.0038	982843.3084	0.0014
HARK-VESL	RMS	57	-4682359.2153	0.0361	-1022566.0165	0.0340	-2195186.0051	0.0623	5271524.5116	0.0348
HARK-VESL	PPB	57	-4682359.2153	6.8457	-1022566.0165	6.4417	-2195186.0051	11.8206	5271524.5116	6.5994
HARK-VESL	SIG	57	-4682359.2153	0.0047	-1022566.0165	0.0039	-2195186.0051	0.0080	5271524.5116	0.0043
HRAO-KERG	RMS	28	-3006878.6301	0.0259	2816086.9596	0.0283	-1522299.1529	0.0475	4391931.1893	0.0306
HRAO-KERG	PPB	28	-3006878.6301	5.8941	2816086.9596	6.4537	-1522299.1529	10.8115	4391931.1893	6.9761
HRAO-KERG	SIG	28	-3006878.6301	0.0034	2816086.9596	0.0047	-1522299.1529	0.0075	4391931.1893	0.0044
HRAO-MALI	RMS	60	2402192.7381	0.0381	1379407.0674	0.0250	-630390.5760	0.0699	2840895.2967	0.0261
HRAO-MALI	PPB	60	2402192.7381	13.3994	1379407.0674	8.8165	-630390.5760	24.6220	2840895.2967	9.2002
HRAO-MALI	SIG	60	2402192.7381	0.0039	1379407.0674	0.0041	-630390.5760	0.0096	2840895.2967	0.0032
HRAO-MAW1	RMS	59	-4426627.5590	0.0321	1404219.8918	0.0142	-2030165.6059	0.0435	5068376.2132	0.0298
HRAO-MAW1	PPB	59	-4426627.5590	6.3271	1404219.8918	2.8011	-2030165.6059	8.5918	5068376.2132	5.8762
HRAO-MAW1	SIG	59	-4426627.5590	0.0041	1404219.8918	0.0030	-2030165.6059	0.0058	5068376.2132	0.0031
HRAO-NAMI	RMS	46	323458.6564	0.0149	-1083951.1703	0.0610	-99890.2731	0.0326	1135585.1833	0.0597
HRAO-NAMI	PPB	46	323458.6564	13.1522	-1083951.1703	53.6743	-99890.2731	28.6802	1135585.1833	52.6006
HRAO-NAMI	SIG	46	323458.6564	0.0027	-1083951.1703	0.0062	-99890.2731	0.0097	1135585.1833	0.0058
HRAO-OHIG	RMS	39	-5017011.9887	0.0434	-2862943.0127	0.0293	-3711475.5644	0.0635	6865996.1298	0.0466
HRAO-OHIG	PPB	39	-5017011.9887	6.3184	-2862943.0127	4.2611	-3711475.5644	9.2505	6865996.1298	6.7843

Table C.5: HartRAO regional GPS network, baseline repeatability; continued

Stations		Days	N	±	E	±	U	±	Length	±
HRAO-PALM	RMS	62	-5212769.2312	0.0518	-2724423.1309	0.0458	-3954141.4685	0.0724	7087360.5246	0.0514
HRAO-PALM	PPB	62	-5212769.2312	7.3084	-2724423.1309	6.4633	-3954141.4685	10.2182	7087360.5246	7.2458
HRAO-PALM	SIG	62	-5212769.2312	0.0058	-2724423.1309	0.0056	-3954141.4685	0.0085	7087360.5246	0.0060
HRAO-SEY1	RMS	3	1977412.5702	0.0090	2964358.9975	0.0174	-1085122.3294	0.0123	3724926.2018	0.0079
HRAO-SEY1	PPB	3	1977412.5702	2.4189	2964358.9975	4.6654	-1085122.3294	3.3154	3724926.2018	2.1310
HRAO-SEY1	SIG	3	1977412.5702	0.0070	2964358.9975	0.0116	-1085122.3294	0.0144	3724926.2018	0.0091
HRAO-SUTH	RMS	63	-734759.4279	0.0076	-645717.7026	0.0115	-77167.0747	0.0206	981212.2736	0.0120
HRAO-SUTH	PPB	63	-734759.4279	7.7475	-645717.7026	11.7351	-77167.0747	21.0140	981212.2736	12.2680
HRAO-SUTH	SIG	63	-734759.4279	0.0008	-645717.7026	0.0017	-77167.0747	0.0032	981212.2736	0.0013
HRAO-VESL	RMS	62	-4681980.6853	0.0371	-1021937.6294	0.0346	-2194466.3267	0.0626	5270766.7483	0.0347
HRAO-VESL	PPB	62	-4681980.6853	7.0396	-1021937.6294	6.5702	-2194466.3267	11.8690	5270766.7483	6.5853
HRAO-VESL	SIG	62	-4681980.6853	0.0046	-1021937.6294	0.0041	-2194466.3267	0.0074	5270766.7483	0.0041
KERG-MALI	RMS	28	3954119.1742	0.0603	-3190610.5672	0.0477	-2510487.7423	0.0697	5667239.4461	0.0571
KERG-MALI	PPB	28	3954119.1742	10.6479	-3190610.5672	8.4185	-2510487.7423	12.2989	5667239.4461	10.0692
KERG-MALI	SIG	28	3954119.1742	0.0098	-3190610.5672	0.0082	-2510487.7423	0.0106	5667239.4461	0.0072
KERG-MAW1	RMS	26	-2013078.7771	0.0162	-313238.3802	0.0126	-341144.4581	0.0511	2065667.9276	0.0183
KERG-MAW1	PPB	26	-2013078.7771	7.8466	-313238.3802	6.1049	-341144.4581	24.7473	2065667.9276	8.8633
KERG-MAW1	SIG	26	-2013078.7771	0.0034	-313238.3802	0.0034	-341144.4581	0.0094	2065667.9276	0.0028
KERG-NAMI	RMS	17	1081538.5014	0.0244	-4717376.0830	0.0507	-2213894.5433	0.0610	5322094.6711	0.0795
KERG-NAMI	PPB	17	1081538.5014	4.5787	-4717376.0830	9.5283	-2213894.5433	11.4687	5322094.6711	14.9357
KERG-NAMI	SIG	17	1081538.5014	0.0078	-4717376.0830	0.0092	-2213894.5433	0.0166	5322094.6711	0.0092
KERG-OHIG	RMS	9	-5053940.1885	0.0572	-2257919.7771	0.0297	-3231717.4973	0.0586	6409720.0509	0.0542
KERG-OHIG	PPB	9	-5053940.1885	8.9189	-2257919.7771	4.6374	-3231717.4973	9.1501	6409720.0509	8.4614
KERG-OHIG	SIG	9	-5053940.1885	0.0140	-2257919.7771	0.0075	-3231717.4973	0.0109	6409720.0509	0.0098
KERG-PALM	RMS	25	-5198603.7802	0.0399	-1950526.5376	0.0465	-3262978.3026	0.0859	6440268.8174	0.0681
KERG-PALM	PPB	25	-5198603.7802	6.2011	-1950526.5376	7.2159	-3262978.3026	13.3401	6440268.8174	10.5748
KERG-PALM	SIG	25	-5198603.7802	0.0080	-1950526.5376	0.0069	-3262978.3026	0.0144	6440268.8174	0.0084
KERG-SUTH	RMS	27	431372.6336	0.0190	-4097598.2539	0.0278	-1502873.9522	0.0530	4385775.1785	0.0350
KERG-SUTH	PPB	27	431372.6336	4.3234	-4097598.2539	6.3380	-1502873.9522	12.0766	4385775.1785	7.9767
KERG-SUTH	SIG	27	431372.6336	0.0043	-4097598.2539	0.0062	-1502873.9522	0.0083	4385775.1785	0.0054
KERG-VESL	RMS	27	-3502757.5729	0.0332	-1924893.6852	0.0532	-1419042.6697	0.0721	4241250.8075	0.0507
KERG-VESL	PPB	27	-3502757.5729	7.8163	-1924893.6852	12.5442	-1419042.6697	16.9894	4241250.8075	11.9581
MALI-MAW1	RMS	54	-5749831.5041	0.0421	939536.9776	0.0114	-3827463.9655	0.0974	6970851.6312	0.0696
MALI-MAW1	PPB	54	-5749831.5041	6.0340	939536.9776	1.6342	-3827463.9655	13.9722	6970851.6312	9.9855
MALI-MAW1	SIG	54	-5749831.5041	0.0070	939536.9776	0.0028	-3827463.9655	0.0111	6970851.6312	0.0067

Table C.6: HartRAO regional GPS network, baseline repeatability; continued

Stations		Days	N	±	E	±	U	±	Length	±
MALI-NAMI	RMS	43	-2149259.8405	0.0253	-2312882.9156	0.0791	-837827.4990	0.0784	3266603.7656	0.0719
MALI-NAMI	PPB	43	-2149259.8405	7.7579	-2312882.9156	24.2149	-837827.4990	24.0013	3266603.7656	22.0245
MALI-NAMI	SIG	43	-2149259.8405	0.0060	-2312882.9156	0.0082	-837827.4990	0.0266	3266603.7656	0.0092
MALI-OHIG	RMS	36	-5689482.7466	0.0352	-2842845.2805	0.0242	-6487159.1856	0.1091	9084889.5156	0.0979
MALI-OHIG	PPB	36	-5689482.7466	3.8799	-2842845.2805	2.6644	-6487159.1856	12.0093	9084889.5156	10.7758
MALI-OHIG	SIG	36	-5689482.7466	0.0050	-2842845.2805	0.0030	-6487159.1856	0.0148	9084889.5156	0.0110
MALI-PALM	RMS	59	-5774167.2754	0.0427	-2641863.0435	0.0394	-6749514.0481	0.1103	9266951.3838	0.0970
MALI-PALM	PPB	59	-5774167.2754	4.6026	-2641863.0435	4.2465	-6749514.0481	11.9056	9266951.3838	10.4722
MALI-PALM	SIG	59	-5774167.2754	0.0054	-2641863.0435	0.0036	-6749514.0481	0.0157	9266951.3838	0.0116
MALI-SUTH	RMS	60	-3128378.0355	0.0193	-1789957.3980	0.0225	-1121141.7588	0.0857	3774606.6633	0.0375
MALI-SUTH	PPB	60	-3128378.0355	5.1262	-1789957.3980	5.9684	-1121141.7588	22.7061	3774606.6633	9.9474
MALI-SUTH	SIG	60	-3128378.0355	0.0027	-1789957.3980	0.0035	-1121141.7588	0.0107	3774606.6633	0.0040
MALI-VESL	RMS	60	-5948681.8269	0.0519	-1372975.6146	0.0362	-4596349.0841	0.1079	7641878.1997	0.0784
MALI-VESL	PPB	60	-5948681.8269	6.7896	-1372975.6146	4.7418	-4596349.0841	14.1177	7641878.1997	10.2656
MALI-VESL	SIG	60	-5948681.8269	0.0070	-1372975.6146	0.0038	-4596349.0841	0.0140	7641878.1997	0.0089
MAW1-NAMI	RMS	41	2864021.7396	0.0464	-4224088.9650	0.0678	-2536676.7712	0.0504	5699147.0547	0.0448
MAW1-NAMI	PPB	41	2864021.7396	8.1421	-4224088.9650	11.9006	-2536676.7712	8.8373	5699147.0547	7.8573
MAW1-NAMI	SIG	41	2864021.7396	0.0067	-4224088.9650	0.0093	-2536676.7712	0.0135	5699147.0547	0.0080
MAW1-OHIG	RMS	34	-3531945.6936	0.0297	-2467206.9068	0.0232	-1679966.0427	0.0412	4624287.6433	0.0300
MAW1-OHIG	PPB	34	-3531945.6936	6.4256	-2467206.9068	5.0130	-1679966.0427	8.9028	4624287.6433	6.4979
MAW1-OHIG	SIG	34	-3531945.6936	0.0037	-2467206.9068	0.0036	-1679966.0427	0.0085	4624287.6433	0.0044
MAW1-PALM	RMS	56	-3714605.7079	0.0309	-2179058.2754	0.0531	-1678929.5806	0.0526	4622271.6352	0.0436
MAW1-PALM	PPB	56	-3714605.7079	6.6928	-2179058.2754	11.4872	-1678929.5806	11.3714	4622271.6352	9.4242
MAW1-PALM	SIG	56	-3714605.7079	0.0044	-2179058.2754	0.0051	-1678929.5806	0.0108	4622271.6352	0.0056
MAW1-SUTH	RMS	57	2396736.2319	0.0361	-3612912.7342	0.0252	-1687855.0617	0.0395	4652562.4874	0.0269
MAW1-SUTH	PPB	57	2396736.2319	7.7519	-3612912.7342	5.4068	-1687855.0617	8.4811	4652562.4874	5.7849
MAW1-SUTH	SIG	57	2396736.2319	0.0036	-3612912.7342	0.0045	-1687855.0617	0.0091	4652562.4874	0.0044
MAW1-VESL	RMS	56	-1547491.6599	0.0187	-1833745.1120	0.0380	-470200.7084	0.0332	2445084.9227	0.0316
MAW1-VESL	PPB	56	-1547491.6599	7.6678	-1833745.1120	15.5535	-470200.7084	13.5584	2445084.9227	12.9052
MAW1-VESL	SIG	56	-1547491.6599	0.0028	-1833745.1120	0.0038	-470200.7084	0.0088	2445084.9227	0.0038
NAMI-OHIG	RMS	32	-4962528.4815	0.0419	-2773479.5446	0.0289	-3522798.5443	0.0673	6687973.3326	0.0507
NAMI-OHIG	PPB	32	-4962528.4815	6.2640	-2773479.5446	4.3154	-3522798.5443	10.0563	6687973.3326	7.5764
NAMI-OHIG	SIG	32	-4962528.4815	0.0065	-2773479.5446	0.0053	-3522798.5443	0.0062	6687973.3326	0.0052
NAMI-PALM	RMS	47	-5151737.6315	0.0569	-2693157.4658	0.0421	-3795091.8514	0.0758	6942349.7406	0.0538
NAMI-PALM	PPB	47	-5151737.6315	8.1950	-2693157.4658	6.0616	-3795091.8514	10.9231	6942349.7406	7.7495

Table C.7: HartRAO regional GPS network, baseline repeatability; continued

Stations		Days	N	±	E	±	U	±	Length	±
NAMI-SUTH	RMS	46	-1085675.3913	0.0165	350005.7308	0.0502	-105808.1450	0.0479	1145596.1027	0.0342
NAMI-SUTH	PPB	46	-1085675.3913	14.3929	350005.7308	43.7771	-105808.1450	41.8009	1145596.1027	29.8261
NAMI-SUTH	SIG	46	-1085675.3913	0.0027	350005.7308	0.0059	-105808.1450	0.0102	1145596.1027	0.0034
NAMI-VESL	RMS	46	-4854467.1570	0.0378	-685807.2902	0.0418	-2325797.6495	0.0906	5426372.4277	0.0452
NAMI-VESL	PPB	46	-4854467.1570	6.9660	-685807.2902	7.7072	-2325797.6495	16.7001	5426372.4277	8.3358
NAMI-VESL	SIG	46	-4854467.1570	0.0069	-685807.2902	0.0067	-2325797.6495	0.0109	5426372.4277	0.0059
OHIG-PALM	RMS	41	-176108.3926	0.0066	-292043.6520	0.0130	-9577.9569	0.0163	341167.6976	0.0129
OHIG-PALM	PPB	41	-176108.3926	19.2577	-292043.6520	37.9812	-9577.9569	47.8451	341167.6976	37.8642
OHIG-PALM	SIG	41	-176108.3926	0.0010	-292043.6520	0.0018	-9577.9569	0.0034	341167.6976	0.0016
OHIG-SUTH	RMS	40	-591386.4521	0.0231	5288769.0977	0.0323	-2853271.2485	0.0508	6038375.0564	0.0367
OHIG-SUTH	PPB	40	-591386.4521	3.8272	5288769.0977	5.3559	-2853271.2485	8.4060	6038375.0564	6.0754
OHIG-SUTH	SIG	40	-591386.4521	0.0036	5288769.0977	0.0056	-2853271.2485	0.0076	6038375.0564	0.0052
OHIG-VESL	RMS	39	-1695245.9457	0.0146	1649151.6338	0.0222	-457497.4528	0.0283	2408913.4162	0.0146
OHIG-VESL	PPB	39	-1695245.9457	6.0523	1649151.6338	9.2322	-457497.4528	11.7609	2408913.4162	6.0516
OHIG-VESL	SIG	39	-1695245.9457	0.0027	1649151.6338	0.0032	-457497.4528	0.0066	2408913.4162	0.0031
PALM-SUTH	RMS	62	-1019287.6430	0.0596	5371443.7700	0.0343	-3084341.5915	0.0532	6277301.8508	0.0435
PALM-SUTH	PPB	62	-1019287.6430	9.4898	5371443.7700	5.4645	-3084341.5915	8.4817	6277301.8508	6.9344
PALM-SUTH	SIG	62	-1019287.6430	0.0056	5371443.7700	0.0078	-3084341.5915	0.0093	6277301.8508	0.0065
PALM-VESL	RMS	61	-1709883.2161	0.0228	1763115.0749	0.0310	-494342.5669	0.0333	2505324.3211	0.0205
PALM-VESL	PPB	61	-1709883.2161	9.0857	1763115.0749	12.3789	-494342.5669	13.3014	2505324.3211	8.1697
PALM-VESL	SIG	61	-1709883.2161	0.0032	1763115.0749	0.0035	-494342.5669	0.0068	2505324.3211	0.0033
SEY1-SUTH	RMS	3	-3026916.2901	0.0040	-3067787.3671	0.0170	-1682546.5566	0.0164	4626500.2402	0.0075
SEY1-SUTH	PPB	3	-3026916.2901	0.8725	-3067787.3671	3.6765	-1682546.5566	3.5385	4626500.2402	1.6126
SEY1-SUTH	SIG	3	-3026916.2901	0.0043	-3067787.3671	0.0082	-1682546.5566	0.0131	4626500.2402	0.0075
SEY1-VESL	RMS	3	-5927850.1408	0.0479	-1712055.7934	0.0315	-4837166.6681	0.0453	7840199.2135	0.0281
SEY1-VESL	PPB	3	-5927850.1408	6.1067	-1712055.7934	4.0123	-4837166.6681	5.7745	7840199.2135	3.5849
SEY1-VESL	SIG	3	-5927850.1408	0.0210	-1712055.7934	0.0238	-4837166.6681	0.0388	7840199.2135	0.0236
SUTH-VESL	RMS	62	-4122691.4349	0.0305	-807104.3578	0.0295	-1599078.2007	0.0531	4495003.1372	0.0261
SUTH-VESL	PPB	62	-4122691.4349	6.7768	-807104.3578	6.5624	-1599078.2007	11.8163	4495003.1372	5.8120
SUTH-VESL	SIG	62	-4122691.4349	0.0037	-807104.3578	0.0035	-1599078.2007	0.0065	4495003.1372	0.0032

Appendix D

Footprint Data

Table D.1: Adjusted Individual Sessions Outer Network: April 97;

Baseline	Date	Start	H:M	Δx	Δy	Δz	Slope Dist.	Δ H
SLR-LYT	2/5/97	06:20	3:20	-22702.4827	48205.9955	4961.3966	53514.8220	122.3684
SLR-LYT	8/5/97	06:23	3:30	-22702.4890	48205.9916	4961.4011	53514.8217	122.3597
SLR-LYT			Mean	-22702.4858	48205.9936	4961.3988	53514.8218	122.3640
SLR-POT	30/4/97	09:56	2:59	-15741.1116	-31179.8997	-58136.4225	67821.9165	173.7808
SLR-RUS	29/4/97	11:01	2:40	26620.3280	-34735.8775	15921.8755	46569.6164	-94.9739

Table D.2: Outer Network, Before and Final Adjusted Values: April 97;

Station		Before	Min	Sec	Adjust	After	Min	Sec	σ		Old Cartesian	New Cartesian		Adjust (m)
LYT	Lat S	25°	50'	21.900890"	+0.002138"	25°	50'	21.898752"	0.001511m	x	5062698.6576	5062698.5724	dx	-0.0852
	Lon E	28°	13'	01.404355"	+0.003789"	28°	13'	01.408144"	0.001364m	y	2716535.9745	2716536.0486	dy	0.0741
	Height	1529.1763m			-0.0763m	1529.1000m			0.003754m	z	2763727.5525	2763727.4600	dz	-0.0925
RUS	Lat S	25°	43'	49.850977"	+0.002128"	25°	43'	49.848849"	0.002144m	x	5112021.4683	5112021.3869	dx	-0.0814
	Lon E	27°	15'	23.279459"	+0.003813"	27°	15'	23.283271"	0.002100m	y	2633594.1016	2633594.1792	dy	0.0776
	Height	1311.8351m			-0.0724m	1311.7627m			0.005652m	z	2752767.0735	2752766.9831	dz	-0.0904
POT	Lat S	26°	28'	24.737701"	+0.002128"	26°	28'	24.735573"	0.001948m	x	5069660.0286	5069659.9483	dx	-0.0803
	Lon E	27°	28'	57.635609"	+0.003809"	27°	28'	57.639417"	0.002011m	y	2637150.0794	2637150.1566	dy	0.0772
	Height	1580.5898m			-0.0724m	1580.5174m			0.004708m	z	2826825.3716	2826825.2806	dz	-0.0910

Table D.3: Adjusted Individual Sessions Intermediate Network: April 97;

Baseline	Date	Start	H:M	Δx	Δy	Δz	Slope Dist.	Δ H
SLR-SYF	21/4/97	10:01	3:47	2510.9646	-20939.2358	-16066.0896	26511.8044	318.0701
SLR-MAG	18/4/97	09:39	2:20	9203.1530	-13301.0066	3094.8072	16467.9274	441.6762
SLR-MAG	18/4/97	12:01	1:35	9203.1598	-13301.0051	3094.8030	16467.9292	441.6840
SLR-MAG			Mean	9203.1564	-13301.0058	3094.8051	16467.9283	441.6801
SLR-B16	6/5/97	07:45	3:56	-3110.6927	16732.6399	10329.0959	19908.4874	37.1060
SLR-TWE	7/5/97	09:28	2:51	-7964.3846	11910.7686	-3502.8522	14750.1798	180.4984

Table D.4: Intermediate Network, Before and Final Adjusted Values: April 97;

Station		Before	Min	Sec	Adjust	After	Min	Sec	σ		Old Cartesian	New Cartesian		Adjust (m)
SYF	Lat S	26°	02'	58.476514"	+0.002159"	26°	02'	58.474355"	0.002547m	x	5087912.0706	5087912.0152	dx	-0.0554
	Lon E	27°	29'	21.444431"	+0.003753"	27°	29'	21.448184"	0.002497m	y	2647390.7275	2647390.8163	dy	0.0888
	Height	1724.8376m			-0.0416m	1724.7960m			0.006333m	z	2784755.0210	2784754.9430	dz	-0.0780
MAG	Lat S	25°	51'	24.255716"	+0.002104"	25°	51'	24.253613"	0.002206m	x	5094604.2933	5094604.2140	dx	-0.0793
	Lon E	27°	31'	33.816467"	+0.003789"	27°	31'	33.820255"	0.002241m	y	2655028.9725	2655029.0501	dy	0.0776
	Height	1848.4852m			-0.0696m	1848.4156m			0.005385m	z	2765594.1418	2765594.0532	dz	-0.0886
TWE	Lat S	25°	55'	26.619216"	+0.002128"	25°	55'	26.617088"	0.001930m	x	5077436.7556	5077436.6740	dx	-0.0816
	Lon E	27°	49'	42.075756"	+0.003802"	27°	49'	42.079558"	0.002054m	y	2680240.7477	2680240.8243	dy	0.0766
	Height	1587.3074m			-0.0724m	1587.2350m			0.004706m	z	2772191.8012	2772191.7106	dz	-0.0906
B16	Lat S	25°	47'	09.528145"	+0.002135"	25°	47'	09.526010"	0.001408m	x	5082290.4411	5082290.3645	dx	-0.0766
	Lon E	27°	50'	53.787812"	+0.003870"	27°	50'	53.791682"	0.001404m	y	2685062.6129	2685062.6944	dy	0.0815
	Height	1443.9057m			-0.0647m	1443.8410m			0.003507m	z	2758359.8493	2758359.7619	dz	-0.0874

Table D.5: Adjusted Individual Sessions Inner Network: April 97;

Baseline	Date	Start	H:M	Δx	Δy	Δz	Slope Dist.	Δ H
SLR-413	17/4/97	10:46	1:37	-558.6233	1377.0804	-76.3473	1488.0321	164.1047
SLR-413	14/5/97	07:26	6:02	-558.6201	1377.0885	-76.3520	1488.0386	164.1126
SLR-413			Mean	-558.6217	1377.0844	-76.3496	1488.0354	164.1086
SLR-411	17/4/97	08:01	1:59	470.8376	760.4395	1185.4410	1485.0005	175.5057
SLR-411	12/5/97	07:58	5:00	470.8489	760.4458	1185.4388	1485.0056	175.5184
SLR-411			Mean	470.8432	760.4426	1185.4399	1485.0030	175.5120
SLR-B44	16/4/97	09:33	2;26	959.9801	-846.2560	474.1345	1364.7397	204.1365
SLR-B44	16/4/97	12:01	1:34	959.9847	-846.2546	474.1337	1364.7418	204.1410
SLR-B44			Mean	959.9824	-846.2553	474.1341	1364.7408	204.1388
SLR-415	22/4/97	11:59	1:34	41.6983	-956.5427	888.9790	1306.5207	21.6848
SLR-414	22/4/97	09:15	0:41	-421.0879	302.1011	-669.5002	846.6467	83.2112
SLR-414	22/4/97	10:01	0:59	-421.0891	302.1011	-669.4975	846.6451	83.2090
SLR-414			Mean	-421.0885	302.1011	-669.4988	846.6459	83.2101

Table D.6: Inner Network, Before and Final Adjusted Values: April 97;

Station		Before	Min	Sec	Adjust	After	Min	Sec	σ		Old Cartesian	New Cartesian		Adjust (m)
SLR	Lat S	25°	53'	22.953502"	+0.000000"	25°	53'	22.953502"	FIXED	x	5085401.0587	5085401.0587	dx	0.0000
	Lon E	27°	41'	10.226915"	+0.000000"	27°	41'	10.226915"	FIXED	y	2668330.0559	2668330.0559	dy	0.0000
	Height	1406.7366m			+0.0000m	1406.7366m			FIXED	z	2768688.8585	2768688.8585	dz	0.0000
411	Lat S	25°	52'	37.383036"	+0.002130"	25°	52'	37.380906"	0.001005m	x	5085871.9761	5085871.9006	dx	-0.0755
	Lon E	27°	41'	26.548861"	+0.003775"	27°	41'	26.552636"	0.000899m	y	2669090.4200	2669090.4991	dy	0.0791
	Height	1582.3128m			-0.0652m	1582.2476m			0.002421m	z	2767503.5053	2767503.4179	dz	-0.0874
413	Lat S	25°	53'	23.125085"	+0.002084"	25°	53'	23.123001"	0.000656m	x	5084842.5170	5084842.4384	dx	-0.0786
	Lon E	27°	42'	03.340680"	+0.004004"	27°	42'	03.344684"	0.000657m	y	2669707.0595	2669707.1442	dy	0.0847
	Height	1570.9137m			-0.0647m	1570.8490m			0.001634m	z	2768765.2963	2768765.2104	dz	-0.0859
B44	Lat S	25°	53'	02.615924"	+0.002149"	25°	53'	02.613775"	0.002054m	x	5086361.1204	5086361.0408	dx	-0.0796
	Lon E	27°	40'	27.292261"	+0.003792"	27°	40'	27.296053"	0.002108m	y	2667483.7231	2667483.8006	dy	0.0775
	Height	1610.9455m			-0.0704m	1610.8751m			0.005233m	z	2768214.8145	2768214.7243	dz	-0.0902
414	Lat S	25°	53'	45.820947"	+0.002150"	25°	53'	45.818797"	0.001994m	x	5084980.0524	5084979.9704	dx	-0.0820
	Lon E	27°	41'	26.858824"	+0.003817"	27°	41'	26.862641"	0.001915m	y	2668632.0801	2668632.1571	dy	0.0770
	Height	1490.0202m			-0.0731m	1489.9471m			0.004853m	z	2769358.4492	2769358.3578	dz	-0.0914
415	Lat S	25°	53'	54.717698"	+0.002128"	25°	53'	54.715570"	0.001788m	x	5085442.8386	5085442.7570	dx	-0.0816
	Lon E	27°	40'	39.103100"	+0.003805"	27°	40'	39.106906"	0.001807m	y	2667373.4363	2667373.5132	dy	0.0769
	Height	1428.4938m			-0.0724m	1428.4214m			0.004851m	z	2769577.9280	2769577.8374	dz	-0.0906

Table D.7: Adjusted Individual Sessions Inner Network: September 97;

Baseline	Date	Start	H:M	Δx	Δy	Δz	Slope Dist.	Δ H
SLR-413	04/09/97	08:47	05:08	-558.6146	1377.0920	-76.3555	1488.0399	164.1148
SLR-411	23/09/97	13:00	10:54	470.8538	760.4417	1185.4418	1485.0075	175.5147
SLR-411	24/09/97	00:01	23:57	470.8626	760.4492	1185.4358	1485.0093	175.5275
SLR-411	25/09/97	00:01	07:27	470.8601	760.4520	1185.4368	1485.0107	175.5262
SLR-411	25/09/97	07:29	05:45	470.8568	760.4540	1185.4377	1485.0115	175.5241
SLR-411			Mean	470.8583	760.4492	1185.4380	1485.0098	175.5231
SLR-B44	18/09/97	08:29	03:46	959.9904	-846.2529	474.1289	1364.7431	204.1513
SLR-415	17/09/97	07:47	05:40	41.7014	-956.5396	888.9812	1306.5201	21.6946
SLR-414	09/05/97	07:27	06:26	-421.0834	302.1061	-669.5004	846.6464	83.2167

Table D.8: Inner Network, Before and Final Adjusted Values: September 97;

Station		Before	Min	Sec	Adjust	After	Min	Sec	σ		Old Cartesian	New Cartesian		Adjust (m)
411	Lat S	25°	52'	36.480314"	-0.900420"	25°	52'	37.380734"	0.001087m	x	5085882.6237	5085871.9192	dx	-10.7045
	Lon E	27°	41'	26.552750"	-0.000229"	27°	41'	26.552521"	0.001013m	y	2669096.1302	2669090.5052	dy	-5.6250
	Height	1582.2619m			+0.0045m	1582.2665m			0.002691m	z	2767478.4820	2767503.4214	dz	+24.9394
413	Lat S	25°	53'	23.121901"	-0.001112"	25°	53'	23.123013"	0.003020m	x	5084842.5203	5084842.4441	dx	-0.0762
	Lon E	27°	42'	03.345091"	-0.000385"	27°	42'	03.344706"	0.002931m	y	2669707.2000	2669707.1478	dy	-0.0522
	Height	1570.9420m			-0.0854m	1570.8566m			0.007040m	z	2768765.2205	2768765.2140	dz	-0.0065
B44	Lat S	25°	53'	01.713535"	-0.900274"	25°	53'	02.613810"	0.004871m	x	5086371.7684	5086361.0490	dx	-10.7194
	Lon E	27°	40'	27.295741"	+0.000249"	27°	40'	27.295991"	0.004777m	y	2667489.4168	2667483.8030	dy	-5.6138
	Height	1610.8879m			-0.0030m	1610.8849m			0.011777m	z	2768189.7989	2768214.7295	dz	+24.9306
414	Lat S	25°	53'	44.918972"	-0.899762"	25°	53'	45.818734"	0.003574m	x	5084990.6844	5084979.9753	dx	-10.7091
	Lon E	27°	41'	26.862803"	-0.000089"	27°	41'	26.862714"	0.003427m	y	2668637.7850	2668632.1619	dy	-5.6231
	Height	1489.9533m			+0.0002m	1489.9535m			0.008138m	z	2769333.4439	2769358.3588	dz	+24.9149
415	Lat S	25°	53'	53.815828"	-0.899748"	25°	53'	54.715576"	0.004725m	x	5085453.4803	5085442.7601	dx	-10.7202
	Lon E	27°	40'	39.106666"	+0.000286"	27°	40'	39.106952"	0.004541m	y	2667379.1302	2667373.5163	dy	-5.6139
	Height	1428.4312m			-0.0051m	1428.4261m			0.010971m	z	2769552.9282	2769577.8397	dz	+24.9115
SLR	Lat S	25°	53'	22.953502"	+0.000000"	25°	53'	22.953502"	FIXED	x	5085401.0587	5085401.0587	dx	0.0000
	Lon E	27°	41'	10.226915"	+0.000000"	27°	41'	10.226915"	FIXED	y	2668330.0559	2668330.0559	dy	0.0000
	Height	1406.7366m			+0.0000m	1406.7366m			FIXED	z	2768688.8585	2768688.8585	dz	0.0000

Table D.9: Adjusted Individual Sessions Inner network: January 98;

Baseline	Date	Start	H:M	Δx	Δy	Δz	Slope Dist.	Δ H
SLR-B44	27/01/98	12:01	1:52	959.8597	-846.3228	474.2068	1364.7216	203.9810
SLR-B44	12/03/98	09:52	2:07	959.9711	-846.2621	474.1369	1364.7380	204.1256
SLR-411	26/01/98	12:00	1:59	470.7170	760.3788	1185.5078	1484.9846	175.3551
SLR-411	26/01/98	14:01	1:59	470.7405	760.3878	1185.4989	1484.9895	175.3816
SLR-411	26/01/98	16:01	1:59	470.7561	760.3972	1185.4962	1484.9971	175.3991
SLR-411	26/01/98	18:01	1:59	470.7406	760.3865	1185.5009	1484.9905	175.3802
SLR-411	26/01/98	20:01	1:59	470.7310	760.3787	1185.5013	1484.9838	175.3692
SLR-411	26/01/98	22:01	1:58	470.7369	760.3742	1185.4951	1484.9784	175.3747
SLR-411	27/01/98	00:01	1:59	470.7429	760.3930	1185.5068	1484.9992	175.3822
SLR-411	27/01/98	02:01	1:59	470.7333	760.3819	1185.5053	1484.9893	175.3706
SLR-411	27/01/98	04:01	1:59	470.7263	760.3805	1185.5078	1484.9884	175.3633
SLR-411	27/01/98	06:01	1:59	470.7319	760.3822	1185.5123	1484.9946	175.3665
SLR-411	27/01/98	08:01	1:59	470.7284	760.3771	1185.5024	1484.9830	175.3659
SLR-411	27/01/98	10:01	1:59	470.7257	760.3730	1185.5048	1484.9820	175.3610
SLR-411	27/01/98	12:01	1:59	470.6994	760.3624	1185.4981	1484.9628	175.3386
SLR-411	27/01/98	14:01	1:59	470.7402	760.3857	1185.4996	1484.9889	175.3802
SLR-411	27/01/98	16:01	1:58	470.7592	760.3929	1185.4912	1484.9920	175.4020
SLR-411	27/01/98	18:01	1:58	470.7453	760.3900	1185.4982	1484.9916	175.3866
SLR-411	27/01/98	20:01	1:58	470.7425	760.3850	1185.4952	1484.9858	175.3837
SLR-411	27/01/98	22:01	1:58	470.7449	760.3789	1185.4925	1484.9812	175.3841
SLR-411	28/01/98	00:01	1:59	470.7503	760.3967	1185.5038	1485.0011	175.3910
SLR-411	28/01/98	02:01	1:59	470.7368	760.3833	1185.5030	1484.9893	175.3749
SLR-411	28/01/98	04:01	1:59	470.7250	760.3791	1185.5067	1484.9864	175.3622
SLR-411	28/01/98	06:01	1:59	470.7332	760.3825	1185.5078	1484.9916	175.3696
SLR-411	28/01/98	08:01	1:59	470.7317	760.3784	1185.4987	1484.9817	175.3707
SLR-411			Mean	470.7356	760.3829	1185.5015	1484.9875	175.3745
SLR-414	29/01/98	08:00	1:59	-421.1313	302.0740	-669.4783	846.6413	83.1557
SLR-414	29/01/98	10:01	1:59	-421.1380	302.0733	-669.4752	846.6419	83.1487
SLR-414	29/01/98	12:01	1:59	-421.1252	302.0850	-669.4816	846.6448	83.1667
SLR-414	10/02/98	08:40	1:13	-421.1249	302.0754	-669.4794	846.6394	83.1619
SLR-414	10/02/98	10:00	1:59	-421.1354	302.0738	-669.4767	846.6420	83.1517
SLR-414			Mean	-421.1310	302.0763	-669.4782	846.6419	83.1569
SLR-606	30/01/98	09:20	4:04	-657.8895	2063.1954	447.7468	2211.3505	143.1893
SLR-415	29/01/98	08:30	1:28	41.6867	-956.5512	-888.9754	1306.5241	21.6704
SLR-415	29/01/98	10:01	1:59	41.6880	-956.5505	-888.9756	1306.5238	21.6719
SLR-415	29/01/98	12:01	1:59	41.6926	-956.5484	-888.9765	1306.5230	21.6768
SLR-415	05/02/98	08:01	1:58	41.6841	-956.5536	-888.9731	1306.5242	21.6663
SLR-415	05/02/98	10:01	1:59	41.6803	-956.5523	-888.9752	1306.5246	21.6648
SLR-415	05/02/98	12:01	1:13	41.6849	-956.5531	-888.9715	1306.5228	21.6665
SLR-415			Mean	41.6861	-956.5515	-888.9746	1306.5238	21.6694
SLR-415	12/03/98	09:05	3:30	41.6970	-956.5426	-888.9744	1306.5174	21.6817

Table D.10: Inner Network, Before and Final Adjusted Values: January 98;

Station		Before	Min	Sec	Adjust	After	Min	Sec	σ		Old Cartesian	New Cartesian		Adjust (m)
413	Lat S	25°	53'	23.123007"	+0.000000"	25°	53'	23.123007"	0.002141m	x	5084842.3244	5084842.3252	dx	0.0008
	Lon E	27°	42'	03.344501"	+0.000000"	27°	42'	03.344501"	0.001760m	y	2669707.0785	2669707.0790	dy	0.0005
	Height	1570.7029m			+0.0011m	1570.7040m			0.005355m	z	2768765.1467	2768765.1472	dz	0.0005
414	Lat S	25°	53'	45.818870"	+0.000000"	25°	53'	45.818870"	0.001713m	x	5084979.9274	5084979.9283	dx	0.0009
	Lon E	27°	41'	26.862538"	+0.000000"	27°	41'	26.862538"	0.001391m	y	2668632.1313	2668632.1318	dy	0.0005
	Height	1489.8926m			+0.0011m	1489.8937m			0.004412m	z	2769358.3360	2769358.3365	dz	0.0005
415	Lat S	25°	53'	54.715599"	+0.000000"	25°	53'	54.715599"	0.001331m	x	5085442.7494	5085442.7503	dx	0.0009
	Lon E	27°	40'	39.106834"	+0.000000"	27°	40'	39.106834"	0.001139m	y	2667373.5070	2667373.5074	dy	0.0004
	Height	1428.4111m			+0.0011m	1428.4122m			0.003736m	z	2769577.8337	2769577.8342	dz	0.0005
B44	Lat S	25°	53'	02.613839"	+0.000000"	25°	53'	02.613839"	0.002493m	x	5086360.9528	5086360.9537	dx	0.0009
	Lon E	27°	40'	27.295839"	+0.000000"	27°	40'	27.295839"	0.002229m	y	2667483.7477	2667483.7482	dy	0.0005
	Height	1610.7621m			+0.0011m	1610.7632m			0.007450m	z	2768214.6767	2768214.6772	dz	0.0005
411	Lat S	25°	52'	37.380848"	+0.000000"	25°	52'	37.380848"	0.001427m	x	5085871.7981	5085871.7990	dx	0.0009
	Lon E	27°	41'	26.552494"	+0.000000"	27°	41'	26.552494"	0.001328m	y	2669090.4409	2669090.4413	dy	0.0004
	Height	1582.1158m			+0.0011m	1582.1169m			0.003572m	z	2767503.3588	2767503.3592	dz	0.0004
SLR	Lat S	25°	53'	22.953502"	+0.000000"	25°	53'	22.953502"	FIXED	x	5085401.0587	5085401.0587	dx	0.0000
	Lon E	27°	41'	10.226915"	+0.000000"	27°	41'	10.226915"	FIXED	y	2668330.0559	2668330.0559	dy	0.0000
	Height	1406.7366m			+0.0000m	1406.7366m			FIXED	z	2768688.8585	2768688.8585	dz	0.0000

Table D.11: Adjusted Individual Sessions Inner Network: April 98

Date	H:M	Δx	σ	Δy	σ	Δz	σ	Slope Dist.	σ	Δ H	σ
4/21/98	0:59	1029.4765	0.890	-616.6364	0.547	1261.7845	0.472	1741.3105	0.406	11.4171	0.997
4/21/98	0:59	1029.4760	0.758	-616.6369	0.617	1261.7830	0.618	1741.3093	0.462	11.4171	0.957
4/21/98	0:59	1029.4735	0.969	-616.6386	0.608	1261.7869	0.577	1741.3113	0.542	11.4127	0.108
4/21/98	0:59	1029.4796	0.109	-616.6350	0.604	1261.7821	0.579	1741.3101	0.496	11.4212	0.119
413-411	Mean	1029.4764		-616.6367		1261.7841		1741.3103		11.4170	
4/23/98	0:59	-137.5470	0.644	1074.9774	0.408	593.1578	0.349	1235.4480	0.305	80.8813	0.726
4/23/98	0:59	-137.5437	0.683	1074.9765	0.543	593.1563	0.567	1235.4461	0.408	80.8842	0.856
414-413	Mean	-137.5454		1074.9770		593.1570		1235.4470		80.8828	
4/23/98	0:37	462.7715	0.120	-1258.6508	0.592	-219.4706	0.515	1358.8696	0.455	-61.5446	0.126
4/23/98	0:59	462.7732	0.784	-1258.6496	0.453	-219.4748	0.457	1358.8697	0.358	-61.5410	0.876
4/23/98	0:59	462.7746	0.931	-1258.6483	0.516	-219.4737	0.771	1358.8689	0.376	-61.5398	0.118
414-415	Mean	462.7731		-1258.6496		-219.4730		1358.8694		-61.5418	
4/28/98	0:54	918.3027	0.901	110.2928	0.639	1363.1024	0.591	1647.2682	0.389	182.4757	0.108
4/28/98	0:59	918.3077	0.673	110.2957	0.505	1363.0984	0.527	1647.2678	0.414	182.4826	0.807
4/28/98	0:59	918.3020	0.738	110.2934	0.366	1363.1029	0.318	1647.2682	0.358	182.4751	0.775
4/28/98	0:59	918.3049	0.609	110.2932	0.329	1363.1017	0.440	1647.2689	0.305	182.4779	0.707
4/28/98	0:58	918.3096	0.128	110.2949	0.897	1363.0991	0.966	1647.2694	0.563	182.4835	0.163
415-B44	Mean	918.3054		110.2940		1363.1009		1647.2685		182.4790	
4/22/98	0:59	-489.1402	0.133	1606.6980	0.829	711.3069	0.712	1823.9227	0.621	-28.6279	0.149
4/22/98	0:59	-489.1328	0.115	1606.7087	0.922	711.3045	0.948	1823.9292	0.710	-28.6165	0.145
4/22/98	0:59	-489.1433	0.123	1606.6998	0.767	711.3119	0.710	1823.9271	0.556	-28.6318	0.137
4/22/98	0:59	-489.1345	0.101	1606.7059	0.572	711.3061	0.561	1823.9278	0.546	-28.6198	0.111
4/22/98	0:59	-489.1432	0.919	1606.7016	0.506	711.3104	0.750	1823.9280	0.396	-28.6304	0.116
B44-411	Mean	-489.1388		1606.7028		711.3080		1823.9270		-28.6253	
4/21/98	0:59	519.3999	0.888	694.8155	0.550	1228.2785	0.473	1503.7330	0.411	168.0562	0.998
4/21/98	0:59	519.4062	0.869	694.8148	0.707	1228.2766	0.709	1503.7332	0.542	168.0618	0.110
4/21/98	0:59	519.4128	0.117	694.8203	0.740	1228.2729	0.703	1503.7351	0.588	168.0710	0.131
4/21/98	0:59	519.4113	0.130	694.8204	0.723	1228.2745	0.694	1503.7359	0.608	168.0692	0.143
4/22/98	0:59	519.4002	0.123	694.8130	0.763	1228.2785	0.657	1503.7319	0.560	168.0555	0.138
4/22/98	0:59	519.4085	0.118	694.8168	0.945	1228.2756	0.968	1503.7342	0.632	168.0650	0.148
4/22/98	0:59	519.4018	0.110	694.8178	0.676	1228.2767	0.629	1503.7332	0.536	168.0596	0.121
4/22/98	0:59	519.4130	0.102	694.8228	0.578	1228.2719	0.569	1503.7355	0.488	168.0727	0.113
4/22/98	0:59	519.4094	0.831	694.8212	0.447	1228.2721	0.683	1503.7337	0.361	168.0690	0.104
HRAO-411	Mean	519.4070		694.8181		1228.2753		1503.7340		168.0644	
4/21/98	0:59	-510.0762	0.778	1311.4520	0.487	-33.5062	0.412	1407.5535	0.374	156.6396	0.873
4/21/98	0:59	-510.0701	0.746	1311.4513	0.606	-33.5064	0.605	1407.5506	0.512	156.6442	0.939
4/21/98	0:59	-510.0610	0.109	1311.4589	0.698	-33.5140	0.661	1407.5546	0.567	156.6580	0.122
4/21/98	0:59	-510.0684	0.139	1311.4554	0.769	-33.5074	0.732	1407.5538	0.602	156.6478	0.152
4/23/98	0:59	-510.0677	0.737	1311.4550	0.473	-33.5096	0.400	1407.5532	0.373	156.6491	0.832
4/23/98	0:59	-510.0616	0.854	1311.4584	0.681	-33.5096	0.708	1407.5542	0.574	156.6554	0.107
HRAO-413	Mean	-510.0675		1311.4552		-33.5089		1407.5533		156.6490	
4/23/98	0:59	-372.5213	0.114	236.4777	0.722	-626.6673	0.618	766.4240	0.493	75.7674	0.128
4/23/98	0:59	-372.5177	0.812	236.4821	0.644	-626.6662	0.674	766.4227	0.533	75.7716	0.102
4/23/98	0:59	-372.5211	0.128	236.4815	0.770	-626.6689	0.698	766.4264	0.647	75.7698	0.140
4/23/98	0:59	-372.5208	0.102	236.4796	0.591	-626.6674	0.596	766.4244	0.452	75.7686	0.114
4/23/98	0:59	-372.5222	0.898	236.4758	0.498	-626.6678	0.745	766.4251	0.446	75.7672	0.114
HRAO-414	Mean	-372.5206		236.4793		-626.6675		766.4245		75.7689	

Table D.12: Adjusted Individual Sessions Inner Network April 98, continued;

Date	H:M	Δx	σ	Δy	σ	Δz	σ	Slope Dist.	σ	Δ H	σ
4/23/98	0:37	90.2529	0.105	-1022.1694	0.571	-846.1415	0.496	1330.0117	0.367	14.2280	0.112
4/23/98	0:59	90.2530	0.768	-1022.1696	0.445	-846.1427	0.445	1330.0127	0.361	14.2285	0.855
4/23/98	0:59	90.2523	0.984	-1022.1699	0.545	-846.1414	0.813	1330.0121	0.459	14.2273	0.124
4/28/98	0:59	90.2499	0.730	-1022.1704	0.526	-846.1407	0.469	1330.0118	0.374	14.2249	0.869
4/28/98	0:59	90.2511	0.618	-1022.1710	0.462	-846.1380	0.483	1330.0106	0.345	14.2244	0.739
4/28/98	0:59	90.2544	0.751	-1022.1687	0.401	-846.1420	0.347	1330.0117	0.269	14.2297	0.802
4/28/98	0:59	90.2569	0.752	-1022.1660	0.413	-846.1432	0.544	1330.0105	0.386	14.2333	0.874
4/28/98	0:58	90.2513	0.123	-1022.1692	0.865	-846.1403	0.932	1330.0108	0.591	14.2263	0.157
HRAO-415	Mean	90.2527		-1022.1693		-846.1412		1330.0115		14.2278	
4/22/98	0:59	1008.5399	0.130	-911.8847	0.808	516.9715	0.687	1454.6291	0.694	196.6832	0.145
4/22/98	0:59	1008.5415	0.124	-911.8918	0.993	516.9711	0.102	1454.6345	0.800	196.6816	0.156
4/22/98	0:59	1008.5450	0.106	-911.8821	0.670	516.9647	0.618	1454.6286	0.616	196.6913	0.118
4/22/98	0:59	1008.5476	0.959	-911.8831	0.544	516.9658	0.530	1454.6314	0.498	196.6925	0.106
4/22/98	0:59	1008.5554	0.958	-911.8785	0.526	516.9602	0.812	1454.6320	0.415	196.7031	0.121
4/28/98	0:54	1008.5508	0.747	-911.8775	0.535	516.9625	0.495	1454.6290	0.422	196.6988	0.897
4/28/98	0:59	1008.5589	0.670	-911.8752	0.500	516.9602	0.527	1454.6323	0.437	196.7072	0.803
4/28/98	0:59	1008.5570	0.852	-911.8752	0.423	516.9607	0.368	1454.6312	0.460	196.7055	0.894
4/28/98	0:59	1008.5622	0.700	-911.8725	0.378	516.9578	0.507	1454.6321	0.349	196.7120	0.813
4/28/98	0:59	1008.5601	0.620	-911.8742	0.439	516.9589	0.473	1454.6321	0.285	196.7092	0.795
HRAO-B44	Mean	1008.5518		-911.8795		516.9633		1454.6312		196.6984	
4/21/98	0:59	48.5515	0.623	-65.6273	0.385	42.8358	0.331	92.1905	0.288	-7.4587	0.700
4/21/98	0:59	48.5554	0.491	-65.6303	0.456	42.8370	0.417	92.1953	0.373	-7.4574	0.654
4/21/98	0:59	48.5564	0.489	-65.6275	0.319	42.8348	0.301	92.1928	0.275	-7.4545	0.554
4/21/98	0:59	48.5579	0.616	-65.6267	0.343	42.8340	0.328	92.1926	0.268	-7.4526	0.675
4/21/98	0:59	48.5583	0.577	-65.6280	0.309	42.8333	0.488	92.1934	0.243	-7.4526	0.726
4/22/98	0:59	48.5510	0.628	-65.6284	0.393	42.8367	0.337	92.1915	0.297	-7.4599	0.706
4/22/98	0:59	48.5547	0.511	-65.6307	0.484	42.8364	0.443	92.1949	0.398	-7.4579	0.687
4/22/98	0:59	48.5533	0.574	-65.6285	0.365	42.8360	0.332	92.1924	0.313	-7.4579	0.641
4/22/98	0:59	48.5539	0.612	-65.6272	0.348	42.8357	0.342	92.1917	0.270	-7.4567	0.677
4/22/98	0:59	48.5552	0.608	-65.6285	0.322	42.8355	0.502	92.1932	0.251	-7.4562	0.762
4/23/98	0:59	48.5555	0.652	-65.6283	0.432	42.8341	0.349	92.1925	0.275	-7.4552	0.770
4/23/98	0:59	48.5508	0.594	-65.6281	0.377	42.8369	0.322	92.1913	0.286	-7.4601	0.669
4/23/98	0:59	48.5536	0.422	-65.6294	0.406	42.8359	0.372	92.1932	0.336	-7.4580	0.572
4/23/98	0:59	48.5522	0.580	-65.6286	0.351	42.8363	0.318	92.1921	0.303	-7.4590	0.638
4/23/98	0:59	48.5538	0.585	-65.6271	0.339	42.8353	0.343	92.1914	0.260	-7.4566	0.654
4/23/98	0:59	48.5552	0.553	-65.6282	0.307	42.8357	0.458	92.1931	0.235	-7.4561	0.699
4/23/98	0:54	48.5518	0.559	-65.6306	0.473	42.8363	0.303	92.1934	0.263	-7.4601	0.705
4/28/98	0:59	48.5507	0.702	-65.6268	0.497	42.8372	0.453	92.1904	0.382	-7.4598	0.836
4/28/98	0:59	48.5554	0.428	-65.6292	0.358	42.8380	0.347	92.1950	0.309	-7.4574	0.535
4/28/98	0:59	48.5557	0.600	-65.6278	0.297	42.8349	0.258	92.1927	0.261	-7.4552	0.630
4/28/98	0:59	48.5553	0.587	-65.6272	0.320	42.8340	0.424	92.1916	0.258	-7.4549	0.683
4/28/98	0:59	48.5580	0.442	-65.6288	0.315	42.8351	0.337	92.1947	0.219	-7.4539	0.568
4/28/98	0:24	48.5529	0.118	-65.6270	0.101	42.8370	0.561	92.1916	0.512	-7.4581	0.147
HRAO-SLR	Mean	48.5543		-65.6283		42.8357		92.1927		-7.4569	
4/21/98	0:59	470.8484	0.888	760.4428	0.549	1185.4427	0.473	1485.0070	0.413	175.5150	0.997
4/21/98	0:59	470.8520	0.819	760.4481	0.762	1185.4376	0.695	1485.0068	0.423	175.5224	0.109
4/21/98	0:59	470.8570	0.118	760.4492	0.756	1185.4369	0.756	1485.0084	0.586	175.5271	0.132
4/21/98	0:59	470.8535	0.136	760.4471	0.754	1185.4405	0.723	1485.0091	0.634	175.5219	0.149
4/22/98	0:59	470.8483	0.130	760.4412	0.803	1185.4422	0.694	1485.0058	0.594	175.5145	0.146
4/22/98	0:59	470.8546	0.116	760.4481	0.113	1185.4392	0.996	1485.0089	0.615	175.5237	0.157
4/22/98	0:59	470.8484	0.114	760.4460	0.723	1185.4408	0.660	1485.0072	0.554	175.5172	0.127
4/22/98	0:59	470.8591	0.996	760.4500	0.566	1185.4362	0.556	1485.0089	0.479	175.5294	0.110
4/22/98	0:59	470.8531	0.863	760.4488	0.457	1185.4373	0.711	1485.0073	0.376	175.5237	0.108
SLR-411	Mean	470.8527		760.4468		1185.4393		1485.0077		175.5217	

Table D.13: Adjusted Individual Sessions Inner Network April 98, continued;

Date	H:M	Δx	σ	Δy	σ	Δz	σ	Slope Dist.	σ	Δ H	σ
4/21/98	0:59	-558.6279	0.887	1377.0792	0.548	-76.3419	0.470	1488.0324	0.422	164.0981	0.995
4/21/98	0:59	-558.6248	0.785	1377.0832	0.737	-76.3443	0.668	1488.0350	0.609	164.1032	0.105
4/21/98	0:59	-558.6166	0.117	1377.0874	0.749	-76.3497	0.703	1488.0361	0.613	164.1140	0.131
4/21/98	0:59	-558.6261	0.143	1377.0821	0.796	-76.3415	0.762	1488.0343	0.621	164.1006	0.157
4/23/98	0:59	-558.6189	0.952	1377.0831	0.605	-76.3464	0.517	1488.0328	0.479	164.1088	0.107
4/23/98	0:59	-558.6144	0.965	1377.0893	0.928	-76.3465	0.849	1488.0369	0.767	164.1151	0.131
SLR-413	Mean	-558.6214		1377.0840		-76.3450		1488.0346		164.1066	
4/23/98	0:18	-421.0768	0.165	302.1093	0.979	-669.5025	0.912	846.6459	0.722	83.2244	0.188
4/23/98	0:59	-421.0722	0.943	302.1057	0.599	-669.5041	0.513	846.6436	0.415	83.2274	0.106
4/23/98	0:59	-421.0716	0.820	302.1102	0.785	-669.5015	0.724	846.6428	0.603	83.2285	0.111
4/23/98	0:59	-421.0731	0.976	302.1101	0.589	-669.5053	0.535	846.6466	0.498	83.2289	0.107
4/23/98	0:59	-421.0747	0.847	302.1067	0.491	-669.5026	0.496	846.6440	0.375	83.2251	0.947
4/23/98	0:59	-421.0775	0.651	302.1066	0.361	-669.5034	0.539	846.6460	0.318	83.2232	0.823
4/23/98	0:21	-421.0690	0.110	302.1148	0.945	-669.5059	0.708	846.6467	0.524	83.2345	0.141
SLR-414	Mean	-421.0736		302.1091		-669.5036		846.6451		83.2274	
4/23/98	0:37	41.6948	0.135	-956.5423	0.667	-888.9766	0.578	1306.5186	0.421	21.6811	0.141
4/23/98	0:59	41.6988	0.815	-956.5428	0.472	-888.9774	0.481	1306.5197	0.383	21.6844	0.912
4/23/98	0:59	41.6971	0.965	-956.5418	0.536	-888.9771	0.798	1306.5187	0.459	21.6834	0.122
4/28/98	0:59	41.6984	0.974	-956.5435	0.688	-888.9776	0.627	1306.5203	0.481	21.6840	0.116
4/28/98	0:59	41.6957	0.647	-956.5413	0.535	-888.9762	0.520	1306.5177	0.362	21.6821	0.803
4/28/98	0:59	41.6997	0.939	-956.5408	0.466	-888.9770	0.405	1306.5180	0.308	21.6858	0.986
4/28/98	0:59	41.7018	0.758	-956.5385	0.411	-888.9778	0.549	1306.5169	0.388	21.6888	0.882
4/28/98	0:58	41.6924	0.121	-956.5406	0.848	-888.9748	0.913	1306.5161	0.579	21.6791	0.154
SLR-415	Mean	41.6973		-956.5414		-888.9768		1306.5182		21.6836	
4/22/98	0:59	959.9861	0.137	-846.2567	0.827	474.1361	0.129	1364.7450	0.745	204.1402	0.153
4/22/98	0:59	959.9865	0.124	-846.2617	0.118	474.1353	0.107	1364.7480	0.848	204.1388	0.167
4/22/98	0:59	959.9918	0.112	-846.2537	0.710	474.1287	0.645	1364.7446	0.659	204.1492	0.125
4/22/98	0:59	959.9938	0.886	-846.2559	0.503	474.1301	0.494	1364.7477	0.465	204.1493	0.980
4/22/98	0:59	959.9996	0.109	-846.2501	0.577	474.1250	0.895	1364.7465	0.474	204.1586	0.136
4/28/98	0:54	960.0004	0.807	-846.2507	0.578	474.1249	0.534	1364.7474	0.459	204.1590	0.969
4/28/98	0:59	960.0031	0.780	-846.2464	0.646	474.1227	0.627	1364.7459	0.526	204.1639	0.970
4/28/98	0:59	960.0015	0.101	-846.2475	0.502	474.1259	0.438	1364.7466	0.553	204.1608	0.106
4/28/98	0:59	960.0069	0.696	-846.2452	0.376	474.1238	0.503	1364.7482	0.352	204.1669	0.809
4/28/98	0:59	960.0019	0.637	-846.2455	0.451	474.1240	0.486	1364.7449	0.295	204.1628	0.817
SLR-B44	Mean	959.9972		-846.2513		474.1276		1364.7465		204.1550	

Table D.14: Inner Network, Before and Final Adjusted Values: April 98;

Station		Before	Min	Sec	Adjust	After	Min	Sec	σ		Old Cartesian	New Cartesian		Adjust (m)
411	Lat S	25°	52'	37.380744"	-0.000043"	25°	52'	37.380787"	0.000387m	x	5085871.9116	5085871.9088	dx	-0.0028
	Lon E	27°	41'	26.552530"	+0.000029"	27°	41'	26.552559"	0.000417m	y	2669090.5015	2669090.5010	dy	-0.0005
	Height	1582.2572m			-0.0024m	1582.2548m			0.000961m	z	2767503.4176	2767503.4177	dz	0.0001
413	Lat S	25°	53'	23.122895"	+0.000038"	25°	53'	23.122857"	0.000412m	x	5084842.4306	5084842.4330	dx	0.0024
	Lon E	27°	42'	03.344440"	+0.000101"	27°	42'	03.344541"	0.000479m	y	2669707.1324	2669707.1368	dy	0.0044
	Height	1570.8336m			+0.0042m	1570.8377m			0.001022m	z	2768765.2007	2768765.2014	dz	0.0007
414	Lat S	25°	53'	45.818734"	+0.000023"	25°	53'	45.818711"	0.000365m	x	5084979.9743	5084979.9797	dx	0.0054
	Lon E	27°	41'	26.862539"	+0.000063"	27°	41'	26.862601"	0.000387m	y	2668632.1559	2668632.1607	dy	0.0048
	Height	1489.9494m			+0.0075m	1489.9569m			0.000917m	z	2769358.3570	2769358.3597	dz	0.0027
415	Lat S	25°	53'	54.715513"	+0.000002"	25°	53'	54.715511"	0.000336m	x	5085442.7488	5085442.7521	dx	0.0033
	Lon E	27°	40'	39.106862"	+0.000065"	27°	40'	39.106927"	0.000355m	y	2667373.5076	2667373.5113	dy	0.0037
	Height	1428.4096m			+0.0051m	1428.4147m			0.000835m	z	2769577.8307	2769577.8329	dz	0.0022
B44	Lat S	25°	53'	02.613759"	+0.000011"	25°	53'	02.613748"	0.000318m	x	5086361.0516	5086361.0544	dx	0.0028
	Lat S	27°	40'	27.295865"	+0.000049"	27°	40'	27.295914"	0.000338m	y	2667483.8003	2667483.8034	dy	0.0031
	Height	1610.8853m			+0.0042m	1610.8895m			0.000795m	z	2768214.7283	2768214.7298	dz	0.0015
HRAO	Lat S	25°	53'	24.382820"	+0.000000"	25°	53'	24.382820"	FIXED	x	5085352.5003	5085352.5003	dx	0.0000
	Lon E	27°	41'	13.124400"	+0.000000"	27°	41'	13.124400"	FIXED	y	2668395.6811	2668395.6811	dy	0.0000
	Height	1414.1880m			+0.0000m	1414.1880m			FIXED	z	2768731.6920	2768731.6920	dz	0.0000
SLR	Lat S	25°	53'	22.953531"	+0.000023"	25°	53'	22.953508"	0.000187m	x	5085401.0585	5085401.0551	dx	-0.0034
	Lon E	27°	41'	10.226831"	+0.000054"	27°	41'	10.226885"	0.000202m	y	2668330.0531	2668330.0531	dy	0.0000
	Height	1406.7354m			-0.0038m	1406.7317m			0.000469m	z	2768688.8588	2768688.8565	dz	-0.0023

Table D.15: Adjusted Individual Sessions Intermediate Network: July 98. (σ is in millimetres, H=HRAO)

Date	H:M	Δx	σ	Δy	σ	Δz	σ	Slope Dist.	σ	Δ H	σ
02/7/98	5:59	-3062.1084	0.16	16667.0069	0.10	10371.9101	0.10	19868.1189	0.79	29.6808	0.18
03/7/98	10:40	-3062.1282	0.94	16667.0005	0.63	10371.9293	0.61	19868.1266	0.45	29.6540	0.11
H-BRO	Mean	-3062.1183		16667.0037		10371.9197		19868.1228		29.6674	
02/7/98	13:22	9251.7323	0.47	-13366.6156	0.29	3137.6288	0.29	16556.1371	0.20	434.2532	0.55
03/7/98	13:00	9251.7394	0.59	-13366.5983	0.39	3137.6194	0.37	16556.1254	0.28	434.2701	0.69
H-MAG	Mean	9251.7358		-13366.6070		3137.6241		16556.1312		434.2616	
02/7/98	15:58	48.5563	0.14	-65.6253	0.91	42.8359	0.89	92.1917	0.62	-7.4542	0.16
03/7/98	13:22	48.5511	0.15	-65.6281	0.10	42.8385	0.10	92.1921	0.07	-7.4606	0.18
22/7/98	23:58	48.5507	0.13	-65.6313	0.85	42.8373	0.08	92.1937	0.06	-7.4617	0.15
23/7/98	12:05	48.5508	0.15	-65.6307	0.10	42.8369	0.10	92.1931	0.07	-7.4613	0.18
H-SLR	Mean	48.5522		-65.6288		42.8372		92.1926		-7.4594	
22/7/98	3:59	2559.5491	0.24	-21004.8468	0.16	-16023.2448	0.17	26542.4049	0.12	310.6400	0.29
22/7/98	4:58	2559.5097	0.11	-21004.8807	0.67	-16023.2353	0.66	26542.4221	0.44	310.5903	0.13
23/7/98	4:27	2559.5155	0.37	-21004.8625	0.26	-16023.2254	0.15	26542.4023	0.24	310.5982	0.34
H-SYF	Mean 2	2559.5248		-21004.8633		-16023.2352		26542.4098		310.6095	
22/7/98	2:58	-7915.7867	0.10	11845.1562	0.60	-3460.0275	0.62	14660.8047	0.36	173.0879	0.12
23/7/98	10:59	-7915.8114	0.48	11845.1425	0.33	-3460.0169	0.31	14660.8045	0.23	173.0578	0.57
H-TWE	Mean	-7915.7990		11845.1494		-3460.0222		14660.8046		173.0728	
02/7/98	4:23	-12313.8339	0.39	30033.6188	0.57	7234.2804	0.18	33256.3314	0.46	-404.5681	0.50
03/7/98	10:40	-12313.8726	0.13	30033.5984	0.91	7234.3108	0.89	33256.3339	0.65	-404.6206	0.16
MAG-BRO	Mean	-12313.8532		30033.6086		7234.2956		33256.3326		-404.5944	
02/7/98	5:59	-3110.6600	0.16	16732.6345	0.11	10329.0716	0.10	19908.4651	0.80	37.1407	0.19
03/7/98	10:32	-3110.6797	0.97	16732.6280	0.65	10329.0910	0.63	19908.4728	0.46	37.1139	0.11
SLR-BRO	Mean	-3110.6629		16732.6246		10329.0764		19908.4597		37.1322	
2/7/98	13:22	9203.1820	0.44	-13300.9868	0.26	3094.7897	0.27	16467.9243	0.18	441.7150	0.51
3/7/98	12:52	9203.1884	0.60	-13300.9699	0.40	3094.7808	0.38	16467.9126	0.29	441.7310	0.71
SLR-MAG	Mean 2	9203.1852		-13300.9784		3094.7852		16467.9184		441.7230	
22/7/98	3:59	2510.9955	0.36	-20939.2289	0.48	-16066.0744	0.15	26511.7927	0.37	318.0904	0.43
22/7/98	4:58	2510.9750	0.98	-20939.2438	0.56	-16066.0803	0.55	26511.8061	0.39	318.0705	0.11
23/7/98	4:27	2510.9659	0.37	-20939.2310	0.26	-16066.0626	0.15	26511.7844	0.24	318.0608	0.34
SLR-SYF	Mean	2510.9788		-20939.2346		-16066.0724		26511.7944		318.0739	
22/7/98	2:58	-7964.3576	0.93	11910.7816	0.55	-3502.8552	0.54	14750.1765	0.35	180.5269	0.10
23/7/98	10:59	-7964.3624	0.49	11910.7733	0.34	-3502.8538	0.32	14750.1720	0.24	180.5189	0.59
SLR-TWE	Mean	-7964.3600		11910.7774		-3502.8545		14750.1742		180.5229	

Table D.16: Intermediate Network, Before and Final Adjusted Values: July 98;

Station		Before	Min	Sec	Adjust	After	Min	Sec	σ		Old Cartesian	New Cartesian		Adjust (m)
BRO	Lat S	25°	47'	09.526170"	-0.000012"	25°	47'	09.526182"	0.002177m	x	5082290.3816	5082290.3804	dx	-0.0012
	Lon E	27°	50'	53.791056"	-0.000015"	27°	50'	53.791041"	0.002310m	y	2685062.6837	2685062.6826	dy	-0.0011
	Height	1443.8546m			-0.0016m	1443.8531m			0.006285m	z	2758359.7723	2758359.7720	dz	-0.0003
HRAO	Lat S	25°	53'	24.382820"	+0.000000"	25°	53'	24.382820"	FIXED	x	5085352.5003	5085352.5003	dx	0.0000
	Lon E	27°	41'	13.124400"	+0.000000"	27°	41'	13.124400"	FIXED	y	2668395.6811	2668395.6811	dy	0.0000
	Height	1414.1880m			+0.0000m	1414.1880m			FIXED	z	2768731.6920	2768731.6920	dz	0.0000
MAG	Lat S	25°	51'	24.253602"	-0.000004"	25°	51'	24.253606"	0.001441m	x	5094604.2343	5094604.2360	dx	0.0017
	Lon E	27°	31'	33.820492"	+0.000023"	27°	31'	33.820515"	0.001558m	y	2655029.0682	2655029.0698	dy	0.0016
	Height	1848.4447m			+0.0025m	1848.4472m			0.006464m	z	2765594.0656	2765594.0668	dz	0.0012
SLR	Lat S	25°	53'	22.953503"	+0.000003"	25°	53'	22.953501"	0.000411m	x	5085401.0526	5085401.0538	dx	0.0012
	Lon E	27°	41'	10.226911"	-0.000003"	27°	41'	10.226908"	0.000437m	y	2668330.0526	2668330.0531	dy	0.0005
	Height	1406.7289m			+0.0013m	1406.7303m			0.001401m	z	2768688.8551	2768688.8557	dz	0.0006
SYF	Lat S	26°	02'	58.473919"	+0.000031"	26°	02'	58.473887"	0.002947m	x	5087912.0242	5087912.0255	dx	0.0013
	Lon E	27°	29'	21.447804"	-0.000001"	27°	29'	21.447804"	0.003062m	y	2647390.8091	2647390.8097	dy	0.0006
	Height	1724.7946m			+0.0010m	1724.7957m			0.018255m	z	2784754.9304	2784754.9300	dz	-0.0004
TWE	Lat S	25°	55'	26.616819"	+0.000011"	25°	55'	26.616808"	0.001457m	x	5077436.6898	5077436.6921	dx	0.0023
	Lon E	27°	49'	42.079276"	-0.000072"	27°	49'	42.079204"	0.001554m	y	2680240.8237	2680240.8227	dy	-0.0010
	Height	1587.2463m			+0.0015m	1587.2478m			0.004763m	z	2772191.7081	2772191.7085	dz	0.0004

Table D.17: Adjusted Individual Sessions Inner Network: June 99;

Date	H:M	Δx	σ	Δy	σ	Δz	σ	Slope Dist.	σ	Δ H	σ
6/10/99	5:05	1029.4725	0.336	-616.6372	0.230	1261.7860	0.217	1741.3096	0.161	11.4130	0.398
413-411											
6/09/99	4:23	-137.5421	0.260	1074.9779	0.186	593.1546	0.177	1235.4464	0.135	80.8868	0.317
414-413											
6/08/99	4:21	462.7683	0.305	-1258.6516	0.218	-219.4693	0.194	1358.8690	0.159	-61.5481	0.363
414-415											
6/24/99	4:44	918.2917	0.413	110.2899	0.285	1363.1098	0.258	1647.2680	0.209	182.4624	0.486
415-B44											
6/11/99	0:06	-489.1362	1.821	1606.7006	0.799	711.3082	1.067	1823.9245	0.626	-28.6242	2.070
6/23/99	4:29	-489.1350	0.365	1606.6971	0.249	711.3057	0.223	1823.9201	0.181	-28.6236	0.427
B44-411	Mean	-489.1356		1606.6988		711.3070		1823.9223		-28.6239	
6/10/99	5:05	519.4115	0.346	694.8220	0.238	1228.2724	0.223	1503.7350	0.180	168.0709	0.410
6/11/99	0:06	519.4119	1.588	694.8243	0.696	1228.2713	0.929	1503.7353	0.589	168.0727	1.804
6/23/99	4:59	519.4086	0.305	694.8181	0.210	1228.2746	0.195	1503.7340	0.158	168.0660	0.361
HRAO-411	Mean	519.4107		694.8215		1228.2728		1503.7348		168.0699	
6/09/99	4:23	-510.0609	0.252	1311.4578	0.181	-33.5140	0.171	1407.5535	0.133	156.6577	0.307
6/10/99	5:47	-510.0608	0.296	1311.4594	0.200	-33.5136	0.192	1407.5549	0.150	156.6582	0.351
HRAO-413	Mean	-510.0608		1311.4586		-33.5138		1407.5542		156.6580	
6/08/99	4:21	-372.5181	0.332	236.4817	0.236	-626.6700	0.197	766.4258	0.147	75.7728	0.394
6/09/99	5:54	-372.5190	0.226	236.4799	0.152	-626.6688	0.144	766.4248	0.107	75.7708	0.267
HRAO-414	Mean	-372.5186		236.4808		-626.6694		766.4253		75.7718	
6/08/99	5:15	90.2507	0.345	-1022.1686	0.234	-846.1385	0.214	1330.0091	0.168	14.2253	0.409
6/24/99	4:59	90.3409	0.309	-1022.1223	0.214	-846.1893	0.197	1330.0120	0.155	14.3387	0.366
HRAO-415	Mean	90.2958		-1022.1454		-846.1639		1330.0106		14.2820	
6/11/99	5:59	1008.5536	0.267	-911.8762	0.179	516.9641	0.174	1454.6307	0.136	196.7009	0.316
6/23/99	4:59	1008.5436	0.357	-911.8787	0.247	516.9687	0.220	1454.6269	0.184	196.6899	0.420
6/24/99	4:59	1008.6325	0.357	-911.8325	0.247	516.9205	0.223	1454.6425	0.184	196.8010	0.421
HRAO-B44	Mean	1008.5766		-911.8625		516.9511		1454.6334		196.7306	
6/08/99	5:59	48.5562	0.227	-65.6262	0.151	42.8346	0.141	92.1917	0.105	-7.4540	0.268
6/09/99	6:48	48.5560	0.193	-65.6265	0.126	42.8352	0.121	92.1921	0.091	-7.4546	0.225
6/10/99	5:59	48.5562	0.212	-65.6262	0.143	42.8347	0.137	92.1917	0.102	-7.4541	0.251
6/11/99	8:23	48.5557	0.178	-65.6265	0.115	42.8350	0.113	92.1918	0.086	-7.4547	0.208
6/22/99	5:59	48.5563	0.214	-65.6267	0.144	42.8343	0.138	92.1920	0.103	-7.4541	0.254
6/23/99	4:59	48.5566	0.228	-65.6260	0.158	42.8345	0.146	92.1917	0.113	-7.4536	0.270
HRAO-SLR	Mean	48.5562		-65.6264		42.8347		92.1918		-7.4542	
6/10/99	5:05	470.8550	0.344	760.4482	0.235	1185.4377	0.220	1485.0079	0.180	175.5247	0.406
6/11/99	0:06	470.8538	0.870	760.4475	0.821	1185.4420	1.096	1485.0105	0.689	175.5216	2.126
6/23/99	4:59	470.8512	0.309	760.4438	0.210	1185.4402	0.195	1485.0065	0.160	175.5188	0.364
SLR-411	Mean	470.8533		760.4465		1185.4400		1485.0083		175.5217	
6/09/99	4:23	-558.6169	0.291	1377.0845	0.209	-76.3491	0.198	1488.0335	0.153	164.1122	0.355
6/10/99	5:45	-558.6171	0.317	1377.0856	0.214	-76.3482	0.205	1488.0346	0.159	164.1122	0.375
SLR-413	Mean	-558.6170		1377.0850		-76.3486		1488.0340		164.1122	
6/08/99	4:21	-421.0744	0.306	302.1084	0.219	-669.5050	0.194	846.6464	0.148	83.2271	0.364
6/09/99	5:54	-421.0751	0.260	302.1063	0.175	-669.5040	0.166	846.6452	0.122	83.2253	0.306
SLR-414	Mean	-421.0748		302.1074		-669.5045		846.6458		83.2262	
6/08/99	5:15	41.6948	0.325	-956.5423	0.224	-888.9742	0.211	1306.5170	0.163	21.6801	0.386
6/24/99	4:59	41.6973	0.335	-956.5418	0.232	-888.9763	0.214	1306.5182	0.167	21.6832	0.397
SLR-415	Mean	41.6960		-956.5420		-888.9752		1306.5176		21.6816	

Table D.18: Inner Network, Before and Final Adjusted Values: June 99;

Station		Before	Min	Sec	Adjust	After	Min	Sec	σ		Old Cartesian	New Cartesian		Adjust (m)
411	Lat S	25°	52'	37.380794"	+0.000002"	25°	52'	37.380792"	0.001694m	x	5085871.9144	5085871.9123	dx	0.0021
	Lon E	27°	41'	26.552534"	+0.000000"	27°	41'	26.552534"	0.001727m	y	2669090.5031	2669090.5020	dy	0.0011
	Height	1582.2616m			-0.0027m	1582.2589m			0.004160m	z	2767503.4209	2767503.4197	dz	0.0012
413	Lat S	25°	53'	23.122892"	+0.000001"	25°	53'	23.122891"	0.001523m	x	5084842.4413	5084842.4404	dx	0.0009
	Lon E	27°	42'	03.344521"	+0.000000"	27°	42'	03.344521"	0.001545m	y	2669707.1406	2669707.1401	dy	0.0005
	Height	1570.8483m			-0.0011m	1570.8472m			0.003757m	z	2768765.2070	2768765.2065	dz	0.0005
414	Lat S	25°	53'	45.818726"	+0.000001"	25°	53'	45.818725"	0.001469m	x	5084979.9835	5084979.9827	dx	0.0008
	Lon E	27°	41'	26.862605"	+0.000000"	27°	41'	26.862605"	0.001499m	y	2668632.1628	2668632.1625	dy	0.0003
	Height	1489.9619m			-0.0009m	1489.9610m			0.003616m	z	2769358.3623	2769358.3618	dz	0.0005
415	Lat S	25°	53'	54.715465"	+0.000000"	25°	53'	54.715465"	0.002329m	x	5085442.7527	5085442.7519	dx	0.0008
	Lon E	27°	40'	39.106962"	+0.000000"	27°	40'	39.106962"	0.002418m	y	2667373.5127	2667373.5123	dy	0.0004
	Height	1428.4153m			-0.0010m	1428.4143m			0.005791m	z	2769577.8319	2769577.8314	dz	0.0005
B44	Lat S	25°	53'	02.613693"	+0.000004"	25°	53'	02.613689"	0.001620m	x	5086361.0634	5086361.0534	dx	0.0100
	Lon E	27°	40'	27.296019"	+0.000000"	27°	40'	27.296019"	0.001672m	y	2667483.8114	2667483.8061	dy	0.0053
	Height	1610.9017m			-0.0126m	1610.8890m			0.003988m	z	2768214.7336	2768214.7280	dz	0.0056
HRAO	Lat S	25°	53'	24.382820"	+0.000000"	25°	53'	24.382820"	FIXED	x	5085352.5003	5085352.5003	dx	0.0000
	Lon E	27°	41'	13.124400"	+0.000000"	27°	41'	13.124400"	FIXED	y	2668395.6811	2668395.6811	dy	0.0000
	Height	1414.1880m			+0.0000m	1414.1880m			FIXED	z	2768731.6920	2768731.6920	dz	0.0000
SLR	Lat S	25°	53'	22.953503"	+0.000001"	25°	53'	22.953502"	0.000844m	x	5085401.0602	5085401.0587	dx	0.0015
	Lon E	27°	41'	10.226914"	+0.000000"	27°	41'	10.226915"	0.000867m	y	2668330.0567	2668330.0559	dy	0.0008
	Height	1406.7385m			-0.0018m	1406.7366m			0.002095m	z	2768688.8593	2768688.8585	dz	0.0008

Appendix E

Baseline Results of Hill 411

Table E.1: Thermal Experiment: GPS and thermal results, Data Set A;

Point	MJD	Δ X	Δ Y	Δ Z	Height	Slope Distance	Surface T (°C)	T at 40 cm (°C)
1	50742.479167	470.8526	760.4472	1185.4401	175.5214	1485.0086	31.537463	22.380056
2	50742.541667	470.8592	760.4501	1185.4365	175.5294	1485.0093	31.847553	23.945821
3	50742.625000	470.8561	760.4489	1185.4393	175.5252	1485.0098	30.483906	26.170559
4	50742.708333	470.8576	760.4463	1185.4376	175.5260	1485.0077	27.472345	28.004626
5	50742.791667	470.8582	760.4475	1185.4373	175.5271	1485.0082	23.637997	28.956592
6	50742.875000	470.8578	760.4473	1185.4391	175.5259	1485.0094	20.026498	28.771359
7	50742.958333	470.8607	760.4502	1185.4379	175.5300	1485.0109	17.623513	27.498578
8	50743.041667	470.8593	760.4472	1185.4380	175.5276	1485.0089	17.091382	25.479259
9	50743.125000	470.8575	760.4477	1185.4385	175.5262	1485.0091	18.591611	23.254521
10	50743.208333	470.8578	760.4473	1185.4392	175.5259	1485.0095	21.741642	21.420454
11	50743.291667	470.8572	760.4467	1185.4366	175.5264	1485.0069	25.717355	20.468488
13	50743.458333	470.8596	760.4505	1185.4360	175.5301	1485.0092	32.023598	21.926502
14	50743.541667	470.8574	760.4473	1185.4385	175.5260	1485.0088	32.704175	23.945821
15	50743.625000	470.8606	760.4497	1185.4362	175.5305	1485.0092	31.352047	26.170559
16	50743.708333	470.8600	760.4487	1185.4357	175.5298	1485.0082	28.348230	28.004626
17	50743.791667	470.8605	760.4487	1185.4363	175.5299	1485.0088	24.515811	28.956592
18	50743.875000	470.8632	760.4505	1185.4378	175.5321	1485.0117	20.899819	28.771359
19	50743.958333	470.8598	760.4499	1185.4381	175.5290	1485.0106	18.487214	27.498578
20	50744.041667	470.8604	760.4490	1185.4389	175.5288	1485.0110	17.942875	25.479259
21	50744.125000	470.8564	760.4473	1185.4394	175.5247	1485.0092	19.431578	23.254521
22	50744.208333	470.8552	760.4455	1185.4391	175.5231	1485.0077	22.573851	21.420454
23	50744.291667	470.8556	760.4473	1185.4367	175.5253	1485.0069	26.547648	20.468488
24	50744.375000	470.8590	760.4485	1185.4392	175.5274	1485.0105	30.308196	20.653721
25	50744.458333	470.8556	760.4457	1185.4358	175.5250	1485.0053	32.867942	21.926502
26	50744.541667	470.8644	760.4497	1185.4370	175.5331	1485.0111	33.560724	23.945821
27	50744.625000	470.8617	760.4493	1185.4375	175.5306	1485.0105	32.220127	26.170559
28	50744.708333	470.8625	760.4495	1185.4356	175.5319	1485.0092	29.224085	28.004626
29	50744.791667	470.8626	760.4502	1185.4363	175.5323	1485.0102	25.393600	28.956592
30	50744.875000	470.8618	760.4491	1185.4369	175.5308	1485.0099	21.773184	28.771359
31	50744.958333	470.8554	760.4444	1185.4393	175.5228	1485.0074	19.350982	27.498578
32	50745.041667	470.8520	760.4439	1185.4415	175.5188	1485.0078	18.794442	25.479259
33	50745.125000	470.8516	760.4447	1185.4409	175.5191	1485.0076	20.271606	23.254521
34	50745.208333	470.8510	760.4413	1185.4403	175.5175	1485.0051	23.406090	21.420454
35	50745.291667	470.8510	760.4415	1185.4412	175.5172	1485.0060	27.377934	20.468488
36	50745.375000	470.8482	760.4411	1185.4409	175.5150	1485.0046	31.142887	20.653721
37	50745.458333	470.8547	760.4446	1185.4378	175.5229	1485.0060	33.712217	21.926502
38	50745.541667	470.8519	760.4422	1185.4397	175.5189	1485.0054	34.417197	23.945821

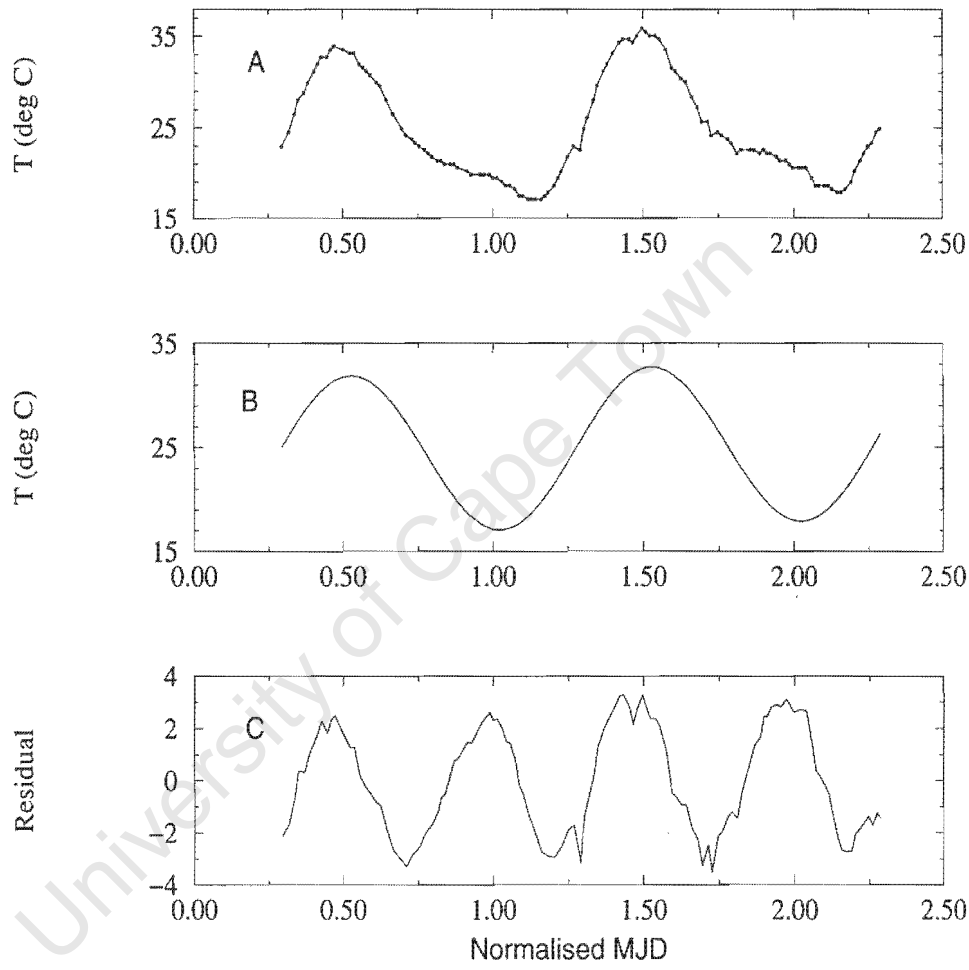

Figure E.1: Data set A: (A) Surface temperature as a function of time (day). (B) Sinusoidal fit to surface temperature data. (C) Residuals of fit.

Table E.2: Thermal Experiment: GPS and thermal results, Data Set B;

Point	MJD	Δ X	Δ Y	Δ Z	Height	Slope Distance	Surface T ($^{\circ}C$)	T at 40 cm ($^{\circ}C$)
39	50748.791667	470.8455	760.4388	1185.4468	175.5092	1485.0074	18.888494	14.205621
40	50748.875000	470.8514	760.4431	1185.4471	175.5157	1485.0116	15.501510	18.360915
41	50748.958333	470.8530	760.4461	1185.4432	175.5198	1485.0106	13.332046	22.624188
42	50749.041667	470.8499	760.4431	1185.4451	175.5153	1485.0096	12.945249	25.853137
43	50749.125000	470.8513	760.4458	1185.4435	175.5181	1485.0101	14.433169	27.182498
44	50749.208333	470.8523	760.4442	1185.4415	175.5193	1485.0080	17.390301	26.256120
45	50749.291667	470.8504	760.4434	1185.4409	175.5177	1485.0066	21.021287	23.322179
46	50749.375000	470.8501	760.4422	1185.4424	175.5163	1485.0070	24.351810	19.166885
47	50749.541667	470.8462	760.4411	1185.4451	175.5115	1485.0073	26.850719	11.674663
48	50749.625000	470.8433	760.4412	1185.4458	175.5090	1485.0071	25.334684	10.345302
49	50749.708333	470.8445	760.4390	1185.4456	175.5090	1485.0062	22.331055	11.271680
50	50749.791667	470.8428	760.4416	1185.4462	175.5086	1485.0074	18.626304	14.205621
51	50749.875000	470.8487	760.4418	1185.4438	175.5143	1485.0075	15.193106	18.360915
52	50749.958333	470.8466	760.4410	1185.4451	175.5118	1485.0075	12.931939	22.624188
53	50750.041667	470.8483	760.4438	1185.4441	175.5147	1485.0086	12.432286	25.853137
54	50750.125000	470.8467	760.4423	1185.4454	175.5123	1485.0084	13.816150	27.182498
55	50750.208333	470.8466	760.4405	1185.4447	175.5118	1485.0069	16.705640	26.256120
56	50750.291667	470.8466	760.4425	1185.4451	175.5124	1485.0082	20.323351	23.322179
57	50750.375000	470.8457	760.4400	1185.4440	175.5111	1485.0057	23.698487	19.166885
58	50750.458333	470.8471	760.4432	1185.4419	175.5145	1485.0062	25.924754	14.903612
59	50750.541667	470.8435	760.4407	1185.4434	175.5099	1485.0050	26.400709	11.674663
60	50750.625000	470.8475	760.4423	1185.4443	175.5134	1485.0078	24.989417	10.345302
61	50750.708333	470.8431	760.4384	1185.4451	175.5080	1485.0050	22.054824	11.271680
62	50750.791667	470.8424	760.4398	1185.4467	175.5072	1485.0068	18.365082	14.205621
63	50750.875000	470.8473	760.4419	1185.4481	175.5114	1485.0105	14.888882	18.320915
64	50750.958333	470.8447	760.4419	1185.4467	175.5099	1485.0086	12.538115	22.624188
65	50751.041667	470.8455	760.4419	1185.4464	175.5107	1485.0087	11.926042	25.853137
66	50751.125000	470.8446	760.4421	1185.4467	175.5100	1485.0086	13.204503	27.182498
67	50751.208333	470.8468	760.4405	1185.4452	175.5117	1485.0073	16.023578	26.256120
68	50751.291667	470.8439	760.4409	1185.4457	175.5093	1485.0071	19.624550	23.322179
69	50751.375000	470.8430	760.4404	1185.4453	175.5086	1485.0062	23.041065	19.166885
70	50751.458333	470.8483	760.4404	1185.4473	175.5119	1485.0094	25.355849	14.903612

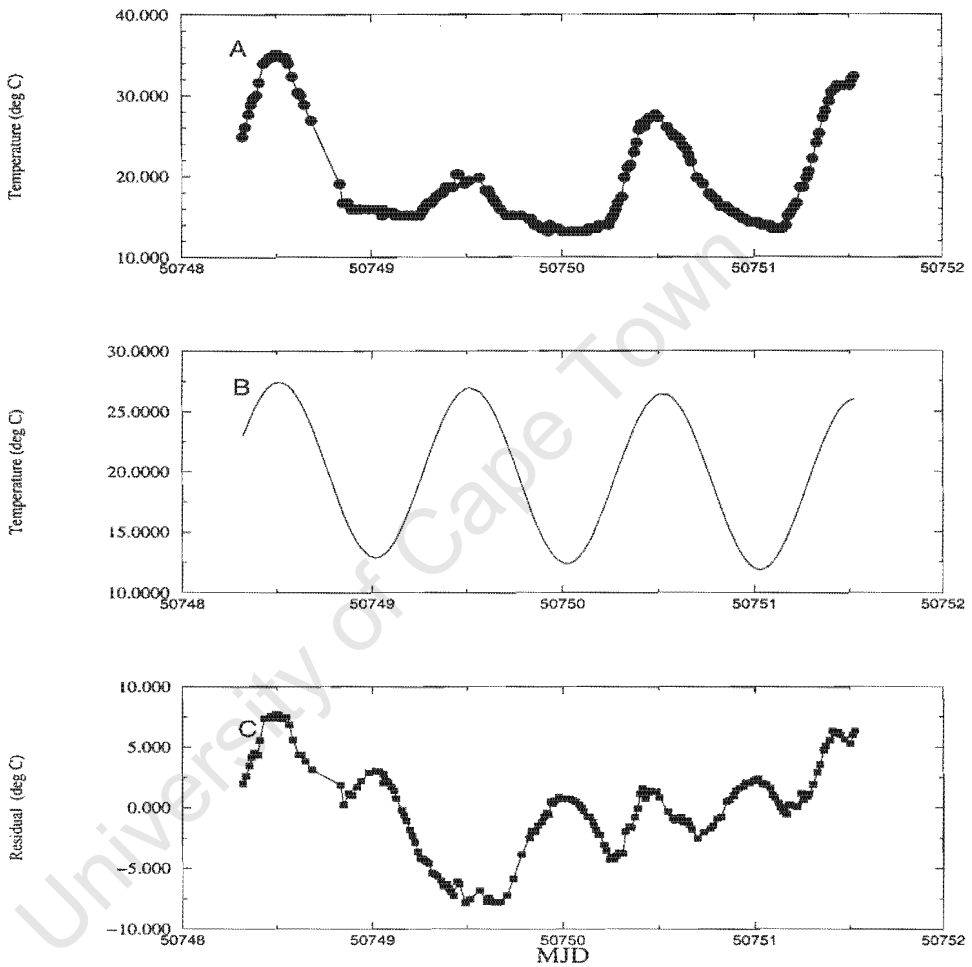

Figure E.2: Data set B: (A) Surface temperature as a function of time (day). (B) Sinusoidal fit to surface temperature data. (C) Residuals of fit.

Table E.3: Thermal Experiment: GPS and thermal results, Data Set C;

Point	MJD	Δ X	Δ Y	Δ Z	Height	Slope Distance	Surface T (°C)	T at 40 cm (°C)
71	50756.375000	470.8508	760.4441	1185.4389	175.5191	1485.0054	31.587931	24.407825
72	50756.458333	470.8528	760.4454	1185.4394	175.5211	1485.0071	34.282841	27.003754
73	50756.541667	470.8560	760.4463	1185.4394	175.5239	1485.0086	34.815137	29.667170
74	50756.625000	470.8497	760.4447	1185.4411	175.5175	1485.0071	33.116823	31.684356
75	50756.708333	470.8447	760.4408	1185.4421	175.5115	1485.0043	29.663208	32.514845
76	50756.791667	470.8478	760.4428	1185.4426	175.5146	1485.0067	25.357044	31.936096
77	50756.875000	470.8492	760.4430	1185.4452	175.5146	1485.0094	21.308877	30.103195
78	50756.958333	470.8478	760.4424	1185.4445	175.5136	1485.0080	18.566269	27.507266
79	50757.041667	470.8466	760.4423	1185.4441	175.5128	1485.0073	17.858858	24.843850
80	50757.125000	470.8443	760.4415	1185.4459	175.5098	1485.0076	19.420613	22.826664
81	50757.208333	470.8456	760.4399	1185.4442	175.5109	1485.0059	22.932797	21.996175
82	50757.291667	470.8439	760.4400	1185.4446	175.5095	1485.0057	27.601717	22.574924
83	50757.375000	470.8458	760.4408	1185.4434	175.5118	1485.0058	32.351783	24.407825
84	50757.458333	470.8514	760.4442	1185.4396	175.5194	1485.0062	36.087803	27.003754
85	50757.541667	470.8433	760.4407	1185.4453	175.5090	1485.0064	37.961517	29.667170
86	50757.625000	470.8435	760.4438	1185.4456	175.5103	1485.0083	37.578187	31.684356
87	50757.708333	470.8430	760.4389	1185.4453	175.5080	1485.0054	35.092870	32.514845
88	50757.791667	470.8480	760.4437	1185.4448	175.5142	1485.0090	31.172481	31.936096
89	50757.875000	470.8499	760.4427	1185.4458	175.5149	1485.0099	26.833602	30.103195
90	50757.958333	470.8512	760.4435	1185.4462	175.5160	1485.0111	23.194606	27.507266
91	50758.041667	470.8483	760.4430	1185.4442	175.5144	1485.0083	21.203435	24.843850
92	50758.125000	470.8488	760.4437	1185.4432	175.5155	1485.0080	21.406755	22.826664
93	50758.208333	470.8491	760.4427	1185.4423	175.5157	1485.0068	23.816667	21.996175
94	50758.375000	470.8487	760.4413	1185.4392	175.5161	1485.0036	32.745688	24.407825
95	50758.458333	470.8459	760.4404	1185.4400	175.5132	1485.0029	37.213349	27.003754

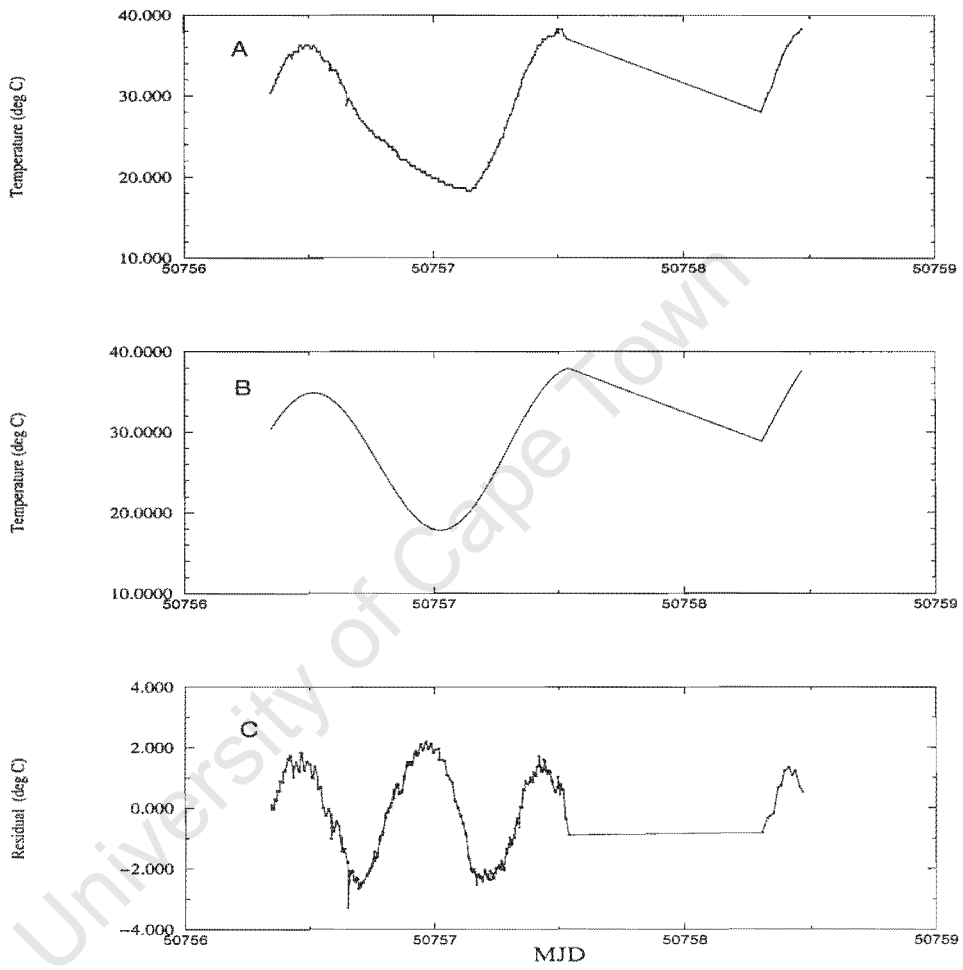

Figure E.3: Data set C: (A) Surface temperature as a function of time (day). (B) Sinusoidal fit to surface temperature data. (C) Residuals of fit. The straight line represents lost data.

Table E.4: Thermal Experiment: GPS and thermal results, Data Set D;

Point	MJD	Δ X	Δ Y	Δ Z	Height	Slope Distance	Surface T ($^{\circ}C$)	T at 40 cm ($^{\circ}C$)
96	50763.375000	470.8416	760.4406	1185.4457	175.5074	1485.0061	24.870389	23.011816
97	50763.458333	470.8448	760.4387	1185.4453	175.5093	1485.0059	27.432586	18.998520
98	50763.541667	470.8450	760.4399	1185.4454	175.5099	1485.0066	28.452226	15.958901
99	50763.625000	470.8427	760.4404	1185.4453	175.5083	1485.0060	27.663700	14.707488
100	50763.708333	470.8402	760.4376	1185.4466	175.5046	1485.0048	25.298124	15.579547
101	50763.791667	470.8437	760.4400	1185.4482	175.5077	1485.0085	22.019747	18.341456
102	50763.875000	470.8444	760.4417	1185.4491	175.5086	1485.0103	18.743671	22.253104
103	50763.937500	470.8505	760.4446	1185.4445	175.5167	1485.0100	16.845555	25.314737
104	50763.979167	470.8543	760.4450	1185.4422	175.5209	1485.0096	16.023836	27.155928
105	50764.041667	470.8499	760.4452	1185.4448	175.5163	1485.0104	15.604095	29.306019
106	50764.125000	470.8471	760.4421	1185.4445	175.5130	1485.0077	16.632009	30.557432
107	50764.208333	470.8486	760.4427	1185.4445	175.5143	1485.0085	19.200116	29.685373
108	50764.291667	470.8465	760.4419	1185.4438	175.5127	1485.0068	22.617527	26.923464
109	50764.375000	470.8472	760.4428	1185.4444	175.5134	1485.0080	25.959939	23.011816
110	50764.458333	470.8441	760.4379	1185.4462	175.5080	1485.0060	28.323764	18.998520
111	50764.541667	470.8452	760.4444	1185.4449	175.5122	1485.0086	29.074184	15.958901
112	50764.625000	470.8376	760.4371	1185.4487	175.5014	1485.0055	28.019545	14.707488
113	50764.708333	470.8462	760.4431	1185.4462	175.5119	1485.0093	25.464060	15.579547
114	50764.791667	470.8426	760.4384	1185.4502	175.5053	1485.0089	22.124142	18.341456
115	50764.875000	470.8453	760.4437	1185.4480	175.5106	1485.0107	18.931800	22.253104
116	50764.958333	470.8479	760.4422	1185.4482	175.5120	1485.0109	16.778389	26.266400
117	50765.041667	470.8425	760.4416	1185.4494	175.5069	1485.0099	16.269926	29.306019
118	50765.125000	470.8419	760.4391	1185.4475	175.5062	1485.0069	17.560585	30.557432
119	50765.208333	470.8444	760.4398	1185.4456	175.5093	1485.0065	20.310319	29.685373
120	50765.291667	470.8445	760.4386	1185.4439	175.5096	1485.0046	23.778347	26.923464
121	50765.375000	470.8474	760.4422	1185.4428	175.5140	1485.0065	27.026460	23.011816
122	50765.458333	470.8463	760.4375	1185.4431	175.5110	1485.0040	29.176976	18.998520
123	50765.541667	470.8397	760.4366	1185.4467	175.5037	1485.0043	29.653665	15.958901
124	50765.625000	470.8420	760.4369	1185.4479	175.5052	1485.0061	28.340073	14.707488
125	50765.708333	470.8450	760.4393	1185.4453	175.5097	1485.0063	25.611537	15.579547
126	50765.791667	470.8431	760.4406	1185.4457	175.5085	1485.0066	22.232009	18.341456
127	50765.875000	470.8468	760.4401	1185.4470	175.5107	1485.0085	19.144377	22.253104
128	50765.958333	470.8497	760.4383	1185.4471	175.5123	1485.0086	17.211234	26.266400
129	50766.041667	470.8541	760.4433	1185.4467	175.5181	1485.0123	16.978093	29.306019
130	50766.125000	470.8441	760.4350	1185.4484	175.5058	1485.0062	18.523497	30.557432
131	50766.208333	470.8446	760.4373	1185.4451	175.5086	1485.0049	21.437424	29.685373
132	50766.375000	470.8295	760.4441	1185.4502	175.4972	1485.0077	28.067153	23.011816

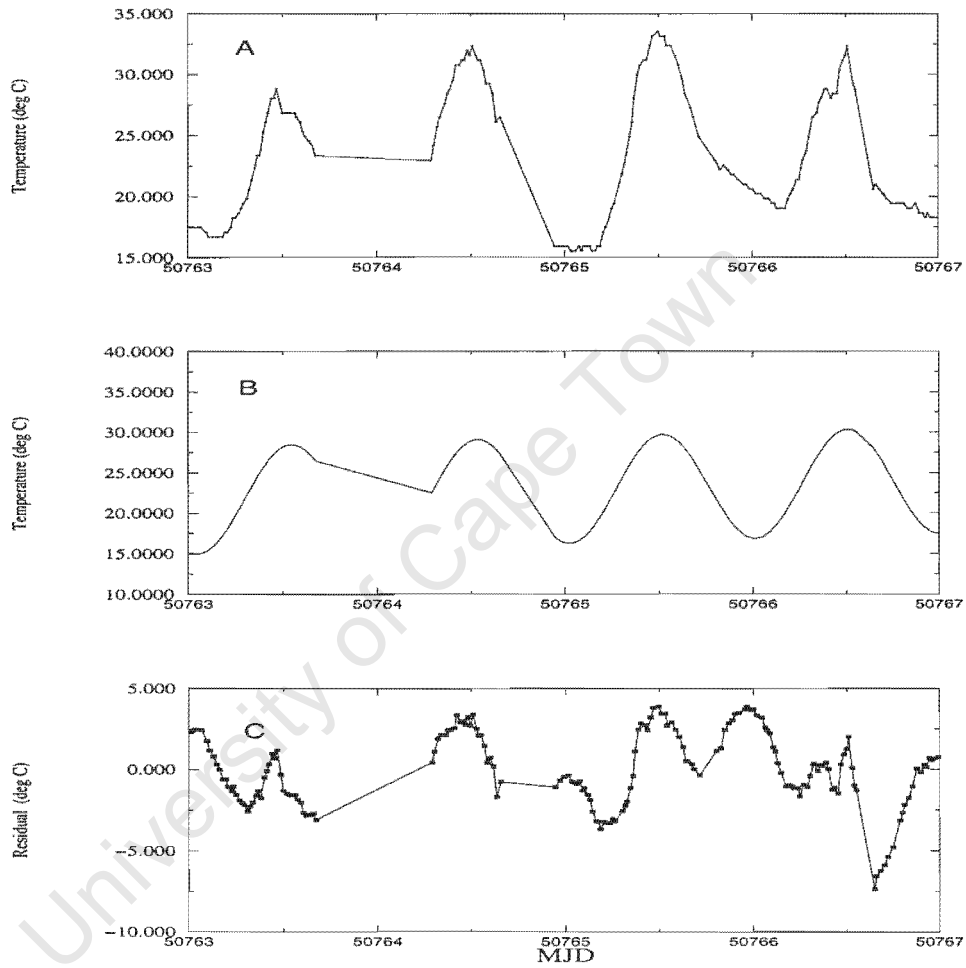

Figure E.4: Data set D: (A) Surface temperature as a function of time (day). (B) Sinusoidal fit to surface temperature data. (C) Residuals of fit. The straight line represents lost data.

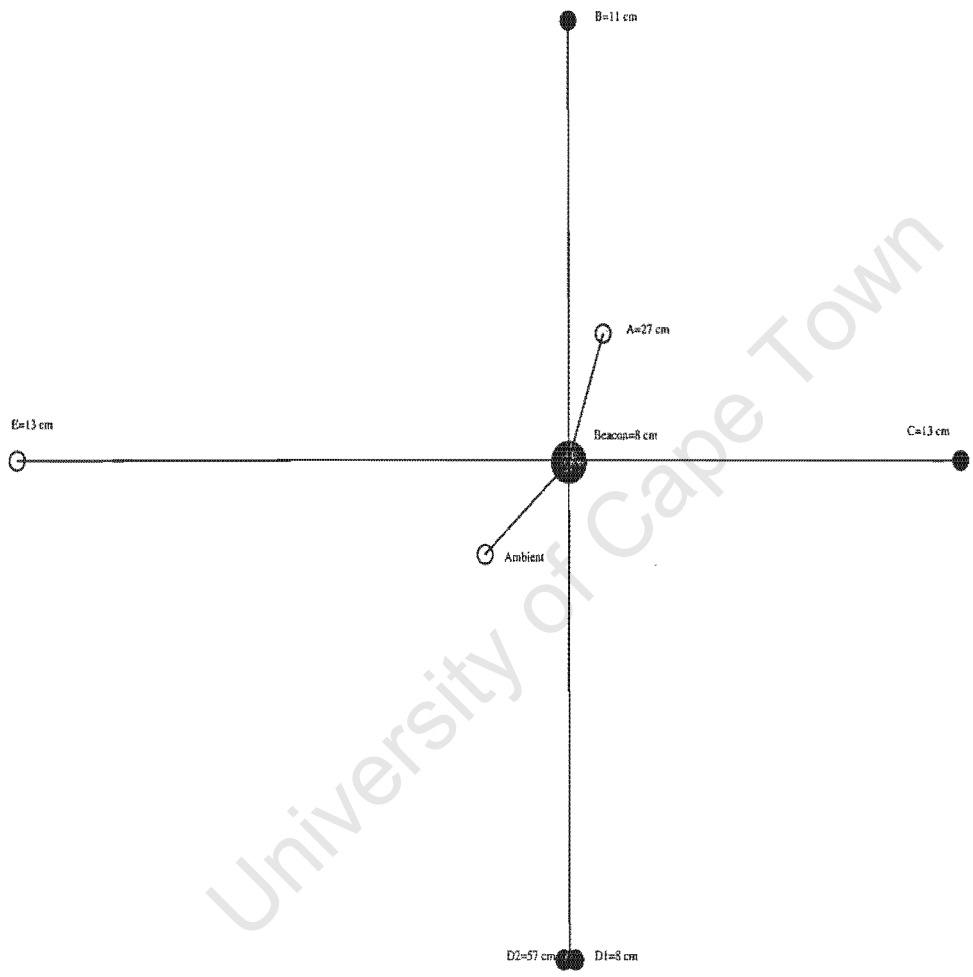

Figure E.5: Geometry of thermal transducers surrounding beacon on Hill 411.

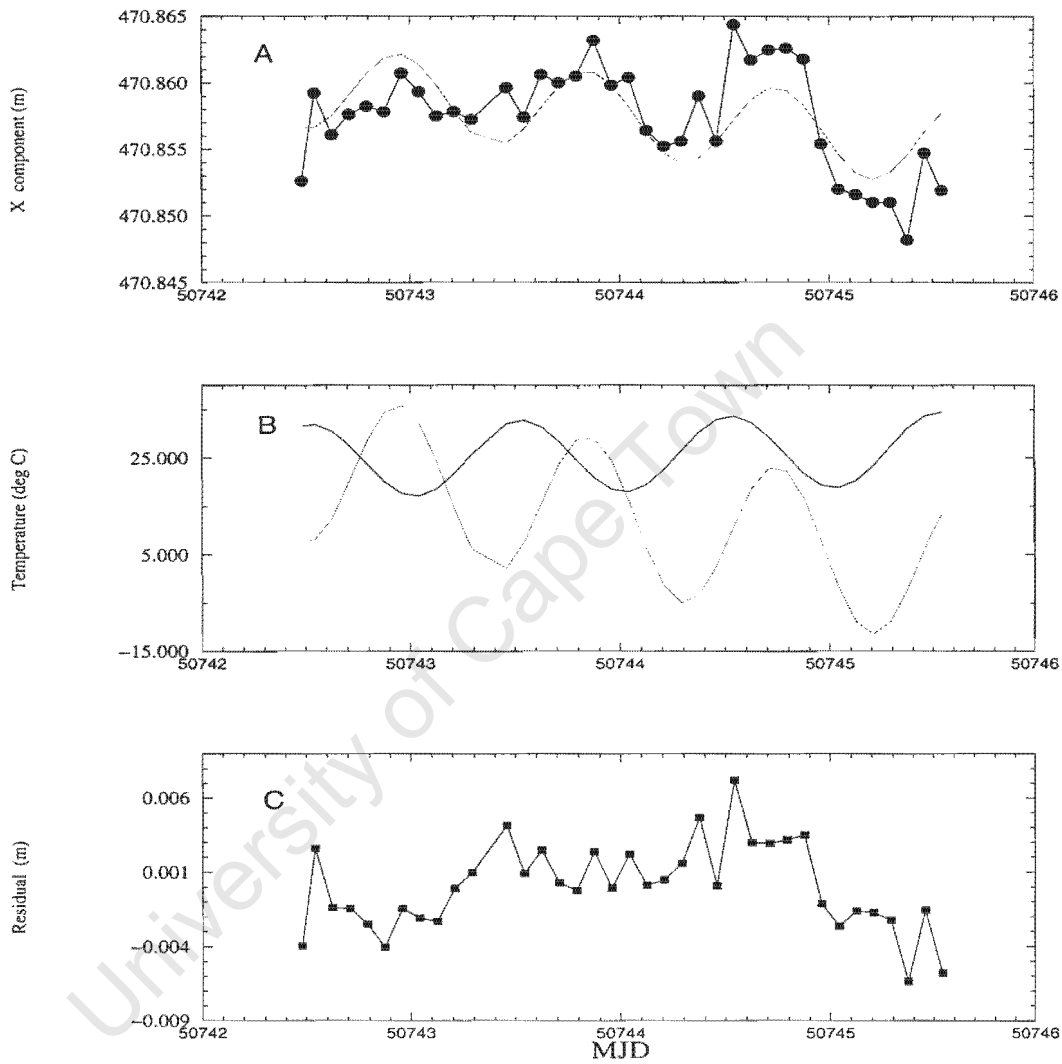

Figure E.6: Data set A: (A) X component, SLR to 411 and sinusoid with linear trend fitted to the X component data. (B) Sinusoidal fit to surface temperature data, overlaid with sinusoidal fit (red) to X component data points. (C) Residuals of (A).

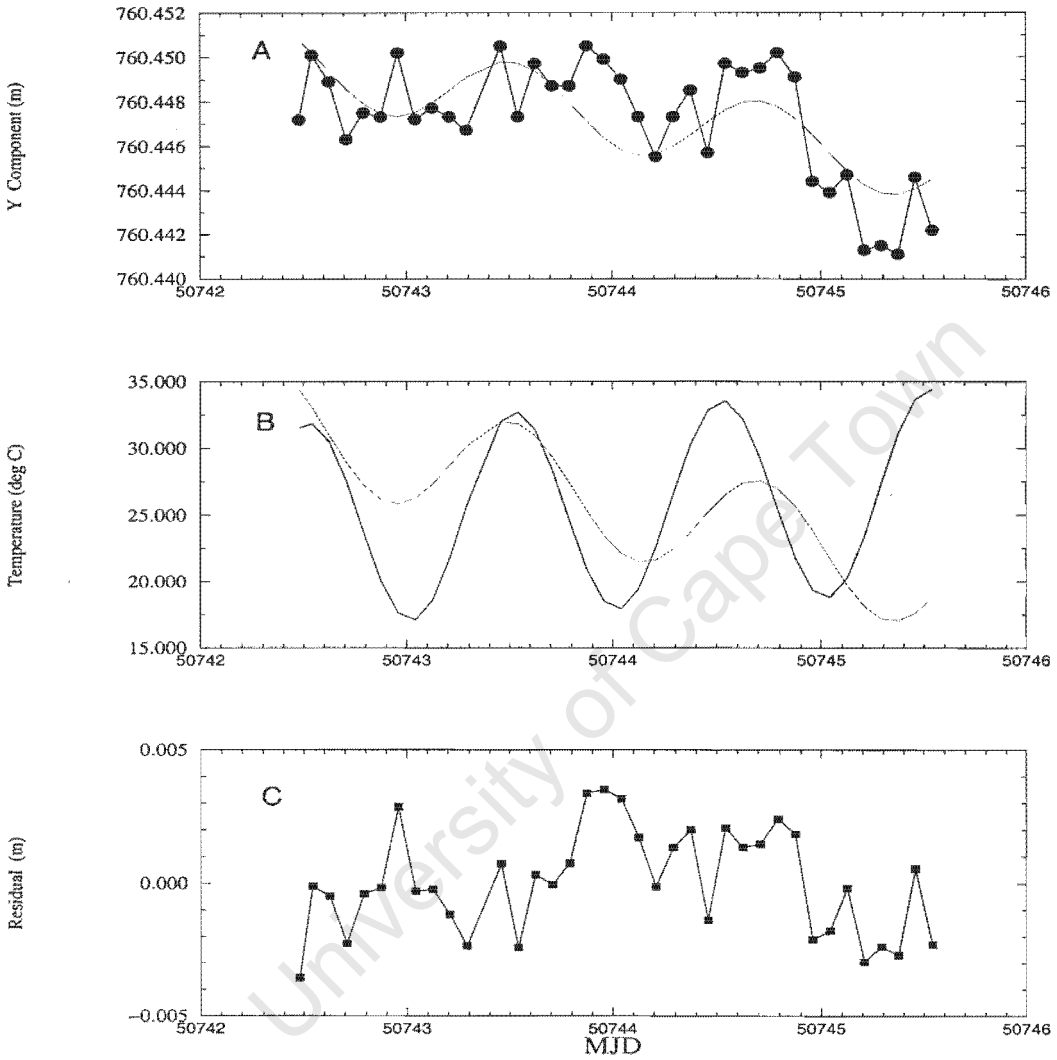

Figure E.7: Data set A: (A) Y component, SLR to 411 and sinusoid with linear trend fitted to the Y component data. (B) Sinusoidal fit to surface temperature data, overlaid with sinusoidal fit (red) to X component data points. (C) Residuals of (A).

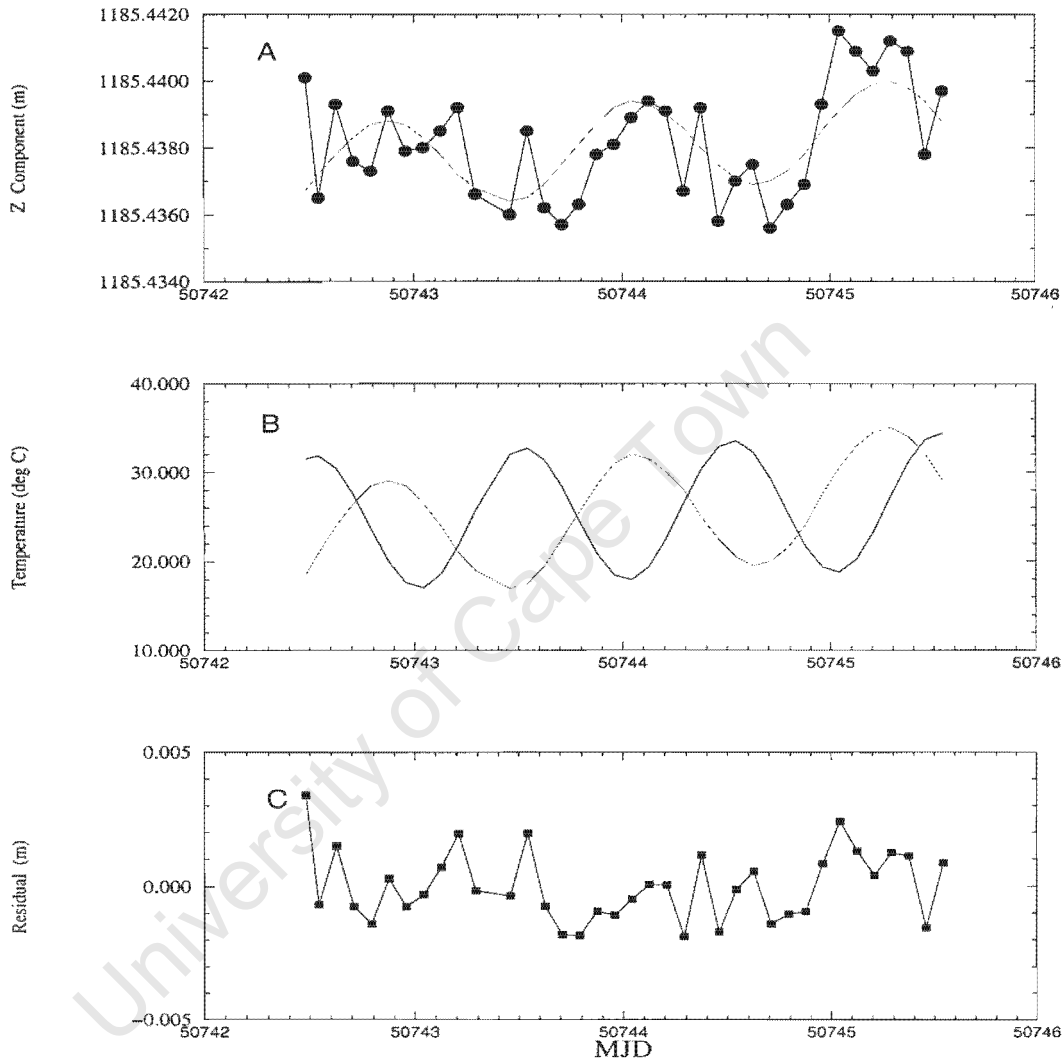

Figure E.8: Data set A: (A) Z component, SLR to 411 and sinusoid with linear trend fitted to the Y component data. (B) Sinusoidal fit to surface temperature data, overlaid with sinusoidal fit (red) to X component data points. (C) Residuals of (A).

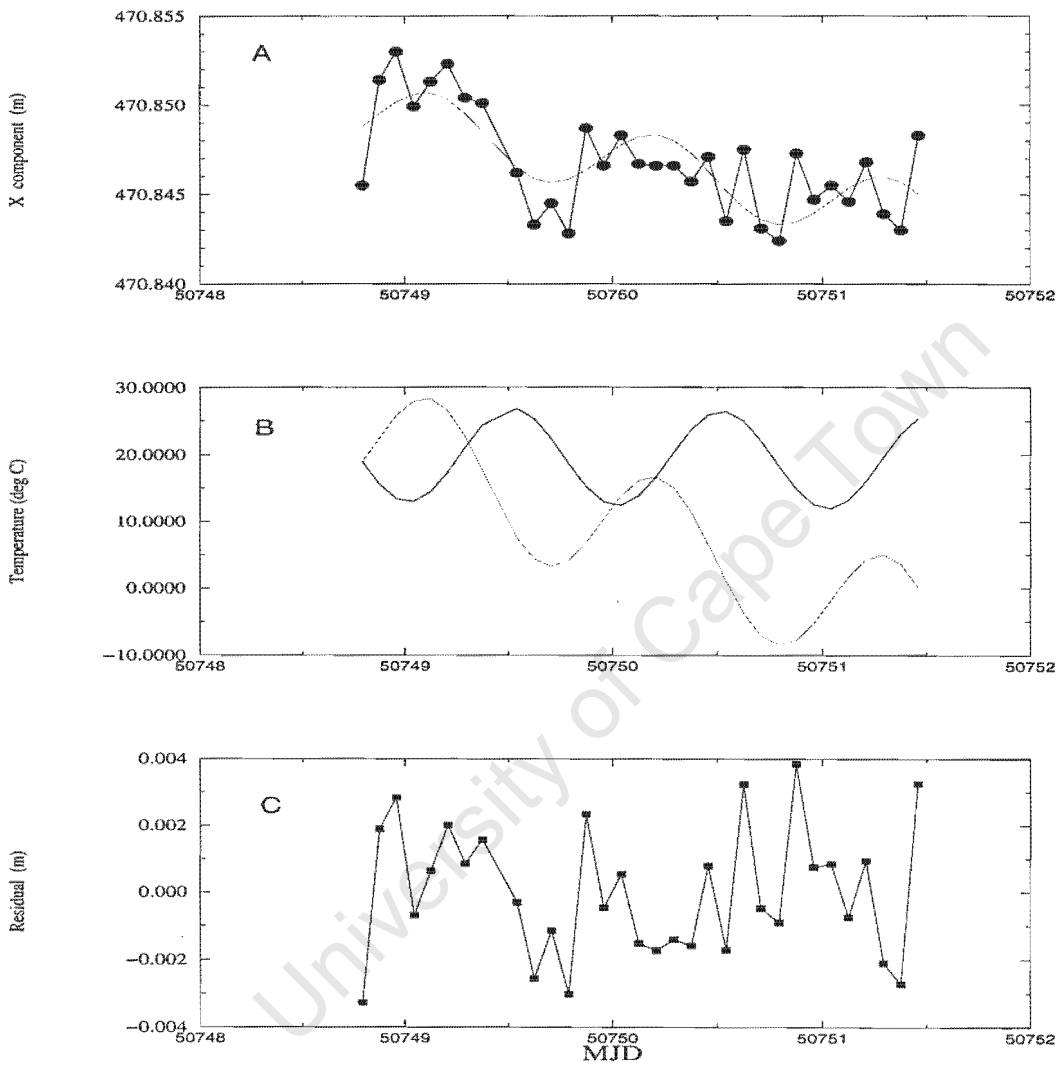

Figure E.9: Data set B: (A) X component, SLR to 411 and sinusoid with linear trend fitted to the X component data. (B) Sinusoidal fit to surface temperature data, overlaid with sinusoidal fit (red) to X component data points. (C) Residuals of (A).

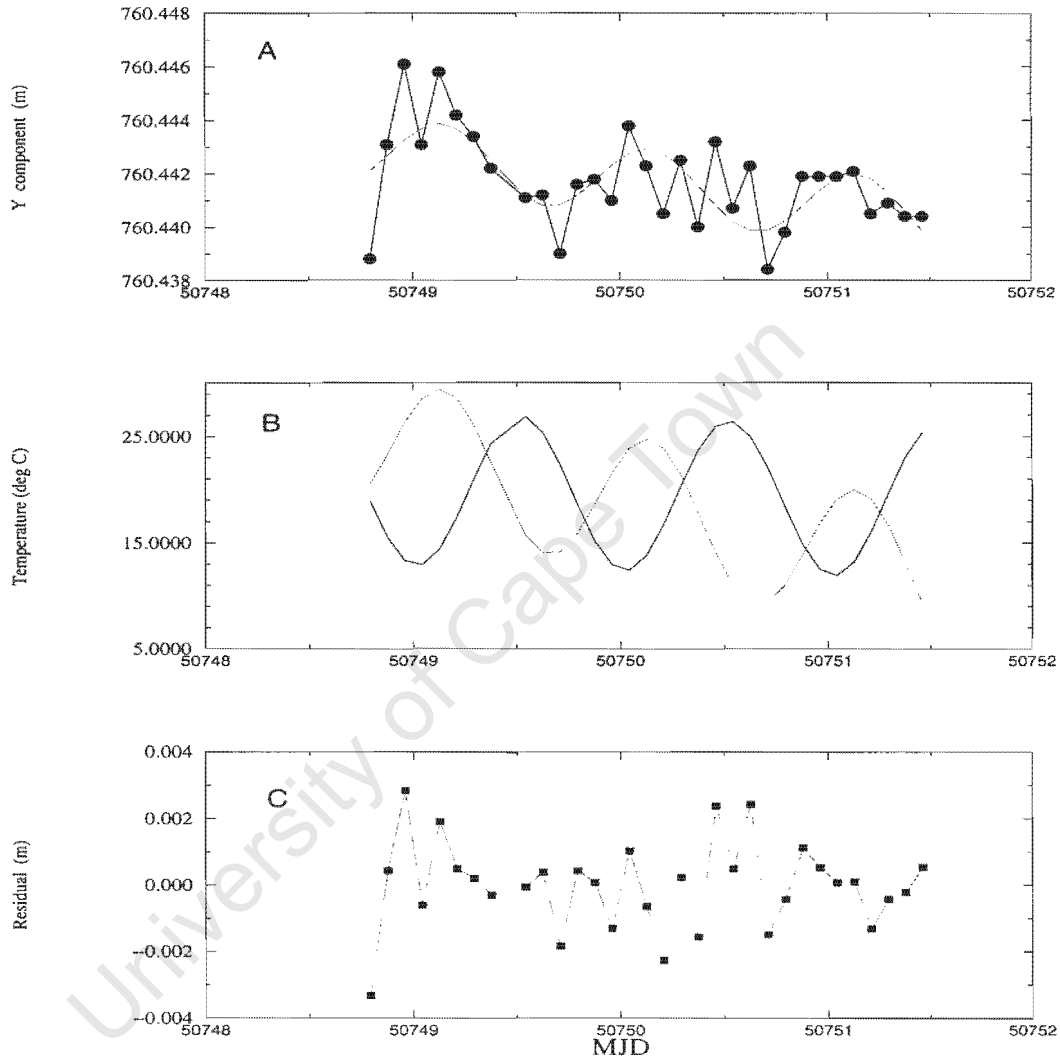

Figure E.10: Data set B: (A) Y component, SLR to 411 and sinusoid with linear trend fitted to the Y component data. (B) Sinusoidal fit to surface temperature data, overlaid with sinusoidal fit (red) to X component data points. (C) Residuals of (A).

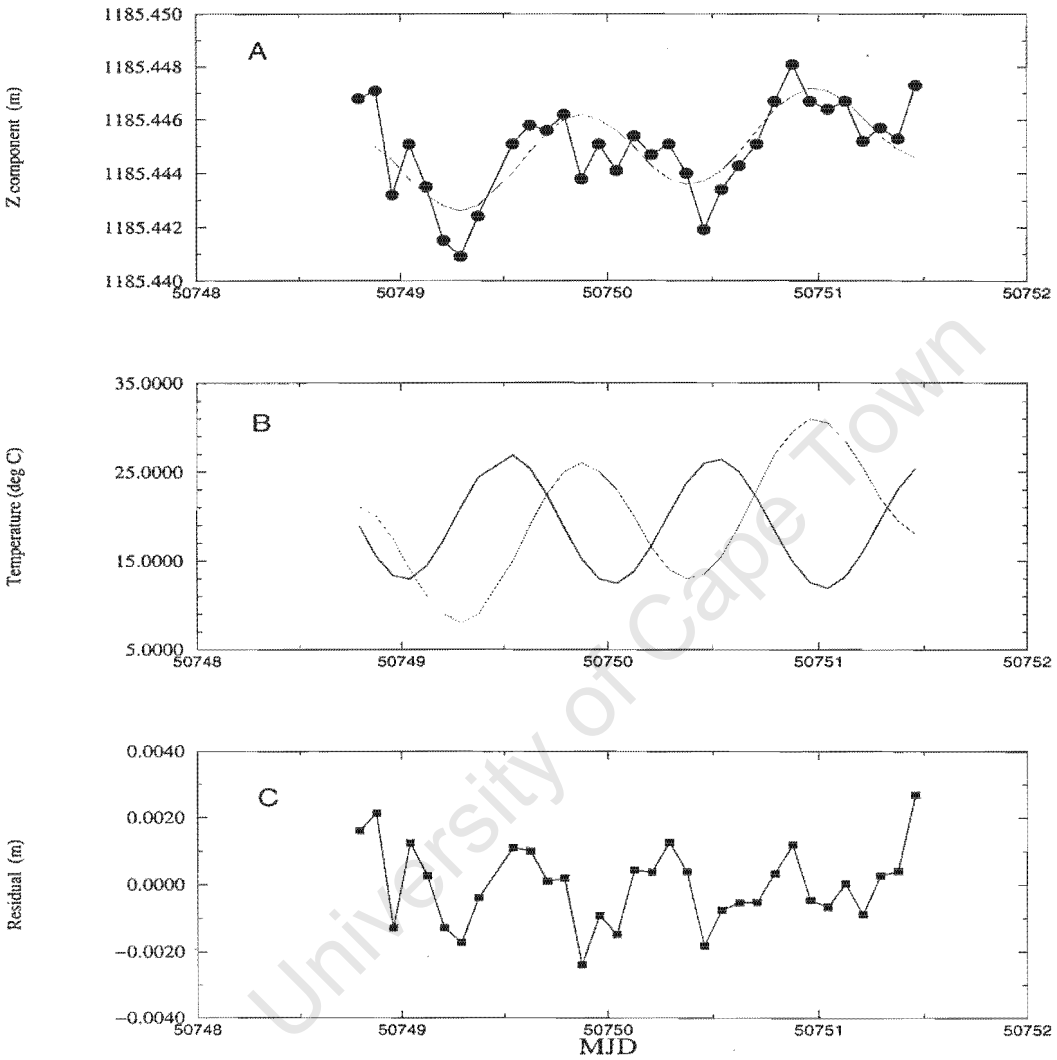

Figure E.11: Data set B: (A) Z component, SLR to 411 and sinusoid with linear trend fitted to the Y component data. (B) Sinusoidal fit to surface temperature data, overlaid with sinusoidal fit (red) to X component data points. (C) Residuals of (A).

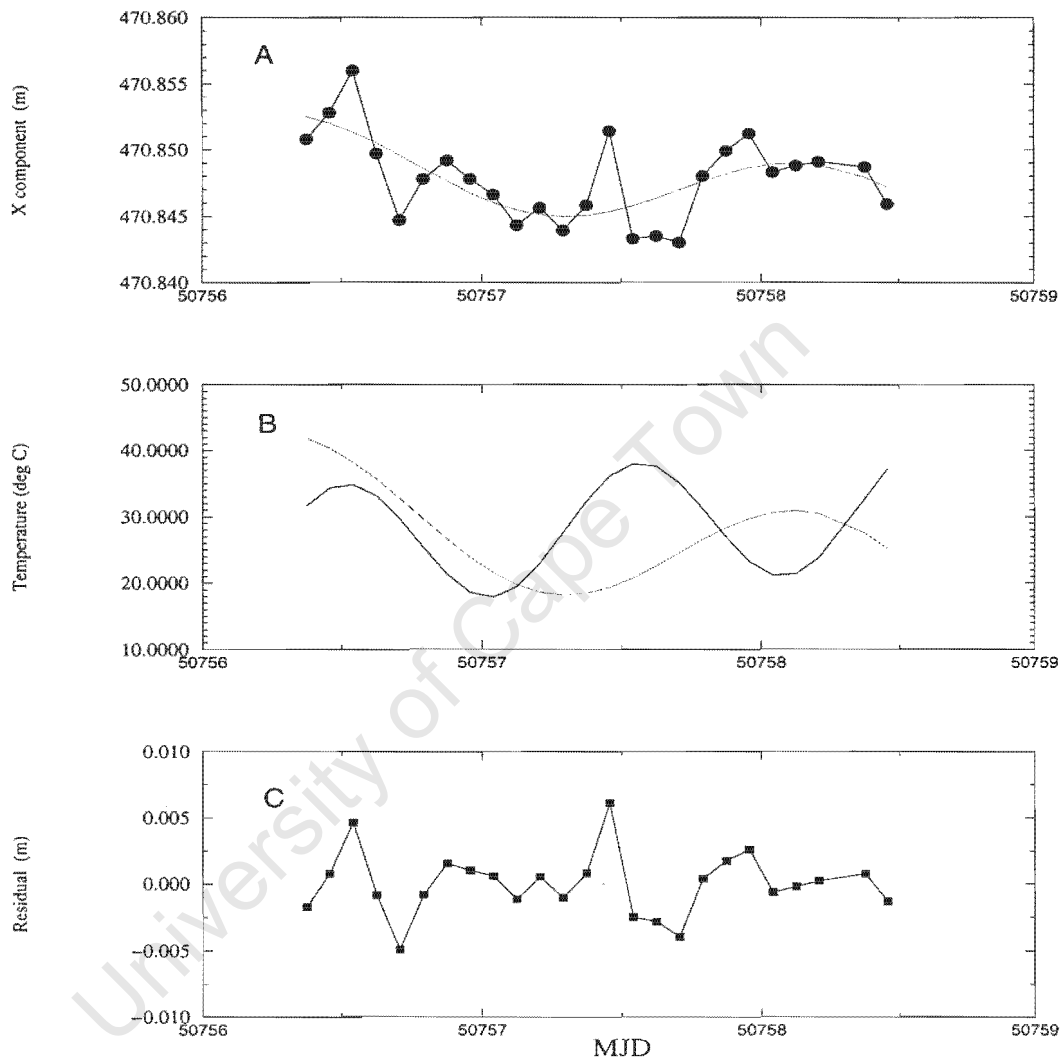

Figure E.12: Data set C: (A) X component, SLR to 411 and sinusoid with linear trend fitted to the X component data. (B) Sinusoidal fit to surface temperature data, overlaid with sinusoidal fit (red) to X component data points. (C) Residuals of (A).

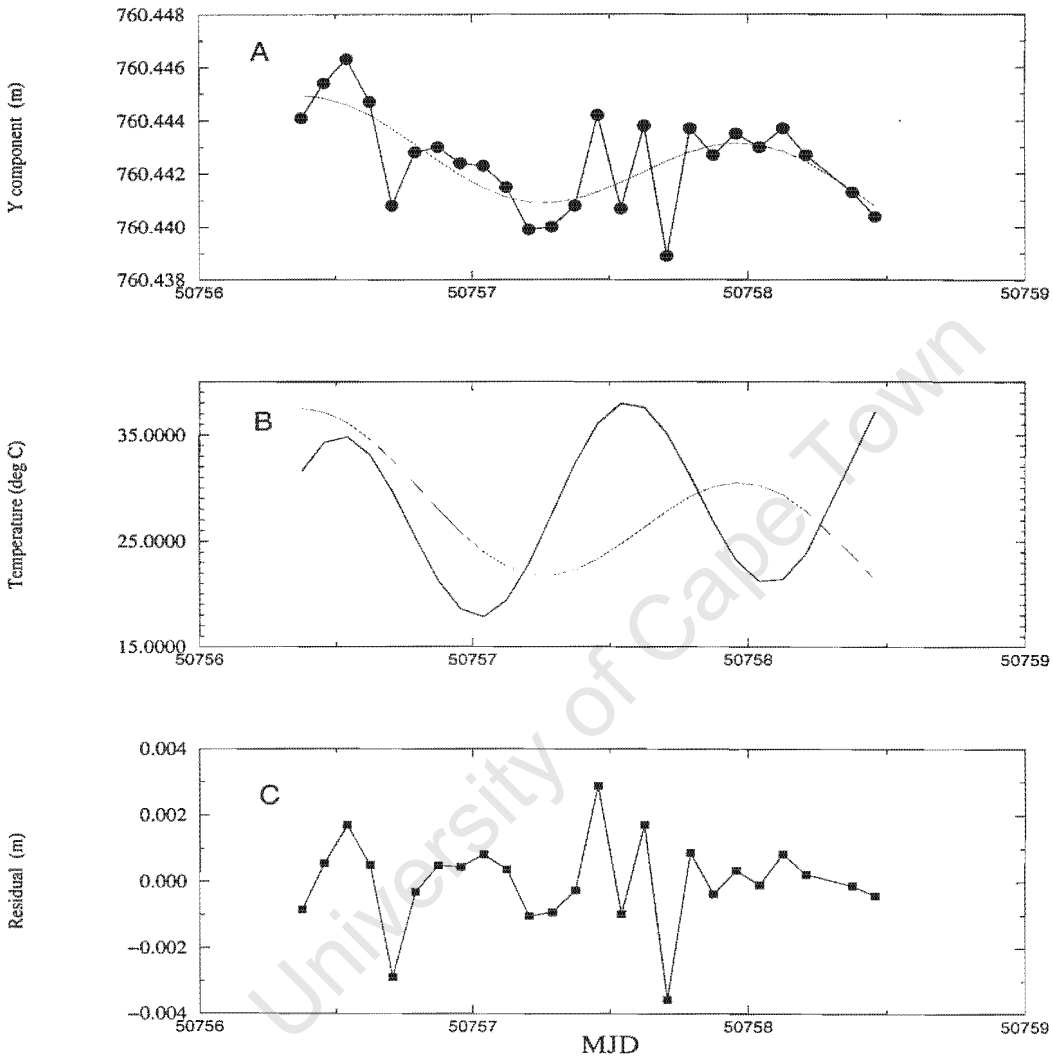

Figure E.13: Data set C: (A) Y component, SLR to 411 and sinusoid with linear trend fitted to the Y component data. (B) Sinusoidal fit to surface temperature data, overlaid with sinusoidal fit (red) to X component data points. (C) Residuals of (A).

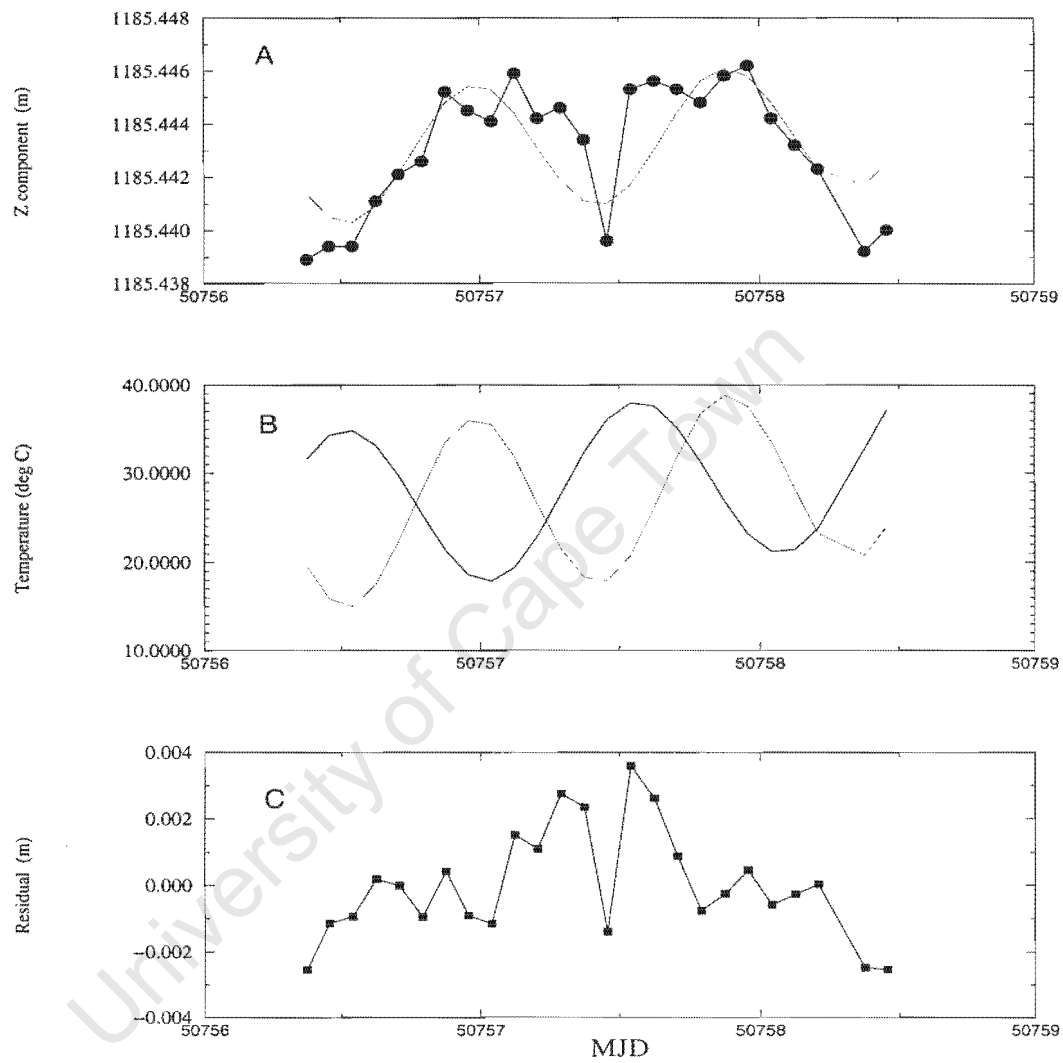

Figure E.14: Data set C: (A) Z component, SLR to 411 and sinusoid with linear trend fitted to the Y component data. (B) Sinusoidal fit to surface temperature data, overlaid with sinusoidal fit (red) to X component data points. (C) Residuals of (A).

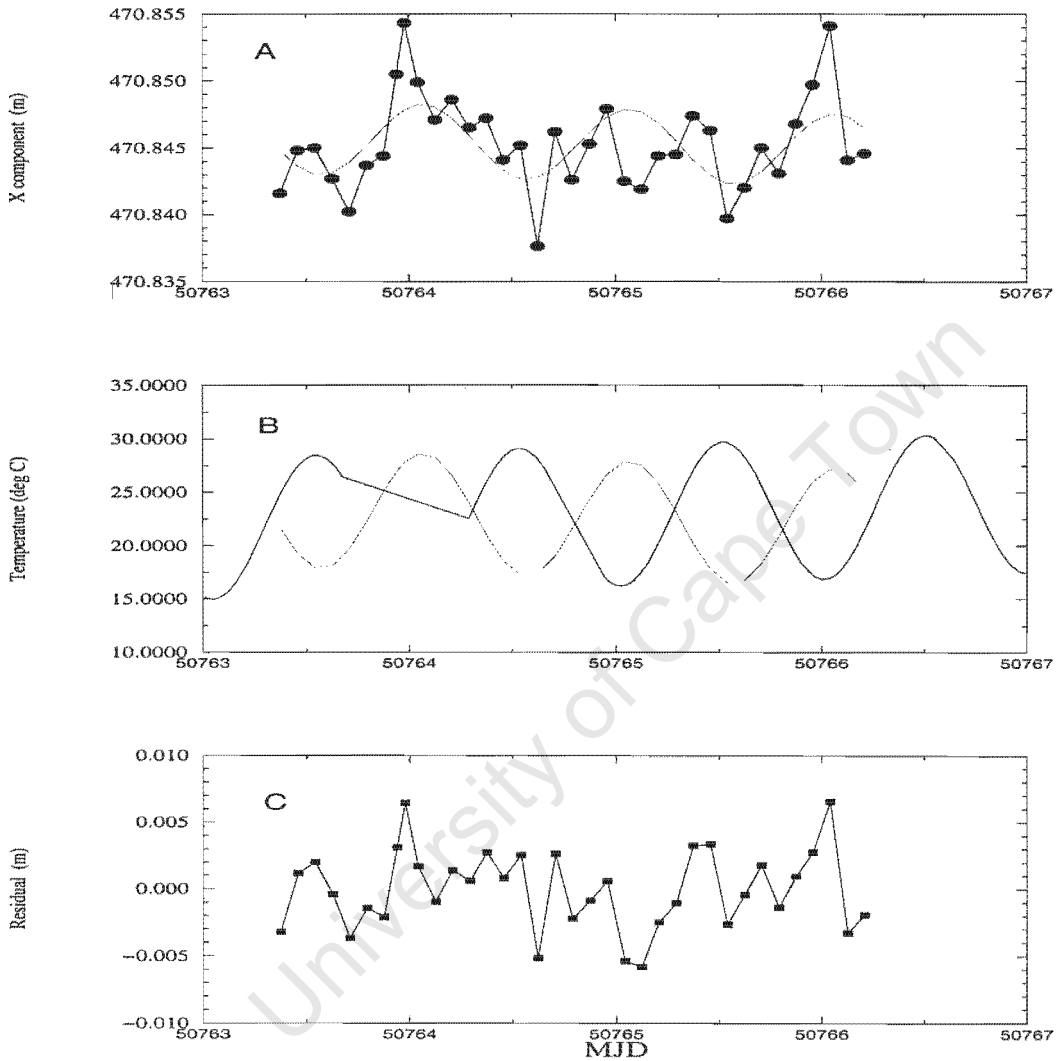

Figure E.15: Data set D: (A) X component, SLR to 411 and sinusoid with linear trend fitted to the X component data. (B) Sinusoidal fit to surface temperature data, overlaid with sinusoidal fit (red) to X component data points. (C) Residuals of (A).

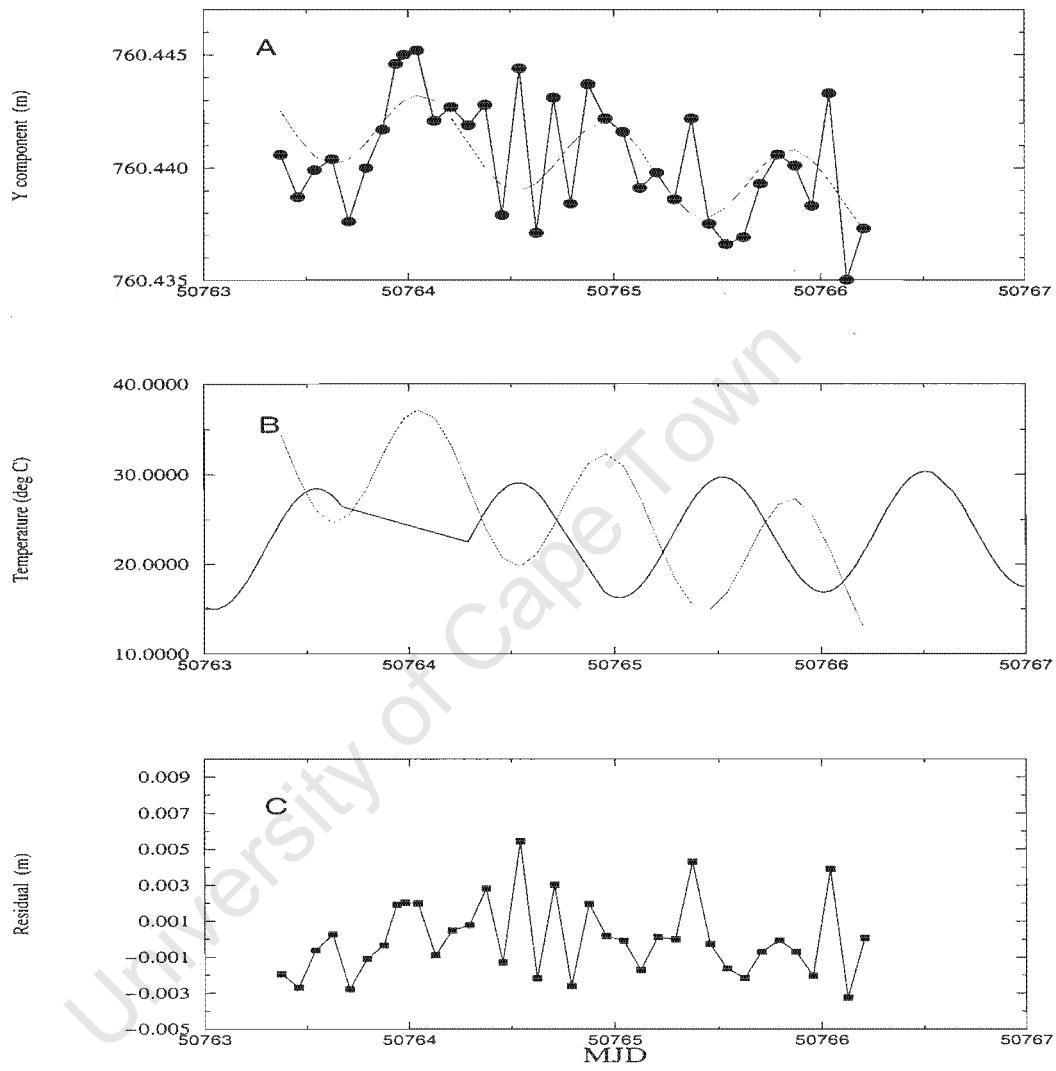

Figure E.16: Data set D: (A) Y component, SLR to 411 and sinusoid with linear trend fitted to the Y component data. (B) Sinusoidal fit to surface temperature data, overlaid with sinusoidal fit (red) to X component data points. (C) Residuals of (A).

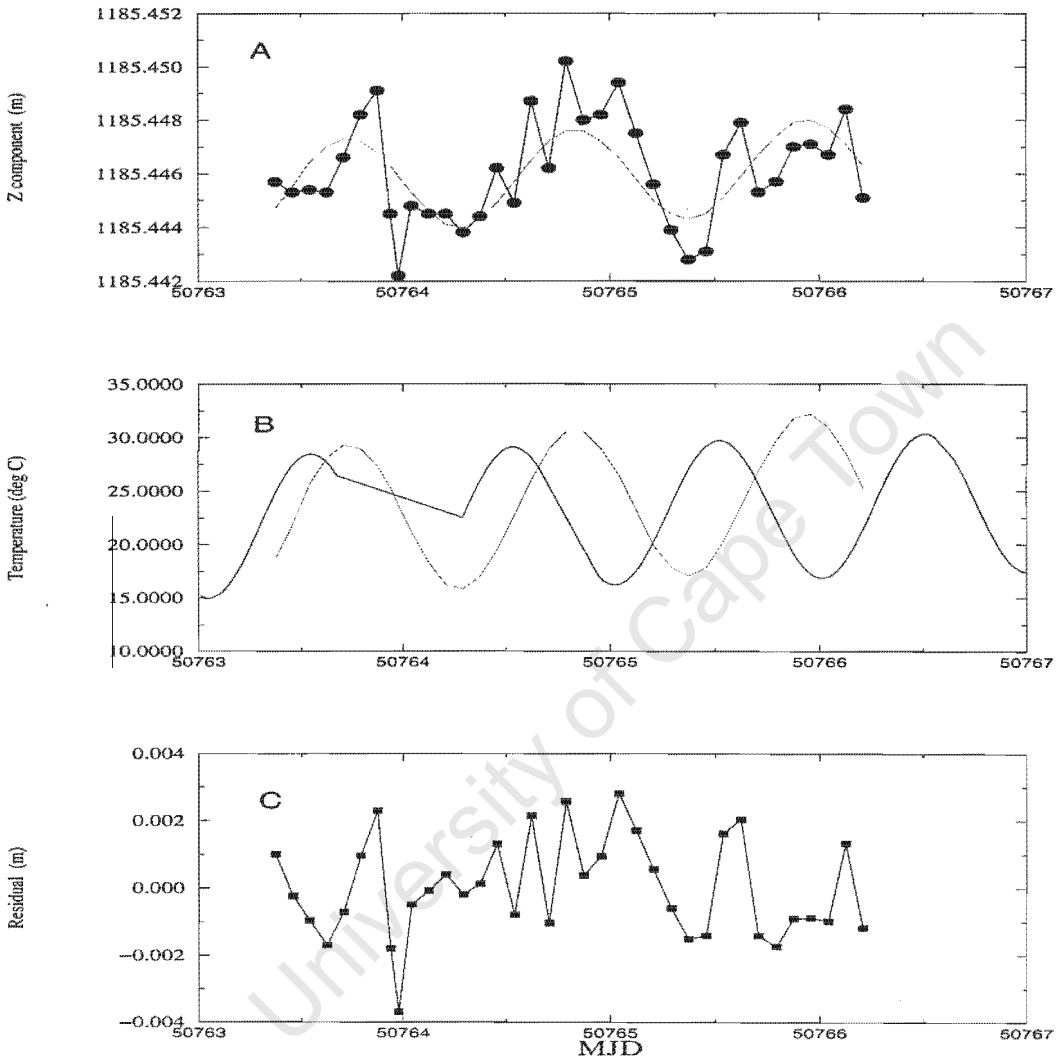

Figure E.17: Data set D: (A) Z component, SLR to 411 and sinusoid with linear trend fitted to the Y component data. (B) Sinusoidal fit to surface temperature data, overlaid with sinusoidal fit (red) to X component data points. (C) Residuals of (A).

Appendix F

Monument Located on Clay Data

Table F.1: Monument located on expansive clay

Session	MJD	Δx	Δy	Δz	Slope Distance	Δ Height
1	51197.531250	11.683100	-1.544800	15.114300	2.061900	19.165700
2	51197.750000	11.683300	-1.545400	15.114300	2.061900	19.165900
3	51198.000000	11.683500	-1.545800	15.114100	2.061900	19.165900
4	51198.250000	11.685200	-1.545800	15.113900	2.063300	19.166700
5	51198.500000	11.683100	-1.546500	15.115000	2.060900	19.166400
6	51198.750000	11.683400	-1.546000	15.114700	2.061500	19.166300
7	51199.000000	11.682300	-1.547300	15.116600	2.059300	19.167200
8	51199.250000	11.681700	-1.548100	15.115900	2.058700	19.166400
9	51199.500000	11.682900	-1.547500	15.115500	2.060100	19.166800
10	51199.750000	11.683600	-1.547000	15.114600	2.061400	19.166300
11	51200.000000	11.684500	-1.547500	15.114600	2.061800	19.167000
13	51200.500000	11.684200	-1.547300	15.114500	2.061700	19.166700
14	51200.750000	11.684800	-1.547400	15.114500	2.062200	19.167100
15	51201.000000	11.686600	-1.547600	15.114100	2.063600	19.167900
16	51201.250000	11.684900	-1.547400	15.114100	2.062300	19.166800
17	51201.500000	11.684900	-1.547500	15.115000	2.061900	19.167500
18	51201.750000	11.685700	-1.547300	15.114000	2.063100	19.167200
19	51202.000000	11.686400	-1.547800	15.114800	2.063100	19.168300
20	51202.250000	11.685500	-1.547500	15.114200	2.062800	19.167300
21	51202.500000	11.684200	-1.547100	15.114400	2.061800	19.166600
22	51202.750000	11.684400	-1.547100	15.114400	2.062000	19.166700
23	51203.000000	11.685000	-1.547300	15.114000	2.062600	19.166800
24	51203.250000	11.685200	-1.547800	15.114400	2.062400	19.167300
25	51203.500000	11.684500	-1.547100	15.114300	2.062100	19.166700
26	51203.750000	11.684300	-1.547300	15.114400	2.061800	19.166700
27	51204.000000	11.684400	-1.547600	15.114100	2.061900	19.166500
28	51204.250000	11.685800	-1.547500	15.114000	2.063100	19.167300
29	51204.500000	11.684700	-1.546000	15.114400	2.062700	19.166800
30	51205.347222	11.686100	-1.548000	15.113900	2.063200	19.167500
31	51205.500000	11.684500	-1.547200	15.114400	2.062000	19.166800
32	51205.750000	11.684300	-1.547300	15.114600	2.061700	19.166800
33	51206.000000	11.684600	-1.547200	15.114100	2.062300	19.166600
34	51206.250000	11.686200	-1.547000	15.113700	2.063800	19.167300
35	51206.500000	11.684500	-1.547800	15.114300	2.061800	19.166800
36	51206.750000	11.684300	-1.547700	15.114600	2.061500	19.166800
37	51207.000000	11.684900	-1.547700	15.114600	2.062000	19.167200
38	51207.250000	11.683600	-1.548500	15.114800	2.060600	19.166600
39	51207.500000	11.684300	-1.547300	15.114400	2.061800	19.166700
40	51207.750000	11.684500	-1.547700	15.114500	2.061800	19.166900
41	51208.000000	11.684800	-1.547500	15.114200	2.062200	19.166800
42	51208.250000	11.685500	-1.547500	15.114100	2.062800	19.167200
43	51208.500000	11.684700	-1.547400	15.114400	2.062100	19.166900
44	51208.750000	11.684200	-1.547900	15.114700	2.061300	19.166900
45	51209.000000	11.684700	-1.547700	15.114300	2.062000	19.167000
46	51209.250000	11.684700	-1.547800	15.114800	2.061700	19.167300
47	51209.500000	11.684700	-1.547800	15.115700	2.061400	19.168000
48	51209.750000	11.684500	-1.549500	15.116200	2.060300	19.168400
49	51210.000000	11.687900	-1.548000	15.114200	2.064500	19.168800
50	51210.250000	11.686100	-1.547900	15.114000	2.063100	19.167500
51	51217.312500	11.683700	-1.548500	15.114200	2.060900	19.166000
52	51224.312500	11.686200	-1.547200	15.113900	2.063600	19.167500
53	51231.306250	11.686600	-1.548400	15.114200	2.063300	19.168000
54	51231.312500	11.685900	-1.548000	15.113500	2.063200	19.167000
55	51238.306250	11.688600	-1.547700	15.112200	2.066100	19.167600
56	51238.312500	11.685400	-1.548200	15.114100	2.062500	19.167200
57	51245.306250	11.686800	-1.549200	15.113800	2.063300	19.167900
58	51245.312500	11.685100	-1.549500	15.114300	2.061600	19.167200
59	51253.306250	11.686800	-1.549200	15.113800	2.063300	19.167900
60	51253.312500	11.685100	-1.549500	15.114300	2.061600	19.167200
61	51260.306250	11.684600	-1.550400	15.114200	2.060900	19.167000
62	51260.312500	11.684400	-1.552400	15.114600	2.059700	19.167300
63	51266.306250	11.685800	-1.549400	15.112700	2.062800	19.166500
64	51266.312500	11.683500	-1.548900	15.113700	2.060800	19.165800
65	51275.306250	11.686800	-1.547900	15.112300	2.064400	19.166600
66	51275.312500	11.684600	-1.549700	15.114200	2.061100	19.166900
67	51287.306250	11.684700	-1.550700	15.113700	2.060900	19.166600
68	51287.312500	11.684000	-1.550100	15.114100	2.060400	19.166500
69	51297.306250	11.685500	-1.547800	15.113500	2.062900	19.168800
70	51297.312500	11.683500	-1.548600	15.115200	2.060200	19.166900
71	51311.306250	11.683900	-1.550500	15.114000	2.060300	19.166400
72	51323.306250	11.683100	-1.549900	15.114400	2.059700	19.166200
73	51336.306250	11.683900	-1.549300	15.114500	2.060500	19.166600
74	51343.306250	11.684800	-1.549900	15.114700	2.060900	19.167500

Appendix G

Footprint Error Ellipses

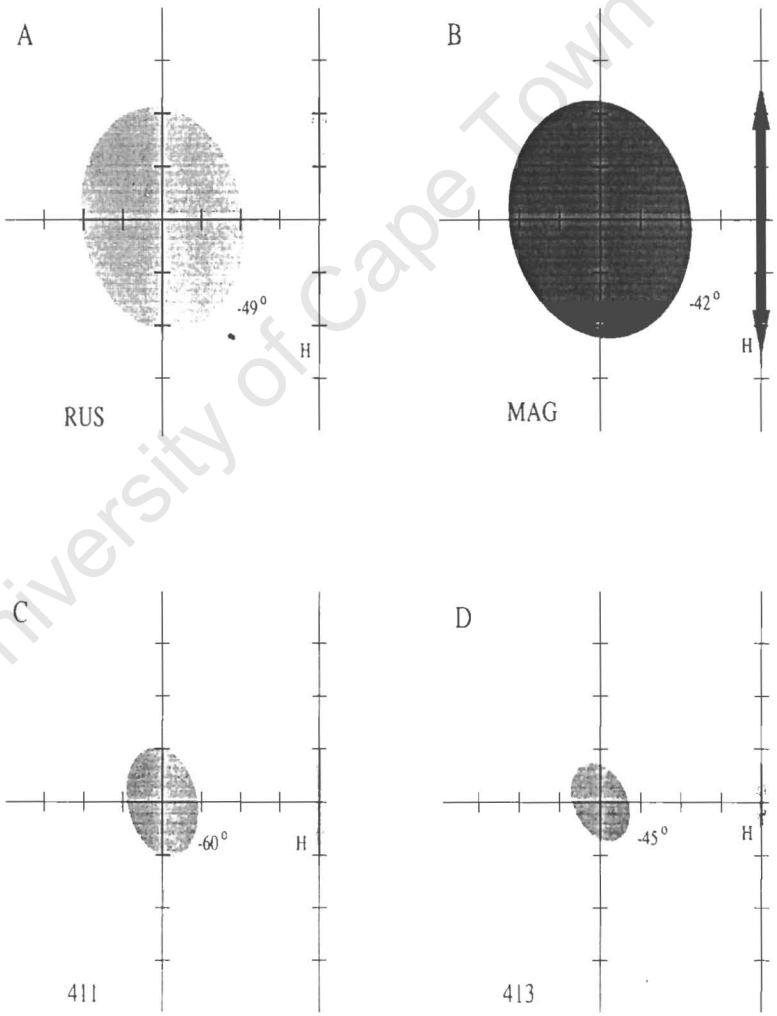

Figure G.1: Error ellipses, April 1997. (A) RUS, (B) MAG, (C) 411, (D) 413. Bar scale tick = 1 mm. Horizontal and vertical error (1σ)

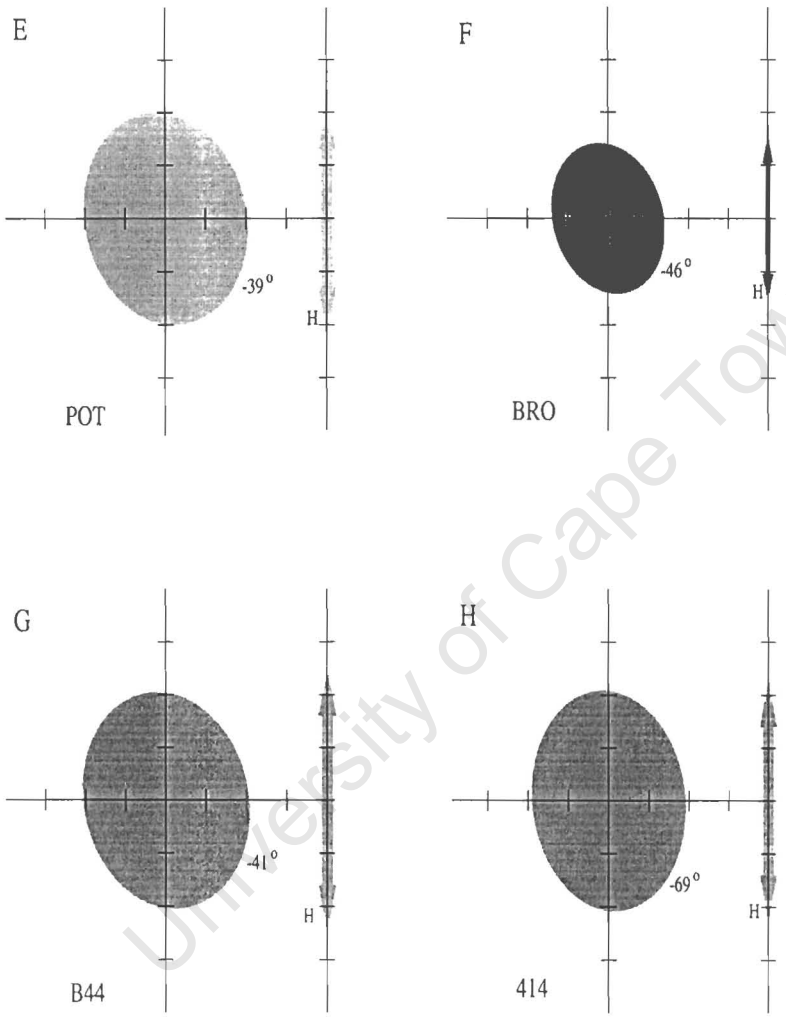

Figure G.2: Error ellipses, April 1997. (E) POT, (F) BRO, (G) B44, (H) 414. Bar scale tick = 1 mm. Horizontal and vertical error (1σ)

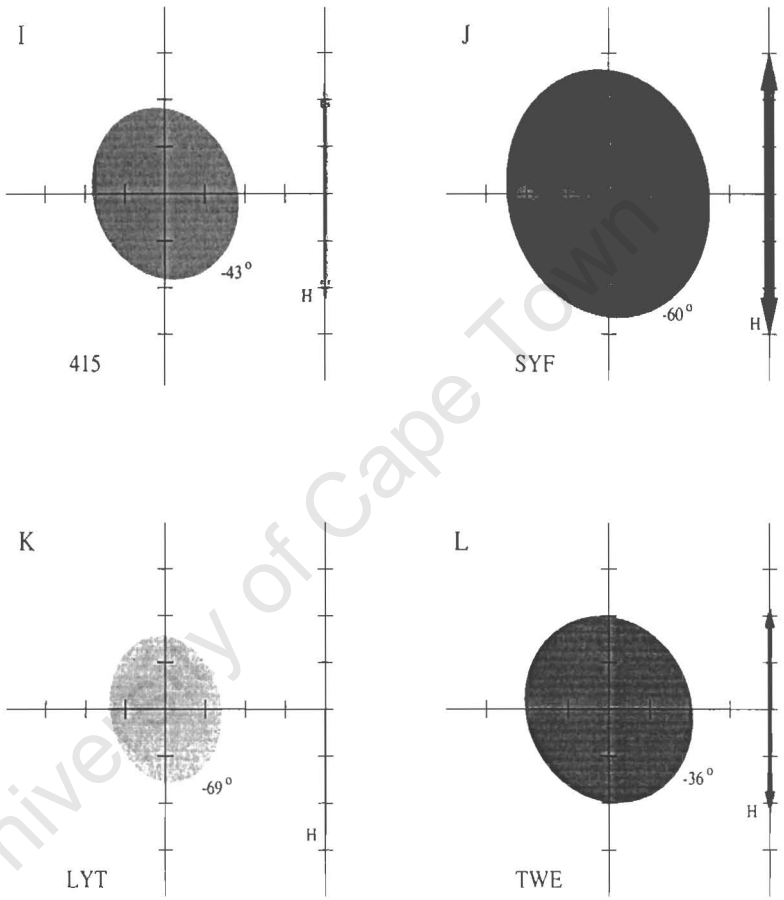

Figure G.3: Error ellipses, April 1997. (I) 415, (J) SYF, (K) LYT, (L) TWE. Bar scale tick = 1 mm. Horizontal and vertical error (1σ)

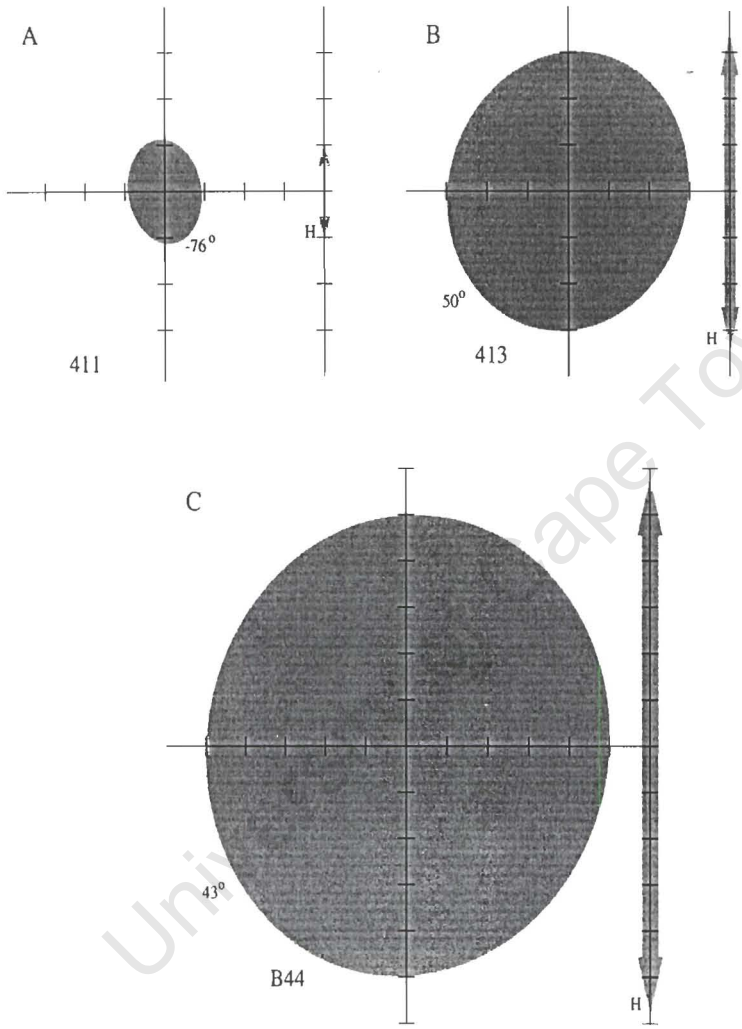

Figure G.4: Error ellipses, inner network September 1997. (A) 411, (B) 413, (C) B44.Bar scale tick = 1 mm. Horizontal and vertical error (1σ)

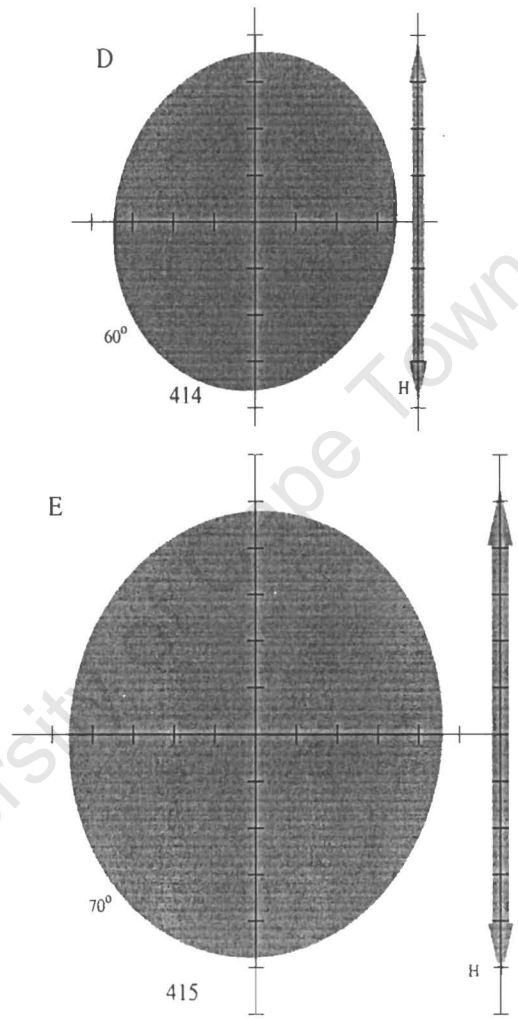

Figure G.5: Error ellipses, inner network September 1997. (D) 414, (E) 415. Bar scale tick = 1 mm. Horizontal and vertical error (1σ)

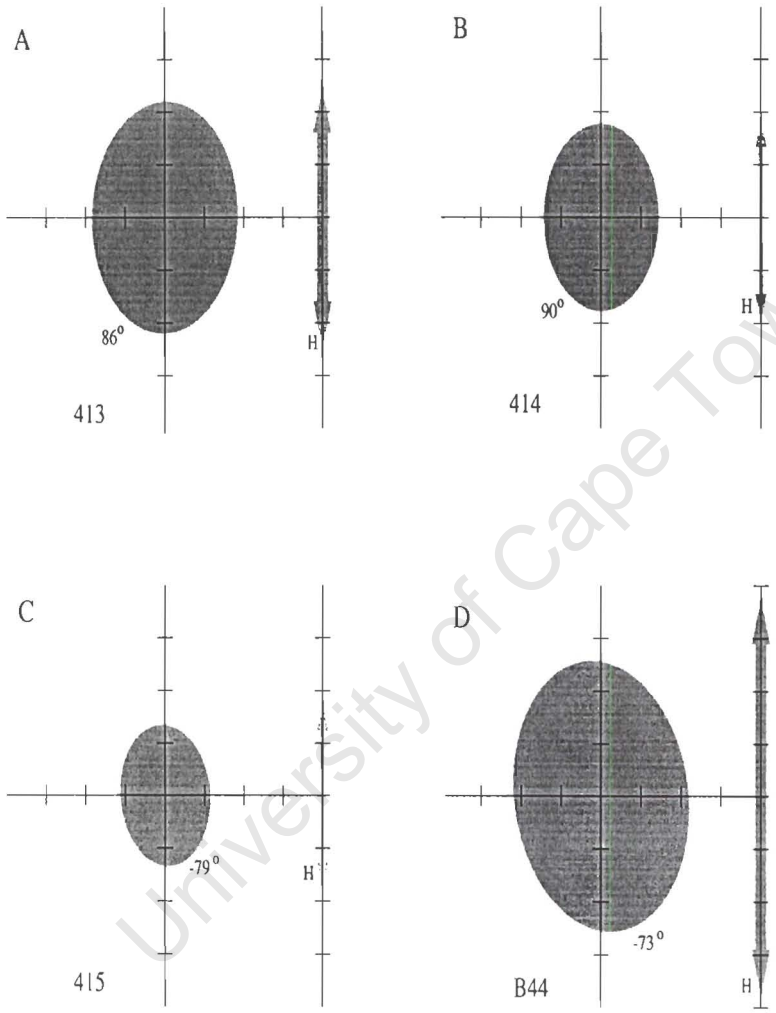

Figure G.6: Error ellipses, inner network January 1998. (A) 413, (B) 414, (c) 415, (D) B44. Bar scale tick = 1 mm. Horizontal and vertical error (1σ)

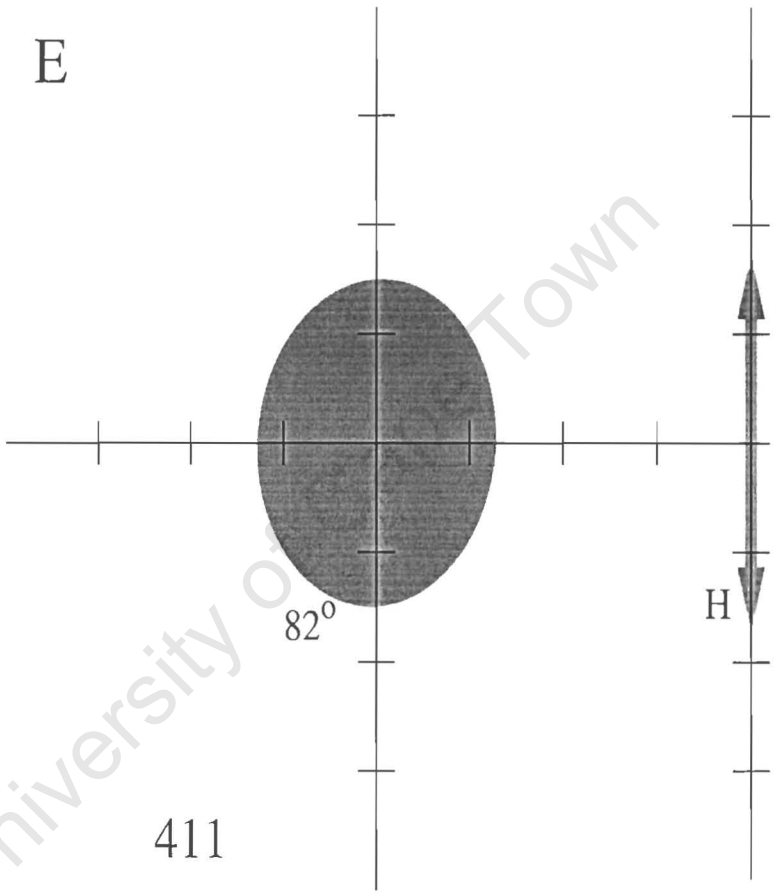

Figure G.7: Error ellipse, inner network January 1998. (E) 411. Bar scale tick = 1 mm. Horizontal and vertical error (1σ)

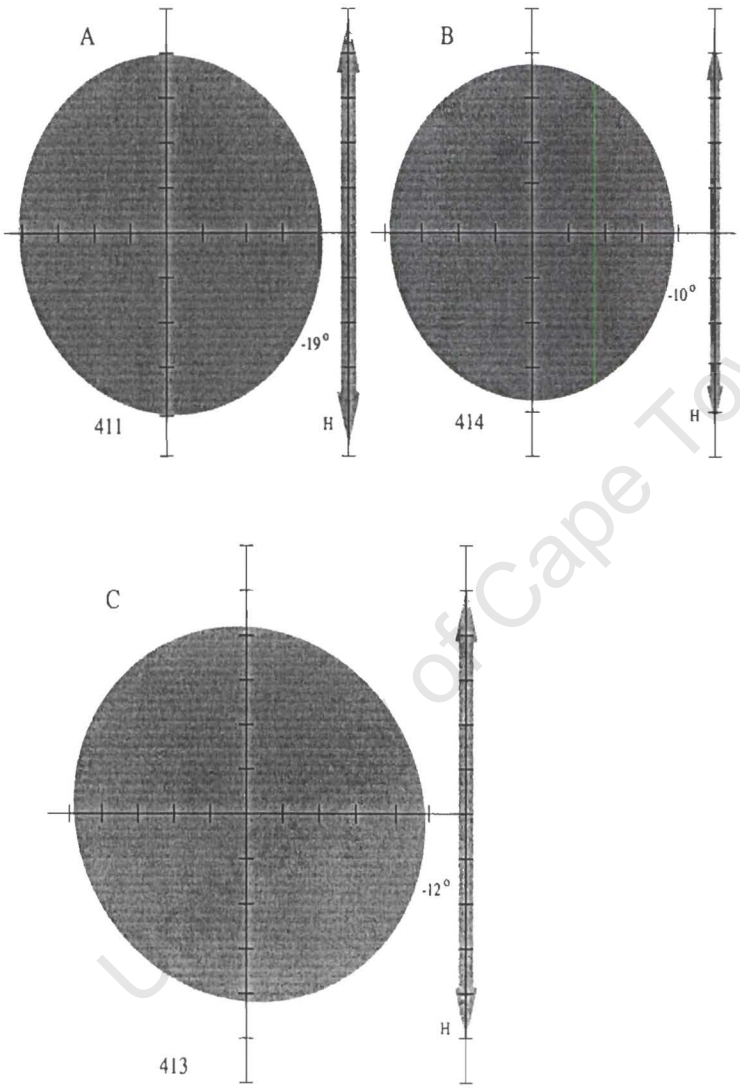

Figure G.8: Error ellipses, inner network April 1998. (A) 411, (B) 414, (C) 413. Bar scale tick = 0.1 mm. Horizontal and vertical error (1σ)

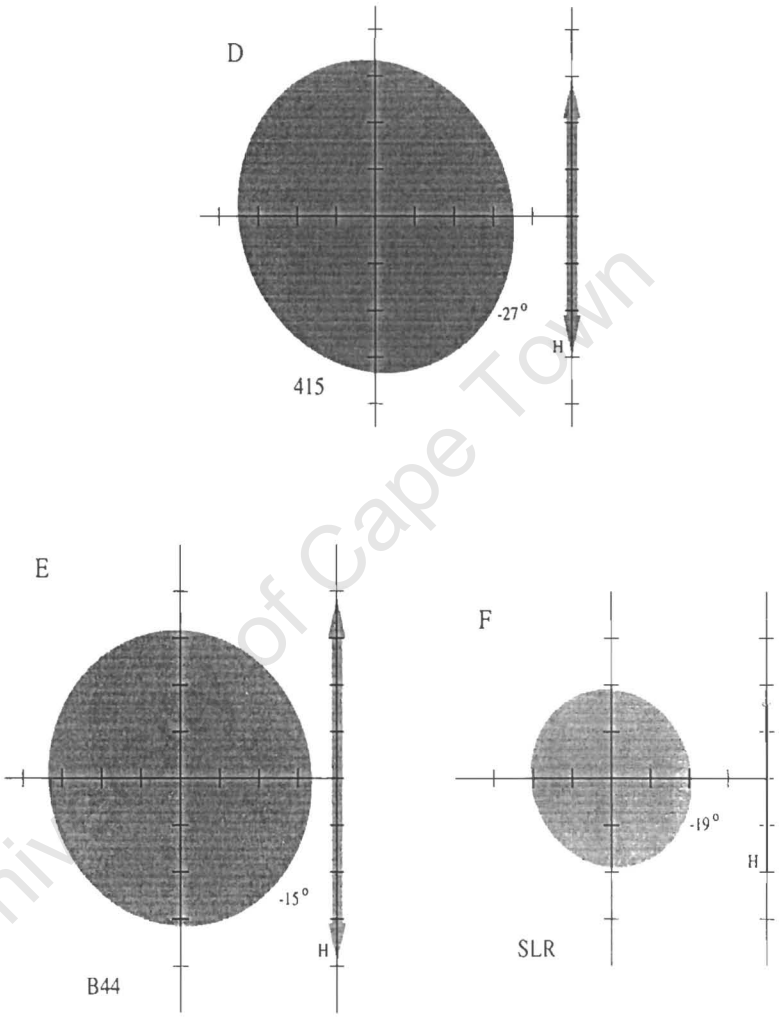

Figure G.9: Error ellipses, inner network April 1998. (D) 415, (E) B44, (F) SLR. Bar scale tick = 0.1 mm. Horizontal and vertical error (1σ)

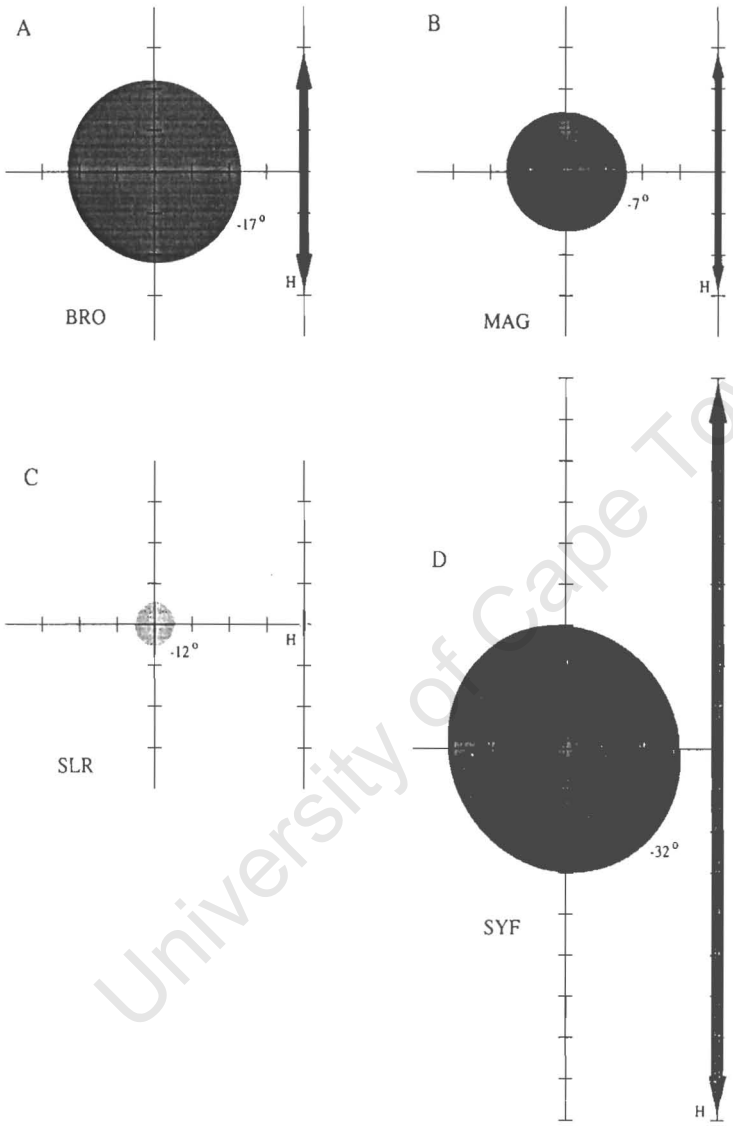

Figure G.10: Error ellipses, inner/intermediate network July 1998. (A) BRO, (B) MAG, (C) SLR, (D) SYF. Bar scale tick = 1 mm. Horizontal and vertical error (1σ)

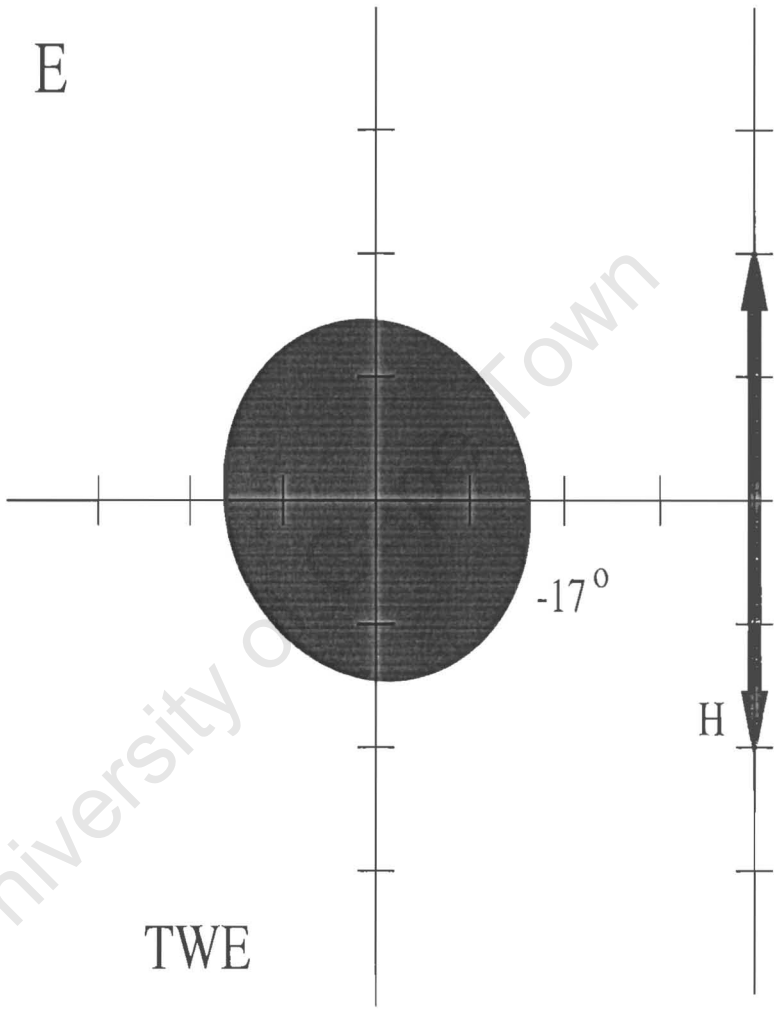

Figure G.11: Error ellipses, intermediate network July 1998. (E) TWE. Bar scale tick = 1 mm. Horizontal and vertical error (1σ)

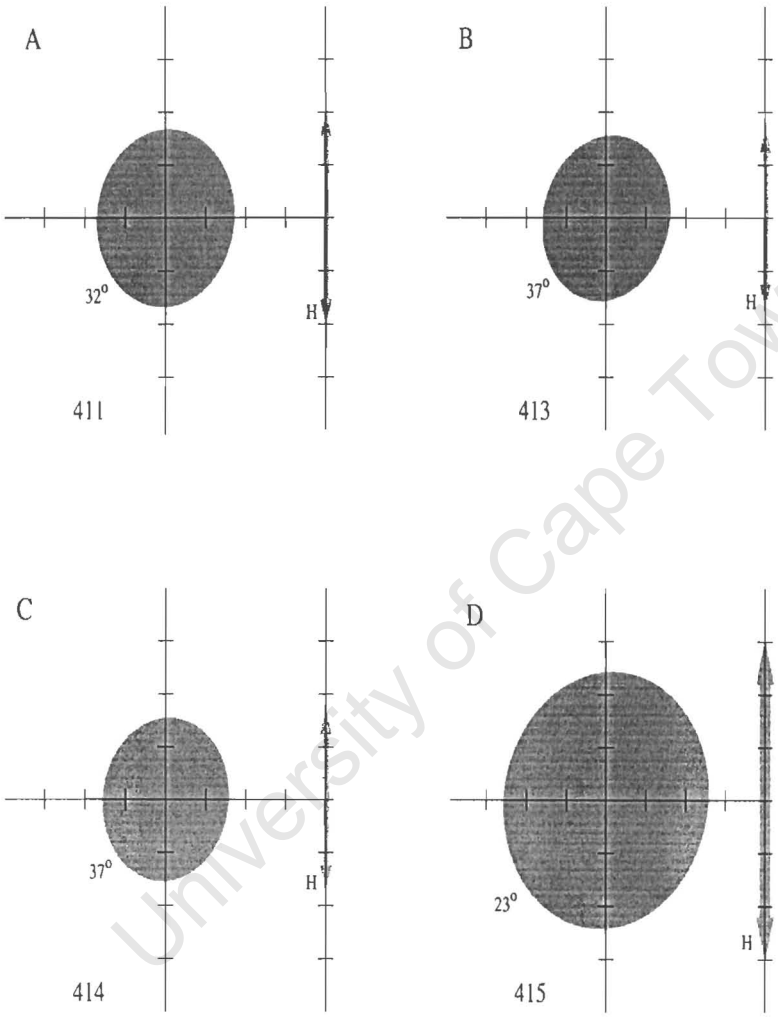

Figure G.12: Error ellipses, inner network June 1999. (A) 411, (B) 413, (C) 414, (D) 415. Bar scale tick = 1 mm. Horizontal and vertical error (1σ)

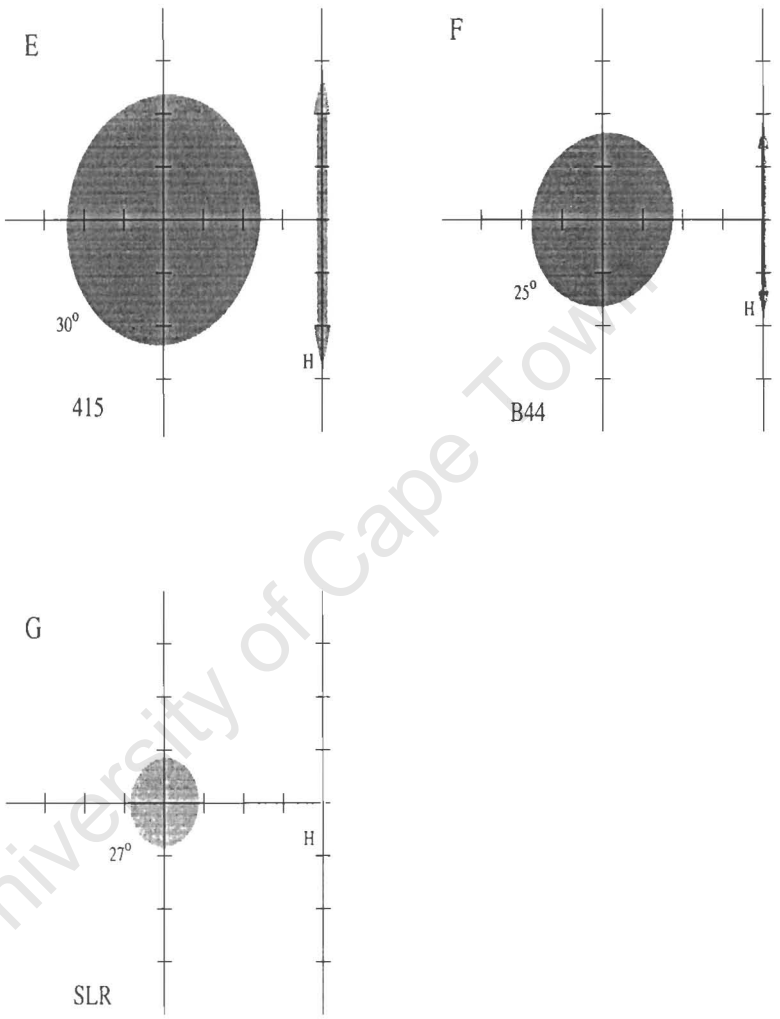

Figure G.13: Error ellipses, inner network June 1999. (E) 415, (F) B44, (G) SLR. Bar scale tick = 1 mm. Horizontal and vertical error (1σ)

Appendix H

Baseline plots

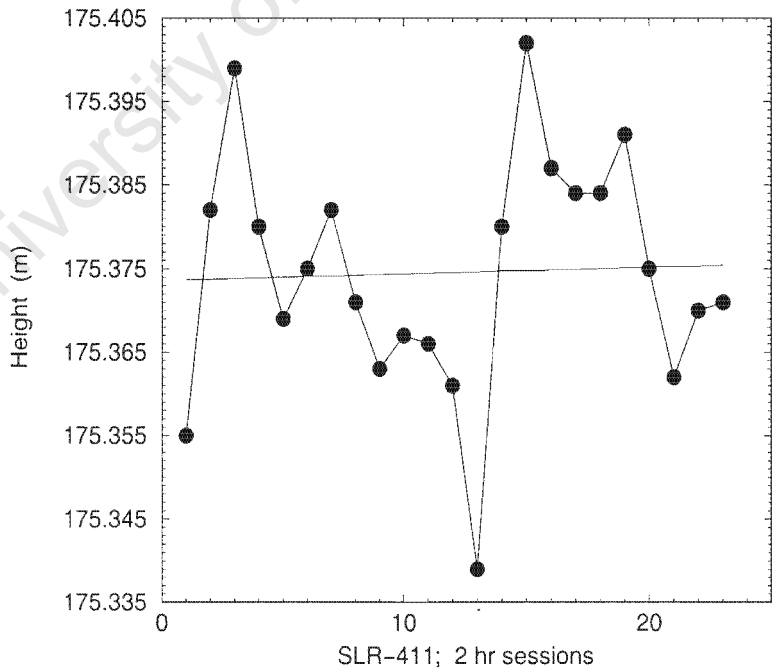

Figure H.1: Inner network January 1998, 23 two hour duration sessions. Baseline SLR to 411, height, linear regression.

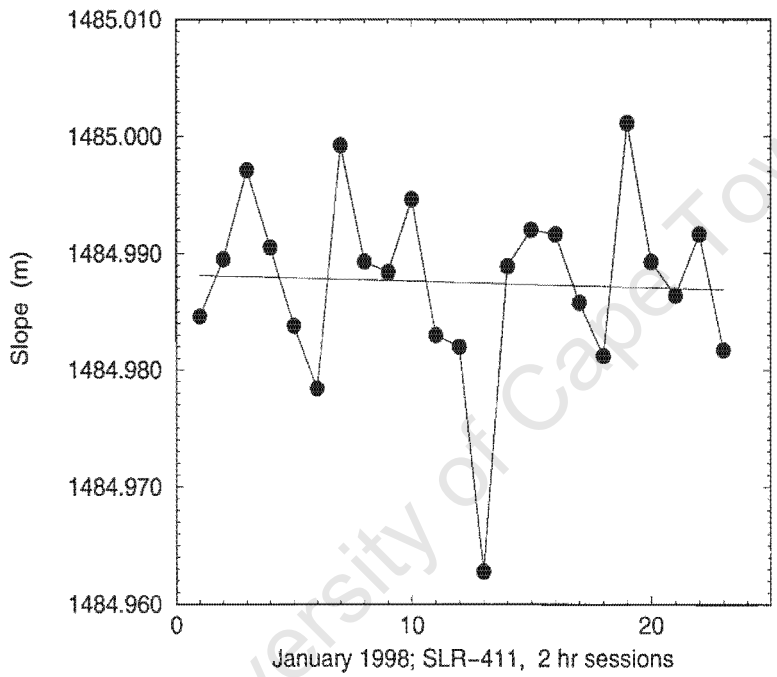

Figure H.2: Inner network January 1998, 23 two hour duration sessions. Baseline SLR to 411, slope distance, linear regression.

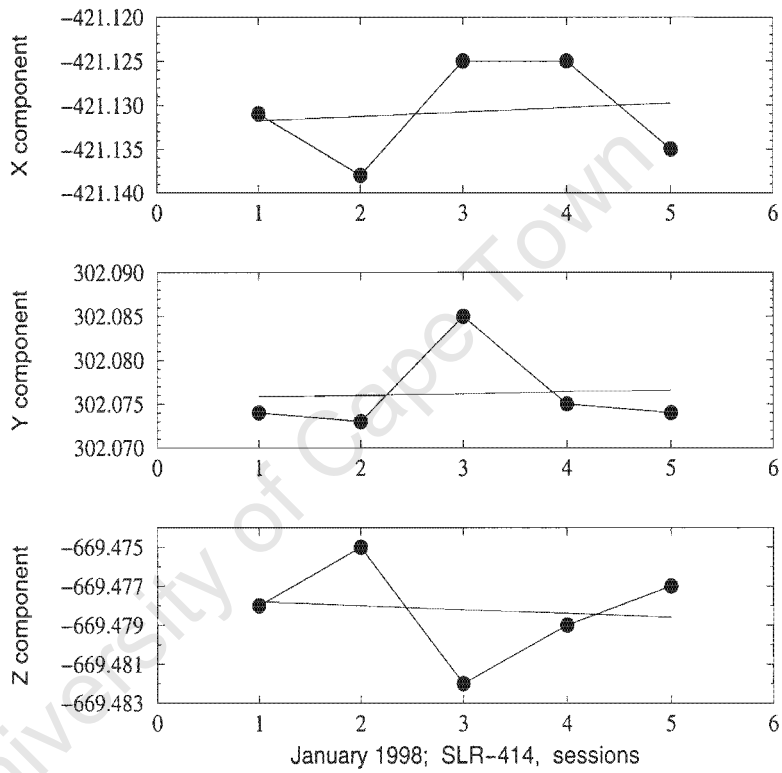

Figure H.3: Inner network January 1998, 5 sessions. Baseline SLR to 414, X, Y and Z components, linear regression.

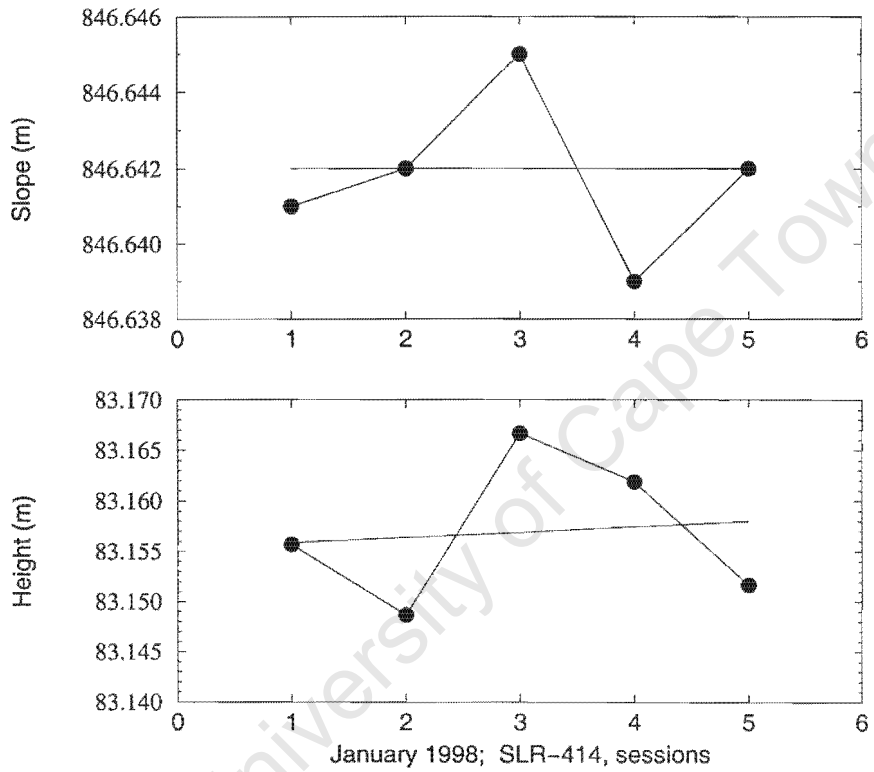

Figure H.4: Inner network January 1998, 5 sessions. Baseline SLR to 414, slope distance and height, linear regression.

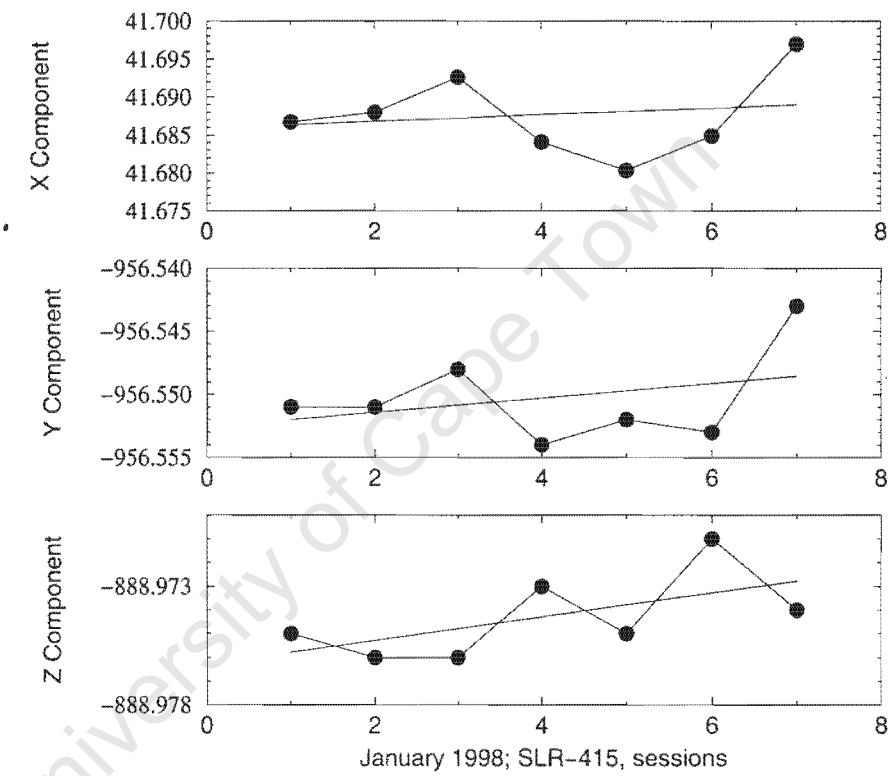

Figure H.5: Inner network January 1998, 7 sessions. Baseline SLR to 415, X, Y and Z components, linear regression.

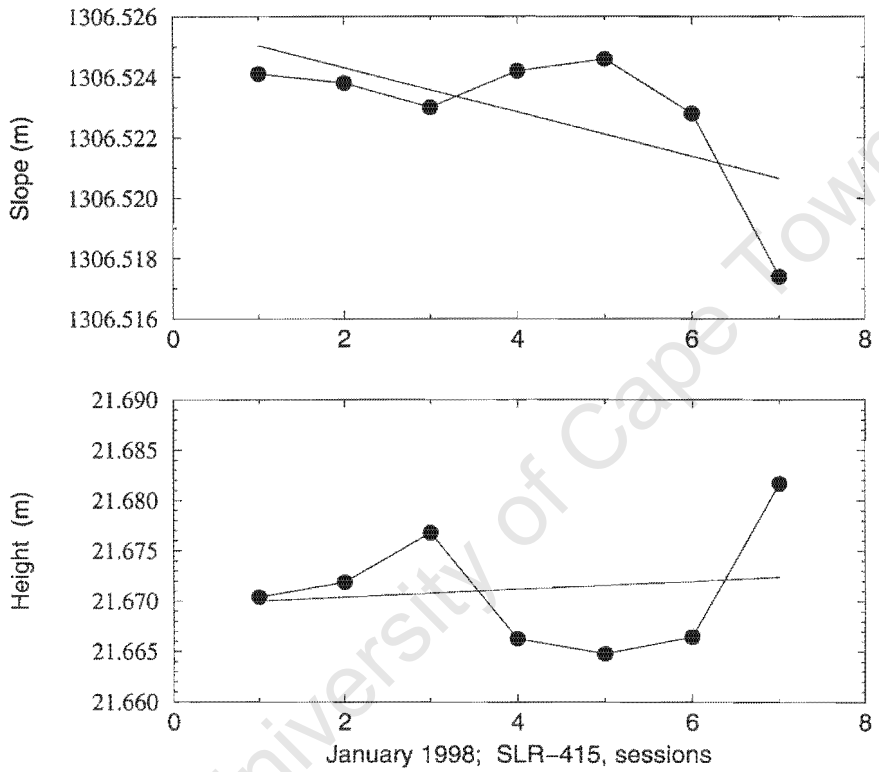

Figure H.6: Inner network January 1998, 7 sessions. Baseline SLR to 414, slope distance and height, linear regression.

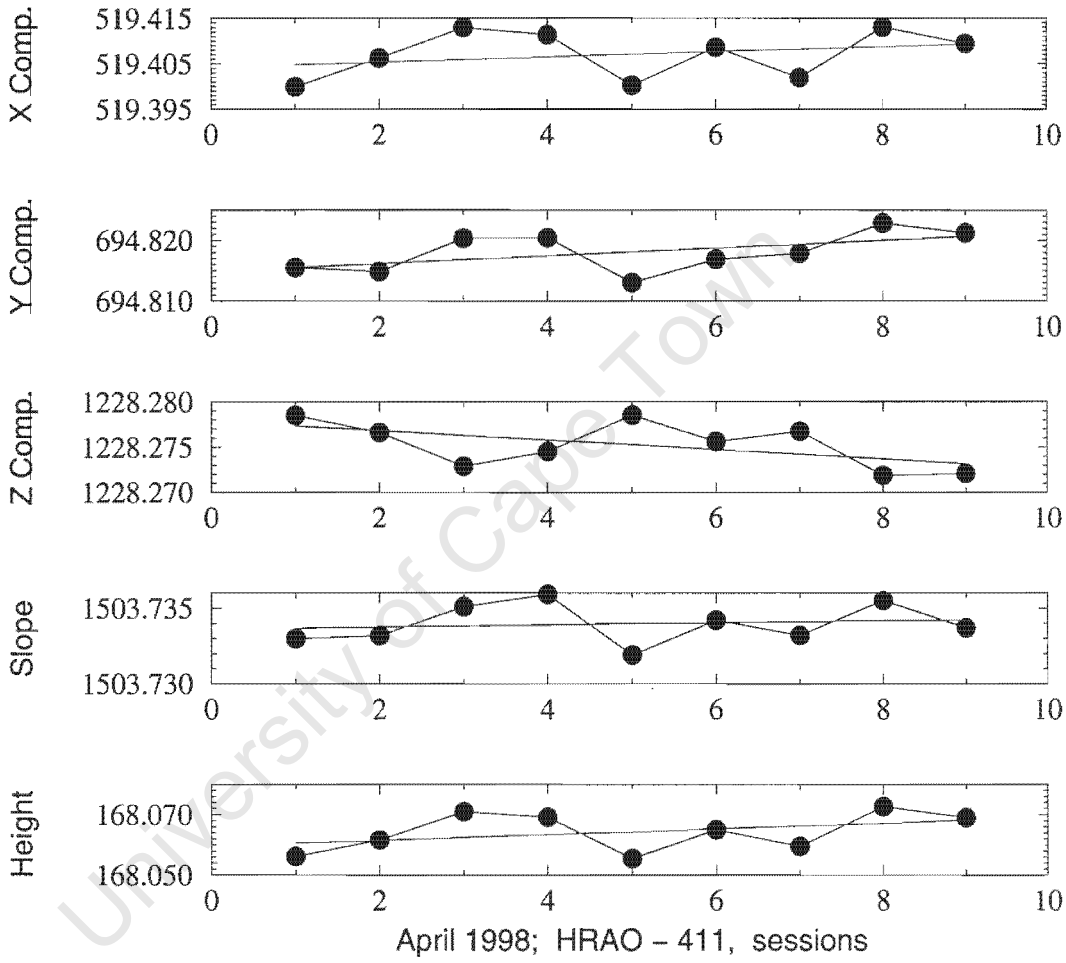

Figure H.7: Inner network April 1998, 9 sessions. Baseline SLR to 411, X, Y, Z components, slope distance and height (metres), linear regression.

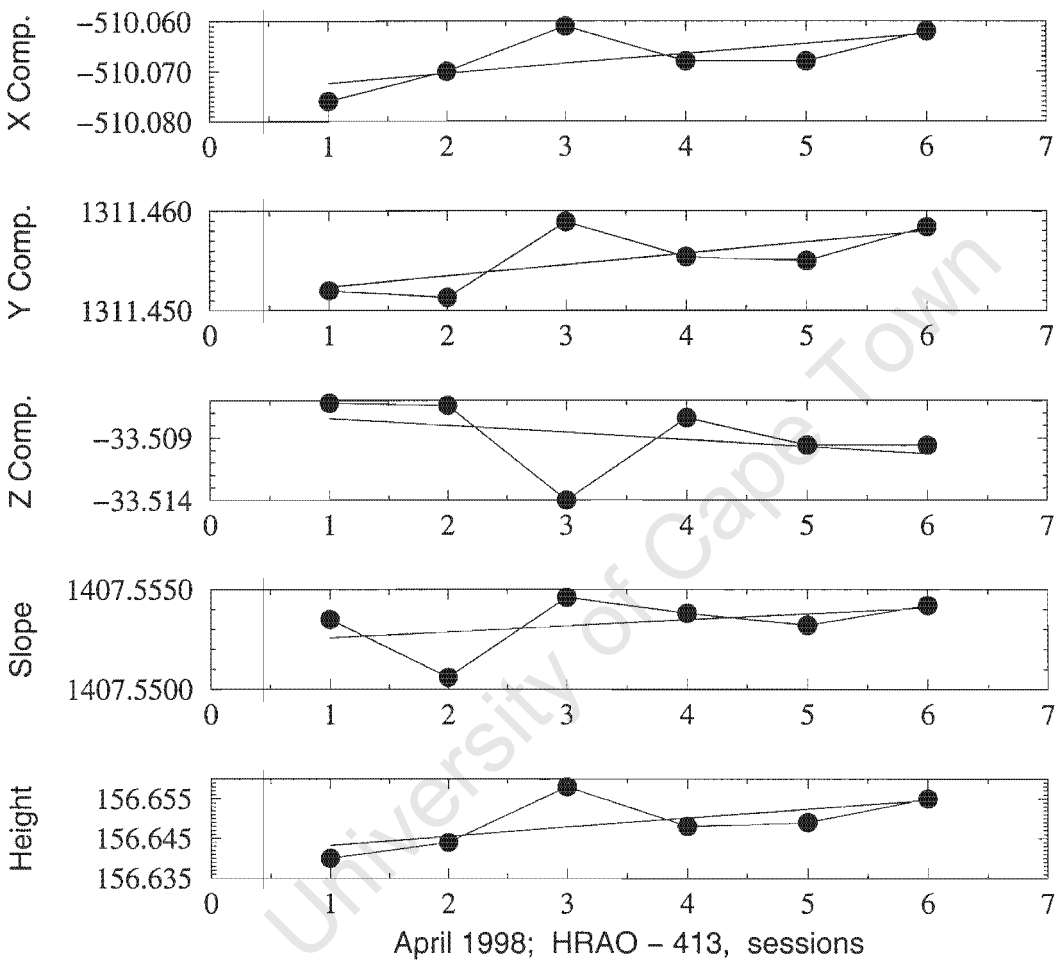

Figure H.8: Inner network April 1998, 6 sessions. Baseline SLR to 413, X, Y, Z components, slope distance and height (metres), linear regression.

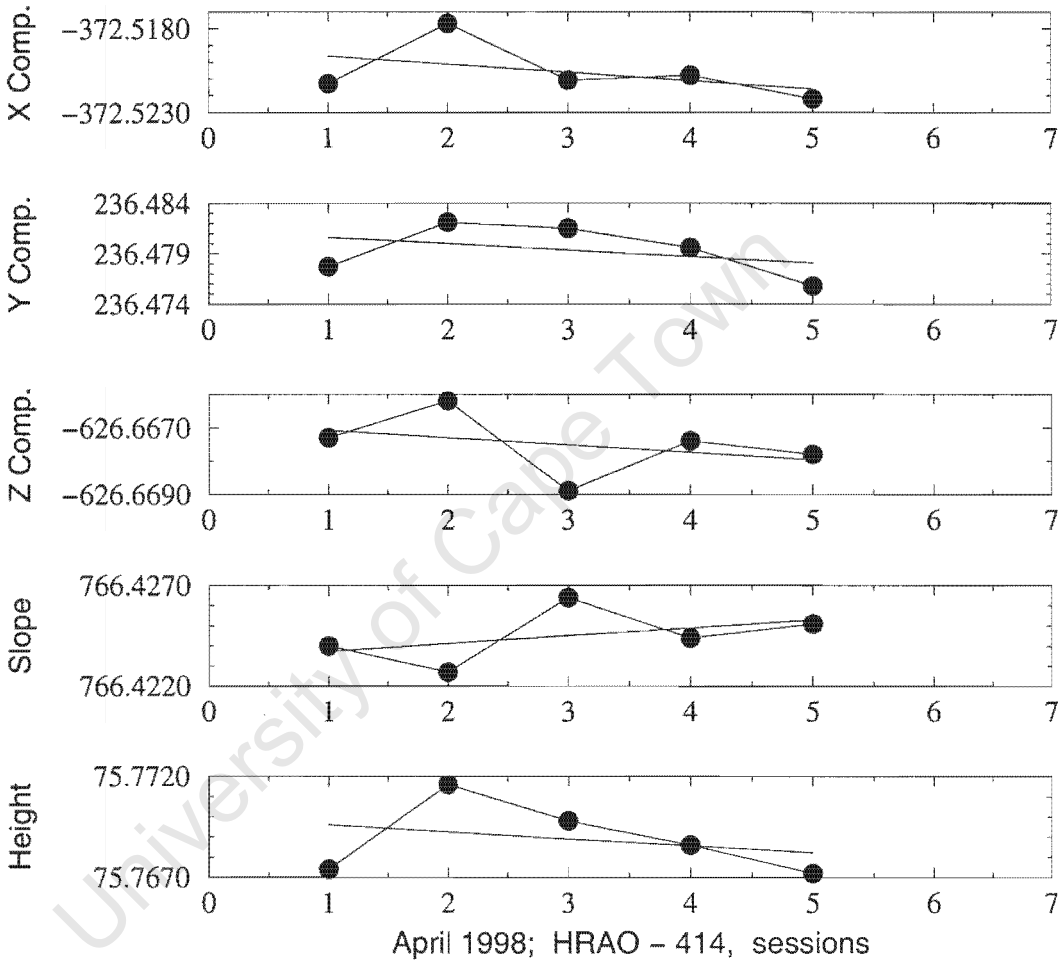

Figure H.9: Inner network April 1998, 5 sessions. Baseline SLR to 414, X, Y, Z components, slope distance and height (metres), linear regression.

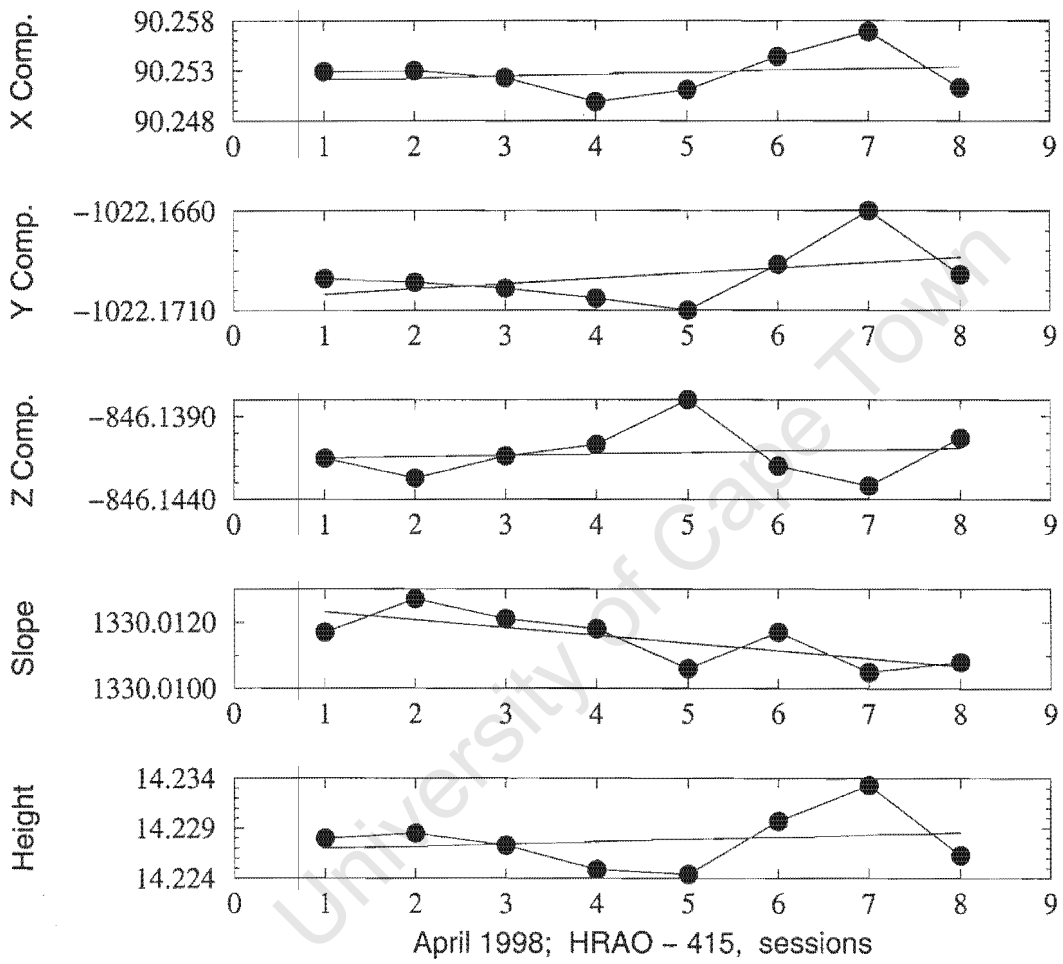

Figure H.10: Inner network April 1998, 8 sessions. Baseline SLR to 415, X, Y, Z components, slope distance and height (metres), linear regression.

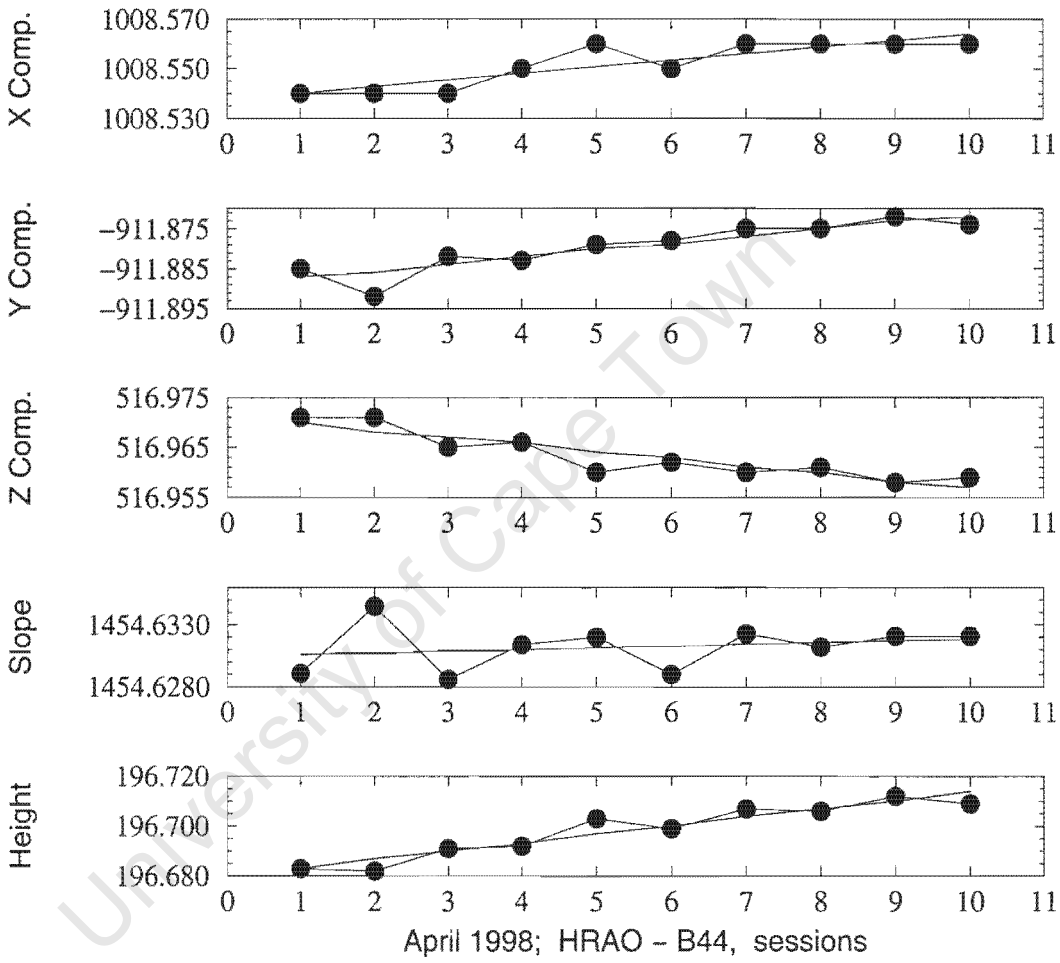

Figure H.11: Inner network April 1998, 10 sessions. Baseline SLR to B44, X, Y, Z components, slope distance and height (metres), linear regression.

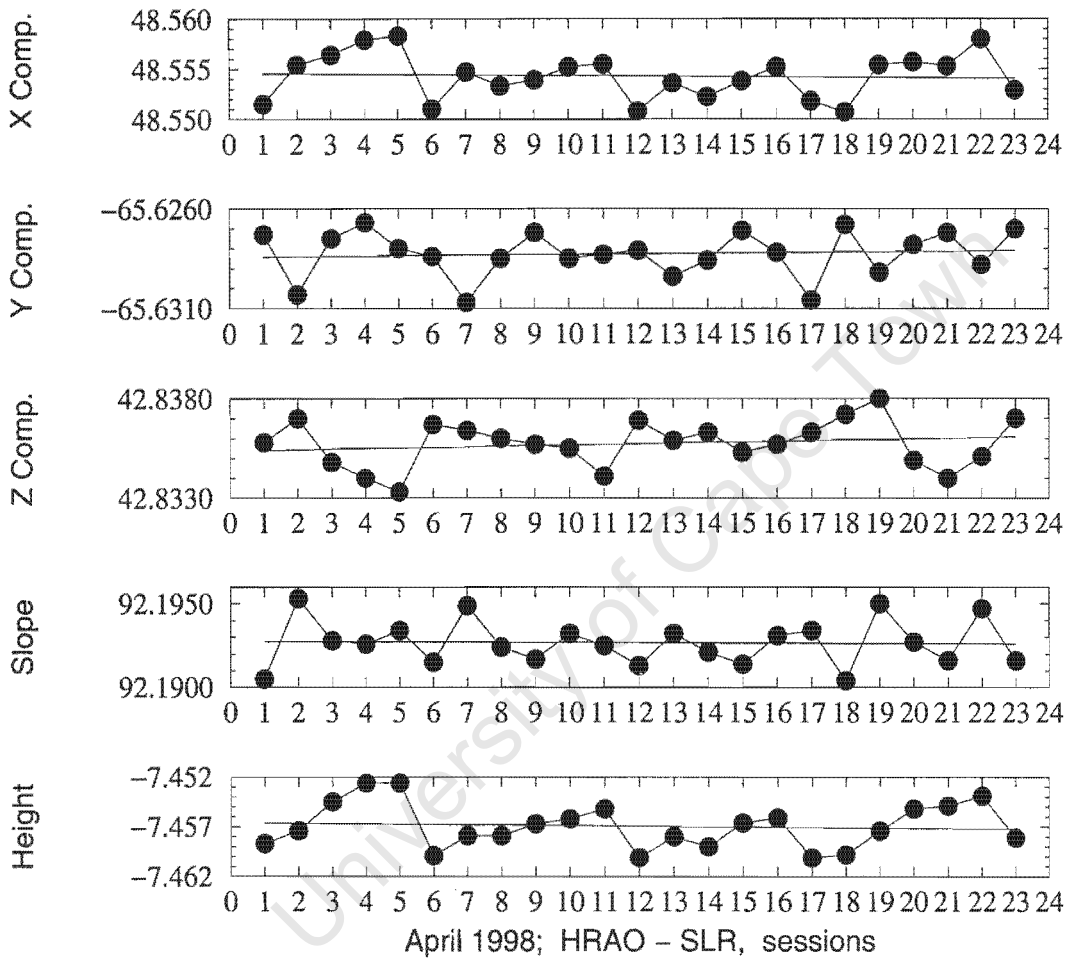

Figure H.12: Inner network April 1998, 23 sessions. Baseline HRAO to SLR, X, Y, Z components, slope distance and height (metres), linear regression.

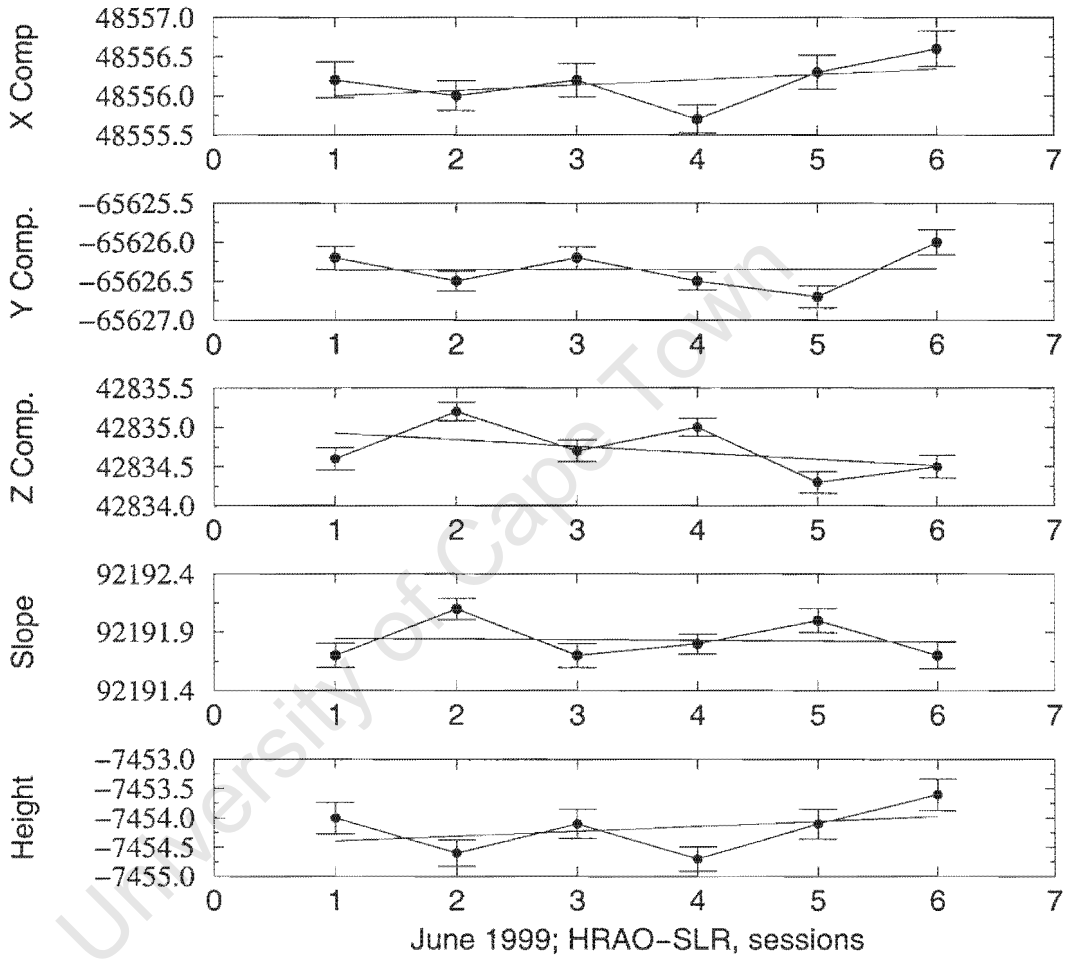

Figure H.13: June 1999, 6 sessions, 6, 7, 6, 8, 6 and 5 hour duration respectively. Baseline HRAO to SLR, X, Y, Z components, slope distance and height (mm), linear regression.

Appendix I

Thermal Monitoring Equipment

Copper rod was cut and drilled to provide a housing for the transducers. The front part of the housing was rounded to allow easy installation into the rock. Heatsink paste was used when installing the transducer into its housing to ensure good thermal conductivity between the copper and the transducer.

The thermal transducer used in this project is a type AD592 two terminal monolithic integrated circuit that provides an output current which is proportional to absolute temperature. The transducer acts as a high impedance temperature dependent current source of $1\mu A/K$. Due to its high impedance current output the transducer is immune to voltage drops and voltage noise over long lines, which made it very suitable for populating the hill used in this study. The calculated self-heating error with the transducer in free air, that is not contained in a heat sinking package, was only $0.2°C$. The specified accuracy which we required was 0.5°, a limit set by the resolution of the A/D converter used in the telemetry transmitter.

Each of the 8 AD592 transducers had to be properly calibrated via a calibrating circuit. A stable 2.5 V reference voltage was used in conjunction with an operational amplifier to produce an output of 0 to 5 V which represented $-50°C$ to $50°C$, so that $0°C$=2.5 V. Output level after the operational amplifier was 50 mV/K. A separate regulated power supply (derived from a 12 V battery supply) provided input voltage to the AD592 transducers. The operational amplifiers (8 off) can be balanced (nulled) by potentiometers and a calibration potentiometer was set to calibrate the AD592.

The function of the telemetry transmit system is to condition, digitise and transmit via radio link, the thermal data to a remote receiver and PC. A block diagram which describes the system is depicted in (Figure I.1). Although the author was involved with parts of the conceptual design, credit for the design and construction of the electronics of the data telemetry system must be given to R Uytenbogaardt. Most of the construction and testing was done after hours, and the resulting unit is an example of very high quality, meticulous work, which greatly aided this research work. No electronic circuits

are described here as it falls outside the scope of this work, but a functional description should allow any reader to understand the unit's operation.

- Power for the unit is generated by a small solar panel, which feeds a 12 V battery. This battery voltage is monitored by the unit and the voltage value is transmitted via the telemetry system for monitoring purposes.
- A power board provides regulated 5 V outputs, as well as a switched 12 V supply to the rf transmitter.
- A crystal oscillator with a fundamental frequency of 32 Khz drives a timing control circuit and an electronic switch (8.5 minute or 17 minute selectable).
- The transducer conditioning module is interfaced to an 8 channel, 8 bit analogue to digital converter (AD7828KN). In order to select a specific transducer, a 3 bit address had to be selected via an 8 channel counter, driven by the timing control circuitry.
- The 8 bit output of the analogue to digital converter is the input to a 20 bit shift register. The shift register is also fed the 3 bit address, a battery level and a station number. This allowed a 20 bit digital data stream to be transferred to a tone encoder, which in turn frequency shifted the rf transmitter.

While R Uytenbogaardt constructed the telemetry unit, the author designed and constructed a radio receiver (direct conversion, crystal controlled) which had to receive the frequency shift keyed (fsk) data, demodulate it and feed this demodulated signal to a tone decoder. The tone decoder in turn interfaced to a logic circuit which was read by a PC14B I/O card situated in a PC. It was necessary to spend a large amount of time to optimise the cicuit of the decoder in order to have a high success rate of data decoding, through ionospheric and other noise present on the rf frequency the equipment was operating on. The details of all this is beyond the scope of this work, so a short description of the receiver and tone decoder must suffice. The receiver description follows the path of the rf, starting at the antenna:

- Short whip antenna tuned by a variable inductor
- Rf amplifier (10 dB) with two tuned circuits for selectivity
- Doubly balanced mixer fed by crystal controlled local oscillator and the amplified incoming signal, resulting in an intermediate frequency at audio frequencies, the local oscillator acting simultaneously as beat frequency oscillator, after detection generating an audio tone (1KHz).
- A narrowband audio filter, centred on 1 KHz, followed by a 110 dB audio amplifier, driving the tone detector.
- The tone detector is a FX105A monolithic CMOS tone operated switch, designed for tone decoding in single and mulititone signalling systems.

It was selected because of its inherent immunity to high levels of harmonic and sub-harmonic interference, excellent noise immunty and constant bandwidth over varying levels of input signal strength. It was found to work very well but only at slow data transmission rates.

- Peripheral circuits were constructed to facilitate operation of the receiver, such as a power supply, signal level meter driving circuit and audio tape recorder electronic switch.

The receiver had to be very frequency stable, as there were severe constraints on receiver drift due to the narrowband audio filter, low transmitter power and characteristics of the tone decoder, which gave a workable audio bandwidth of about 40 Hz. This was achieved by using 3.581 MHz crystals in both the transmitter and receiver, so that once adjusted, frequency drift was within the required specifications. After construction the telemetry unit, transmitter/encoder and receiver/decoder was found to be adequate for its designed purpose. The transmitter/decoder unit operated unattended for several months before being severely damaged by lightning, but has since been repaired.

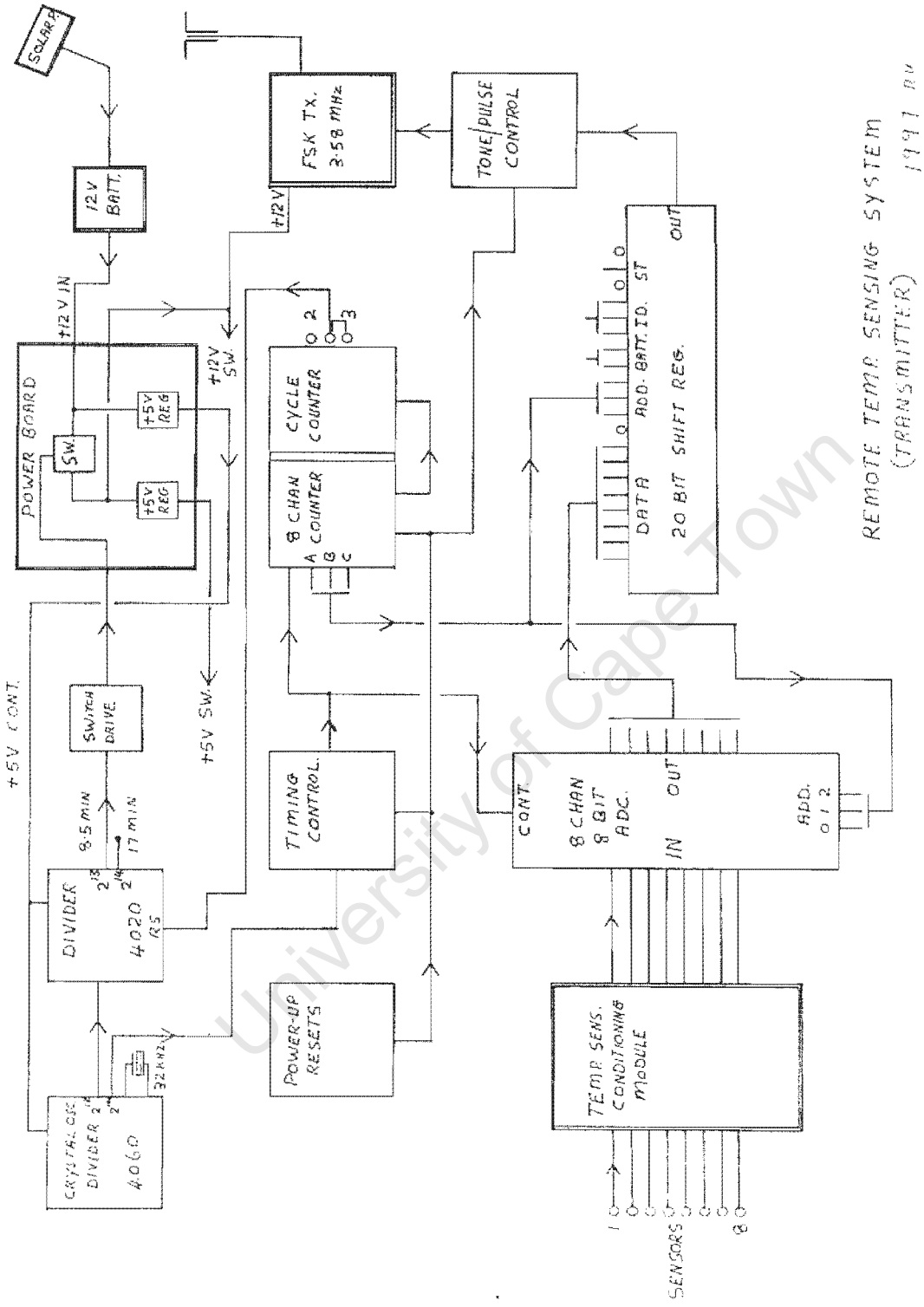

Figure I.1: Block diagram of the thermal data telemetry system, describing the signal conditioning, digitising, logic and rf transmission components. (R. Uytenbogaardt, 1997)

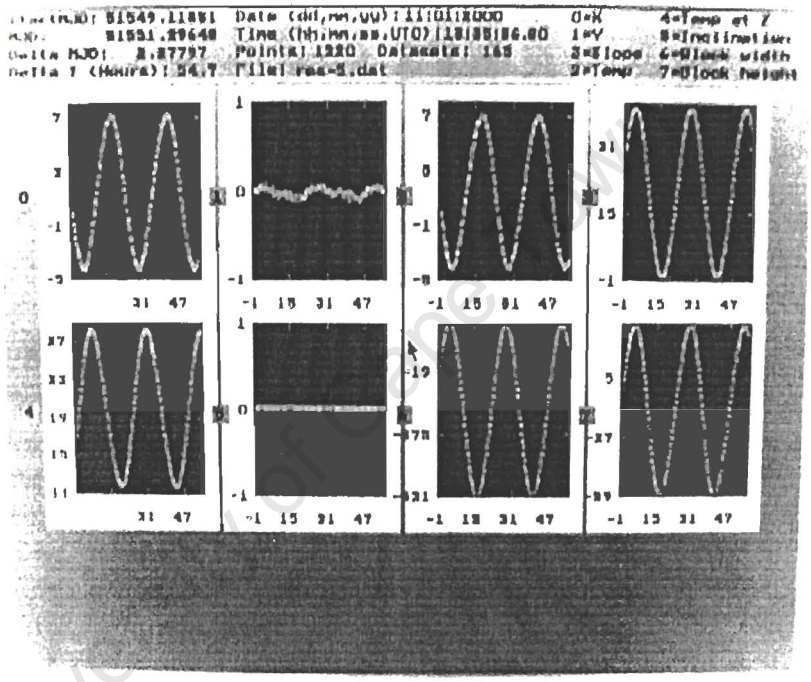

Figure I.2: NTM results based on thermal expansion of a 200 metre diameter hill, coefficient of expansion set to 1×10^{-5}. The slope distance variation is unrealistically large.

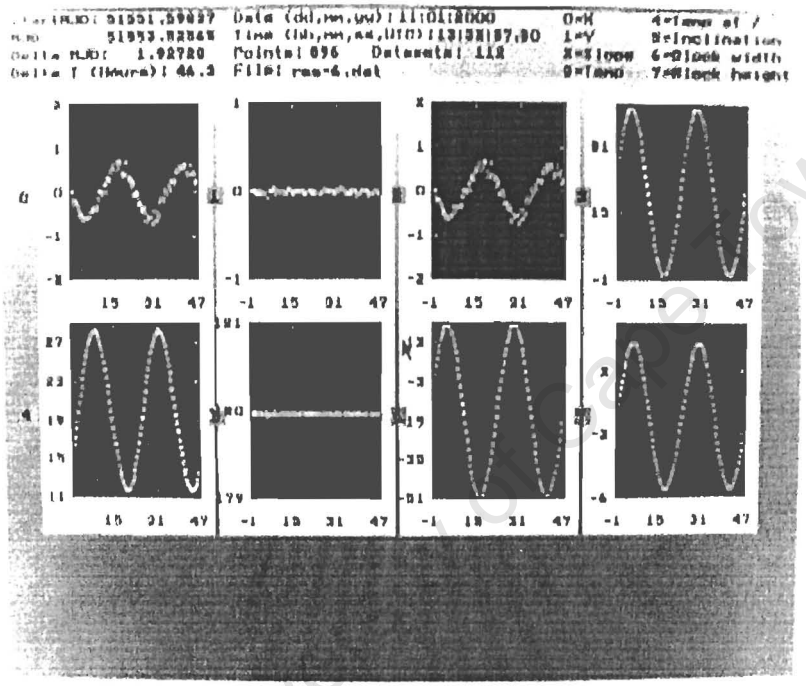

Figure I.3: NTM results based on thermal expansion of a 200 metre diameter hill, coefficient of expansion set to 1×10^{-6}. Peak to peak amplitude of slope distance variation is approximately 5 mm when scaled to a 1000 metre diameter hill.

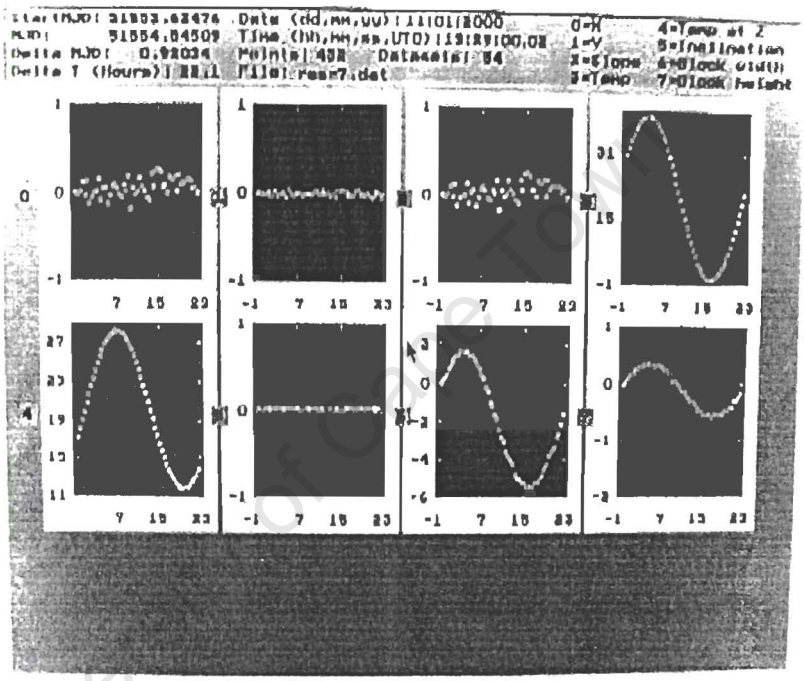

Figure I.4: NTM based on thermal expansion of a 200 metre diameter hill, coefficient of expansion set to 1×10^{-7}. The slope distance variation signal is lost in the noise generated by the blocky hill structure.